

6S RNAs in *Bacillus subtilis*
**Investigation of biological function and molecular
mechanism**

Dissertation

zur

Erlangung des Doktorgrades
der Naturwissenschaften
(Dr. rer. nat.)

dem

Fachbereich Pharmazie der
Philipps-Universität Marburg

vorgelegt von

Sweetha Ganapathy M. Tech
aus **Chennai, Indien**

Marburg (Lahn) **2021**

Erstgutachter: **Prof. Dr. Roland K. Hartmann**
(Philipps-Universität Marburg)
Zweitgutachter: **Prof. Dr. Arnold Grünweller**
(Philipps-Universität Marburg)

Eingereicht am **06.12.2021**

Tag der mündlichen Prüfung am **25.01.2022**

Hochschulkennziffer: 1180

Abstract

6S-1 RNA (*bsrA*) is a 190 nucleotides small non-coding RNA found in *Bacillus subtilis*, which binds to the housekeeping sigma A (σ^A) RNA polymerase holoenzyme (RNAP). 6S-1 RNA levels peak in stationary phase where the RNA supports adaptation to nutrient scarcity (or other stresses) and prepares cells for an instant outgrowth from stationary phase upon nutrient re-supply. In addition to inhibiting cellular transcription by binding to σ^A -RNAP, 6S-1 RNA also serves as a template for this enzyme to direct the synthesis of small product RNAs (pRNAs) in an RNA-dependent RNA polymerization reaction. These pRNAs, if long enough (~ 14-mer), are able to rearrange the structure of 6S-1 RNA such that the polymerase is released from the 6S-1 RNA and transcription of DNA promoters can be resumed. The kinetics of the process and key nucleotides involved in release and rearrangement of 6S-1 are unknown. Towards a deeper understanding of this process, we introduce substitutions/deletions along the secondary structure of 6S-1 RNA and analyse the impact thereof on the kinetics of 6S-1 rearrangement. In our study, we found that mutations C44/45 in the 5'-Central Bulge (CB) weaken 6S-1 RNA: σ^A -RNAP ground state binding two- to threefold while stabilizing the Central Bulge Collapse Helix (CBC) and shifting the pRNA length pattern to shorter pRNAs. A 6S-1 RNA variant with a weakened helix P2 and CBC stabilized by the the C44/45 mutation was more effectively rearranged and released from the enzyme. Our mutational analysis also revealed that formation of a second short hairpin in 3'-CB is detrimental to 6S-1 RNA release. From our results we infer that formation of the CBC subtly supports pRNA-induced 6S-1 RNA rearrangement and release. Additionally, truncated variants of 6S-1 RNA, solely consisting of the CB flanked by two short helical arms, can still traverse the functional 6S RNA cycle *in vitro*, despite decreased σ^A -RNAP affinity. This indicates that the '- 35-like' region is not strictly essential for 6S-1 RNA function, at least in *B. subtilis*. We also showed that pRNA-isosequential locked nucleic acids (pLNAs) as short as 6 nt were able to induce 6S-1 RNA rearrangement and disrupt/prevent complex formation with σ^A -RNAP. Additionally, we analyzed the spatial dimensions of free 6S-1 RNA versus 6S-1:pLNA complexes by atomic force microscopy, revealing that 6S-1:pRNA hybrid structures, on average, adopt a more bent/constrained

structure than 6S-1 RNA alone. The pLNA studies help us interpret the 6S-1 rearrangement to be a progressive process with intermediate states, ultimately leading to a maximally constrained and bent structure. Finally, we observed that the pRNA-mediated rearrangement of 6S-1 RNA and its release from σ^A -RNAP largely accelerates at NTP concentrations $> 40 \mu\text{M}$, which supports the role of 6S-1 RNA during nutrient re-supply.

In gel assays, the regulatory 6S-1 and 6S-2 RNAs of *Bacillus subtilis* bind to the housekeeping RNA polymerase holoenzyme (σ^A -RNAP) with submicromolar affinity. We observed copurification of endogenous 6S RNAs from a published *B. subtilis* strain expressing a His-tagged RNAP. Such 6S RNA contaminations in σ^A -RNAP preparations reduce the fraction of enzymes that are accessible for binding to DNA promoters. In addition, this leads to background RNA synthesis by σ^A -RNAP utilizing copurified 6S RNA as template for the synthesis of short abortive transcripts termed product RNAs (pRNAs). To avoid this problem, we constructed a *B. subtilis* strain expressing His-tagged RNAP but carrying deletions of the two 6S RNA genes. The His-tagged, 6S RNA-free σ^A -RNAP holoenzyme can be prepared with sufficient purity and activity by a single affinity step. We also reported expression and separate purification of *B. subtilis* σ^A that can be added to the His-tagged RNAP to maximize the amount of holoenzyme and, by inference, *in vitro* transcription activity.

In order to test our hypothesis that the regulatory role of 6S RNAs may be particularly important under natural, constantly changing environmental conditions, we constructed 6S RNA deletion mutants of the undomesticated *B. subtilis* wild-type strain NCIB 3610. We observed a strong phenotype under stress conditions in which the $\Delta 6\text{S-2}$ RNA strain exhibited retarded swarming activity and earlier spore formation. In contrast, the $\Delta 6\text{S-1\&2}$ double knockout strain exhibited lesser spore formation than the wild-type. Additionally, we could show that 6S mutants grown under nutrient rich conditions revealed no strong phenotype. Our data suggests that both 6S RNAs contributes to the fitness of *B. subtilis* under the unsteady and temporarily harsh conditions encountered in natural habitats.

- This page is intentionally left blank -

Zusammenfassung

6S-1 RNA (*bsrA*) ist eine 190 Nukleotid lange, nicht-kodierende RNA, die in *Bacillus subtilis* vorkommt und an das Housekeeping-Sigma-A (σ^A) RNA-Polymerase-Holoenzym (RNAP) bindet. Die 6S-1 RNA Konzentration erreicht ihren Höhepunkt in der stationären Phase, in der die RNA die Anpassung an Nährstoffknappheit (oder andere Stressfaktoren) unterstützt und die Zellen darauf vorbereitet, bei erneuter Nährstoffzufuhr sofort aus der stationären Phase herauszuwachsen. Neben der Hemmung der zellulären Transkription durch Bindung an σ^A -RNAP dient die 6S-1 RNA auch als Vorlage für dieses Enzym, um die Synthese von kleinen Produkt-RNAs (pRNAs) in einer RNA-abhängigen RNA-Polymerisationsreaktion zu steuern. Diese pRNAs sind, wenn sie lang genug sind (~ 14-mer), in der Lage, die Struktur der 6S-1 RNA so umzugestalten, dass die Polymerase von der 6S-1 RNA freigesetzt wird und die Transkription der DNA-Promotoren wieder aufgenommen werden kann. Die Kinetik des Prozesses und die Schlüsselnukleotide, die an der Freisetzung und Umstrukturierung von 6S-1 beteiligt sind, sind unbekannt. Um diesen Prozess besser zu verstehen, führen wir Substitutionen/Deletionen entlang der Sekundärstruktur der 6S-1 RNA ein und analysieren deren Auswirkungen auf die Kinetik der 6S-1 Umstrukturierung. In unserer Studie fanden wir heraus, dass die Mutationen C44/45 in der 5'-Central Bulge (CB) die 6S-1 RNA: σ^A -RNAP Grundzustandsbindung um das Zwei- bis Dreifache schwächen, während sie die Central Bulge Collapse Helix (CBC) stabilisieren und das pRNA-Längenmuster zu kürzeren pRNAs verschieben. Eine 6S-1 RNA Variante mit einer geschwächten Helix P2 und einer durch die C44/45 Mutation stabilisierten CBC wurde effektiver umstrukturiert und vom Enzym freigesetzt. Unsere Mutationsanalyse ergab außerdem, dass die Bildung einer zweiten kurzen Haarnadel in 3'-CB die Freisetzung von 6S-1 RNA beeinträchtigt. Aus unseren Ergebnissen schließen wir, dass die Bildung der CBC die pRNA-induzierte Umstrukturierung und Freisetzung von 6S-1 RNA auf subtile Weise unterstützt. Darüber hinaus können verkürzte Varianten der 6S-1 RNA, die nur aus der CB bestehen, das von zwei kurzen helikalen Armen flankiert wird, den funktionalen 6S RNA Zyklus *in vitro* trotz verminderter σ^A -RNAP Affinität durchlaufen. Dies

deutet darauf hin, dass die "-35-ähnliche" Region für die Funktion der 6S-1 RNA zumindest in *B. subtilis* nicht unbedingt erforderlich ist. Wir haben auch gezeigt, dass pRNA-isosequentiell verschlossene Nukleinsäuren (pLNAs) mit einer Länge von nur 6 nt in der Lage sind, eine Umstrukturierung der 6S-1 RNA zu bewirken und die Komplexbildung mit σ^A -RNAP zu unterbrechen/verhindern. Darüber hinaus analysierten wir die räumlichen Dimensionen von freier 6S-1 RNA im Vergleich zu 6S-1:pLNA-Komplexen mit Hilfe der Rasterkraftmikroskopie und stellten fest, dass 6S-1:pLNA-Hybridstrukturen im Durchschnitt eine stärker gebogene/begrenzte Struktur aufweisen als 6S-1 RNA allein. Die pLNA-Untersuchungen helfen uns, die 6S-1 Umstrukturierung als einen fortschreitenden Prozess mit Zwischenzuständen zu interpretieren, der schließlich zu einer maximal eingeschränkten und gebogenen Struktur führt. Schließlich beobachteten wir, dass die pRNA-vermittelte Umstrukturierung der 6S-1 RNA und ihre Freisetzung aus σ^A -RNAP bei NTP-Konzentrationen $> 40 \mu\text{M}$ stark beschleunigt wird, was die Rolle der 6S-1 RNA während der Nährstoffversorgung unterstützt.

In Gel-Assays binden die regulatorischen 6S-1 und 6S-2 RNAs von *Bacillus subtilis* mit submikromolarer Affinität an das Holoenzym der Housekeeping-RNA-Polymerase (σ^A -RNAP). Wir haben eine Co-Aufreinigung endogener 6S RNAs aus einem aus der Literatur bekannten *B. subtilis* Stamm beobachtet, der eine His-markierte RNAP exprimiert. Solche 6S RNA Kontaminationen in σ^A -RNAP Präparaten reduzieren den Anteil der Enzyme, die für die Bindung an DNA-Promotoren zugänglich sind. Darüber hinaus führt dies zu einer Hintergrund-RNA-Synthese durch σ^A -RNAP, die die co-aufgereinigte 6S RNA als Vorlage für die Synthese kurzer, fehlgeschlagener Transkripte, so genannter Produkt-RNAs (pRNAs), verwendet. Um dieses Problem zu vermeiden, haben wir einen *B. subtilis* Stamm konstruiert, der His-markierte RNAP exprimiert, aber Deletionen der beiden 6S RNA Gene trägt. Das His-markierte, 6S RNA-freie σ^A -RNAP Holoenzym kann mit ausreichender Reinheit und Aktivität in einem einzigen Affinitätsschritt hergestellt werden. Wir berichteten auch über die Expression und separate Reinigung von *B. subtilis* σ^A , dass der His-markierten RNAP hinzugefügt werden kann, um die Menge des Holoenzym und damit die *in vitro* Transkriptionsaktivität zu maximieren.

Um unsere Hypothese zu testen, dass die regulatorische Rolle der 6S RNAs unter natürlichen, sich ständig ändernden Umweltbedingungen besonders wichtig sein könnte, konstruierten wir 6S RNA Deletionsmutanten des undomestizierten *B. subtilis* Wildtyp Stammes NCIB 3610. Wir beobachteten einen starken Phänotyp unter Stressbedingungen, bei dem der $\Delta 6S-2$ RNA Stamm eine verzögerte Schwarmaktivität und eine frühere Sporenbildung aufwies. Im Gegensatz dazu wies der $\Delta 6S-1\&2$ Doppelknockout Stamm eine geringere Sporenbildung auf als der Wildtyp. Außerdem konnten wir zeigen, dass 6S Mutanten, die unter nährstoffreichen Bedingungen wuchsen, keinen starken Phänotyp aufwiesen. Unsere Daten deuten darauf hin, dass beide 6S RNAs zur Fitness von *B. subtilis* unter den unbeständigen und zeitweise rauen Bedingungen in natürlichen Lebensräumen beitragen.

கற்றது கைமண் அளவு, கல்லாதது உலகளவு

- ஓளவையார்

What you have learnt is a mere handful; What you haven't learnt is the size of the world.

- Avvaiyar

Alles was man gelernt hat passt in eine Hand aber alles was man nicht gelernt hat ist groß wie die ganze Welt.

- Avvaiyar

Acknowledgement

I would like to thank my supervisor Prof. Dr. Roland Hartmann for this opportunity, the invigilation committee members for their participation and careful assessment of the dissertation. I thank Dr. Wiebke Obermann for the documentation of the disputation.

I am grateful for my 6S RNA girls Amri Schlüter, Jana C. Wiegard and Dr. Marietta Thüring for making the entire journey fun, filled with fruitful discussions and clever solutions. Also, for taking time to correct and proofread my thesis. I thank Dr. Katrin Damm, Dr. Nadine Waeber and Dr. Simone Bach for being good mentors and teaching me the ropes.

My büro buddies Swetlana Davydov, Wiebke, Amri and the coffee machine for making it possible for me to complete this programme. I would like to thank the lab fairy Dominik Jens Helmecke for assistance in performing experiments and to whom I probably owe a few reagents. I am grateful to Katja Hütte for being there whenever I have problems.

I thank the entire working group Prof. Dr. Arnold Grünweller, Dr. Markus Gößringer, Jana-Christin Demper, Isabell Schencking, Rebecca Feyh, Paul Klemm, Dr. Harshavardhan Janga, Mahasweta Bordoloi, Ahmad Altoun and Erna Ebert for providing a friendly and productive environment to nurture and grow in.

I would like to thank Ganapathy Ayyamperumal Swaminathan, Revathi Ganapathy, Akhil Ganapathy and my extended family for helping me become the person I am today. I take cognizance of the motto in our household that educated people should empower education which helped me to pursue this outcome.

Finally, I would like to thank my roommates Paula Böcker, Bianca Bickel and most importantly my social clique “BBBBB” for making my life in Marburg enjoyable.

Index

I. List of diagrams	15
II. List of tables	16
III. Abbreviation	17
1 Introduction	19
1.1 Non-coding RNAs.....	19
1.2 6S RNAs	21
1.2.1 General features of 6S RNAs	21
1.2.2 6S RNA cycle	24
1.2.3 Secondary structure of 6S RNAs	26
1.2.4 Mechanistic aspects of 6S RNAs	33
1.2.5 6S RNAs in <i>Bacillus subtilis</i>	37
1.2.6 Phenotypic aspects of 6S RNA knockouts	38
1.3 <i>Bacillus subtilis</i>	43
1.3.1 RNA polymerase	44
1.3.2 Stress response and adaptation in <i>B. subtilis</i>	47
1.3.3 Molecular basis for biofilm formation in <i>B. subtilis</i>	49
1.4 Aim of the projects	50
1.4.1 Impact of secondary structure modifications on 6S-1 RNA and σ^A -RNAP interaction kinetics	50
1.4.2 Construction of 6S RNA free His-tagged RNA polymerase in <i>B. subtilis</i>	51
1.4.3 Phenotypic characterization of 6S RNA knockouts in 3610 strain	52
1.4.4 Transcription of the <i>epsA</i> gene by RemA mutants	52
2 Materials and methods	53
2.1 Bacterial handling techniques.....	53
2.1.1 Preparation of media	53
2.1.2 Solid medium handling	53
2.1.3 Liquid medium handling	53
2.1.4 Growth curve measurements	53
2.1.5 Glycerol stock preparation	54

2.1.6 Harvesting of bacterial cells	54
2.1.7 Inducing chemical competency in bacterial cells	55
2.2 Nucleic acid handling techniques.....	56
2.2.1 Cloning	56
2.2.2 Polymerase chain reaction (PCR)	57
2.2.3 Agarose gel electrophoresis	61
2.2.4 Sequencing of PCR products	61
2.2.5 Gel elution of PCR product	62
2.2.6 Phosphorylation	62
2.2.7 <i>DpnI</i> digestion and ligation	63
2.2.8 Transformation	64
2.2.9 Plasmid preparation for sequencing	64
2.2.10 Preparation of cold RNA	64
2.2.11 Plasmid preparation for cold RNA transcription	65
2.2.12 Linearisation of plasmid	65
2.2.13 Phenol and chloroform extraction of DNA	66
2.2.14 <i>In vitro</i> transcription using T7 RNA polymerase	67
2.2.15 Phenol and chloroform extraction of RNA	67
2.2.16 Extraction of RNA from denaturing polyacrylamide gel	68
2.2.17 Gel elution and precipitation of RNA	68
2.2.18 De-phosphorylation of RNA	68
2.2.19 5' radiolabeling of RNA	69
2.3 Protein handling techniques	71
2.3.1 Cell lysis for purification	71
2.3.2 Nickel-nitrilotriacetic acid (Ni-NTA) column	72
2.3.3 Size exclusion column	73
2.3.4 Heparin column	74
2.3.5 MonoQ column	75
2.3.6 Bradford assay	76
2.3.7 Image lab™ software	76
2.3.8 Sodium dodecyl sulphate polyacrylamide (SDS-PAGE) gel	77
2.3.9 Tris-glycine extended (TGX) gel	78
2.3.10 Schaeffer gel	78
2.3.11 Coomassie blue staining	79

2.3.12 Zinc staining	79
2.3.13 Silver staining	79
2.3.14 Western blot	80
2.4 Assays	81
2.4.1 Electrophoretic mobility shift assay	81
2.4.2 Native electrophoretic mobility shift assay	82
2.4.3 Nucleotide supplemented native electrophoretic mobility shift assay	85
2.4.4 Denaturing electrophoretic mobility shift assay	87
2.4.5 pRNA transcription assay	89
2.4.6 RemA and RNA polymerase transcription assay	91
2.4.7 Motility assay	93
2.4.8 Sporulation assay	94
2.5 Equations	95
2.5.1 Ligand binding - 1 site equation	95
2.5.2 1 st order rate equation	96
2.5.3 Spline curve	97
3. Results and discussion	98
3.1 Structural and functional insight into the mechanism of <i>Bacillus subtilis</i> 6S-1 RNA release from RNA polymerase	98
3.2 Rapid preparation of 6S RNA-free <i>Bacillus subtilis</i> σ^A-RNA polymerase and σ^A	149
3.3 6S-2 RNA deletion in the undomesticated <i>B. subtilis</i> strain NCIB 3610 causes a biofilm derepression phenotype	184
3.4 RemA and RNA polymerase transcription assay	195
4. Summary and Outlook	197
5. Literature review	200
Appendix	211
A. Equipment and disposables	211
B. Chemicals	213
C. Proteins and Enzymes	215
D. Kits	215
E. Bacterial strains and antibiotics	216
F. Plasmids	217

G. Terminology of 6S RNA mutants	218
H. Primers	219
I. Softwares	221
J. Plasmid cards	222
K. RNA folds	237
L. Scientific CV	263
M. Scientific contributions	265

I. List of diagrams

Figure 1: Steps and thermodynamic rate constants involved in the cycle of 6S RNA in <i>B. subtilis</i>	24
Figure 2: Secondary structure of 6S RNAs.....	26
Figure 3: Truncated mutants of <i>E. coli</i> 6S RNA.....	29
Figure 4: Secondary structure modifications of <i>E. coli</i> 6S RNA	30
Figure 5: Structural rearrangement of 6S RNA occurs upon pRNA binding....	36
Figure 6: <i>In vitro</i> mutagenesis.....	57
Figure 7: Brief overview of PCR reaction.....	57
Figure 8: Chemical composition of a nucleotide.....	68
Figure 9: Principle of Ni-NTA column.....	72
Figure 10: Pictorial representation of Electrophoretic Mobility Shift Assay (EMSA).....	81
Figure 11: Ligand binding - 1 site equation.....	94
Figure 12: 1 st order rate equation.....	95
Figure 13: Spline curve diagram.....	96

II. List of tables

Table 1: Mapped interaction partners of RNA polymerase subunits.....	46
Table 2: PCR reaction set-up for <i>in vitro</i> mutagenesis.....	58
Table 3: PCR programme for <i>in vitro</i> mutagenesis.....	58
Table 4: PCR reaction set-up for colony PCR.....	59
Table 5: PCR programme for colony PCR.....	59
Table 6: PCR reaction set-up for two-step PCR.....	60
Table 7: PCR programme for two-step PCR.....	60
Table 8: Resolution of PCR fragment based on agarose percentage of gel.....	61
Table 9: Reaction set up for DNA phosphorylation.....	63
Table 10: Reaction set up for DNA ligation and parent strand digestion.....	63
Table 11: Restriction digestion of plasmid DNA.....	65
Table 12: Reaction set up for <i>in vitro</i> transcription using T7 RNA polymerase....	67
Table 13: Reaction set up for de-phosphorylation of RNA.....	69
Table 14: Reaction set up for radiolabeling of RNA.....	70
Table 15: Pipette scheme for standard BSA assay calibration curve.....	76
Table 16: Dye migration and corresponding nucleotide length based on native polyacrylamide gel percentage	83
Table 17: Pipette scheme for determination of binding affinity (K_d) of σ^A -RNAP and 6S RNA.....	84
Table 18: Pipette scheme for determination of kinetics rate of pRNA:6S RNA complex formation	86
Table 19: 6S RNA re-folding programme	87
Table 20: Dye migration and corresponding nucleotide length based on denaturing polyacrylamide gel percentage.....	88
Table 21: Pipette scheme for pRNA transcription.....	90
Table 22: Empirically derived decay factor of radioactive Phosphorus-32.....	91
Table 23: Pipette scheme to check for <i>epsA</i> gene transcription by mutant RemA.....	92

III. Abbreviation

Symbol	Abbreviation
%	Percentage
γ - ³² P-ATP	Gamma ³² P adenosine triphosphate
°C	Degree Celsius
μg	Microgram
μL	Microliter
μM	Micromolar
APS	Ammonium persulfate
Amp	Ampicillin
bp	Base pair
BPB	Bromophenol blue
Cm	Chloramphenicol
cpm	Counts per minute
ddH₂O	Double distilled water
DMSO	Dimethyl sulfoxide
DNA	Deoxyribonucleic acid
DTT	Dithiothreitol
EDTA	Ethylenediaminetetraacetic acid
f.c.	Final concentration
g	Gravitational force
g	Gram
h	Hour
Hz	Hertz
Kan	Kanamycin
KDa	Kilodalton
LB	Luria bertani
M	Molar
mM	Millimolar
mA	Milliampere
nt	Nucleotide

NTP	Nucleoside triphosphate
OD	Optical density
p.a.	Pro analysi (Analytical grade)
PAA	Polyacrylamide
PAGE	Polyacrylamide gel electrophoresis
PCR	Polymerase chain reaction
pmol	Pico moles
PMSF	Phenylmethylsulphonyl fluoride
pRNA	Product RNA
RNA	Ribonucleic acid
RT	Room temperature
SDS	Sodium dodecyl sulphate
Spec	Spectinomycin
TTC	Tri-phenyl tetrazolium chloride
T4 PNK	T4 polynucleotide kinase
TBE	Tris boric acid EDTA
TAE	Tris acetate EDTA
TE	Tris EDTA
T.G.	Tetrazolium glucose
Tm	Melting temperature
U	Units of enzymatic activity
UV	Ultraviolet
V	Volts
v/v	Volume per volume %
w/v	Weight per volume %
XCB	Xylene cyanol

1 Introduction

1.1 Non-coding RNAs

In the 21st century, the central dogma of molecular biology is truly outdated. The mundane narration of DNA transcribes into RNA and RNA translates into protein is a linear relationship that has been debunked many times. Discovered in the 1950s and often mistaken to be junk elements, non-coding RNAs (ncRNA) are defined as RNAs that do not code for proteins (Palazzo et al., 2015, Joshi et al., 2020). Non-coding RNAs are termed small ncRNAs when shorter than 200 nt and long ncRNAs (lncRNAs) when longer than 200 nt (Joshi et al., 2020, Palazzo et al., 2015). The existence of ncRNAs has been well documented across all three domains of life namely Eukaryotes, Prokaryotes and Archaea (Palazzo et al., 2015, Dennis et al., 2015, Gottesman 2005). Non-coding RNAs can affect gene regions in cis acting (neighbourhood) or trans-acting (faraway) manner (Joshi et al., 2020, UI Haq et al., 2020). They act either by binding to proteins or by base pairing target RNAs or otherwise by exhibiting intrinsic activity such as catalysis (Wassarman et al., 2018). NcRNAs are very versatile and aid in a wide range of functions such as regulation in cell development, cell death and chromosomal inactivation in eukaryotes; protein transport, rRNA processing, ribosomal assembly in archaea and stress response, virulence in prokaryotes (Gottesman 2005, Dennis et al., 2015). The existence of ncRNAs in prokaryotes is special as the genome of a prokaryote is vastly coding with only 12 % being non-protein coding DNA (Vandevenne et al., 2019). On an average, a bacterial cell genome encodes only about 200 to 300 small regulatory RNAs (UI Haq et al., 2020). The prokaryotic system is evolutionarily designed to rely heavily on proteins to accomplish tasks and is effective in weeding out useless RNAs. Therefore, ncRNAs that persist in the prokaryotic genome despite the selection pressure should serve functional significance (Vandevenne et al., 2019). In prokaryotes, majority of the non-coding RNAs act by base pairing target mRNA which results in translation inhibition or stimulation, degradation of the target mRNA or mRNA stabilization (Gottesman 2005). Due to the ability of ncRNAs to form secondary structures, or even tertiary structures in presence of metal ions, the ncRNA emancipates itself from the need to extensively conserve nucleotide sequence in

order to be effective (Joshi et al., 2020, Vandevenne et al., 2019). Therefore, all sequencing strategies designed to detect ncRNAs were not successful and ncRNAs eluded scientists for decades. The earliest ncRNAs were detected while testing their strong interacting partners or just pure luck (Gottesman 2005). As a result, algorithms looking for reading frames outside coding regions were designed to include partial sequence matches along with conservation of secondary structure elements (hairpins) and Rho-independent termination sites to improve accuracy of ncRNA hits. Techniques belonging to Next Generation Sequencing (NGS) such as Psoralen Analysis of RNA Interactions and Structures with High Throughput and Resolution (PARIS), Ligation of Interacting RNA followed by high-throughput Sequencing (LIGR-Seq) are arguably the best to detect intracellular RNA duplexes. High-Throughput Sequencing Crosslinking and Immunoprecipitation (HITS-CLIP), Photoactivatable Ribonucleoside-enhanced Crosslinking and Immunoprecipitation (PAR-CLIP), Individual nucleotide resolution CLIP (iCLIP) aid to detect protein interaction partners of ncRNAs (Vandevenne et al., 2019). Some non-sequencing techniques to study ncRNA and protein interaction are Phenol-Toluol extraction (PTex) method, Systematic Evolution of Ligands by Exponential enrichment (SELEX), RNase footprinting, p-Benzoyl-L-Phenylalanine (BPA) cross linking (Chen et al., 2015), Grad-seq (Gerovac et al., 2021) and Selective 2'-Hydroxyl Acylation analyzed by Primer Extension Sequencing (SHAPE-seq) method. Finally, certain methods help us to study the secondary structure of the ncRNA such as lead probing (Köhler et al., 2015), X-ray diffraction, Nuclear Magnetic Resonance (NMR), Atomic Force Microscopy (AFM), Total Internal Reflection Fluorescence Microscope (TIRFM) and Surface Plasmon Resonance (SPR) (Neidle et al., 2002).

1.2 6S RNAs

The 6S RNA is a small non-coding RNA found in the bacterial kingdom. It was first discovered in *E. coli* as a band migrating slower than the 5S band in a tRNA preparation gel by Hindley (Hindley et al., 1971). Radiolabelled pulse chase experiments showed that the 6S RNA had an unusually long-life time in the prokaryotic cell, making it unlikely to be mRNA. This small ncRNA was later sequenced in *E. coli* (Brownlee et al., 1971, Lee et al., 1978). The heavier than somewhat anticipated sucrose gradient sedimentation profile of the 6S RNA hinted the possibility of a ribonucleic protein complex (Lee et al., 1978). This possibility was confirmed using UV crosslinking experiments which demonstrated that the 6S RNA binds to the housekeeping RNA polymerase (RNAP) in a robust manner (Wassarman et al., 2000). Since then, research on the 6S RNA as a transcriptional regulator has skyrocketed. Questions asking about the expression, function, binding mechanism and phylogeny were open to answers.

1.2.1 General features of 6S RNAs

The 6S RNA predominantly binds to the housekeeping RNAP, however weak binding to alternative sigma factor associated holo and core RNAP has been observed on gel assays (Gildehaus et al., 2007). Most 6S RNAs accumulate towards the end of stationary phase however, there are a few exceptions to this expression profile. *B. subtilis* harbours two 6S RNAs namely 6S-1 RNA and 6S-2 RNA. The 6S-2 RNA peaks in the early to mid-exponential phase and during which was found to be three folds higher in concentration than 6S-1 RNA. 6S-1 RNA appears to peak and accumulate through the stationary phase (Hoch et al., 2016). In certain species such as *S. meliloti* and *R. sphaeroides*, the 6S RNA attains highest concentration towards the transition phase (Burenina et al., 2020). The 6S RNA is widely present throughout the microbial kingdom, an initial phylogenetic analysis conducted by Barrick et al. (2005) found 121 potential 6S RNA harbouring organisms. The phylogenetic data indicated that the RNA has a common ancestral origin and an uninterrupted existence in *E. coli* with no signs of horizontal gene transfer. Intriguingly, the genetic proximity of the 6S RNA gene to *ygfA* gene was phylogenetically conserved across some species. A higher

expression of the *ygfA* gene has been observed in biofilm forming cells in *E. coli*. Nevertheless, no significant relationship between 6S RNA and *ygfA* gene expression has been documented until now (Wehner et al., 2014, Barrick et al., 2005). Detection of 6S RNA has also been done using experimental RNomics where cDNA libraries of a length of 100 - 450 nt were closely inspected for small RNA transcripts. Through this process several mRNAs of unknown proteins, intergenic RNAs (6S RNA) and tRNA antisense transcripts in *A. aeolicus* were found (Willkomm et al., 2005). The 6S RNA was identified in this study by looking for short co-transcripts (~ 200 nt) in proximity to the *ygfA* gene or its phylogenetic equivalent, followed by Rapid Amplification of 5' cDNA Ends (5' RACE) to identify transcription initiation and processing sites of the intergenic RNA and concluded using mfold/RNA fold software (Lorenz et al., 2018) that may or may not reveal the canonical secondary structure (Willkomm et al., 2005). Another study, using an algorithm aimed to detect the secondary structure of 6S RNA in bacterial genomes filtered 1750 6S RNA hits of which 1367 previously unknown were detected. Another aspect of 6S RNAs is their copy number. Most organisms belonging to α , β , γ , ϵ -Proteobacteria and Firmicutes have one copy of 6S RNA with some exceptions having two namely *B. subtilis*, *Prochlorococcus MED4* and speculatively up to four *C. ljungdahlii* but the exact relationship to the number of 6S RNA copies present and function is unknown (Wehner et al., 2014, Rediger et al., 2012). A third atypical 6S RNA (RNA3) in *B. subtilis* that does not bind to σ^{70} -RNAP was proposed and later rejected by Trotochaud et al. (2005) due to non-conformity to the 6S RNA hallmark features. Ms1 RNA found in mycobacteria, is an analogue of the 6S RNA that interacts exclusively with core RNAP (Šíková et al., 2018). Ms1 RNA could be an intriguing suspect for the RNA3 documented in *B. subtilis* but this is purely speculative. Quantitatively, ~ 3.5 billion copies of 6S RNA was observed for every 10 μg of RNAP. Such high levels make 6S RNA a crucial binding partner and an important transcriptional regulator of σ^A -RNAP (Delumeau et al., 2011). At genomic level, 6S RNA in *E. coli* is under the influence of two promoters namely P1 and P2. P1 promoter region is recognized by σ^{70} -RNAP whereas P2 is recognized by σ^{70}/σ^S -RNAP subunit. Both P1 and P2 are actively transcribed during the exponential phase but only P2 is transcribed towards the stationary phase. This phenomenon can be putatively explained by the decrease in availability of σ^{70} -RNAP and increase in

RNAP assembled with alternative sigma factors (σ^S) upon entry into stationary phase. Interestingly, precursor 6S RNA initiated by P1 is processed into mature RNA by RNase E and RNase G but in the case of P2 initiated precursor 6S RNA only RNase E is involved (Kim et al., 2004). RNase BN is identified as a main cleavage enzyme responsible for endo-nucleolytic degradation of 6S RNA at least in the case of *E. coli*. RNase BN production peaks in mid-exponential phase and readily degrades the 6S RNA rearranged complex. Therefore, freshly produced RNase BN could cause the sudden dip in 6S RNA population observed during outgrowth phase or restarted exponential phase of bacterial growth. The newly released σ^{70} -RNAP can now be effectively used by the bacteria to adapt to the new environment (Chen et al., 2016). Unfortunately, there isn't much published information regarding the processing and degradation of 6S-1 and 6S-2 RNA in *B. subtilis*, which is currently one focused theme of our working group.

1.2.2 6S RNA cycle

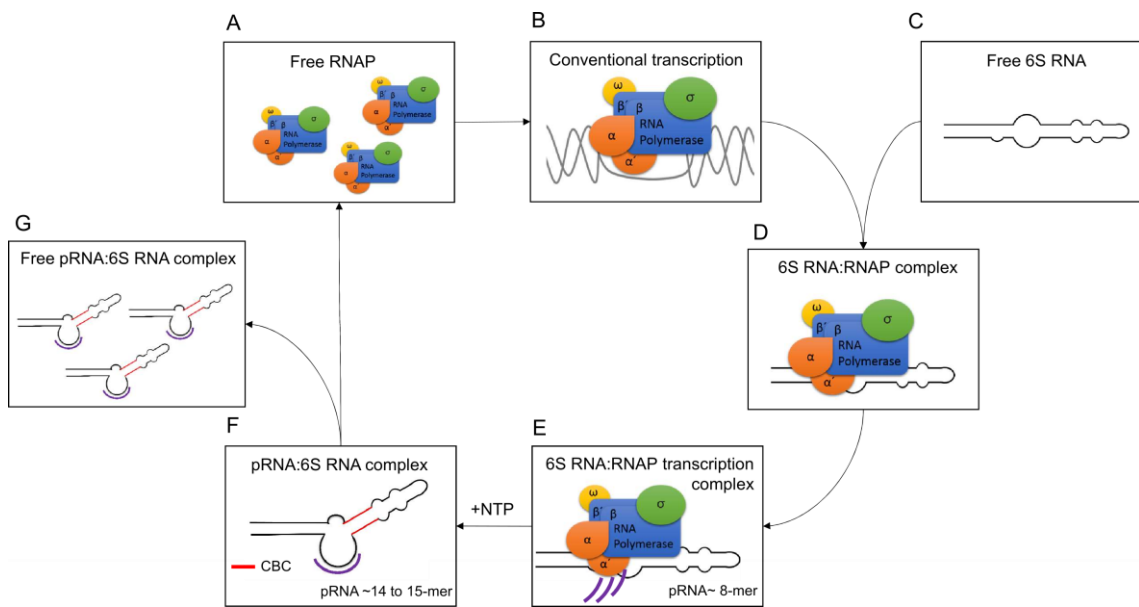


Figure 1: Steps and thermodynamic rate constants involved in the cycle of 6S RNA in *B. subtilis*: (A) Housekeeping σ^A -RNA polymerase (σ^A -RNAP) is in an unbound free state. (B) During early exponential phase, RNAP performs its housekeeping role by transcribing various essential genes (C) The 6S RNA is produced upon entry into late exponential to stationary phase. (D) 6S RNA binds to the RNAP forming a 6S RNA:RNAP complex. K_d : The dissociation constant for binding of 6S RNA to RNAP. (E) This 6S RNA:RNAP complex formation is called the Initial Transcription Complex (ITC). Within this complex the enzyme initiates RNA-templated RNA transcription resulting in the production of short, abortive RNA transcripts called product RNAs (pRNAs). Under nutrient depletion, the pRNAs are typically ~ 8-mer. (F) Upon nutrient replenishment, pRNAs ~ 14 - 15-mer are synthesized. These relatively longer pRNAs are capable of stable binding to the 6S RNA forming a pRNA:6S RNA complex. The binding triggers rearrangement of the 6S RNA into a sterically constrained bent structure and in formation of a new region called the "Central Bulge Collapse helix or Central Bubble Collapse helix" (CBC) is formed. (G) The pRNA:6S RNA complexes are ultimately released from the RNAP and the free RNAP is allowed to resume the cycle (Burenina et al., 2014, Beckmann et al., 2012).

Upon entry into stationary phase, bacterial cells enter into a starvation mode where nutrients are limited and survival is tough. Thus, the stationary phase is a form of stress situation. Luckily, if a resurgence of nutrients occurs the molecular networks in the bacteria re-program and start multiplying. This phase is specifically denoted as the outgrowth phase. The 6S RNA aids in the optimal stress response of bacteria as they move from stationary phase (stress phase) to outgrowth phase (relief phase). Formation of pRNA:6S RNA complex has been

shown to be critical during outgrowth conditions of cells both in *E. coli* and *B. subtilis*. In *E. coli*, 6S RNA mutants that are defective in pRNA synthesis showed a delayed outgrowth phenotype and reduced viability in late stationary phase (~ 24 h). Likewise, a *B. subtilis* 6S-1 knockout strain also showed a delayed outgrowth phenotype (Cavanagh et al., 2011). In both species, the pRNA:6S RNA rearranged complex does not bind back to the RNAP (Cavanagh et al., 2011).

Hallmarks of 6S RNAs

1. 6S RNA should bind to the housekeeping RNA polymerase (RNAP).
2. 6S RNA should serve as a template to produce product RNAs (pRNAs).
3. 6S RNA should be able to compete against DNA for binding to the housekeeping RNAP and inhibit DNA-templated transcription.
4. 6S RNA should bind to pRNAs and result in a rearranged pRNA:6S RNA complex.
5. The pRNA:6S RNA complex should not bind back to the housekeeping RNAP (Burenina et al., 2014).

1.2.3 Secondary structure of 6S RNAs

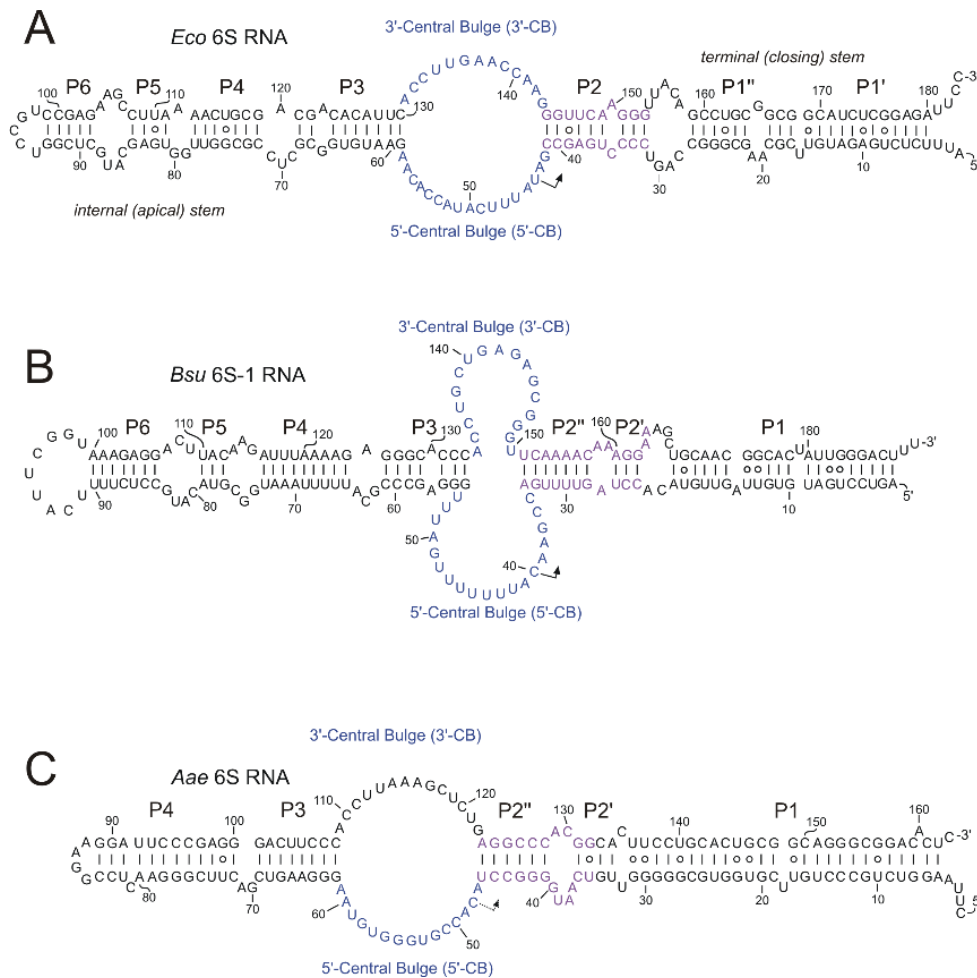


Figure 2: Secondary structure of 6S RNAs: There are three main conserved features of 6S RNA derived from covariance model-based analysis. 1. The terminal (closing) stem is more than 15 nucleotide basepairs long with one or more interruptions (mini-bulges) and some wobble base pairing (G-U) along a complementary double stranded sequence; the unpaired overhang of the closing stem is however highly deviant depending on the species. 2. The central bulge is an open unpaired loop with a 5' and 3' sequence. The 5' sequence is unpaired and low in G residues (~ 11 %) with an average length of 15 nucleotides while the 3' sequence has four conserved bases which might form a short, unstable stem loop (Barrick et al., 2005). 3. The internal (apical) stem ends in an ultimate stem loop and depending on the species may have one mini bulge (β - , δ - proteobacteria, *Spirochetes*), two mini-bulges (γ - proteobacteria, *Bacillus*, *Clostridium*, *Cyanobacteria*) or none (α - proteobacteria) along the double stranded sequence connecting to the central bulge. (A) Secondary structure of *E. coli* 6S RNA: The short stretches of double stranded RNA interrupted by mini bulges, the regions P5 and P6 in *E. coli* are similar to - 35 region of a conventional DNA promoter and 3' central bulge resembles the - 10 region of the DNA promoter, finally the P2 region acts as the downstream helix that is uncoiled gently during transcription by RNA polymerase. Due to the conserved nature of the secondary structure, other

6S RNAs could function in a similar manner. (B) Secondary structure of *B. subtilis* 6S-1 RNA. (C) Secondary structure of *A. aeolicus* 6S RNA. (Hoch et al., 2014, Trotochaud et al., 2005, Barrick et al., 2005).

All cellular RNAs have the potential to form secondary structures. Secondary structures of RNAs are formed due to duplex base pairing of nucleotides influenced by thermodynamic parameters such as Gibbs free energy (G), entropy (S) and enthalpy (H). Modification of these oligonucleotides may either promote or disrupt the base pairing; for example, 2'-O methyl nucleotides stabilizes duplexes whereas phosphonothioate de-stabilizes the duplex formation by 0.3 kcal/mol per modification (Erickson et al., 1992). Although a sequence-based algorithm identified multiple hits for 6S RNA across the γ -proteobacterial genomes, a strikingly similar secondary structure feature of largely double stranded with a single stranded central region was found conserved across domains (Trotochaud et al., 2005, Barrick et al., 2005). The secondary structure consists of an internal stem that mimics the upstream region of a melted promoter DNA template and putatively the -35 region of promoter DNA, a central bulge that mimics the transcription bubble and the -10 region of promoter DNA and finally a terminal stem that presents itself as a transcription template downstream to the transcription start site. Even within the same organism 6S-1 RNA and 6S-2 RNA of *B. subtilis* only show a 46 % sequence conservation but a similar secondary structure. This secondary structure of 6S RNA is well conserved even across widely diverse species such as *E. coli*, *B. subtilis* and *Synechococcus sp.* PCC6301. A machine learning algorithm based on covariance model was fed with known 6S RNA sequences from the *Rfam* database and 121 potential 6S RNA housing organisms were identified (Panchapakesan et al., 2012, Barrick et al., 2005). This ubiquitous yet sequentially poorly conserved secondary structure feature of 6S RNA is typical of canonical ncRNAs. The secondary structure enables binding of 6S RNA to the house keeping RNA polymerase and triggers inhibition of transcription in a global manner, earning the title “ribo-regulator” (Steuten et al., 2014). The presence of minor variations such as loops and bulges within a strongly conserved secondary structure of 6S RNAs could presumably be a response to changes in species-specific RNAP structure or temperature of growth of bacteria. The 6S RNA from *Cyanobacteria sp.* has a highly conserved

- 10 promoter (TAnnnT) region similar to *E. coli* and - 35 region (TTGnnn) of promoter similar to most *Enterobacter* species. Surprisingly, interspecies interaction of 6S RNA and RNAP has been observed leading to the conclusion that the 6S RNAs are orthologs. 6S RNAs from *Cyanobacteria sp.* could recognize RNAP from *E. coli* bind and serve as template for transcription (Rediger et al., 2012). *A. aeolicus* 6S RNA can bind and serve as pRNA transcription template to *B. subtilis* RNAP, diminishing the evolutionary gap of 6S RNA between thermophiles and mesophiles (Köhler et al., 2015). The ability to interact with σ^{70} subunit and the resemblance of the 6S RNA secondary structure to an open promoter complex instigates the theory that the 6S RNA may be involved in DNA mimicry (Wassarman et al., 2000, Barrick et al., 2005).

A 3.8 Å cryo-electron microscope (cryo-EM) structure of *E. coli* 6S RNA interacting with σ^{70} -RNA polymerase confirms the DNA mimicking nature of 6S RNA. In which, 6S RNA resembles a melted promoter DNA element eliminating the need to have a perfect - 10 and - 35 consensus promoter sequence (Chen et al., 2017, Wurm et al., 2010). RNA footprinting and p-Benzoyl-L-Phenylalanine (BPA) crosslinking studies could show that 6S RNA interacts with β , β' and σ subunits of housekeeping RNA polymerase. For the cryo-EM structure, 3DNA software predicted the base pairs in 6S RNA to be stacked in a pattern of alternating grooves; some grooves are narrow while others are wide. This pattern interestingly resembles the grooves of a B-form DNA (Chen et al., 2017). In the same publication, an alignment of 101 enterobacteriaceae 6S RNA sequences revealed a widely conserved secondary structure. Only a few but crucial nucleotide positions were identified to enable binding activity to RNA polymerase (nucleotide position G82) and interact with σ^{70} subunit (nucleotide position U135, G136) were identified. Nevertheless, 6S RNA prefers σ^{70} subunit to σ^S subunit exclusively due to negatively charged amino acids at two positions in the σ^{70} subunit (K593, H600) (Chen et al., 2017). In *E. coli*, Small-Angle X-ray Scattering (SAXS) data of 6S RNA suggests the existence of a stem loop structure in the central bulge region which may be important to orchestrate the release of 6S RNA from RNAP. Mutational analysis of the *E. coli* RNAP σ^{70} 4.2 domain revealed a severe loss of binding to the 6S RNA upon substitution of positive amino acid residues to negatively charged amino acid residues (R588A

and K597A). Therefore, 6S RNA competes with the DNA template for similar binding sites of the RNAP much exclusively at the 4.2 domain of σ^{70} subunit (Klocko et al., 2009).

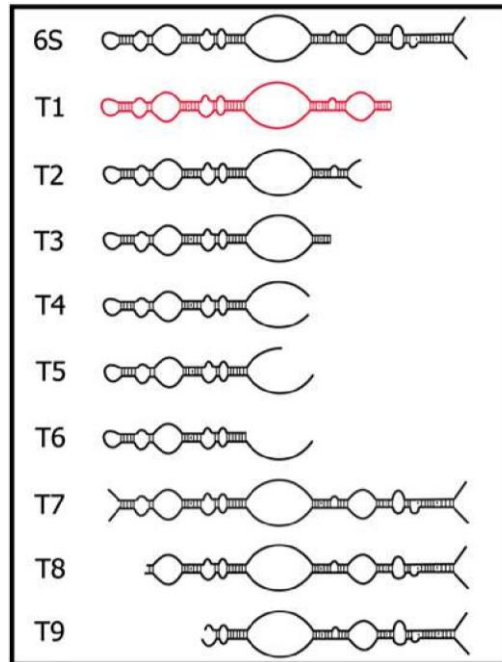


Figure 3: Truncated mutants of *E. coli* 6S RNA: 6S: the wild type, T1 - T5: mutants showed a steady decrease in binding affinity to RNAP. T6, T8 and T9: exhibited a complete loss of RNAP binding activity. T7: no loss in RNAP binding affinity. In summary, the 3' central bulge and -35 promoter mimic region of the internal stem were found to be crucial for recognition and binding to RNAP (Shephard et al., 2010).

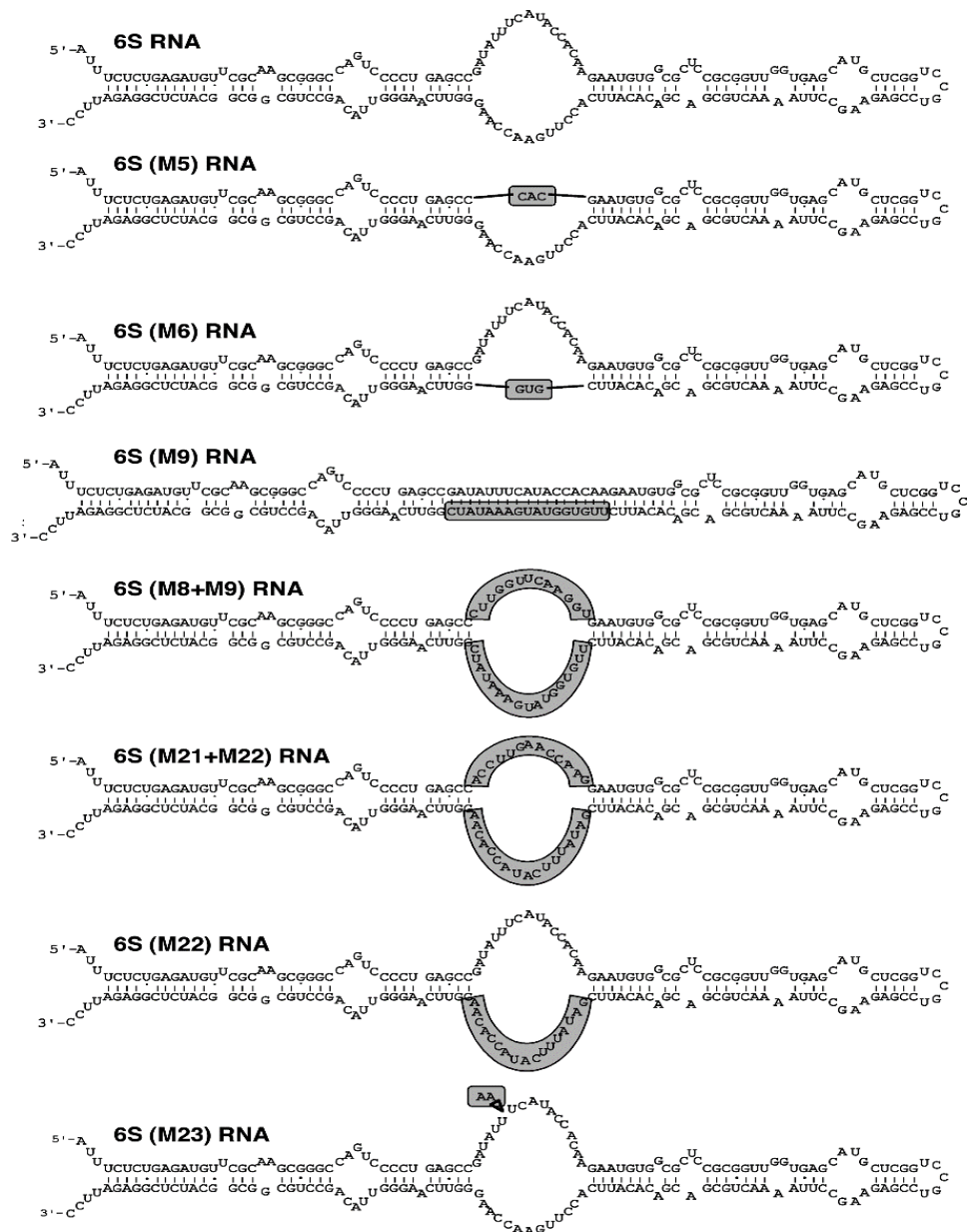


Figure 4: Secondary structure modifications of *E. coli* 6S RNA: 6S RNA: the wild type. 6S (M5) RNA and 6S (M6) RNA: 5' and 3' central bulge deletion mutants, no co-immuno precipitation with RNAP *in vivo*, exhibits destroyed binding activity to RNAP. 6S (M9) RNA: complete base pairing of the central bulge region, no binding to RNAP *in vitro*. 6S (M8+M9) RNA: altered sequences at 5' and 3' central bulge with conserved secondary structure, binds RNAP. 6S (M21+M22) RNA: sequence at 5' central bulge and 3' central bulge is flipped, reduced binding to RNAP *in vitro* (~ 50 %). 6S (M22) RNA: 3' central bulge carries the sequence of 5' central bulge, reduced binding to RNAP *in vitro* (~ 50 %). 6S (M23) RNA: increased number of nucleotides in 5' central bulge region, binds RNAP (~ 95 %) (Trotochaud et al., 2005, Picture source: Prof. Dr. Karen M Wassarman).

Some of the early mutational studies on the secondary structure of 6S RNA were done in *E. coli* by Wassarman et al. 2006 and Trotochaud et al. 2005. A mutant lacking most of the single stranded regions of the 6S RNA secondary structure was constructed and studied by *in vitro* gel assays. Surprisingly, this mutant can neither bind to σ^{70} -RNAP nor shut down conventional DNA-templated transcription. This indicates that an unpaired central bulge region is of prime importance. Iron-directed cleavage assays in the active site of RNAP successfully cleaved 6S RNA at base pair position U44, A43. To confirm the suspicion of possible transcription by RNAP using the 6S RNA as template, radioactive NTPs were supplied and small RNA transcripts were observed. These small RNA transcripts are termed as product RNAs (pRNA). When NTPs were added to radiolabeled 6S RNA, a new 6S RNA signal running higher than the free 6S RNA signal appeared. This new signal upon addition of rifampicin (transcription inhibitor) disappeared. Therefore, the pRNA was deduced to bind to the 6S RNA, inducing a structural rearrangement which results in the appearance of this signal (Wassarman et al., 2006). High throughput analysis of *E. coli* 6S RNA mutants featuring a diversity of 4×10^{12} sequences were examined vigorously for RNAP binding and pRNA-induced release from RNAP. Robust RNA candidates were found to have conserved - 10 and - 35 promoter mimic regions. Point mutations at the - 10 and - 35 region showed severe loss in the binding activity (Shepherd et al., 2010). A library of secondary structure modified mutants of *E. coli* 6S RNA was constructed and based on their 6S RNA release defect profile three classes were made. Class 1 mutants resulted in production of short pRNAs while class 2 mutants resulted in production of long pRNAs, attributable to strand slippage of σ^{70} -RNAP when reading the 6S RNA template. Strand slippage occurs when transcription mistakenly initiates at position - 1 or - 3 nt relative to transcription start site (TSS). Class 3 mutants produced long pRNAs and exhibited the intermediate core 6S RNA:RNAP complex. The class 1 mutant namely R9-33 was most extensively studied due to the ability to retain the 6S RNA: σ^{70} -RNAP complex (~ 85 %) even after addition of NTPs and $MgCl_2$. Overexpression of the R9-33 mutant in *E. coli* cells showed a reduced growth (OD_{600}) during exponential phase. Additional mutations were cloned onto the backbone of R9-33 mainly in the upstream region (- 35 promoter mimic), lower and upper 5' and 3' strand regions of the central bulge. A pRNA release defect phenotype arose due to

mutations in the upstream region (- 35 promoter mimic), the phenotype was explained by possible altered binding affinity that might favor interaction with 2.1 and 3.1 domain over the 4.2 domain of σ^{70} subunit. The pRNA release defect phenotype of R9-33 was explained by the destabilization of the 3' hairpin structure required by the 6S RNA to rearrange and release. However, a lot of functional inconsistencies upon testing the mutants were observed, for example, introducing mutations at the TSS resulted in a mutant with the reduced ability to perform pRNA synthesis. Surprisingly, mutating neighboring nucleotides of the TSS to this mutant recovered the pRNA synthesis. Additionally, when mutations in the top strand of central bulge to this previously mentioned mutant was introduced, a totally new pRNA release defective phenotype emerged. A poor understanding of RNA structural dynamics and enzyme kinetics made it difficult to explain the phenotype of 6S RNA variants with mutations in the CB in particular (Oviedo Ovando et al., 2014).

Structural analysis of *A. aeolicus* 6S RNA (*Aae* 6S RNA) by Köhler et al., (2015) revealed a fair correspondence between secondary structure prediction by RNA fold on basis of minimum free energy and enzymatic/chemical (RNase T1, RNase V1 and Pb^{2+}) probing assay. In this study, a 132 nt truncated *Aae* 6S RNA was constructed by deletion of 15 nucleotides at the terminal stem region from both 5' and 3' ends compared to wild type *Aae* 6S RNA (163 nt). Another 85 nt truncated *Aae* 6S RNA was constructed through complete deletion of region P4 deletion and extreme truncation in P1 region (see Figure 5, sub-section C for details of the *Aae* 6S RNA secondary structure). Although both truncated mutants in both structural probing experiments and NMR data failed to prove the existence of a 3' hairpin, formation of Central Bulge Collapse helix (CBC) was observed in case of 132 nt truncated mutant. Moreover, *A. aeolicus* 6S RNA can act as a template for pRNAs from two different orientations on the 5' and 3' Central Bulge (CB) respectively. RNA-Seq data indicated pRNA transcription from 3' CB to be rather inefficient (9 fold less than 5' CB). To check for any biological significance, artificial pRNAs complementary to 3' CB were used for strand invasion and checked for dissociation of 6S RNA from RNAP. No dissociation of 6S RNA:RNAP complex was observed further discrediting the biological significance of 3' CB initiated pRNAs. NMR data showed that the *A. aeolicus*

6S RNA secondary structure is folded based on traditional *Watson and Crick* base pairing (A·U, G·C) and Wobble base pairs (G·U) (Köhler et al., 2015).

1.2.4 Mechanistic aspects of 6S RNAs

Regulatory systems cushion single celled organisms against turbulent environmental changes stabilizing the genomic and proteomic construct of the organism. They exist due to selective pressure from evolution; some examples are lytic/lysogenic cycles in bacteriophages, inducible/repressible metabolite systems in bacteria. It is not uncommon for ncRNAs to act as regulators for transcription and to play a role in stress situation adaptation. In mouse, B2 RNA (a type of ncRNA) is produced upon heat shock and inhibits RNA polymerase II from active transcription. Likewise in bacteria, 6S RNA can act as a template to σ^A -RNAP and result in production of short transcripts called product RNAs (pRNAs) in a form of RNA-templated RNA polymerization reaction (Gildehaus et al., 2007). 6S RNA is a trans-encoded ncRNA with a global impact on the cellular transcriptomic environment whereas pRNAs are cis-encoded and interact locally with the 6S RNA template imitating a negative feedback inhibition model. The synthesis of pRNAs aid in the release of 6S RNA from RNA polymerase. (Wehner et al., 2014). To obtain a homogenous cryo-EM structure (Chen et al., 2017), the 6S RNA sequence had to be changed in the P2 region (Fig 2A.) to avoid any formation of the iso-energetic structure that is induced and stabilized by pRNA synthesis. pRNA synthesis of 10 - 14-mers have been observed in *E. coli*, *B. subtilis*, *H. pylori* and *Synechocystis sp* whereas longer pRNAs ~ 30-mer were observed in *Cyanobacteria*. Interestingly, both the 5' and 3' central bulges in species such as *H. pylori*, *L. monocytogenes*, *B. subtilis*, *A. aeolicus* and *E. coli* can act as pRNA templates although 5' central bulge transcripts outweigh 3' central bulge transcripts (Wehner et al., 2014, Köhler et al., 2015). Such 3' central bulge initiated pRNA transcripts were not found *in vivo* upon screening of differential RNA-Seq (dRNA-Seq) data (Beckmann et al., 2011). In *B. subtilis*, RNA-Seq data and pRNA primer extension assays were used to detect outbursts of pRNA transcripts for the first time *in vivo*. Such experiments showed us that the increase in pRNAs correlates with the expression profile of 6S RNAs. The initiating nucleotide for pRNA transcription plays a major role in the efficiency of

the synthesis. The pRNA production rate of 6S-2 RNA with a starting nucleotide “A” is inefficient in comparison to 6S-1 RNA with a starting nucleotide “G”. Interestingly in *E. coli*, pRNA transcription initiation is not affected by the starting nucleotide. Promoter positions - 1, + 1 and + 2 of the pRNA transcription start site also play a profound role in the initiation process (Hoch et al., 2016, Cabrera-Ostertag et al., 2013). In *S. meliloti* and *B. japonicum*, the pRNA initiation nucleotide is a “C”, which is a highly inefficient way to produce pRNAs. Although pRNAs are such short transcripts (~ 20-mer), oddly enough many of these pRNAs manage to carry homo-oligomeric nucleotide stretches “CCCCGGGG” in *Rhizobia*, “GGGG” in *E. coli*, “CCCC” in *A. aeolicus*, “AAAA” in *B. subtilis* and “AAAAAA” in *Synechocystis* sp. The purpose of these homo-oligomeric nucleotide stretches is unknown (Burenina et al., 2020). The composition of the pRNA and the stability of 6S RNA secondary structure may play a role in rearrangement and release of RNA polymerase. The more G and C residues are present in the pRNA sequence, the shorter pRNAs can be for effective triggering of the 6S RNA rearrangement. In *B. subtilis*, 6S-1 pRNA has a higher G-C content than 6S-2 pRNA and thus only needs a length of 14 nt to trigger rearrangement while 6S-2 pRNA needs ~ 20 nt for the same purpose. Crucial regions on the secondary structure backbone of 6S RNA namely 3' central bulge and region P2 play a role in stability during rearrangement and might contribute to longer pRNAs (Hoch et al., 2016). In *E. coli*, the pRNA:6S RNA re-arrangement complex is extremely stable ($\Delta G = -40.4$ kcal/mol) even partly surviving harsh 8 M denaturing urea conditions (Wurm et al., 2010). In *E. coli*, 14-mer pRNA invasion is responsible for de-stabilization of region P2, resulting in a hairpin and release of 6S RNA from RNAP. The σ^{70} subunit of RNAP binds to the - 35 promoter mimic region of 6S RNA while the hood domain of β and β' subunits binds to - 10 promoter region mimic region (central bulge) and region P2 of 6S RNA. pRNA invasion at the central bulge leads to the formation of a release hairpin and results in a “scrunch”. The deletion of the release hairpin gives rise to longer pRNAs as now more nucleotides were required to create physical tension in the absence of the hairpin (Panchapakesan et al., 2012). In traditional transcription initiation, transcripts produced by the RNAP leave via the exit tunnel of RNAP. The goal is to effectively displace the 3.2 domain of σ^{70} subunit by weakening the interaction of 4 domain of σ^{70} subunit to the β flap and resulting in σ^{70} subunit dissociation.

However, pRNAs do not use the exit tunnel, instead complementarily basepair with 6S RNA to form ~ 1.3 helical turns in the case of a 14-mer; the resulting structure is too large to fit in the RNAP active complex and presumably clashes with the lid or β flap and induces σ^{70} subunit dissociation (Steuten et al., 2012). Iron chelated Bromoacetamidobenzyl-EDTA (FeBABE) induced cleavage analysis shows that almost all sub-domains of the *E. coli* σ^{70} subunit like 2.1, 2.3, 3.1, 3.2 and 4.2 are in vicinity to 6S RNA (Steuten et al., 2013). Additionally, gel assays could show that the *E. coli* pRNA:6S RNA rearranged complex does not bind to RNAP (Steuten et al., 2012). This fact excludes the possibility of any other side function of the pRNA:6S RNA rearranged complex on the RNAP.

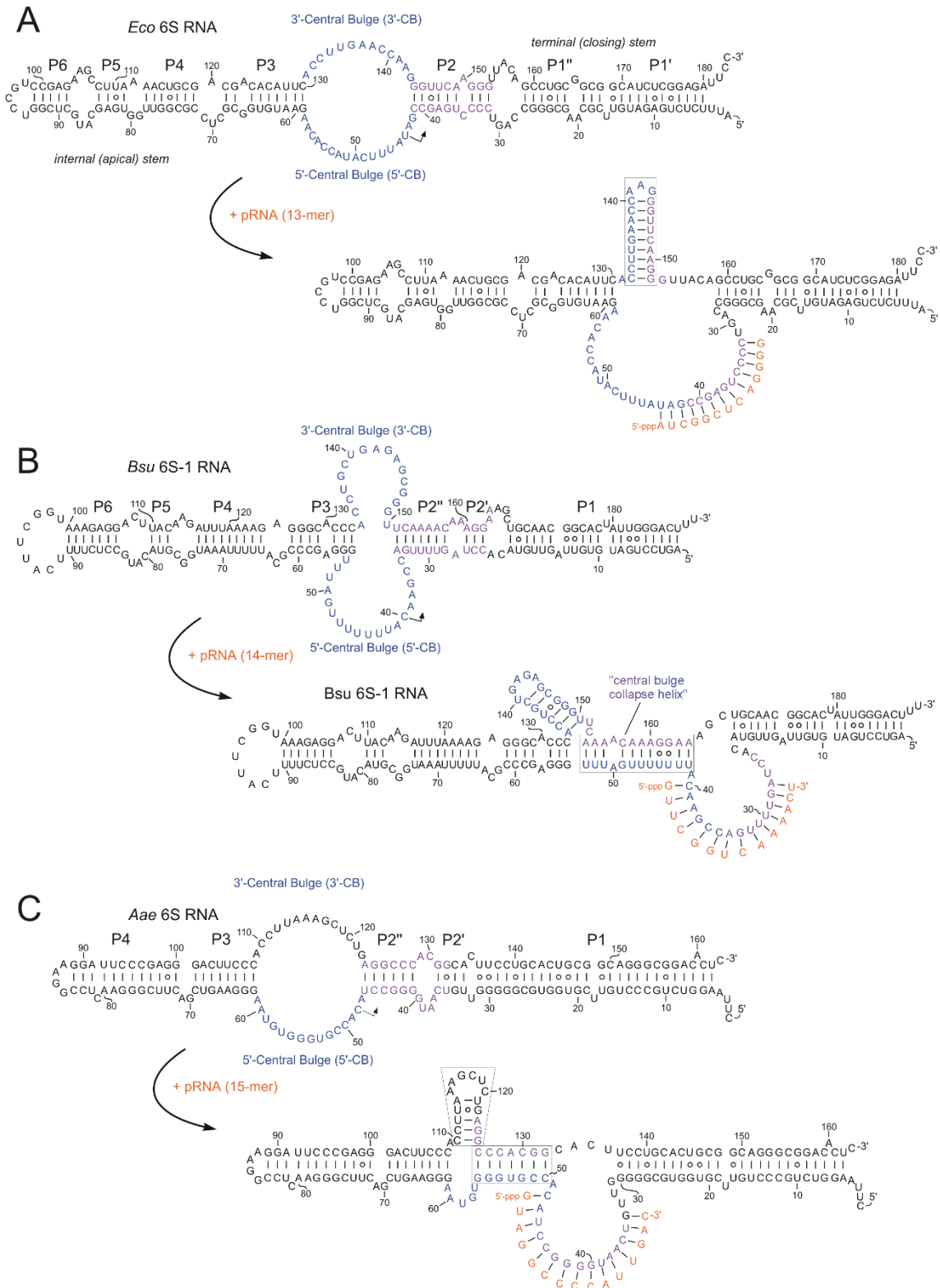


Figure 5: Structural rearrangement of 6S RNA occurs upon pRNA binding: The formation of the pRNA:6S RNA rearranged structure consequently releases itself from the RNA polymerase however the specificity of the process may vary depending on the species. (A) Upon 13-mer pRNA binding to *E. coli* 6S RNA, the upper strand of region P2 uncoils to base pair with 3' Central Bulge (CB) resulting in a stem loop to form the pRNA:6S RNA complex. (B) Upon 14-mer pRNA binding to *B. subtilis* 6S-1 RNA, the helix P2 uncoils but here the lower strand of the P2 region

base pairs with the 5' CB to give rise to a new double stranded region called the Central Bulge Collapse helix (CBC). (C) Upon 15-mer pRNA binding to *A. aeolicus* 6S RNA, the helix P2 uncoils and the upper strand of the helix P2 base pairs with 5' CB to give rise to a new double-stranded region while simultaneously allowing base-pairing with the 3' CB into a small stem-loop. The formation of the pRNA:6S RNA rearranged structure in *A. aeolicus* appears to be a hybrid between the *E. coli* and *B. subtilis* rearrangement model (Steuten et al., 2014).

1.2.5 6S RNAs in *Bacillus subtilis*

There are two types of 6S RNAs in *B. subtilis* namely 6S-1 (*bsrA*) and 6S-2 (*bsrB*) RNA. 6S-2 RNA is predominantly transcribed in mid-exponential phase with a gradual decrease towards the stationary phase while 6S-1 RNA levels peak towards the stationary phase (Barrick et al., 2005, Beckmann et al., 2011). *In vitro* gel assays have established that both 6S RNAs conform to the classical hallmarks of 6S RNAs. Implying, 6S-1 and 6S-2 RNA have very similar features with minor mechanistic differences. *In vivo*, pRNA synthesis was found to be less efficient on 6S-2 RNA compared to 6S-1 RNA as template (Hoch et al., 2016). This deviance is explained by the organism's bias to perform inefficient transcription initiation based on the starting nucleotide. The starting nucleotide for pRNA transcription of 6S-2 RNA is "G", which is much less favored by the *B. subtilis* RNAP in comparison to "A" as the starting nucleotide of 6S-1 RNA (Burenina et al., 2014, Cavanagh et al., 2013).

6S-1 RNA derived pRNAs have been detected *in vivo* using the technique differential high-throughput RNA-Seq. *In vitro* assays indicate that 6S-1 RNA derived pRNAs are normally of length ~ 5-mer, 8-mer, 9-mer and 14-mer. pRNAs with a length of ~14 nt can form stable duplexes with 6S-1 RNA to trigger its rearrangement and release from RNAP. Shorter pRNAs, such as 8-mers, rapidly dissociate from 6S-1 RNA and thus fail to persistently rearrange the 6S-1 RNA structure. However, isosequential pLNA 8-mers, with all RNA residues replaced with locked nucleic acid (LNA) residues, form duplexes stable and long-lived enough to persistently rearrange the structure of 6S-1 RNA. This clearly demonstrated that 6S-1 RNA:pRNA duplex stability plays an important role in the rearrangement of 6S-1 RNA and its release from RNAP (Beckmann et al., 2012).

In *E. coli*, a 6S RNA variant with a point mutation in the -10 like region (mutant C132A) exhibited impaired 6S RNA release from RNAP (Shephard et al., 2010). The defect could be assigned to a destabilization of the hairpin forming in the 3'-CB upon pRNA synthesis and required for release of 6S RNA from RNAP. In light of this data, the 3'-CB hairpin structure found in the free conformer of *B. subtilis* 6S-1 RNA was destabilized by three-point mutations. This mutant *B. subtilis* 6S-1 RNA showed two to three-fold reduced affinity to σ^A -RNAP and a smeary pRNA transcription profile indicating a loose/flexible secondary structure. The 3' central bulge hairpin structure was therefore deemed accessory to the functionality of the 6S RNA cycle and aids only in the optimization of the interaction kinetics (Beckmann et al., 2012). However, when it comes to analyzing the interaction kinetics of 6S RNA, σ^A -RNAP and pRNA, some features remain unexplained. Such as, *in vitro* transcription assays used to study 6S RNA rearranged complexes, the signal corresponding to 6S RNA:RNAP complex weakens but never disappears completely. This sub-population of inert 6S RNA:RNAP complex either produces pRNA but would not rearrange into the pRNA:6S RNA complex or is unable to synthesize any pRNAs in the first place. So far, no actual explanation is possible. 6S RNA in some aspects resembles a riboswitch, taking a free and loose form until ligand binding (RNAP or pRNA) and subsequently undergoing a conformational change into a rigid structure (pRNA:6S RNA rearranged complex), this aspect could be investigated further. Moreover, there is the possibility of a moonlight function of pRNAs other than binding back to 6S RNA but this, likewise needs more investigation (Beckmann et al., 2012).

1.2.6 Phenotypic aspects of 6S RNA knockouts

Many small RNAs play a role in stress management, for example those involved in utilization of carbon substrates (Spot42, CsrB RNA), iron availability (RyhB RNA), detection of free radical species (OxyS RNA), response to low temperature (DsrA RNA) and to osmotic pressure changes (RprA and DsrA RNA) (Trotochaud et al., 2004). The possibility of 6S RNAs to be involved in stress and growth adaptation was first proposed by Neusser et al. (2008). The *E. coli* 6S gene has two promoter regions namely P1 (σ^{70} binding region) and P2 (σ^{70} and σ^S binding region). The transcriptional efficacy of these two promoter sites in presence of

proteins that regulate growth phase adaptation and stress responses such as FIS, H-NS, LRP and StpA was tested. The presence of H-NS, StpA and LRP inhibited *ssrS* transcription (6S RNA gene) indicating a role in stress situations. Moreover, the P1 promoter shows a G-C rich discriminator region that resembles gene promoters that are sensitive to the stringent response. This aspect was further investigated and found to be not true (Neusser et al., 2008). In *B. thuringiensis*, deletion of 6S-1 RNA resulted in an increase in spore and parasporal formation. This phenotype supports the stress regulator function of 6S-1 RNA (Li et al., 2020). Although 6S RNA gene knockout mutant of *R. sphaeroides* showed no phenotype under stress conditions, the mutant exhibited reduced growth under high salt conditions. Due to the genetic proximity in the genome, the function of 6S RNA in *R. sphaeroides* was linked to expression of *sspA* gene that encodes a salt stress responsive membrane protein (Elkina et al., 2017). The deletion of 6S RNA in the soil bacterium *Streptomyces coelicolor* interestingly offers strong phenotypes such as reduced growth and reduced antibiotic production. The researchers attribute the role of 6S RNA to stress response, propose the 6S RNA to be a critical messenger in an adaptation mechanism and the possibility of 6S RNA to act as an interaction partner of ppGpp (Mikulik et al., 2014). 6S RNA has found an economic appeal in the industrial fermentation strain *Clostridium acetobutylicum*. Through plasmid overexpression of 6S RNA in *Clostridium acetobutylicum*, a higher tolerance to butanol presence in the medium and a higher production of butanol during fermentation processes could be observed (Jones et al., 2016). During colonization of host cells, pathogens encounter hostile conditions which is similar to a stress situation where quick reprogramming of cellular networks is required to increase pathogen survivability. qRT-PCR studies on total RNA extracts of *R. conorii* (arthropod pathogen) showed increased expression levels of 6S RNA during host infection, indicative of a role of 6S RNA in virulence (Narra HP et al., 2020). *B. burgdorferi* is a pathogenic bacterium responsible for Lyme disease, whose 6S RNA (Bb6S RNA) is upregulated during host infection and aided the persistence of bacteria in host body (Drecktrah et al., 2020). 6S RNA knockout mutant from *Legionella pneumophila* (a gram-negative pathogen responsible for Legionnaires' disease) was found to disrupt cell division of the pathogen through upregulation of genes involved in general stress response, nutrient intake and type IVB secretion

systems. A computational screening followed by a microarray analysis quickly identified 6S RNA as a critical sRNA in the pathogen (Faucher et al., 2010). Knockout of the 6S RNA gene in the enteric pathogen *Salmonella typhimurium* did not lead to a phenotype under nutrient rich conditions however northern blot studies of RNA extracted post acid stress (~ pH 3.0) showed an upregulation of 6S RNA. Furthermore, *in vivo* and qRT-PCR studies revealed that 6S RNA upregulates genes of the *Salmonella* Pathogenicity Island 1 (SPI-1) aiding in mammalian cell invasion and overall virulence (Ren et al., 2017). RNA-Seq and qRT-PCR analysis of *Yersinia pestis* during nutrient deprived conditions and during infection of host cells from organs such as brain, heart, lung and spleen showed an increased level in production of 6S RNA. The sRNA was detected even under *in vivo* conditions where general sRNA levels drop below detectable range (Yan et al., 2013). Biofilm cells of the opportunistic human pathogen *Burkholderia cenocepacia* J2315 were taken and treated with hydrogen peroxide. These cells showed a significant upregulation in transcription of 6S RNA as a form of stress response against attack by Reactive Oxygen Species (ROS) (Peeters et al., 2010). 6S RNA was newly discovered and profiled in *Coxiella burnetti*. RNA-Seq data revealed a higher transcription of 6S RNA when the bacterium was cultured in host cells in comparison to host free conditions. The role of 6S RNA was speculated to aid in the survival of *Coxiella burnetti* during propagation in intra-cellular host cell conditions (Warrier et al., 2014).

The involvement of 6S RNA in the utilisation of alternative sigma factors with specialised function during nutrient-deprived stress conditions was investigated. In this context, RNA-Seq data from an *E. coli* 6S RNA gene knockout mutant was obtained during different growth phases. Additionally, RNA-Seq data from another mutant lacking the *Rsd* gene was also collected, and the data sets were compared. Overall, 1780 genes were found to be differentially expressed, mathematical modeling revealed that 6S RNA could increase the levels of Rsd protein and in turn increases transcription of σ^{38} - (alternative sigma factor) related genes (Lal et al., 2018). 6S RNA gene knockout mutant of *Synechocystis sp.* PCC 6803 exhibited reduced photosynthetic activity upon relief from stress condition. 6S RNA's role in aiding σ^A -RNA polymerase (housekeeping sigma factor) formation over association with group 2 sigma factors (alternative sigma

factors such as σ^B , σ^C , σ^E) was proposed to be the reason (Heilmann et al., 2017). During long term survival, a subpopulation of the bacterial culture spontaneously mutates to give rise to Growth Advantage in Stationary Phase (GASP) phenotypic cells in order to ensure cellular fitness. Both the wild-type and 6S RNA gene knockout mutant showed no difficulty in generating the GASP phenotypic cells. This empirical evidence discredits the theory that 6S RNA contributes to subpopulation formation and promotes long-term survivability (Trotochaud et al., 2004). Under harsh pH conditions, β -Galactosidase assay in *E. coli* 6S RNA gene knockout mutant showed increased expression levels of σ^{70} -dependent *pspF* gene and increased cell growth. *pspF* gene cluster increases the proton motive force of the cell and sends the cell into a “carpe diem” mode of survival, where cells consume resources uncontrollably. Additionally, the *pspF* gene cluster is speculated to be involved in protein secretion, motility and virulence. In conclusion, the 6S RNA was speculated to influence a much larger regulatory network than the *pspF* gene cluster (Trotochaud et al., 2016).

In some studies, promoters with an extended -10 element and a weak -35 element were found to be selectively down regulated in presence of 6S RNA. 6S RNA gene knocked out in model organism *Escherichia coli* demonstrated a decrease in long term survival (~ 3 weeks post inoculation). Around 106 promoters were studied and 6S RNA was shown to prefer an extended -10 region (containing TGn sequence preceding -10 hexamer) of promoter, which alludes to a theory of 6S RNA occupying the σ^{70} -RNA polymerase as a form of regulation until a strong -35 region competitor could displace out the 6S RNA (Trotochaud et al., 2004). This theory is in line with a study where β -Galactosidase assay displayed genes with extended -10 promoter and weak -35 element to be strongly downregulated by 6S RNA (Cavanagh et al., 2008).

The relationship of 6S RNA to stringent response has been studied in *E. coli* to add an additional layer of regulation. β -Galactosidase assay showed an up-regulation of *relA* mRNA in the absence of 6S RNA. The RelA (ppGpp synthase I) protein up-regulates the production of stringent response regulatory nucleotide (alarmone) ppGpp upon entry into stationary phase (Cavanagh et al., 2010). During exponential phase, genome wide microarray analysis

supplemented by RNA primer extension assay could show that 245 genes, primarily coding transcriptional regulators and transport proteins were altered in a 6S RNA gene knockout mutant. Upon entry into stationary phase, 273 genes were found differentially expressed; most of which specialize in purine metabolism and constitute the translation machinery. The gene profile of the translation machinery encompasses ~ 50 genes coding for ribosomal proteins, transcriptional subunits (*rpoA*, *rpoB* and *rpoC*) and factors involved in translation elongation (*tufA*, *fusA*). The study revealed that 6S RNA gene knockout mutant suffers a loss in translational apparatus and a surge in ppGpp concentration upon entry into stationary phase. The impact of 6S RNA on stringent response was revealed by monitoring levels of *spoT* gene expression (coding for a bifunctional hydrolase and synthase of ppGpp) and although 6S RNA does not directly affect *spoT* levels, the influence of 6S RNA on *spoT* could be a side effect of the downregulation of general purine metabolism (Neusser et al., 2010).

So far, two phenotypic knockout studies of 6S RNA in *B. subtilis* have been performed. 6S-1 RNA gene knockout mutant in *Bacillus subtilis* strain 168 caused an early sporulation phenotype resulting in upregulation of sporulation related genes such as *spoOA*, *spoIIIE* and *kinA* while 6S-2 RNA gene knockout mutant did not show any phenotype. It was speculated that the two RNAs although similar in design may contribute to very different physiological responses. Finally, it was concluded that the main function of 6S-1 RNA is to aid in nutrient resource management (Cavanagh et al., 2013). Knockout studies of 6S-1, 6S-2 and both 6S RNAs of *Bacillus subtilis* PY79 lab strain derivative found two relevant phenotypes. Decreased cell density towards the stationary phase in case of the 6S-1 and 6S- 1 & 2 RNA knockout strains, as well as a faster outgrowth under high pH stress (~ 9.3) was particularly pronounced for the double knockout mutant (Hoch et al., 2015). However, both these studies were done on lab strain derivatives of *B. subtilis* and it could be worth asking the question if they were good models to work with.

1.3 *Bacillus subtilis*

The Gram-positive, spore-forming bacterium *Bacillus subtilis* (*B. subtilis*), belongs to the phylum Firmicutes and is a common bacterial model organism especially for studies on regulation of gene expression. *B. subtilis* is a master adapter to environmental changes with three major triggers of adaptability, i.e. when nutrients are plenty, when nutrient are scarce and when the cell density reaches maximum capacity. A bounty of new phenotypic features appears upon conditions of adversity such as motility: the ability to generate flagella and navigate under pursuit of better nutrition, sporulation: the ability to metabolically shut down and await better conditions to survive and competence: the ability to uptake foreign genetic material to enhance survivability. Interesting to note is the social nature of *B. subtilis* which enables the cells to act in multitudes and perform phenomena like swarming and biofilm formation. All of this rapid response could be possible due to an array of internal molecular networks such as two component systems, multiple alternative sigma factors, regulatory RNA networks, phosphorylation cascades and targeted proteolysis, most of these factors are still of great research interest. Due to both the economic and research incentive to develop this bacterium for efficient results, several strains have been cultured through the years. With a poor understanding of its genetic heritage, subtle changes in proteomic, transcriptomic and metabolomic aspects of the bacterial strains went unnoticed and accumulated until the bacterium class was called “lab strains”. As an undesirable side effect, these lab strain models were no longer optimal to study regulatory networks that rely on the genomic intactness of the primitive ancestral strains they once were. As a prokaryote, *B. subtilis* not always but more likely relies on proteins and manipulation thereof to accomplish tasks. This fact provides researchers motivation to study the single most important protein required to initiate the central dogma of life, the RNA polymerase (Graumann et al., 2017).

1.3.1 RNA polymerase

The *B. subtilis* RNA polymerase (RNAP) is a highly conserved multi subunit enzyme required for transcription of DNA template into RNA. The *B. subtilis* core RNA polymerase with the subunit composition $\beta\beta'(\alpha)_2\delta\epsilon\omega$ (~ 350 kDa) predominantly associates with the housekeeping sigma factor σ^A for recognition of housekeeping DNA promoters during exponential growth phase. The *B. subtilis* RNAP upon association of the housekeeping sigma factor σ^A , is stoichiometrically denoted as $\beta\beta'(\alpha)_2\delta\epsilon\omega\sigma^A$ and is termed as “RNAP holoenzyme”. The σ^{70} subunit (housekeeping sigma factor) of RNAP in the model organism *E. coli* has several regions that interact exclusively with components of the promoter DNA. The homologous σ^{70} subunit is composed of several domains. Domain 1.2 of σ^{70} subunit interacts with the discriminator region element (discriminator region exists between - 10 element and transcription start site of DNA), domain 2 interacts with - 10 element, domain 3 interacts with extended - 10 element of promoter DNA and domain 4 interacts with - 35 region. The 4.2 domain of σ^{70} subunit has a helix-turn-helix motif that recognizes - 35 element of DNA template. This motif is loaded with positively charged amino acids inducing a charge-charge interaction with the negatively charged phosphate backbone of DNA. The sigma factor is therefore an important subunit of RNAP that aids in the recognition of DNA promoter region and in transcription initiation (Klocko AD et al., 2009). Transcription initiation by RNAP in bacteria can be summarized into the three critical steps i.e., melting of the promoter DNA from closed double stranded complex to open complex, isomerization of RNAP to the open complex and once the template strand is delivered into the active site of RNAP, transcription of abortive transcripts (~ 2 - 16-mer) begins. The constant cycling of abortive transcripts is made possible by a scrunching mechanism where the downstream DNA from the Transcription Start Site (TSS) is being pulled into the active site of RNAP forming a single stranded loop. Upon sudden release of the abortive transcript, the tight hold of the RNAP over the squeezed downstream DNA is released and the downstream DNA recoils into a relaxed original state, the scrunch mechanism restarts. The recoiling scrunch process is stochastic and can shift the TSS by position -1 or -3 bp upstream. The cycle of producing abortive transcripts continues until transitioning into Ternary Elongation Complex (TEC).

The TEC is an intermediate state composed of RNAP, DNA template and RNA transcript. The TEC complex is comparatively stable and once formed gives rise to longer transcripts ending the transcription initiation process (Beckmann et al., 2012). Transcription profile of RNAP can be dynamically varied depending on association with ~ 20 alternative or phage sigma factors, numerous transcription regulators and cofactors. As of March 2021, the *Subtiwiki* database lists the following proteins as interaction factors for the *B. subtilis* RNAP as represented in Table 1 (Zhu et al., 2018).

Table 1: Mapped interaction partners of RNA polymerase subunits

RNAP subunit	Subunit designation	Molecular weight (kDa)	Interacting protein partners
RpoB	Beta (β)	133.38	RpoC, RpoA, SigL, SigH, SigA, SigB, SigD, YlaC, SigF, SigM, SigW, SigV, SigE, SigG, SigI, SigX, Xpf, SigK, SigY, SigZ, NusA, CshA, PcrA, SpX, MgsR, RpoE, Btr, RpoY, YlyA, GreA, SigO, Mfd
RpoC	Beta prime (β')	133.92	RpoB, RpoA, SigL, SigH, SigA, SigB, SigD, YlaC, SigF, SigM, SigW, SigV, SigE, SigG, SigI, SigX, Xpf, SigK, SigY, SigZ, RpoE, RpoY, YloH, NusA, GreA, CshA, PcrA, SpX, MgsR, Btr, YlyA, NusG, RsoA, SigKC, Fin
RpoA	Alpha (α)	34.64	RpoA, RpoB, RpoC, SigL, SpX, NusA, GreA, CshA, PcrA, MgsR, Btr, SigA, YlyA, RpoY, CcpN, CcpA, CodY, ComA, YopJ
RpoE	Delta (δ)	20.25	RpoB, RpoC, GreA, PcrA, CshA, RpoY, MgsR, NusA, YlyA
RpoY	Epsilon (ϵ)	8.12	RpoB, RpoC, RpoE, SigA, NusA, GreA, CshA, PcrA, SpX, MgsR, Btr, YlyA, RpoA
RpoZ/YloH	Omega (ω)	7.62	RpoC
RpoD	Sigma A (σ^A)	42.80	RpoB, RpoC, BsrA, BsrB, RpoA, MgsR, GreA, RpoY, CshA, YlyA, Btr, PcrA, SpX, NusA, ComA, Spo0A

1.3.2 Stress response and adaptation in *B. subtilis*

B. subtilis is adept at surviving harsh conditions by forming multicellular stress responses based on social behavior. Formation of biofilm, pellicles, fruiting bodies, the ability to exhibit motility, form spores, secrete surfactin and even exhibit cannibalistic tendencies have been documented as multicellular stress responses in wild-type *B. subtilis*. Motility has been categorized into swimming, swarming and sliding. An integral aspect of motility is the use of a proteinaceous nanomachine namely the flagella. The flagella is roughly made of three parts (1) basal body: a ring structure deeply seated in the cellular membrane, (2) cytoplasmic basal body: consists of C-ring and C-rod, C-ring aids in flagellar rotation whereas C-rod regulates protein export, (3) hook and filament: a type III secretion system which aids in the formation of a universal hook joint and adds proteins to the growing end of a flagella. The molecular basis of flagella formation is under the influence of the *fla/che* operon, second flagellar cluster genes and the *eps* operon. The most important gene of the *fla/che* operon is *sigD*, this gene encodes for the alternative sigma factor σ^D which in turn activates the secondary flagella gene cluster. Swimming as a motility phenomenon occurs on an individual basis in a liquid medium. The cells can exhibit 3-dimensional movement driven by aerotaxis, chemotaxis or phototaxis, in patterns such as tumbles and runs. Swimming is flagella-dependent. *Bacillus subtilis* is hyperflagellated by nature, with flagella protruding pervasively all over the microbial cell body. When the flagella unanimously rotates counter clockwise, the bacteria moves along a smooth forward trajectory called run and when the flagella system is confused likely due to a sensory trigger, then part of the flagella rotates counter clock wise while the others clock wise, then the bacteria appears misoriented fumbling around in the same position called tumble. Evolutionarily, it is advantageous that motility is sequestered in a sub-population. The ability to form sub-populations is beneficial due to the reduced adaptation time required during stress without compromising the current metabolic opportunity for the colony. Swarming is a flagella-dependent, multicellular surface movement. In bacteria, it can be observed by spotting cells onto 0.5 - 0.7 % agar plates and by subsequently observing growth in two forms, a localized spot during initial swarming stages consisting of σ^D inactive cells and outward growing rings of swarming cells which

are σ^D transcriptionally active. Surfactin is an amphipathic lipopeptide secreted by *B. subtilis* to reduce the surface tension and aid in swarming. Other factors that influence swarming are cell length, flagellar number and proteins such as SwrB and Elongation Factor P (EF-P). Sliding is a passive, flagellar independent form of movement, enhanced by Extracellular Polysaccharide (EPS) production. The cells literally slide over the substrate due to lack of friction however it is surfactin dependent. Interestingly, swarming movement is always inversely correlated to biofilm formation. The biofilm matrix component BslA coats the biofilm and is a potent hydrophobin that increases surface tension. The EpsA protein aids in cell cohesion and also forms the matrix component of biofilm. These matrix components co-ordinate the spatial organization and also inadvertently advocate sliding movement. Meanwhile, nutrient starvation conditions such as carbon, nitrogen and phosphorous depletion trigger spore formation. Spores are metabolically dormant cells that persist against heat, radiation, oxidizing agents and enzyme exposure. Speculated to stay alive for 100 years or even longer, spores are formed through a complex sporulation process that involves more than 600 genes. Although σ^A -dependent RNAP transcription primarily dominates the sporulation process, alternative sigma factors are also extensively involved. Sporulation is the process of developing a forespore inside a mother cell, which upon maturation is released following the death of the mother cell. Alternative sigma factors like σ^F and σ^G are involved in transcription of the forespore-specific genes and σ^E and σ^K are responsible for mother cell-specific genes. Sporulation sigma factors are somehow organised into a cascade system of activation of σ^H , followed by σ^F , then σ^E , subsequently σ^G and finally σ^K is spured to action. Existence of such tightly regulated molecular networks illustrate how complex but crucial the stress response system in *B. subtilis* can be (Graumann et al., 2017).

1.3.3 Molecular basis for biofilm formation in *B. subtilis*

One effective form of stress situation adaptation in *B. subtilis* is biofilm formation. Biofilm formation in *B. subtilis* is facilitated on a molecular basis through the expression of the *eps* gene and *tapA-sipW-tasA* operon. RemA is a transcriptional activator of the aforementioned operons, which binds upstream to the promoter thereby contributing to overall biofilm formation. SinR is the functional counterpart of RemA serving as a transcriptional inhibitor of the *eps* gene and the *tapA-sipW-tasA* operon. The *eps* gene codes for synthesis of extracellular polysaccharide which serves as a skeleton for the biofilm in which non-motile cells are enclosed. TasA is an amyloid protein which forms a major component of the biofilm matrix, SipW and TapA aid in the processing and anchoring of TasA. Activation of *eps* increases the expression of EpsE protein which in turn downregulates *fliG* gene required for motility. Downregulation of motility genes due to upregulation of biofilm genes is generally observed in *B. subtilis*, in order for the cells to form nucleation sites and trigger biofilm formation. Although RemA has no predestined DNA binding motif, at least in *in vitro* assays, RemA shows preference in transcription activation of P_{eps} and P_{tapA} promoters. The mechanism of transcription activation is mysterious as RemA has no DNA interacting helix-turn-helix motif. DNase I footprinting studies revealed that RemA binds to a weakly conserved AGNAAAA sequence that is enhanced through co-operative binding, each sequence stretch separated by 3 bp. Bending of the DNA occurs upon binding to RemA which exposes the DNA grooves and becomes vulnerable to DNase I digestion. RemA chooses the face of the DNA to bind and bend, thereby exposing a part of the DNA bearing the promoter to RNAP for transcription (Winkelman et al., 2013, Graumann et al., 2017).

1.4 Aim of the projects

1.4.1 Impact of secondary structure modifications on 6S-1 RNA and σ^A -RNAP interaction kinetics

product RNAs (pRNAs) have been detected *in vitro* from *E. coli*, *B. subtilis* and *R. sphaeroides* 6S RNAs (Burenina et al., 2020). This provides us incentive to analyze the impact of pRNA length on 6S RNA rearrangement kinetics in these organisms. pRNA upon binding to 6S RNA triggers formation of either Central Bulge Collapse helix (CBC) or hairpin depending on the organism, that triggers 6S RNA and RNAP dissociation (Köhler et al., 2015). In *E. coli*, a pRNA of 13-mer was found necessary to release the 6S RNA from RNA polymerase and result in a pRNA:6S RNA rearranged complex. The formation of a 3' hairpin upon pRNA binding was found to be responsible for masking the -10 region and in release of 6S RNA from RNAP via scrunching mechanism. Many promoter elements of *E. coli* are not active in *B. subtilis* driving the need for 6S RNA fine tuning in order to compete with DNA promoter elements specific for the *B. subtilis* RNAP (Cabrera-Ostertag et al., 2013). The 6S RNA rearrangement based on phylogeny, could differ between an α -proteobacter like *B. subtilis* and a γ -proteobacter like *E. coli*. In *E. coli*, an intermediate state of 6S RNA bound core RNAP could be visualized on native gels however such a state is completely absent in *B. subtilis* under similar conditions (Wassarman et al., 2006). Finally, the pRNA:6S RNA release complex in *B. subtilis* is triggered through the formation of a duplex region called the central bulge collapse helix instead of a 3' hairpin. All of which instigates us to ask if the secondary structure of *B. subtilis* 6S-1 RNA has an impact on binding, pRNA transcription and rearrangement, if there is a threshold of pRNA length for the pRNA:6S RNA rearrangement to occur and if the CBC of the *B. subtilis* 6S-1 RNA plays an important role in pRNA:6S RNA rearrangement.

1.4.2 Construction of 6S RNA free His-tagged RNA polymerase in *B. subtilis*

B. subtilis RNAP is a crucial protein responsible for house-keeping transcription. Additionally, it can exert promoter specificity, influence gene expression profiles, affect the kinetics of transcription and modulate the transcription process primarily in response to altered environment and multiple stress conditions. Altogether, this justifies a central interest in RNAP purification protocols for the *in vitro* study of many aspects of gene expression control in *B. subtilis*. Preparation of the native *B. subtilis* RNAP is complex, laborious and sometimes hard to reproduce. A 13-kb plasmid-encoded *B. subtilis* core RNAP including all subunits and a His-tagged *rpoC* subunit was overexpressed in *E. coli* and purified by Ni-NTA affinity and MonoQ anion-exchange chromatography (Yang et al., 2008). In our hands, this approach gave rise to only moderate expression levels. Later, derivatives of *B. subtilis* strain JH642 carrying a chromosomal *rpoC* copy encoding a β' subunit with a C-terminal His tag were constructed, enabling the isolation of the *B. subtilis* RNAP holoenzyme by a single Ni-NTA affinity chromatography step (Qi and Hulett, 1998; Fujita and Sadaie, 1998). This protocol was more robust and efficient than other multi-step protocols for the isolation of native RNAP although this single-step isolation of His-tagged RNAP directly from cell lysates bears the risk of co-purifying cellular interaction partners. The copurification of transcription factor HelD with His-tagged *B. subtilis* RNAP from lysates of strain MH5636 was already described (Wiedermannova et al., 2014). In our case, 6S RNA co-purification with His-tagged RNAP was observed. For this purpose, we aimed to introduce a Histag into the *rpoC* gene of *B. subtilis* PY79 strain where 6S RNAs are knocked out for obtaining 6S RNA-free RNAP holoenzyme. This strain was intended to be used for interaction studies with mutated *B. subtilis* 6S-1 RNAs.

1.4.3 Phenotypic characterization of 6S RNA knockouts in 3610 strain

The widely used lab strains of *B. subtilis* still present poor models to study global regulatory networks. Most lab strains lack the ability to produce antibiotics, to swarm/swim on semisolid media, can neither form biofilm nor sporulate. The source of such incapacitated behavior can be attributed to Single Nucleotide Polymorphisms (SNPs), for example sequencing detected 22 SNPs in the W168 strain (lab strain) compared to NCIB 3610 strain (wild-type strain) which could be due to the harsh handling conditions such as UV and X-ray exposure used to domesticate the lab strains. The W168 strain also has dysfunctional genes such as *sfp* and *swrA* that are involved in surfactant production and swarming, therefore cannot be used to study complex adaptations such as motility (Zeigler et al., 2008). NCIB 3610 is an ancestral strain of many lab strains which exhibits robust environmental adaptations unseen in lab strains. Under the light of this information, our working group hypothesized that 6S RNA being a global transcriptional regulator might exert unforeseen, biologically relevant phenotypes when knocked out in a wild-type strain. My aim in this subproject was to test the swarming and sporulation ability of the NCIB 3610 6S-1 RNA, 6S-2 RNA and 6S-1&2 RNA knockout strains and to document growth curves in conditions where excessive nutrients are readily available.

1.4.4 Transcription of the *epsA* gene by RemA mutants

As a collaboration project with the Bange Lab at Synmikro of our University, I initially aimed at reproducing RemA stimulation of *epsA* gene transcription published by Winkelmann et al. 2013. The ultimate goal was to evaluate several RemA mutants in terms of *in vitro* transcription activation efficacy of the *epsA* gene and check for correlation between *in vitro* gel assay data and *in vivo* biofilm phenotypes.

2 Materials and methods

2.1 Bacterial handling techniques

2.1.1 Preparation of media

All bacterial growth media used are autoclaved at 121 °C for 20 min under 1 bar pressure. After cooling, heat sensitive ingredients that cannot be autoclaved such as glucose, tri-phenyl tetrazolium chloride, antibiotics (strain-specific) are sterile filtered and added as mentioned.

LB medium (1 L)

Casein peptone	10 g
Yeast extract	5 g
NaCl	10 g
Adjust pH 7.5	

Low salt LB medium (1 L)

Casein peptone	10 g
Yeast extract	5 g
NaCl	10 g
Adjust pH 7.5	
1 M Glucose	5 mM

2.1.2 Solid medium handling

Glycerol stocks stored at -80 °C are taken and streaked out onto 1.5 % LB agarose plates (antibiotic supplemented, for more details see appendix E) using the quadrant streaking technique to recover isolated single colonies.

2.1.3 Liquid medium handling

Overnight grown single colonies are inoculated into LB broth (antibiotic supplemented) taken in test tubes or in conical baffled flasks with a head space of 1:5 and are incubated overnight at shaking air incubators at 200 rpm, 37 °C.

2.1.4 Growth curve measurements

The overnight culture was introduced into a pre-culture composed of fresh prewarmed (37 °C) LB broth (antibiotic supplemented). The volume transferred was at a dilution of 1:1000 the volume of the pre-culture. For example: 20 µL of

overnight culture into 20 mL of pre-culture. The pre-culture was left shaking at 37 °C at 200 rpm in a water incubator until the OD₆₀₀ 0.3 to 0.5 was reached. Subsequently, the pre-culture was inoculated into a main culture in appropriate volumes to reach a set start point OD₆₀₀ of 0.05.

For example: the volume of preculture required to inoculate a 100 mL main culture would be calculated as

$$20 \text{ mL pre-culture} \times XX = 100 \text{ mL main culture} \times 0.05$$

XX – OD₆₀₀ value obtained through the trial

The main culture was maintained at 28 °C and 220 rpm in a shaking water incubator. Serological pipettes were used to withdraw small quantities of main culture and after diluting the drawn sample by a factor of 10 (dilution was made only if the OD₆₀₀ values crossed a threshold of 0.8) with LB broth and OD₆₀₀ value was documented.

2.1.5 Glycerol stock preparation

Overnight culture was made according to section 2.1.3 with the exemption of antibiotics supplementation for the purpose of long-term storage. 250 µL of the overnight culture was mixed in 250 µL of glycerol and snap frozen in liquid nitrogen followed by storage at - 80 °C.

2.1.6 Harvesting of bacterial cells

Bacterial cells were harvested for the purpose of tagged protein purification. A single colony from agar plates was picked to inoculate 40 mL LB broth (antibiotic supplemented), followed by overnight growth at 37 °C in a shaking air incubator at 200 rpm. 36 mL of overnight culture was used to inoculate 1.8 L LB medium (prewarmed to 37 °C, antibiotics supplemented) in a 5 L baffled Erlenmeyer flask, the culture was grown at 37 °C under shaking conditions (220 rpm) to late exponential phase (OD₄₂₀ of 1.5 to 2.0) and then harvested by centrifugation at 17,700 x g (JA - 10 rotor, Beckmann ultracentrifuge). Cell pellets were snap frozen in liquid nitrogen and stored at - 80 °C until further use.

2.1.7 Inducing chemical competency in bacterial cells

Modified competence medium		10 x MC medium	
10 x MC	10 % (v/v)	Potassium hydrogen phosphate trihydrate	0.62 M
1 M MgSO ₄	3.33 % (v/v)	Potassium dihydrogen phosphate	0.39 M
ddH ₂ O	make up	Glucose	1.11 M
		Trisodium citrate	33 mM
		Ferric ammonium citrate	0.84 mM
		Casein hydrolysate	0.01 g/mL
		Potassium glutamate	0.11 M
		ddH ₂ O	make up

Chemical competency is useful to introduce foreign DNA from a strain carrying the desired modification into a DNA permissive host strain. In this protocol, 6 mL of LB broth overnight culture (antibiotics supplemented) was inoculated with a single colony of a bacterial strain which carries the desired modification. OD₆₀₀ was measured at 1:10 dilution to calculate cell count (standard conversion factor OD₆₀₀ of 1 corresponds to 8 x 10⁸ cells/mL). Overnight culture containing 2 x 10⁹ cells was centrifuged at ~ 7300 x g for 10 min. The supernatant was discarded and the cell pellet was resuspended in lysis buffer and processed further as instructed by the protocol of the DNeasy Blood and Tissue extraction kit (Qiagen, Cat. No. / ID: 69504). The eluted genomic DNA of the desired strain was quantified using UV spectroscopy. Host strain was streaked onto LB plates containing antibiotics and incubated at 37 °C for 18 h. Isolated colonies were picked and inoculated into 7 mL LB medium (antibiotics supplemented) in a 100 mL baffled Erlenmeyer flask that was incubated at 30 °C overnight in a water bath (Aquatron, Infors AG, Switzerland) under shaking at 200 rpm. The OD was measured at 600 nm (1:10 dilution). Approx. 150 µL of the overnight culture were added to 10 mL modified competence medium in a 250 mL baffled flask, thereby adjusting the OD₆₀₀ to 0.08; this culture was shaken at 200 rpm and 37 °C. The 10 x MC medium was not autoclaved instead sterile filtered and stored at - 20 °C in small aliquots that are easily discarded after one-time use. At an OD₆₀₀ of

~ 1.4, 1 mL of cell culture was transferred to a 13 mL polypropylene reaction tube (Sarstedt, order number 62.515.006) and 500 ng of genomic DNA (strain with desired modification) was added. The reaction mixture was shaken for 2 h at 200 rpm, 37 °C in an air shaking incubator (GFL). 200 µL of the suspension was then plated on screening plates (containing antibiotics) and incubated overnight at 37 °C. Screening and selection of positive clones was achieved by genomic DNA extraction from overnight colonies, followed by a PCR reaction with a locus-specific primer pair to confirm the presence of the recombined locus encoding the desired modification.

2.2 Nucleic acid handling techniques

In order to hijack the cellular machinery, biological entities prefer to inject RNA into a host cell rather than DNA as it is only one step away from translation and perhaps for this very reason are RNAses active and present everywhere as a form of defence mechanism against invading RNA. In our lab, RNase inactivating surface decontaminants are used before starting benchwork. RNA and DNA are re-suspended in double distilled water and kept at - 20 °C for long term storage. The stock is distributed into aliquots to reduce freeze thaw cycles and stored on ice during experiments.

2.2.1 Cloning

Sequence modifications were done on the plasmid level by designing primers using Snapgene 4.1.9. The primers were designed to align the desired mutable sequence complementarily or back-to-back orientation. The melting temperature (T_M) of the primers and off target binding sites were also determined using Snapgene 4.1.9.

Primer design parameters:

1. The primer must have starting and ending nucleotides with G or C.
2. The ideal primer is approximately 20 nucleotides long.
3. The optimal melting temperature (T_M) of a primer should be 55 to 60 °C.
4. The primer pair should not form homo and hetero dimers.

5. The difference of melting temperature (T_M) between the primer pair should not be more than 5 °C.

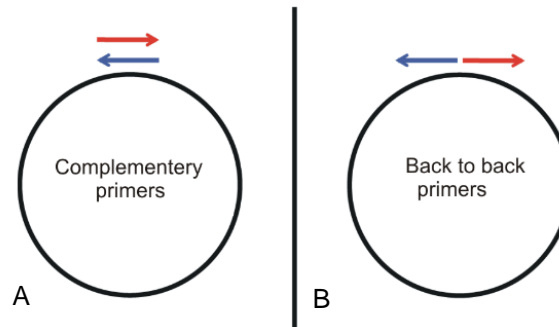


Figure 6: *In vitro* mutagenesis: *In vitro* mutagenesis can be done using two different cloning strategies via primer design. (A) Complementary primers are overlapping primers with a 5' overhang namely sticky ends, the amplified products from complementary primers need not be ligated. (B) Back-to-back primers do not share overlapping sequences and generate blunt end amplicons that need to be ligated.

2.2.2 Polymerase chain reaction (PCR)

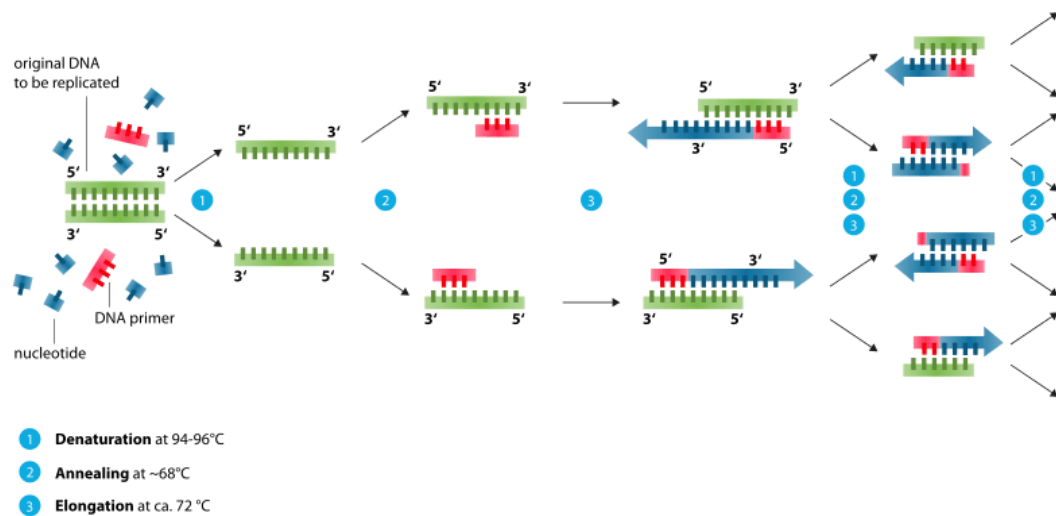


Figure 7: Brief overview of PCR reaction: The DNA template is indicated in green, primer in red and freshly amplified fragments sequestered by nucleotides in blue. 1. The DNA template uncoils. 2. Primers anneal to the uncoiled DNA. 3. Extension of primers along the 3' end. Source: Wikimedia Commons.

Polymerase Chain Reaction (PCR) is a powerful technique used to amplify small fragments of DNA ultimately aiding in detection, modification, sequencing or verification of the DNA sequence of interest. Every PCR step has three main

phases namely, 1. The denaturation step: uncoiling of the double stranded DNA template occurs, 2. The annealing step: primers target and bind to the single stranded template, 3. The elongation step: polymerase recognises the primer and extends the templates along the 3' end. The process repeats and templates amplify exponentially, this can be calculated with the formula $[(2^n - 2n) x]$ where n is the number of cycles and x is the number of copies of the initial template. The type of polymerase used varies upon the purpose of the PCR reaction.

Table 2: PCR reaction set-up for *in vitro* mutagenesis

Components	Final concentration	50 μL reaction
ddH₂O	--	fill to 50 μ L
2 x Phusion master mix (or) 2 x Platinum super fi master mix	1 x	25 μ L
Forward primer (10 μM)	0.5 μ M	2.5 μ L
Reverse primer (10 μM)	0.5 μ M	2.5 μ L
Plasmid DNA (or) Genomic DNA	10 ng 300 ng	varies

Table 3: PCR programme for *in vitro* mutagenesis

Cycle step	3-step protocol	Time	Cycles
Initial denaturation	98 °C	30 sec	1
Denaturation	98 °C	10 sec	35
Annealing	XX °C	10 sec	
Extension	72 °C	YY sec	
Final extension	72 °C	300 sec	1
Hold	4 °C	00 (forever)	
XX – T_M of the primers used, YY – 15 - 30 sec per kb of PCR product			

Colony PCR

Overnight single colonies are obtained by following section 2.1.2. The colonies are picked with a clean pipette tip and shortly resuspended in an Eppendorf containing 50 μL ddH₂O. The mixture was then heated at 95 °C for 5 min using a thermal heat block.

Table 4: PCR reaction set-up for colony PCR

Components	Final concentration	20 μL Reaction
ddH ₂ O	--	fill to 20 μL
5 x Cytopol hot bench MM	1 x	4 μL
Forward primer (10 μM)	0.5 μM	1 μL
Reverse primer (10 μM)	0.5 μM	1 μL
Template DNA (from the heated sample)	~ 10 ng	Varies

Table 5: PCR programme for colony PCR

Cycle step	3-step protocol	Time	Cycles
Initial denaturation	95 °C	900 sec	1
Denaturation	95 °C	15 sec	30
Annealing	XX °C	20 sec	
Extension	72 °C	20 sec	
Final extension	72 °C	60 sec	1
Hold	4 °C	00 (forever)	
XX – T _M of the primers used			

Two-step PCR

Long PCR fragments from genomic DNA were amplified using a two-step protocol, followed by gel elution according to section 2.2.5 to prepare samples destined for sequencing.

Table 6: PCR reaction set-up for two-step PCR

Components	Final concentration	25 μ L reaction
ddH ₂ O	--	fill to 25 μ L
10 x long PCR buffer with 15 mM MgCl ₂	2.5 μ L	2.5 μ L
dNTP 2.5 mM each	0.2 mM	2 μ L
Forward primer (10 μ M)	0.5 μ M	1.25 μ L
Reverse Primer (10 μ M)	0.5 μ M	1.25 μ L
Long PCR master mix (5 U / μ L)	2.5 U	0.5 μ L
Genomic DNA	100 ng	Varies

Table 7: PCR programme for two-step PCR

Step	Temperature	Time	Number of cycles
Initial denaturation	94 °C	180 sec	1
Denaturation	96 °C	20 sec	10
Annealing/extension	68 °C	YY sec	
Denaturation	94 °C	20 sec	25
Annealing/extension	68 °C	YY sec + X sec /cycle	
Final extension	68 °C	600 sec	1

X - correction factor, time increase per cycle due to length of the product, YY - depends on the length of the PCR product, refer long PCR enzyme mix manual (Thermo Fisher Scientific) for more details.

2.2.3 Agarose gel electrophoresis

5 x TBE Buffer

Tris base	445 mM
Boric acid 99.8 %	445 mM
EDTA	10 mM
ddH ₂ O	make up

5 x DNA loading dye

Bromophenol blue	0.25 % (w/v)
Xylene cyanol blue	0.25 % (w/v)
Glycerol	25 % (v/v)
5 x TBE buffer	make up

Based on the length of the PCR product of interest, 1 % agarose gel was made by mixing 50 mL 1 x TBE buffer and 0.5 g agarose powder followed by heating until homogeneity is observed. 2 µL of GelRed[®] was then added to the lukewarm solution, shaken and poured into gel tray (7 cm x 7 cm). A 15 well comb was inserted and the set up was left undisturbed for 15 min. The gel was run at 120 V for 45 min. The sensitivity of GelRed[®] is generally as low as 250 ng of nucleic acid. The agarose gel was then visualised using Dark Hood DH-50 and Gerix 1000 imaging system.

Table 8: Resolution of PCR fragments based on agarose percentage of the gel

% agarose in TBE buffer (w/v)	Size of PCR product separated (bp)
0.5	1000 - 30,000
0.7	800 - 12,000
1	500 - 10,000
1.2	400 - 7,000
1.5	200 - 3,000
3-4 (sieving agarose)	10 - 1,000

2.2.4 Sequencing of PCR products

The DNA sequence of the investigated strains were analysed using Snapgene 4.1.9 to design primers or to identify commercial primer binding sites with the aim to sequence the PCR product. A 25 µL PCR reaction containing the long PCR master mix (Thermo Fisher Scientific, see section 2.2.2 two-step PCR), a unique set of primer pairs and 100 ng of genomic DNA template from the strain of interest

was set up to amplify short PCR fragments. Only 3 μL of the reaction mixture were loaded onto a 0.5 % agarose gel to check for successful amplification of products. The remaining 22 μL PCR reaction mixture was cleaned up using Monarch PCR & DNA Clean-up Kit (New England Biolabs) and recovered in 12 μL elution volume. The eluted product was not quantified and sent away directly for sequencing.

2.2.5 Gel elution of PCR product

Gel elution of the PCR product from the agarose gel is usually done for the purpose of cloning. To optimise effective recovery of PCR products upon usage of gel solubilisation buffer, 0.5 % agarose gels are preferred. The Monarch DNA Gel Extraction Kit (New England Biolabs, #T1020L) was used to extract the desirable PCR product from the agarose gel. Elution volumes less than 15 μL are not recommended, so 20 μL elution buffer was used.

2.2.6 Phosphorylation

When PCR reactions containing primers of unphosphorylated 5' ends are set up, the *in vitro* amplified PCR products have 5' hydroxyl ends that are not natural and are not recognised by enzymes. Therefore, phosphorylation of 5' end is required. The T4 Polynucleotide Kinase (PNK) catalyses the transfer of a phosphate molecule from adenosine triphosphate (ATP) to the 5' hydroxyl end of the PCR product. The reaction mixture was pipetted and incubated at 37 °C for 30 min followed by heat inactivation of T4 PNK at 75 °C for 10 min.

Table 9: Reaction set up for DNA phosphorylation

Components	20 μ L reaction
PCR product	10 μ L
10 x buffer A for T4 PNK	2 μ L
T4 PNK	1 μ L
10 mM ATP	2 μ L
ddH ₂ O	5 μ L

2.2.7 *DpnI* digestion and ligation

DpnI is a restriction digestion enzyme that recognizes and cleaves distinct nucleotide sequence namely 5'-GATC-3' only when the adenine residues are methylated. *DpnI* digestion is done to remove natural DNA or parental strands used as template for PCR reaction as *in vitro* synthesized PCR products lack epigenetic modifications. Back-to-back primers give rise to blunt end PCR products that cannot be ligated by cellular mechanisms in the bacteria unlike sticky end PCR products. T4 DNA ligase effectively recognizes and creates phosphodiester bonds between adjacent 5' phosphate and 3' hydroxyl blunt ends of the PCR fragment. Under such circumstances, ligation of blunt end PCR products can be done simultaneously along with *DpnI* digestion. The *DpnI* digestion/ligation reaction mixture was pipetted and incubated at 37 °C anywhere from 1 h to overnight followed by heat inactivation at 80 °C for 20 min.

Table 10: Reaction set up for DNA ligation and parent strand digestion

Components	50 μ L reaction
Phosphorylated product (total reaction mixture from section 2.2.6)	20 μ L
10 x ligase buffer	5 μ L
T4 DNA ligase	1 μ L (5 U)
<i>DpnI</i> enzyme (10 U/ μ L)	2 μ L
ddH ₂ O	22 μ L

2.2.8 Transformation

Transformation is the process of introducing foreign DNA into a competent (DNA permissive) cell and resulting in a recombinant cell. Chemically competent *E. coli* DH5 α cells were taken from - 80 °C storage and thawed on ice. 10 μ L of reaction mixture from section 2.2.7 was taken and added to 50 μ L of competent cells. The reaction mixture was gently mixed on ice and left standing on ice for 30 min. A quick heat shock was delivered by incubating the reaction mixture at 42 °C for 45 sec followed by a cold shock incubating samples on ice for 2 min. 600 μ L of LB broth was added (pre-warmed to room temperature) to the reaction mixture and incubated at 37 °C for 60 min. 35 μ L and 15 μ L of the bacterial suspension were used to plate onto 1.5 % agarose plates using glass beads. The plates were incubated overnight at 37 °C to get isolated single colonies.

2.2.9 Plasmid preparation for sequencing

Isolated overnight colonies obtained from section 2.2.8 were picked, streaked onto 1.5 % LB agar plates and directly inoculated into overnight culture of 3 mL volume (antibiotic supplemented). GeneJET plasmid mini-prep kit (Thermo Fisher Scientific, # K0502) was used to isolate the plasmid DNA. The plasmid DNA was recovered in ddH₂O and quantified using UV spectroscopy. The plasmid was diluted to a concentration of 70 ng/ μ L in 12 μ L volume and 3 μ L of a sequencing primer (final concentration 4 μ M) was added, making a total final volume of 15 μ L and sent away for sequencing.

2.2.10 Preparation of cold RNA

Gene of interest was placed under the influence of a T7 promoter in a pUC18 plasmid (see Appendix: F. Plasmids for more details) carried by *E. coli* DH5 α strain. This plasmid was recovered and cold RNA was transcribed for further *in vitro* analyses.

2.2.11 Plasmid preparation for cold RNA transcription

150 mL of LB broth was inoculated with isolated single colonies (see section 2.1.2) and left shaking at 37 °C and 200 rpm overnight. The cells were harvested by centrifugation at 6000 x g and 4 °C for 15 min. NucleoBond Xtra Maxi kit (Macharey Nagel, AX 500) was used to isolate the plasmid DNA. The plasmid DNA was eluted using ddH₂O and quantified using UV spectroscopy.

2.2.12 Linearisation of plasmid

For the purpose of *in vitro* transcription, *Hind*III restriction enzyme is used to linearize the plasmid and expose the T7 RNA polymerase promoter binding site. The reaction mixture was pipetted as described and incubated at 37 °C for 1 h. 5 µL of the reaction mixture was taken and checked on a 1 % agarose gel. The reaction was stopped by incubation at 80 °C for 10 min to avoid star activity of Fast Digest (FD) *Hind* III.

Table 11: Restriction digestion of plasmid DNA.

Components	Final concentration	500 µL reaction
FD <i>Hind</i> III	20 U	20 µL
10 x FD green buffer	1 x	50 µL
Plasmid DNA	120 µg	Varies
ddH ₂ O		fill to 500 µL

2.2.13 Phenol and chloroform extraction of DNA

500 μL of the reaction mixture from section 2.2.12 was taken and mixed with 500 μL phenol (ROTI®Phenol, Carl Roth). The mixture was shaken using a vortex mixer for 5 min at room temperature followed by centrifugation at 16,000 x g, room temperature (Biofuge Fresco, Fixed-angle rotor 7500 3325). By careful pipetting, the supernatant was discarded without disturbing the lower phase and transferred to a new reaction tube. 500 μL chloroform was added to the supernatant and vortexed at room temperature for 5 min. The reaction mixture was centrifuged for 5 min at 16,000 x g, room temperature. Only the supernatant was recovered without the lower phase (chloroform) and transferred to the new reaction tube. In a 2 mL Eppendorf vial, 50 μL of pH 5 adjusted 3 M Sodium acetate (NaCH_3COO), 1250 μL of ethanol absolute p.a. was taken along with 500 μL of supernatant. The reaction mixture was snap frozen at $-196\text{ }^\circ\text{C}$ (liquid nitrogen) for 1 min, followed by centrifugation at 16,000 x g, $4\text{ }^\circ\text{C}$. The supernatant was discarded and a translucent pellet was observed. Pellet was air dried for at least 5 min with precaution not to over dry, 50 μL of ddH₂O was then added and incubated for another 5 min. The linearized DNA was quantified using UV spectroscopy.

2.2.14 *In vitro* transcription using T7 RNA polymerase

Reaction mixture was set up as described in the pipette scheme with linearized DNA from section 2.2.13. *In vitro* transcription was aided by T7 RNA polymerase (self-prepared, approximately 40 U/ μ L according to Burenina OY et al., 2014). The efficiency of the reaction could be improved by adding T7 RNA polymerase twice.

Table 12: Reaction set up for *in vitro* transcription using T7 RNA polymerase

Components	Stock concentration	Final concentration	200 μ L reaction
ddH ₂ O			110.8 μ L
MgCl ₂	3 M	33 mM	2.2 μ L
Hepes pH 7.5	1.0 M	80 mM	16 μ L
Spermidine	0.1 M	1 mM	2 μ L
DTT	0.1 M	5 mM	10 μ L
Pyrophosphatase	200 U/mL	0.05 U	1 μ L
Linearized DNA	1 μ g/ μ L	14 μ g	14 μ L
Nucleotide mix	25 mM each	4 mM	30 μ L
DMSO	100 %	5 %	10 μ L
T7 RNA polymerase			4 μ L
Total volume			200 μ L
Incubation at 37 °C			2 h
T7 RNA polymerase			4 μ L
Incubation at 37 °C			2 h

2.2.15 Phenol and chloroform extraction of RNA

The phenol and chloroform extraction protocol for RNA is the same as phenol chloroform extraction protocol for DNA (see section 2.2.13) with the exception of using ROTI®Aqua-Phenol meant for RNA extraction (Carl Roth). The dried pellet was re-suspended in ddH₂O and immediately stored at - 20 °C due to the heat sensitive nature of RNA.

2.2.16 Extraction of RNA from denaturing polyacrylamide gel

The freshly transcribed and purified RNA from section 2.2.15 was mixed with 2 x denaturing RNA loading dye and heated at 95 °C for 3 min. Based on the size of the RNA product the percentage of polyacrylamide (PAA) was chosen (see table 20 for more details). Gel dimensions are 30 cm x 20 cm x 1 mm (breadth x height x thickness). It was run until the bromophenol blue (BPB) bands of the dye reached the end of the gel. The gel was visualized under UV shadowing to visualize the RNA and to excise them using a clean scalpel.

2.2.17 Gel elution and precipitation of RNA

The excised RNA from section 2.2.16 was taken up in a 50 mL falcon containing 5 mL of pH 5.0 adjusted 1 M sodium acetate and was left shaking overnight at 4 °C. The supernatant was recovered and filtered with centrifugal filter (VWR) for 2 min at 14,000 x g (Biofuge fresco). In a 2 mL Eppendorf vial, 50 µL of pH 5 adjusted 3 M Sodium acetate (NaCH₃COO), 1250 µL of ethanol absolute p.a. was taken along with 500 µL of supernatant. The reaction mixture was snap frozen at - 196 °C (liquid nitrogen) for 1 min, followed by centrifugation at 14,000 x g, 4 °C. The supernatant was discarded and a translucent pellet was observed. After 5 min of air drying, at least 50 µL of ddH₂O was added and incubated for another 5 min. The vial was stored on ice, the RNA was quantified using UV spectroscopy and stored at - 20 °C in small aliquots for long term usage.

2.2.18 De-phosphorylation of RNA

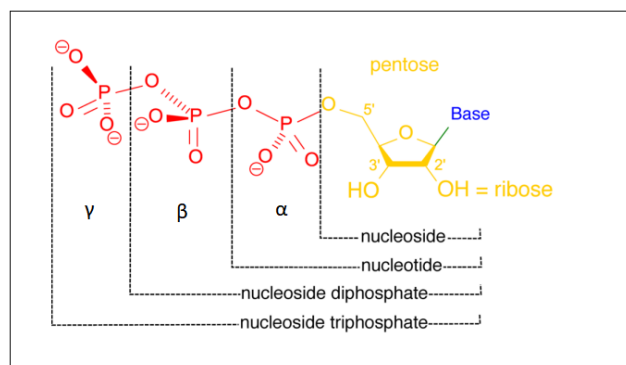


Figure 8: Chemical composition of a nucleotide: A nucleotide is composed of sugar, base and phosphate back bone. Dephosphorylation of a nucleotide is necessary to introduce modifications to the 5' end of sugar moiety. Source: Wikimedia Commons.

Changes in conformational states of RNA can be studied effectively *in vitro* by radiolabeling the 5' end of the RNA transcript with a radioactive phosphate (^{32}P). In order to achieve this, de-phosphorylation of the tri-phosphate chain must be done. FastAP™ thermosensitive alkaline phosphatase (Thermo Fisher Scientific) helps with the cleavage of phosphate priming the RNA for radiolabeling. The reaction mixture was pipetted as described below and incubated at 37 °C for 1 h. Due to the heat sensitive nature of RNA, heat inactivation of the enzyme was avoided instead phenol chloroform extraction of RNA protocol from section 2.2.15 was done. The recovered RNA was quantified using UV spectroscopy and stored at - 20 °C for long term usage.

Table 13: Reaction set up for de-phosphorylation of RNA

Components	Final concentration	100 μL reaction
RNA	100 μg	Varies
10 x FastAP™ buffer	1 x	10 μL
FastAP™ (1 U/ μL)	8 U	8 μL
ddH ₂ O		fill to 100 μL

2.2.19 5' radiolabeling of RNA

γ - ^{32}P -ATP (3.75 MBq activity in 10 μL stock) was used as the substrate by T4 Polynucleotide kinase (T4 PNK, Thermo Fisher Scientific) to remove and introduce radiolabeled phosphate (^{32}P) to the 5' end of the de-phosphorylated RNA from section 2.2.18. The reaction mixture was pipetted as described below and incubated at 37 °C for 1 h. The reaction mixture was shortly centrifuged at 14,000 x g (Biofuge fresco) for 2 min and mixed in equal parts with 2 x denaturing RNA loading dye.

Table 14: Reaction set up for radiolabeling of RNA

Components	Final concentration	10 μL reaction
RNA	60 pmol	Varies
10 x T4 PNK buffer A	1 x	1 μ L
γ-³²P-ATP	0.75 Mbq	2 μ L
T4 PNK (10 U/μL)	10 U	1 μ L
ddH₂O		fill to 10 μ L

Ideally, gel cast with dimensions 16.5 cm x 24 cm x 1 mm (breadth x height x thickness) was chosen and cast with 8 % polyacrylamide solution. The gel was run for 3 - 4 h at 20 mA until the Xylene Cyanol Blue (XCB) signal reached the middle of the gel. The gel was exposed to an imaging plate for 1 min and the imaging plate was developed using a phospho-imager (Fujifilm). The radiolabeled RNA band was identified, excised using a scalpel and introduced in a vial containing 500 μ L of pH 5 adjusted 1 M sodium acetate and 0.05 % SDS. The eppendorf vial was allowed to shake at 8 °C, overnight. The supernatant was filtered with VWR centrifugal filter by spinning at 14000 x g, for 2 min. In a new 2 mL Eppendorf vial, 1250 μ L of ethanol absolute p.a., 2 μ L of GlycobluTM (Thermo Fisher Scientific) was taken and 500 μ L of supernatant was added. The Eppendorf vial was snap frozen at -196 °C (liquid nitrogen) followed by centrifugation for 1 h at 14,000 x g, 4 °C (Biofuge Fresco). The supernatant was discarded and the pellet was air dried for 5 min at room temperature. The pellet subsequently was re-suspended in 10 μ L of ddH₂O and incubated for 5 min. 1 μ L of the radiolabeled sample was loaded and the radioactivity was counted using a scintillator (TriCarb, Perkin Elmer). The stocks were stored in a lead container at - 20 °C. The radioactive decay of the sample was calculated using table 22.

2.3 Protein handling techniques

Proteins are strings of amino acids that form multimeric subunits and are often more complex in terms of composition than nucleic acids. Under suboptimal conditions, they can unfold and lose activity or exhibit sensitivity to freeze thaw cycles. Therefore, handling techniques are often gentle with storage in glycerol-based buffers at -20 °C. Protein purification strategies were mostly based on the strain carrying the protein of interest, properties of the protein of interest and presence or absence of a purification tag.

2.3.1 Cell lysis for purification

Sonication buffer

Tris pH 7.8	50 mM
NaCl	300 mM
MgCl ₂	5 mM
Glycerol	20 %
Imidazole	0 mM
ddH ₂ O	make up

Cell harvest from the bacterial strain of interest was done according to section 2.1.6. Pellet weighing 15 - 20 g was taken and carefully re-suspended in at least 20 mL of sonication buffer not exceeding 50 mL of total volume. 2 mL from 100 mg/mL of lysozyme solution (f. c. 4 mg/mL) was added and stirred thoroughly for 30 min at 4 °C. Additionally, 460 µL of 110 mM PMSF was added and the cells were sonicated (output 4, duty cycle 50 %, S-250 Branson sonifier) in eight cycles each lasting 30 sec with intervals of 2 min on ice. The sonicated cell lysate was centrifuged at ~ 10,200 x g, 4 °C for 1 h. The supernatant was processed further by filtering through 0.2 µM filter (Sarstedt) and stored on ice.

2.3.2 Nickel-nitrilotriacetic acid (Ni-NTA) column

Binding buffer

Tris pH 7.8	50 mM
NaCl	300 mM
MgCl ₂	5 mM
Glycerol	20 %
Imidazole	30 mM
ddH ₂ O	make up

Elution buffer

Tris pH 7.8	50 mM
NaCl	300 mM
MgCl ₂	5 mM
Glycerol	20 %
Imidazole	400 mM
ddH ₂ O	make up

RNA polymerase storage buffer

Tris pH 8.0	10 mM
MgCl ₂	10 mM
EDTA	0.1 mM
DTT	0.1 mM
NaCl	0.1 M
Glycerol	50 % (v/v)
ddH ₂ O	make up

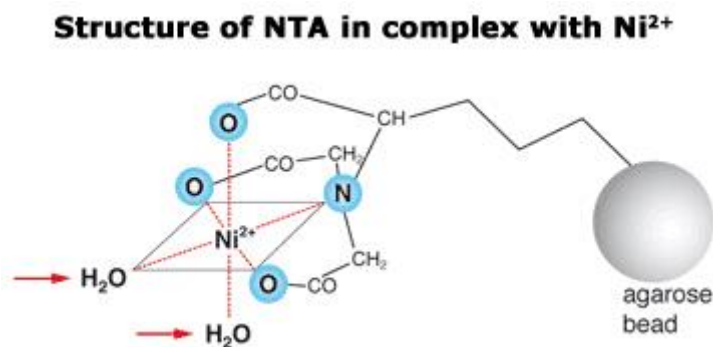


Figure 9: Principle of Ni-NTA column: The principle of Ni-NTA column is based on the protein's histidine affinity to Ni²⁺ ions chelated with nitrilotriacetic acid (NTA) that is in turn affixed to agarose beads in a polypropylene column. NTA is a tetradentate chelator which occupies four of the six binding sites in the coordination sphere of the Ni²⁺ ion. The remaining two coordination sites are usually occupied by water molecules and can be exchanged with histidine residues of the protein of interest. The interaction of histidine with these coordination sites facilitates binding that is tight but also reversible under unfavourable conditions. Source: Macherey Nagel.

Histidine-tagged proteins can be purified using Nickel-nitrilotriacetic acid (Ni-NTA) column. Histidine uses an imidazole side chain to bind with the Ni-NTA

complex, this interaction can be easily displaced upon introduction of imidazole compound. Buffers which differ in imidazole concentration were used, namely the binding buffer (30 mM imidazole) and the elution buffer (400 mM imidazole). The Ni-NTA column (HisTrap HP 5 mL, GE Healthcare) was equilibrated by passing 5 column volumes (CV) of binding buffer. The supernatant was loaded onto the column at a rate of 1 CV per min. After loading the supernatant, the column was washed in binding buffer until baseline at $A_{280\text{nm}}$ of the detector was reached. Overall, 15 column volumes were eluted, 1 CV per collected fraction. The eluted fractions were analyzed using 12 % stain-free SDS-PAGE gels (Biorad, #1610185, see section 2.3.9) and fractions containing the major amount of RNA polymerase were pooled and dialyzed into RNA polymerase storage buffer and stored at -20 °C. The Ni-NTA column was washed in 15 CV of elution buffer followed by 5 CV of binding buffer, after which 15 CV of ddH₂O and finally, 15 CV of 20 % ethanol. The column was stored in a cool, dry place until further use.

2.3.3 Size exclusion column

Modified sonication buffer

Tris pH 7.8	50 mM
NaCl	150 mM
MgCl ₂	5 mM
Glycerol	5 %
ddH ₂ O	make up

The Size exclusion column (SEC) aims to separate proteins based on size. The time taken for the protein to flow through a porous matrix of the column is shorter for bigger proteins and longer for smaller proteins. The column is ideal for further purification of already purified proteins with residual side products and to study the ability of the protein to make higher associative complexes i.e., dimers or tetramers. Hiprep™ 26/60 Sephacryl™ S-300 HR (CV 320 mL) was used to purify the His-tagged RNA polymerase, but the protein concentration suffered an undesired side effect of over-dilution. The use of centricons (Merck Millipore) could not recover the loss of concentration. The column was washed with 0.5 CV of ddH₂O and equilibrated with 2 CV of modified sonication buffer using a

peristaltic pump. 10 mL of sample was loaded and injected, elution begins immediately as the SEC column does not bind to the protein of interest and therefore serves no resistance. 2 CV of modified sonication buffer was used to elute the protein in 2 mL fractions. The eluted fractions were loaded onto SDS gels and visualized using zinc staining (see section 2.3.8 and 2.3.12). The column was washed further with 1 CV of modified sonication buffer (fractions not collected), 0.5 CV of 0.2 M NaOH, 2 CV of ddH₂O and 2 CV of 20 % ethanol. The column was stored with a 20% ethanol filled pressure gauge at room temperature.

2.3.4 Heparin column

BII binding buffer

Tris pH 8	20 mM
NaCl	200 mM
EDTA	0.1 mM
Glycerol	5 %
DTT	2.5 mM
ddH ₂ O	make up

BII elution buffer

Tris pH 8	20 mM
NaCl	1000 mM
EDTA	0.1 mM
Glycerol	5 %
DTT	2.5 mM
ddH ₂ O	make up

Upon DTT addition, store at 4 - 7 °C and use within one week.

Heparin column is a type of adsorption chromatography, which has the ability to bind a wide variety of biomolecules such as enzymes, proteins, DNA-binding proteins and hormone receptors. It can also be used as a cation exchanger due to the presence of sulphate groups in heparin structure. The column is interesting to our project due to the nucleic acid binding nature of RNAP. 1 mL HiTrap Heparin HP (GE healthcare) was used to purify native RNA polymerase. The column was washed in 5 CV ddH₂O and 5 CV of BII binding buffer. 22 mL of the sample was loaded in steps using a 2 mL superloop, consecutively not more than 2 mL at a time. The column afterwards was washed with BII binding buffer until the occurrence of a baseline. A linear gradient was set up to initiate elution using BII binding buffer (200 mM NaCl) as the starting buffer and BII elution buffer (1000 mM NaCl) as ending. 20 CV were eluted with 2 CV collected in every fraction. The eluted fractions were checked on SDS gel followed by Coomassie

blue staining (see section 2.3.8 and 2.3.11). The column was washed in 5 CV of 2 M NaCl, 5 CV of ddH₂O and 5 CV of 20 % ethanol.

2.3.5 MonoQ column

MonoQ start buffer

Tris pH 8.4	25 mM
KCl	100 mM
EDTA	1 mM
Glycerol	10 %

MonoQ elution buffer

Tris pH 8.4	25 mM
KCl	1000 mM
EDTA	1 mM
Glycerol	10 %

MonoQ is a strong anion column for high performance ion exchange of proteins, peptides and other biomolecules. It can be used to concentrate proteins and is usually used as the last step during a purification protocol. MonoQ column 5/50 GL (1 mL) was used to concentrate the native RNA polymerase. The column was washed with 5 CV ddH₂O, 5 CV MonoQ start buffer, 5 CV MonoQ elution buffer and again 5 CV MonoQ start buffer. Sample was loaded using a 2 mL superloop and the column was washed of MonoQ start buffer until baseline was reached. A linear gradient of 5 CV with MonoQ start buffer and subsequently 5 CV MonoQ elution buffer was set up. The eluted fractions were tested on SDS gel and stained with Coomassie to visualize the protein (see section 2.3.11). The column was washed with 5 CV of MonoQ elution buffer, 2 CV of 2 M NaCl, 4 CV of 1 M NaOH, ddH₂O until baseline was reached and 5 CV of 20 % ethanol. The column was stored in 20 % ethanol, in a dry place.

Quantitative evaluation of proteins

2.3.6 Bradford assay

The principle of Bradford assay involves a color change at 595 nm from brown to blue upon protein binding to Coomassie dye under acidic conditions. Bradford assay can be used to detect and quantify proteins based on this colorimetric change extrapolated against a standard calibration curve. Bovine Serum Albumin (BSA) protein with a stock concentration 100 µg/mL was taken and diluted in ddH₂O (see table 15 for further details) to a final concentration of 0, 2, 4, 6, 8 to 10 µg/mL. Upon addition of 200 µL Bradford reagent, the mixture was vortexed and incubated for 5 min. The sample was then measured at 595 nm. Appropriate volume of sample protein was taken and filled to a final volume of 800 µL with ddH₂O. The protocol was repeated to quantify the unknown concentration.

Table 15: Pipette scheme for standard BSA assay calibration curve

Components	0 µg/mL	2 µg/mL	4 µg/mL	6 µg/mL	8 µg/mL	10 µg/mL
ddH₂O	800 µL	780 µL	760 µL	740 µL	720 µL	700 µL
BSA (100 µg/mL)	----	20 µL	40 µL	60 µL	80 µL	100 µL
Bradford reagent	200 µL	200 µL	200 µL	200 µL	200 µL	200 µL

2.3.7 Image lab™ software

Protein can also be quantified by loading the sample against a protein standard of known concentration onto SDS gel followed by Coomassie blue staining (see section 2.3.8 and 2.3.11). The stained gel was scanned using ChemiDoc™ MP Imaging system (Bio-Rad) and the image was quantified in Image Lab™ software (Bio-Rad, version 6.1) using relative quantity tool.

Separation of proteins

2.3.8 Sodium dodecyl sulphate polyacrylamide (SDS-PAGE) gel

4 x resolution gel buffer

Tris/HCl pH 8.8	1.5 M
SDS	0.6 % (v/v)
ddH ₂ O	make up

4 x stacking gel buffer

Tris/HCl pH 6.8	0.5 M
SDS	0.6 % (v/v)
ddH ₂ O	make up

12 % resolution gel

30 % PAA	3.2 mL
4 x Resolution gel buffer	2 mL
ddH ₂ O	2.8 mL
10 % APS	20 µL
TEMED	80 µL

12 % stacking gel

30 % PAA	0.375 mL
4 x Stacking gel buffer	0.9 mL
ddH ₂ O	2.5 mL
10 % APS	20 µL
TEMED	80 µL

4 x Laemmli buffer

Tris/HCl pH 6.8	100 mM
SDS	8 % (w/v)
Mercapto ethanol	8 % (w/v)
Bromophenol Blue	0.04 % (w/v)
Glycerol	30 % (v/v)
ddH ₂ O	make up

Sodium dodecyl sulphate polyacrylamide gel electrophoresis (SDS-PAGE) is a technique that separates proteins based on their molecular weight. Protein samples are mixed in 4 x Laemmli buffer and heated at 95 °C for 5 min using a thermal heating block. The samples are then loaded onto a 12 % SDS gel (gel dimensions 8.6 cm x 6.7 cm x 0.1 mm) and run at 150 V in 1 x running buffer (Rotiphorese[®] 10 x SDS-PAGE) until the blue band runs out.

2.3.9 Tris-glycine extended (TGX) gel

12 % Tris-Glycine extended (TGX) Stain-Free™ FastCast™ acrylamide kit (Bio-Rad, #1610175) was taken and the standard solutions were mixed as instructed and gels were cast. The TGX gels are handled in a manner similar to SDS gels. TGX gels have trihalo-compounds that detect and modify tryptophan residues in proteins resulting in fluorescence upon UV activation therefore no extra staining procedure is required to detect proteins. The protein lanes in the gel are visualized using ChemiDoc™ MP Imaging system (Bio-Rad).

2.3.10 Schaeffer gel

5 x anode buffer

Tris/HCl pH 8.9	1 M
ddH ₂ O	make up

5 x cathode buffer

Tris/HCl pH 8.25	0.5 M
Tricine	0.5 M
20 % SDS	0.1 % (v/v)
ddH ₂ O	make up

3 x gel buffer

Tris/HCl pH 8.45	3 M
20 % SDS	0.4 %
ddH ₂ O	make up

16 % resolution gel

30 % PAA	5.3 mL
3 x gel buffer	3.3 mL
ddH ₂ O	1.4 mL
10 % APS	20 µL
TEMED	80 µL

Schaeffer stacking gel

30 % PAA	0.670 mL
3 x gel buffer	1.7 mL
ddH ₂ O	2.63 mL
10 % APS	20 µL
TEMED	80 µL

Schaeffer gel can be used to study small proteins or small subunits of multimeric proteins. To run a Schaeffer gel, the gel was taken in a Mini-PROTEAN tetra vertical electrophoresis cell (Bio-Rad) with cathode buffer inside the gel cassette and anode buffer outside. The samples were mixed with 4 x Laemmli buffer heated at 95 °C for 5 min and loaded. The gel was initially run at 30 V until the

blue band reaches the resolution gel and afterwards the gel was run at 300 V until the blue band runs out. The gel was recovered and subsequently silver stained (see section 2.3.13).

Qualitative analysis of proteins

2.3.11 Coomassie blue staining

Coomassie blue solution

Coomassie brilliant blue G-250	0.2 % (w/v)
Acetic acid	10 % (v/v)
Methanol	50 % (v/v)
ddH ₂ O	make up

SDS gels were soaked for 30 min in Coomassie blue staining solution under shaking conditions. The gels were taken in ddH₂O and either left to de-stain overnight under shaking conditions or microwaved shortly until only the stained bands remain.

2.3.12 Zinc staining

The SDS gels were shaken in 0.2 M Imidazole solution for 7 min after which the solution was discarded. The gel was then introduced into a 0.2 M Zinc sulphate solution and shaken vigorously for 30 sec against a dark background until translucent bands appear. The reaction was stopped by transferring the gel into ddH₂O. To de-stain the gel, 2 % citric acid solution was added and the gel was left shaking for 10 min followed by storage in ddH₂O.

2.3.13 Silver staining

Silver staining was done on Schaeffer gel using the PagesilverTM silver staining kit (Fermentas, #K0681) and by following the instructions.

2.3.14 Western blot

Transfer buffer		20 x TBS buffer	
Tris/HCl pH 8.3	25 mM	Tris	200 mM
Glycine	192 mM	NaCl	3000 mM
Methanol	10 %	pH	7.6
ddH ₂ O	make up	ddH ₂ O	make up

TBST buffer		Blocking buffer	
Tris	10 mM	Skimmed milk powder	5 % (v/v)
NaCl	150 mM	TBST Buffer	95 % (v/v)
pH	7.6	ddH ₂ O	make up
Tween 20	0.1 % (v/v)		
ddH ₂ O	make up		

Samples were loaded onto SDS gel and were run as described in section 2.3.8. The SDS gel was then blotted onto nitrocellulose membrane (Immobilin[®]- E, Sigma-Aldrich) using the electro blotter (Bio-Rad) and afterwards run for 7 min at 25 V (7.5 mA). The membrane was left shaking in blocking buffer overnight at room temperature (RT). The membrane was washed in TBST buffer three times with an interval of 10 min between each wash. Primary antibody namely anti- His- tag, rabbit origin (PA1-983B, Thermo Fisher Scientific) of dilution 1: 10,000 was added and incubated for 1 h at RT. The membrane was washed again three times in TBST as described above. Secondary antibody namely anti-rabbit, goat origin (A9169-2ml, Sigma-Aldrich) of dilution 1: 5,000 was added and incubated for 1 h at RT. The washing step with TBST was repeated. Reagents of Clarity[™] Western ECL Substrate Kit (Bio-Rad) was taken in 1:1 ratio and dropped onto the membrane followed by incubation for 5 min. The membrane was then detected using chemiluminescence mode on Chemidoc[™] MP Imaging system (Bio-Rad) set for 5 min. Overall, 15 photos were made with the first one recorded after 10 sec of exposure.

2.4 Assays

2.4.1 Electrophoretic mobility shift assay

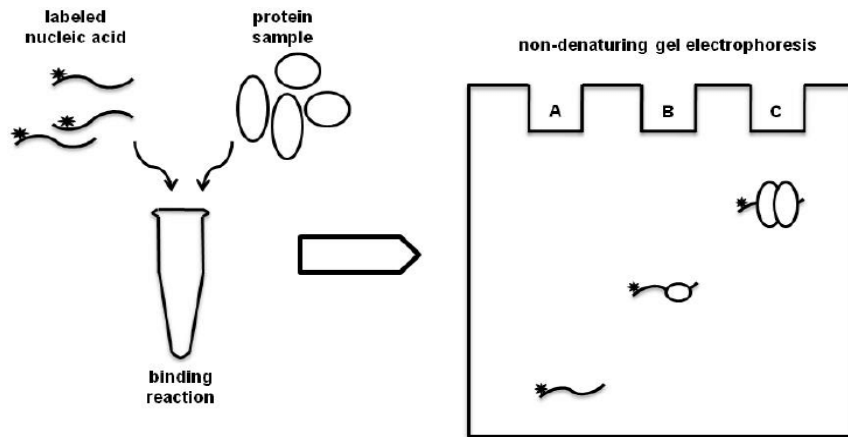


Figure 10: Pictorial representation of electrophoretic mobility shift assay (EMSA): Nucleic acid and protein interaction can be studied in an EMSA assay detected by radio- or fluorescence labeling the nucleic acid of interest. A reaction mixture is usually set up allowing the nucleic acid strand and protein to interact. The sample is loaded onto a gel and any form of interaction is signified by retardation as the nucleic strand moves along the gel. Source: Alves and Cunha (2012).

Electrophoretic mobility shift assay (EMSA) is an *in vitro* gel retardation assay used to study protein and DNA or RNA interactions. The principle of the assay is based on the property of DNA or RNA to travel slower along a gel upon complex formation or due to secondary structure modifications.

2.4.2 Native electrophoretic mobility shift assay

Native 20 % PAA gel (1 L)

50 % PAA	400 mL
5 x TBE	200 mL
ddH ₂ O	make up

5 x transcription buffer

Tris HCl pH 8.0	200 mM
MgCl ₂	25 mM
KCl	800 mM
DTT	5 mM
ddH ₂ O	make up

2 x native RNA loading dye

Glycerol	10 % (v/v)
MgCl ₂	10 mM
BPB	0.025 % (w/v)
XCB	0.025 % (w/v)
ddH ₂ O	make up

To test the binding affinity of 6S-1 RNA (190 nt) to RNA polymerase, a 10 μ L reaction mixture was set up. The reaction mixture consists of heparin (f. c. 80 ng/ μ L), 1 x transcription buffer, trace amounts of radioactive RNA (2500 cpm per lane) and cold RNA (f. c. 10 nM, if needed). Further, RNA polymerase fractions of different dilutions were added in the described order as shown in the pipette scheme (see table 17 for more details). The RNA polymerase enzyme was diluted in RNAP storage buffer to attain the desired end concentration. The reaction mixture was incubated at 37 °C for 30 min. Following incubation, 10 μ L of 2 x native loading dye was added to the reaction mixture and loaded onto a 7.5 % native PAA gel (1 x TBE). The samples were run at 25 mA for 3 h.

Variations in native electrophoretic mobility shift assay

The kinetics of EMSA can be modified by varying many parameters such as addition of cold RNA that slows the visualization of the labeled RNA turnover, decreasing the temperature of the gel which decreases the dissociation of complexes during the gel run and selecting protein concentrations that can help to optimize data points on the curve to obtain optimal fitting. The activity of RNA polymerase can be enhanced through the addition of purified His-tagged σ^A factor

in 10-molar excess to the RNAP holoenzyme with a subsequent incubation step at 30 °C for 15 min before starting the reaction. The addition of σ^A factor dilutes the volume of the RNAP holoenzyme and as a result the stock concentration was adjusted. The binding activity of such σ^A factor associated fractions were higher due to availability of more active RNAP holoenzyme complexes. Throughout the project, owing to minor activity differences in protein purification batches and activity as well as differences in RNA due to mutations to the secondary structure, the native EMSA parameters were constantly changed to get optimal data.

Table 16: Dye migration and corresponding nucleotide length based on native polyacrylamide gel percentage: The following table represents empirically derived data indicating length of nucleotides corresponding to dye migration on a native polyacrylamide (PAA) gel. Source: In house data provided by technician Dominik Helmecke.

% PAA of gel	BPB (nt)	XCB (nt)
3.5	100	460
5	65	260
8	45	160
12	20	70
20	12	45

Table 17: Pipette scheme for determination of binding affinity (K_d) of σ^A -RNAP and 6S RNA:

The values indicated in the table are listed as volumes (μL) if otherwise indicated for their corresponding components. To attain varying stock concentration of σ^A -RNAP, the stock was diluted in RNAP storage buffer. Varying stock concentrations of σ^A -RNAP can ease pipetting and handling while working across a wide range of protein concentrations.

Components	RNA polymerase (μM)						
	0	0.03	0.125	0.25	0.5	1	2
RNA (100 nM)	1	1	1	1	1	1	1
γ-³²P-radiolabeled RNA (5,000 cpm/μL)	0.5	0.5	0.5	0.5	0.5	0.5	0.5
5 x transcription buffer	2	2	2	2	2	2	2
Heparin (400 ng/μL)	2	2	2	2	2	2	2
ddH₂O	4.5	3.75	1.4	3.9	3.28	3.28	2.1
σ^A-RNAP (μL)	0	0.75	3.1	0.61	1.22	1.22	2.44
Stock conc. of σ^A-RNAP (μM)	--	0.41		4.1		8.2	
Incubation at 37 °C for 30 min							
2 x native RNA loading dye (μL)	10	10	10	10	10	10	10

2.4.3 Nucleotide supplemented native electrophoretic mobility shift assay

10 x TE Buffer

Tris	100 mM
EDTA	10 mM
ddH ₂ O	make up

2 x TE Buffer (1 mL)

10 x TE buffer	200 μ L
ddH ₂ O	800 μ L

2 mM nucleotide master mix (100 μ L)

100 mM ATP	2 μ L
100 mM GTP	2 μ L
100 mM CTP	2 μ L
100 mM UTP	2 μ L
ddH ₂ O	make up

In our lab, we have shown that native EMSA helps us to study the binding affinity of 6S RNA to σ^A -RNA polymerase. Interestingly, upon nucleotide addition small transcripts called product RNA (pRNA) production can be triggered. The production of pRNAs results in the formation of a pRNA:6S RNA complex, this complex is sterically bent and runs slowly compared to free 6S RNA band. Therefore, using this gel type we can study the kinetics of pRNA triggered release of 6S RNA from RNA polymerase. For the *in vitro* gel assay, a master mix containing equal parts of radiolabeled 6S RNA and 2 x TE buffer was taken, heated and refolded using 6S RNA re-folding program (See table 19 for more details). Consecutively, 5 x transcription buffer, heparin, ddH₂O, RNA polymerase was added and incubated at 37 °C for 30 min. Control lanes were mixed in parallel as described in the pipette scheme (see table 18 for more details). pRNA formation was triggered upon addition of nucleotides. 10 μ L of reaction mixture was withdrawn at designated time points and mixed in 10 μ L of 2 x native RNA loading dye followed by snap freezing in liquid nitrogen. Shortly before loading, the samples were thawed and loaded onto a 7.5 % native polyacrylamide gel (1 x TBE). The samples were run at 25 mA for 3 h.

Table 18: Pipette scheme for determination of kinetic rates of pRNA:6S RNA complex formation: To a master mix containing 6S RNA and σ^A -RNAP, nucleotides were added and incubated at 37 °C. 10 μ L of reaction mixture from the master mix was withdrawn at indicated time to check for formation of pRNA:6S RNA complex. The symbol " represents seconds and ' represents minutes.

Components	Free 6S RNA	σ^A-RNAP bound 6S RNA	Master mix
γ-³²P-radiolabeled 6S RNA (5000 cpm/μL)	1 μ L	1 μ L	5.5 μ L
2 x TE buffer	1 μ L	1 μ L	5.5 μ L
6S RNA re-folding programme	15 min		
5 x transcription buffer	2 μ L	2 μ L	11 μ L
Heparin (400 ng/μL)	2 μ L	2 μ L	11 μ L
ddH₂O	4 μ L	0.52 μ L	0.1 μ L
σ^A-RNAP (5.75 μM)	0	3.48 μ L	19.14 μ L
Incubation at 37 °C	30 min		
Nucleotide master mix (2 mM)	--	--	2.75 μ L
Incubation at 37 °C	15 min	15 min	10 μ L withdrawn at time points 15", 2', 5', 10', 15'
2 x native RNA loading dye	10 μ L	10 μ L	10 μ L

Table 19: 6S RNA re-folding programme

Temperature	Time
80 °C	2 min
70 °C	2 min
60 °C	2 min
50 °C	2 min
37 °C	Hold

2.4.4 Denaturing electrophoretic mobility shift assay

Denaturing 20 % PAA solution (1 L)

Urea	480 g
50 % PAA	400 mL
5 x TBE	200 mL
ddH ₂ O	make up

8 M urea (1 L)

Urea	480 g
5 x TBE	200 mL
ddH ₂ O	make up

2 x denaturing RNA loading dye

Formamide	95 % (v/v)
SDS	0.025 % (v/v)
Bromophenol blue	0.025 % (v/v)
Xylene cyanol	0.025 % (v/v)
EDTA	0.5 mM
ddH ₂ O	make up

10 % APS (100 mL)

98 % p.a. APS	10 g
ddH ₂ O	make up

Table 20: Dye migration and corresponding nucleotide length based on denaturing polyacrylamide gel percentage: The following table represents empirically derived data indicating the length of nucleotides corresponding to dye migration on a denaturing polyacrylamide (PAA) gel. Source: In house data provided by technician Dominik Helmecke.

% PAA of gel	BPB (nt)	XCB (nt)
5	35	130
6	26	106
8	19	75
10	12	55
20	8	28

The addition of 8 M urea to polyacrylamide solution induces a denaturing condition as the urea can form stacking interaction and multiple hydrogen bonds with nucleobases thereby destroying secondary structure conformations. The denaturing PAGE EMSA is ideal for checking degradation of RNA, for purification of freshly transcribed RNA or to study the length of a transcript. RNA was mixed with 2 x denaturing RNA loading dye and heated at 95 °C for 5 min. Based on the size of the RNA product the percentage of polyacrylamide (PAA) in gel was chosen (see table 20 for more details). The gel was run until the Bromophenol blue (BPB) bands of the dye reached the end of the gel.

2.4.5 pRNA transcription assay

Denaturing 25 % PAA gel (1 L)		10 x TBE buffer (1 L)	
Urea	480 g	Tris base	890 mM
PAA 50 %	500 mL	Boric acid 99.8 %	890 mM
10 x TBE	100 mL	EDTA-disodium	20 mM
ddH ₂ O	make up	ddH ₂ O	make up

pRNA transcription assay should be done using a gel of dimension 420 mm x 335 mm x 3 mm (length x breadth x thickness). 150 mL of a 25 % PAA solution was mixed along with 658 μ L of 10 % APS and 67 μ L of TEMED and poured into the gel mould. The reaction mixtures were pipetted as mentioned in table 21 along with 5 μ L of 1 nt tracer (Orange DNA loading dye, Thermo Fisher Scientific), 2500 cpm/lane of 8 nt RNA marker and 2500 cpm/lane of 14 nt RNA marker as references. A reaction mixture containing equal volumes of 6S RNA and 2 x TE buffer was taken. The reaction mixture was placed in a PCR machine and 6S RNA re-folding programme was run (see table 19 for more details). To this mixture, transcription buffer, σ^A -RNAP and RNase free double distilled water was added. The reaction mixture was incubated for 15 min at 37 °C to facilitate binding of 6S RNA to the RNA polymerase. Initiation of the transcription reaction was achieved by the addition of nucleotide master mix with a final concentration of 200 μ M ATP, GTP, CTP and UTP each and 250,000 cpm of radioactive α -³²P UTP. The total end volume of the reaction mixture was 10 μ L containing a final concentration of \sim 1 μ M cold RNA, 1 μ M RNA polymerase and 200 μ M nucleotides. After 60 min of incubation at 37 °C, 5 μ L of the reaction mixture was mixed with 15 μ L of 2 x denaturing loading dye heated for 3 min at 98 °C followed by cooling on ice for 5 min. The samples were electrophoresed on a 25 % polyacrylamide denaturing gel (8 M Urea, 1 x TBE) for 16 h at 1200 V.

Table 21: Pipette scheme for pRNA transcription: A master mix containing 6S RNA and σ^A -RNAP was taken and nucleotides were added along with radioactive UTP to visualize the freshly transcribed pRNAs in a 25 % denaturing polyacrylamide gel.

Components	Free 6S RNA	σ^A-RNAP bound 6S RNA	Master mix
6S RNA (15.15 μM)	----	0.7 μ L	0.7 μ L
2 x TE Buffer	0.7 μ L	0.7 μ L	0.7 μ L
6S RNA re-folding programme	15 min		
5 x transcription buffer	2 μ L	2 μ L	2 μ L
σ^A-RNAP (5.34 μM)	1.88 μ L	----	1.88 μ L
ddH₂O	3.45 μ L	4.63 μ L	2.75 μ L
Incubation at 37 °C	15 min		
α-³²P-UTP (250,000 cpm/lane)	0.97 μ L	0.97 μ L	0.97 μ L
Nucleotide master mix (2 mM)	1 μ L	1 μ L	1 μ L
Incubation at 37 °C	60 min		
Volume of sample withdrawn	5 μ L	5 μ L	5 μ L
2 x denaturing RNA loading dye	15 μ L	15 μ L	15 μ L

Dilution of α -³²P-UTP stock

3.75 MBq of α -³²P-UTP was ordered. 5 μ L stock dissolved in 95 μ L ddH₂O was aliquoted into four fractions of 25 μ L each and stored away in separate lead containers. 1 μ L of the diluted UTP stock equates to approximately 350,000 cpm and can be used in the pRNA transcription assay. The decay rate of any ³²P substrate can be calculated (see table 22 for more details) and the volume of the radioactive UTP to be added, can be adjusted accordingly in the pipette scheme.

Table 22: Empirically derived decay factor of radioactive Phosphorus-32: Source: Environmental health and safety department, Worcester Polytechnique Institute

Days elapsed	Decay factor	Days elapsed	Decay factor
0	1.00	16	0.460
1	0.953	17	0.438
2	0.908	18	0.418
3	0.865	19	0.398
4	0.824	20	0.379
5	0.785	21	0.361
6	0.748	22	0.344
7	0.712	23	0.328
8	0.678	24	0.312
9	0.646	25	0.297
10	0.616	26	0.283
11	0.587	27	0.270
12	0.559	28	0.257
13	0.532	29	0.245
14	0.507	30	0.233
15	0.483		

2.4.6 RemA and RNA polymerase transcription assay

RemA storage buffer (1 L)

2.5 M KCl	20 mM
2 M MgCl ₂	20 mM
1 M Hepes	20 mM
5 M NaCl	1 M
Glycerol	50 %

A 25 μ L reaction was set up as described in the pipette scheme below. Using this gel, *in vitro* transcription activation efficiency of RemA mutants were studied using the exopolysaccharides (*epsA*) gene as template. Due to the presence of multiple binding sites for RemA on the *epsA* gene promoter region, more RemA is needed

in comparison to RNA polymerase. Therefore, the final ratio of RemA to RNA polymerase was 35:1 to optimize performance activity. The transcription reaction was terminated through the addition of 2 x denaturing RNA loading dye and the mixture was loaded onto a 7.5 % polyacrylamide gel of dimensions 30 cm x 20 cm x 1 mm (length x breadth x thickness). The gel was run at 200 V for roughly 2.5 h.

Table 23: Pipette scheme to check for *eps* gene transcription by mutant RemA: The values indicated in the table are listed in volumes (μL) of the corresponding components. WT RemA lane represents the *epsA* gene transcription activity by wild type native RemA. Mutant RemA lane represents the *epsA* gene transcription activity by mutant RemA variant.

Components	No RemA	No Plasmid	No RNAP	WT RemA	Mutant RemA
Plasmid DNA 170 (100 ng/μL)	0.5	---	0.5	0.5	0.5
Tris-HCl pH 8.0 (200 mM)	1.25	1.25	1.25	1.25	1.25
MgCl₂ (200 mM)	1.25	1.25	1.25	1.25	1.25
KCl (2.5 M)	1	1	1	1	1
DTT (10 mM)	2.5	2.5	2.5	2.5	2.5
BSA (5 mg/mL)	0.5	0.5	0.5	0.5	0.5
ATP (10 mM)	1.25	1.25	1.25	1.25	1.25
GTP (10 mM)	0.5	0.5	0.5	0.5	0.5
CTP (10 mM)	0.5	0.5	0.5	0.5	0.5
UTP (5 μM)	0.5	0.5	0.5	0.5	0.5
α-³²P-UTP (100,000 cpm/lane)	0.8	0.8	0.8	0.8	0.8
ddH₂O	13.51	12.26	12.7	11.76	11.76
RemA protein (100 μM)	---	1.75	1.75	1.75	1.75
Incubation at 22 °C	10 min				
σ^A-RNAP (5.34 μM)	0.94	0.94	---	0.94	0.94
Incubation at 37 °C	15 min				
2 x denaturing RNA loading dye	25	25	25	25	25

2.4.7 Motility assay

TG Agar (1 L)

Casein peptone	10 g
Meat extract	10 g
NaCl	5 g
Agarose	0.7 % (w/v)
Adjust pH to 7.0 - 7.3 (after autoclaving and before usage)	
1 M Glucose	55 mM
Tri-phenyl tetrazolium chloride	0.3 mM

Overnight colonies from bacterial strain of interest were obtained according to section 2.1.2 and overnight culture was inoculated according to section 2.1.3. A preculture flask is needed to break spores and get metabolically active cells. 20 mL of LB medium was prewarmed to 37 °C in 100 mL unbaffled Erlenmeyer flasks and was termed “preculture flask”. The preculture has a dilution factor of 1:1000, which is achieved by introducing 20 µL of overnight culture into 20 mL of LB medium (antibiotic supplemented). The preculture flask was incubated at 37 °C in a water incubator (Aquatron) and shaken at 220 rpm until the OD₆₀₀ reaches 0.3 to 0.6. In the meantime, a main culture containing 50 mL LB medium in 250 mL baffled Erlenmeyer flask was pre-warmed to 37 °C. The pre-culture was then used to inoculate a main culture to an end point OD₆₀₀ of 0.05. Afterwards, main culture was grown at 37 °C, 220 rpm in a water incubator. Once an OD₆₀₀ of 2.0 was reached, 2 µL of cell culture was spotted onto a 0.7 % TG agar swarming plate. The plates were air dried at room temperature for exactly 20 min under a laminar flow hood. The plates were visually inspected for wetness. Plates that looked overly dried and overly wet (water droplets running around) were excluded before the start of the trial. After spotting, plates were incubated at 28 °C in an air incubator. A physical demarcation of the inoculation spot was made and the plates were left undisturbed until the swarm radii could be visualised. The swarm radius is defined as the distance between the inoculation spot and the edge of the swarm front. Upon visualisation of the swarm front, the plates were documented every hour with physical marking. As the swarm front for certain strains is translucent, using Dark Hood DH-50 90 + Gerix 1000 and

setting of the lens focus to f/4 iris, 12 x zoom, 7/20 focus, 0.04 x illumination is set standardly for all images captured. The pictures captured were digitally evaluated using the ImageJ 1.51p software.

2.4.8 Sporulation assay

DSM medium (1 L)

Difco™ nutrient broth	8 g
KCl	1 g
1 M MgSO ₄	1 mL
10 mM MnCl ₂	1 mL
(after autoclaving and before usage)	
1 M CaCl ₂	0.5 mL
100 μM FeSO ₄	100 μL

Heat resistance is a typical characteristic feature of spores. To quantify spores in a bacterial culture, it was exposed to a high temperature for an extended period of time to kill off the heat-sensitive vegetative cells and count only the heat-resistant *B. subtilis* spores. Overnight colonies from bacterial strain of interest were obtained according to section 2.1.2 and overnight culture was inoculated according to section 2.1.3. A preculture flask is needed to break spores and get metabolically active cells to give a “fair head start” to all the bacterial strains. 20 mL of LB medium was prewarmed to 37 °C in 100 mL unbaffled Erlenmeyer flasks and was termed “preculture flask”. The preculture has a dilution factor of 1:1000, which is achieved by introducing 20 μL of overnight culture into 20 mL of LB medium (antibiotic supplemented). The preculture flask was incubated at 37 °C in a water incubator (Aquatron) and shaken at 220 rpm until the OD₆₀₀ reaches 0.3 to 0.6. Upon reaching a similar optical density all the strains were centrifuged and resuspended in Difco™ sporulating medium (DSM). In the meantime, a main culture containing 100 mL LB medium in 1 L baffled Erlenmeyer flask was pre-warmed to 37 °C. The pre-culture was then used to inoculate a main culture to an end point OD₆₀₀ of 0.05. The main culture was then grown at 37 °C, 220 rpm in a water incubator. Eight hours post inoculation, the cells normally enter stationary phase. During this time point, 1 mL of culture was

withdrawn and serial diluted to extreme dilution factors in Gibco PBS buffer (pH 7.4; Thermo Fisher Scientific). 100 μL of each serial dilution concentration was plated onto a 1.5 % LB agar plate with the help of glass beads (total Colony Forming Units (CFU) = heat sensitive + heat-resistant CFUs). The remaining 900 μL was heated to 80 $^{\circ}\text{C}$ for 20 min using a dry heating block and again 100 μL of each dilution sample were plated onto LB agar plates (heat-resistant CFUs). After incubation of plates for 24 h at 37 $^{\circ}\text{C}$, single colonies were counted using ImageJ 1.51p software. The different dilutions yielded anywhere from 10 to 700 distinguishable colonies per plate. The spore forming ability of the strains were calculated using the formula below:

$$\text{Spore forming units} = \frac{\text{CFU/mL heated sample}}{\text{CFU/mL total sample}}$$

2.5 Equations

2.5.1 Ligand binding - 1 site equation

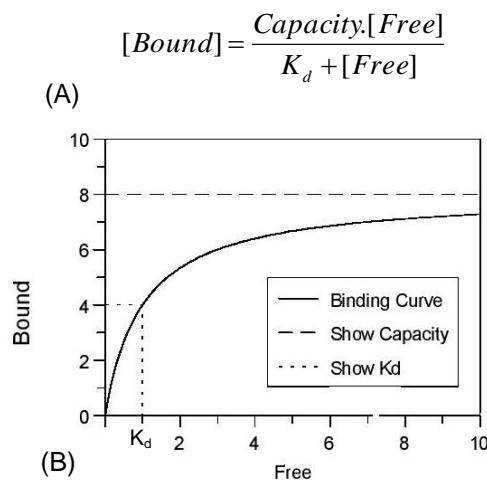


Figure 11. Ligand binding - 1 site equation (A) Formula: [Bound] represents the percentage of ligand in complex with substrate to total ligand available in the gel. [Free] is the varying concentration of substrate added, “ K_d ” is the binding affinity and “Capacity” is the saturation point of ligand-substrate complex formation. **(B) Graphical representation of ligand binding - 1 site equation:** K_d value can be obtained by first plotting the data points. Afterwards, by extrapolating the y-axis point at roughly 50 % complex formation and extending downwards towards the [free] axis from the inflection point of the curve.

Ligand binding - 1 site equation is used to determine the binding affinity (K_d) of ligand to substrate. When this equation was used in Grafit 5, the software automatically fits the data points to a single site saturation curve, where the amount of ligand bound is plotted as a function of the amount free.

2.5.2 1st order rate equation

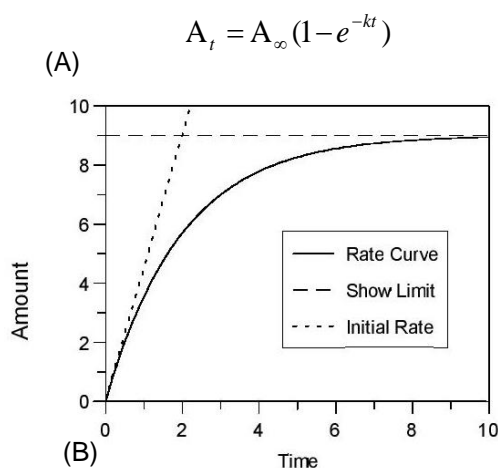


Figure 12: 1st order rate equation (A) Formula: $[A_t]$ Amount of product formed at time t . A_∞ is the amount of product formed at limit as indicated in the graph below. “ K ” is the rate constant and $[t]$ is time taken for the reaction. **(B) 1st order rate equation graph:** The graph was obtained by plotting the percentage of product denoted as $[Amount]$, formed against an incremental time scale denoted as $[Time]$. The initial rate denoted in the graph is used to derive the rate constant K .

1st order rate equation can be used in any experimental set up where product formation steadily increases with time. When this equation was used in Grafit 5, the amount of product formed to substrate available was plotted as the Y-axis against the time scale as the X-axis in order to obtain the rate curve. The rate curve in turn reveals the limit and initial rate. The negative value of initial rate is the rate constant “ K ”.

2.5.3 Spline curve

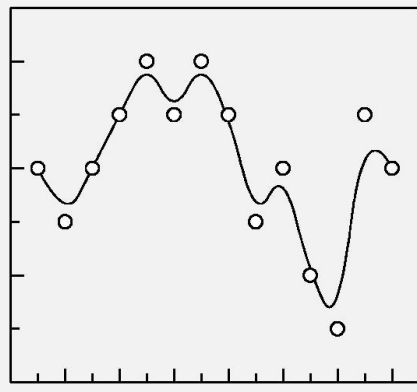


Figure 13: Spline curve diagram: Graphical representation of random data points connected by spline curve of order 3.

In Grafit 5, four orders of spline curve are available namely 3, 4, 5 and 6. The graphical illustration shown is an example from the user manual of Grafit 5. Higher orders give smoother curves. Spline curves smooth out variation in the data however they do not necessarily pass through the data points.

3. Results and discussion

3.1 Structural and functional insight into the mechanism of *Bacillus subtilis* 6S-1 RNA release from RNA polymerase

Sweetha Ganapathy¹, Philipp G. Hoch¹, Marcus Lechner², Malte Bussiek³, Roland K. Hartmann*

¹Institut für Pharmazeutische Chemie, Philipps-Universität Marburg, Marbacher Weg 6, 35037 Marburg, Germany

²Center for Synthetic Microbiology (SYNMIKRO), Bioinformatics Core Facility Karl-von-Frisch-Str. 14, 35032 Marburg, Germany

³University of Kassel, Abt. Genetik and CINSaT, Heinrich-Plett-Strasse 40 34132 Kassel, Germany

*Corresponding author:

E-mail: roland.hartmann@staff.uni-marburg.de

Author Contributions: Conceptualization, R.K.H.; investigation, S.G., P.G.H., M.B.; software, M.L.; validation, S.G., R.K.H.; resources, M.B., M.L., R.K.H.; data curation, M.L.; writing—original draft preparation, S.G., P.G.H., R.K.H.; writing—review and editing, S.G., P.G.H., M.L., M.B., R.K.H.; visualization, S.G., P.G.H., M.L., R.K.H.; supervision, R.K.H.; project administration, R.K.H.; funding acquisition, R.K.H.

Abstract

Here we investigated the refolding of *Bacillus subtilis* 6S-1 RNA and its release from σ^A -RNA polymerase (σ^A -RNAP) using truncated and mutated 6S-1 RNA variants. Truncated 6S-1 RNAs, only consisting of the central bubble (CB) flanked by two short helical arms, can still traverse the mechanistic 6S RNA cycle *in vitro* despite ~ 10-fold reduced σ^A -RNAP affinity. This indicates that the RNA's extended helical arms including the '-35'-like region are not required for basic 6S-1 RNA functionality. The role of the 'central bubble collapse helix' (CBCH) in pRNA-induced refolding and release of 6S-1 RNA from σ^A -RNAP was studied by stabilizing mutations. This also revealed base identities in the 5'-part of the CB (5'-CB), upstream of the pRNA transcription start site (nt 40), that impact ground state binding of 6S-1 RNA to σ^A -RNAP. Stabilization of the CBCH by the C44/45 double mutation shifted the pRNA length pattern to shorter pRNAs and, combined with a weakened P2 helix, resulted in more effective release from RNAP. We conclude that formation of the CBCH supports pRNA-induced 6S-1 RNA refolding and release. Our mutational analysis also unveiled that formation of a second short hairpin in the 3'-CB is detrimental to 6S-1 RNA release. Furthermore, already annealing of an LNA mimic (pLNA) of a pRNA 6-mer to 6S-1 RNA retarded the RNA's gel mobility. This effect incrementally increased with pLNA 7- and 8-mers, suggesting that restricted conformational flexibility introduced into the 5'-CB by base pairing with pRNAs prevents 6S-1 RNA from adopting an elongated shape. Accordingly, atomic force microscopy of free 6S-1 RNA versus 6S-1:pLNA 8- and 14-mer complexes revealed that 6S-1:pRNA hybrid structures, on average, adopt a more compact structure than 6S-1 RNA alone. Overall, our findings also illustrate that the wild-type 6S-1 RNA sequence and structure ensures an optimal balance of the different functional aspects involved in the mechanistic cycle of 6S-1 RNA.

Introduction

Bacterial 6S RNAs are non-coding RNAs (ncRNA) of ~ 200 nt that form a rod-shaped secondary structure with a relatively unstructured region in the center (termed central bubble) that is flanked by two, non-continuously helical arms: the terminal (closing) stem formed by the RNA's 5'- and 3'-proximal sequences and the internal (apical) stem capped by a loop. The helical arms are not perfectly base-paired, but are interspersed with short internal loops and bulges. 6S RNAs bind to the active site of RNA polymerase (RNAP) holoenzymes in complex with the major (housekeeping) sigma factor, σ^{70} and σ^A in the model organisms *Escherichia coli* and *Bacillus subtilis*, respectively. This results in differential and complex transcription inhibition effects at σ^{70}/σ^A -dependent promoters [1-6] and, as a consequence, in global modulation of transcription. A single 6S RNA gene is found in the vast majority of bacterial genomes sequenced so far; some bacteria such as *B. subtilis* even express two 6S paralogs (6S-1 and 6S-2 RNA). A bioinformatic analysis predicted more than 1,700 6S RNAs in >1,600 bacterial species [7], even including extremophiles such as the hyperthermophile *Aquifex aeolicus* [8], although this bacterium has a parsimonious, highly condensed genome and abandoned another prominent ncRNA, the catalytic RNA of RNase P [9]. This indicates an important, though not absolutely essential function of 6S RNA in bacteria. Phenotypic analysis of 6S RNA deficient bacterial strains revealed dysregulations under various stress conditions (reviewed in [4,6,10]. Binding specificity of 6S RNAs for RNAP is achieved by structurally mimicking an open DNA promoter [1,11]. A cryo-EM structure of *E. coli* σ^{70} -RNAP in complex with a 6S RNA derivative revealed B-DNA-like helical parameters in the paired regions of 6S RNA as a major component of this structural mimicry [12]. Based on the cryo-EM structure and biochemical/mutational studies in the *E. coli* system, a '-35'-like region in the internal (apical) arm of 6S RNA and a '-10'-like region located in the 3'-central bubble (3'-CB; see Figure 1) were pinpointed as key recognition elements for binding to σ^{70} -RNAP [12-14]. The open DNA promoter mimicry of 6S RNAs also enables RNAP to utilize the RNA as a template for the transcription of short abortive transcripts termed product RNAs (pRNAs; [15]). The abundance and length pattern of pRNAs

increases with intracellular NTP concentration, particularly of the initiating nucleotide (GTP) in the case of *B. subtilis* 6S-1 RNA-derived pRNA synthesis [15-19]. These pRNAs, when reaching a certain length (13 nt for *E. coli* 6S RNA, 14 nt for *B. subtilis* 6S-1 RNA; [14,16]) and depending on their GC content, have such low rate constants for dissociation from 6S RNA that they stably rearrange the 6S RNA structure. This triggers the release of 6S RNA:pRNA complexes from RNAP as an escape mechanism from the transcriptional block [15,17,20]. In the case of canonical 6S RNAs, this release mechanism is operational during outgrowth of cells from stationary phase upon nutrient resupply [4,17]. The pRNA-induced 6S RNA rearrangement involves unwinding of 6S RNA helix P2 and formation of the 6S RNA hybrid helix between the transcribed pRNA and the 5'-proximal sequence of the 5'-central bubble (5'-CB; Figure 1). For 6S RNAs from *E. coli* and other γ -proteobacteria, unwinding of the helix P2 pendant (also termed downstream helix; [14]) allows formation of a 9-bp long hairpin in the 3'-CB that was shown to make a major contribution to 6S RNA release induced by pRNAs as short as 13-mers [14]. In contrast, other 6S RNAs, such as *A. aeolicus* 6S RNA or *B. subtilis* 6S-1 RNA, do not form such an extended hairpin in the 3'-CB. In the case of *B. subtilis* 6S-1 RNA, a smaller 3'-CB hairpin already forms in free 6S-1 RNA, which appeared to be stabilized in the 6S-1 RNA:pRNA hybrid structure [17]. However, in *B. subtilis* 6S-1 RNA and *A. aeolicus* 6S RNA, another structural element was inferred to form upon pRNA transcription, termed the 'central bubble collapse helix (CBCH)', involving the 3'-strand of P2 and the distal sequence of the 5'-CB (Figure 1; [17,21]. These findings suggest differences in the pRNA-induced 6S RNA release mechanism of *E. coli*- and *B. subtilis*-type 6S RNAs.

Here we show that truncated variants of 6S-1 RNA, solely consisting of the CB flanked by two short helical arms (see Figure 2A, B), can still traverse the mechanistic 6S RNA cycle *in vitro*, despite decreased σ^A -RNAP affinity. This indicates that the '-35' region is not strictly essential for the basic 6S-1 RNA function. Using strategic 6S-1 RNA mutants, we further characterized the role of the CBCH in the kinetics of the 6S-1 RNA rearrangement/release mechanism and its influence on pRNA length patterns. We observed that certain mutations in the 5'-CB upstream of the pRNA transcription start site (nt 40) rapidly impair 6S-1 RNA: σ^A -RNAP ground state binding. Stabilizing the CBCH shifted the pRNA

length pattern to shorter pRNAs. A 6S-1 RNA variant with a weakened helix P2 was more effectively refolded and released from the enzyme in the presence of the stabilized CBCH. Our mutational analysis also revealed that formation of a second short hairpin in 3'-CB is detrimental to 6S-1 RNA release. From our results we conclude that formation of the CBCH supports pRNA-induced 6S-1 RNA refolding and release. We further studied the 6S-1 RNA rearrangement by native PAGE upon stable annealing of LNA versions of pRNAs of different length (6-, 7- and 8-mers) to determine if the rearrangement of 6S-1 RNA structure and 6S-1 RNA: σ^A -RNAP complex decay may require a certain minimum pRNA length. Finally, we analyzed the shape of free 6S-1 RNA versus 6S-1:pLNA complexes by atomic force microscopy, revealing that 6S-1:pRNA hybrid structures, on average, adopt a more compact structure than 6S-1 RNA alone.

Materials and methods

Purification of *B. subtilis* RNA polymerase

Native *B. subtilis* σ^A -RNA polymerase holoenzyme was prepared according to [22] and His-tagged σ^A -RNAP as described recently [23]. σ^A -RNAP concentrations were determined by Bradford assay. A calibration curve was established using quick start bovine serum albumin (BSA) (Cat #5000206, Bio-Rad) to prepare 800 μ L samples with 0, 2, 4, 6, 8 or 10 μ g BSA (referred to the final volume of 1 mL). These samples were mixed with 200 μ L of Protein Assay Dye Reagent Concentrate (Cat # 5000006, Bio-Rad) and incubated for 5 min at room temperature. Samples were then transferred into 1 mL cuvettes and absorption was measured at 595 nm in a spectrophotometer. For measurement of test samples, 2 μ L of the RNAP preparation were diluted with 798 μ L ddH₂O; all following steps were as for the calibration curve samples. For converting weight concentration into molar concentration, we assumed an average molecular weight of 440 kDa for σ^A -RNAP preparations based on ~ 340 kDa for the core enzyme plus 60 kDa for sub-stoichiometric amounts of σ^A , δ and HeID ([23]; Figures 4 and 5 therein).

Cloning of 6S-1 RNA constructs

The pUC18 derivative pUC18_m6S1, encoding the full-length mature 6S-1 RNA (gene: *bsrA*, 190 nt; [16]) under control of a class III T7 promoter, was chosen as the backbone to construct all 6S-1 RNA mutants. Mutagenesis was performed according to standard procedures. Briefly, the entire plasmid was amplified by PCR, using back-to-back primers (manually designed or using Snapgene 4.1.9), one mutagenic primer with 5'-proximal or internal mismatches to introduce nucleotide substitutions (see NEB web page, <https://international.neb.com/applications/cloning-and-synthetic-biology/site-directed-mutagenesis>). After agarose gel purification of the PCR product, the 5'-ends of primer elongation products were phosphorylated using T7 polynucleotide kinase, the template strands were digested with DpnI and the amplified strands were circularized by T4 DNA ligase in a one-tube reaction. For some constructions, primers were already 5'-phosphorylated before the PCR reaction. After transformation into *E. coli* DH5 α cells and selection on ampicillin-containing agar plates, clones were identified by DNA sequencing. For the construction of 6S-1 RNA genes with combined mutations in different regions, the construction was performed in two steps. As an example, the 5'-portion of 6S-1 RNA helix P2 was mutated in the first step as just described. After mutation verification by DNA sequencing, the plasmid obtained after this first PCR mutagenesis round was used as template to introduce the compensatory mutations into the 3'-strand of helix P2 in a second PCR.

In vitro transcription of B. subtilis 6S-1 RNA variants and synthetic pRNA / pLNA oligonucleotides

6S-1 RNA variants were transcribed from linearized plasmid templates by runoff transcription using T7 RNA polymerase as described, followed by transcript purification on usually 7.5% denaturing (8 M urea) polyacrylamide gels as described [23]. Synthetic 6S-1 pRNA 8-mer (5'-OH-GUU CGG UC) and 14-mer (5'-OH-GUU CGG UCA AAA CU) used as size markers were synthesized by Noxxon Pharma AG (Berlin, Germany) or Integrated DNA Technologies (IDT) Europe. All-LNA versions of the 8-mer (5'-GTT CGG TC) and 14-mer (5'-GTT CGG TCA AAA CT) were obtained from Axolabs (Kulmbach, Germany)

6S RNA refolding

To ensure uniform folding of 6S RNA after denaturing gel purification, 100 nM of T7-transcribed RNA, containing trace amounts of the same 5'-³²P-labeled RNA (2,500 Cherenkov c.p.m. per gel lane), were adjusted to 1 x TE buffer (10 mM Tris pH 8.0, 1 mM EDTA). The mixture was then heated to 80°C in a thermocycler (Biometra); after 2 min of holding time at 80°C, the temperature was lowered to 70°C and kept for 2 min at 70°C; this was repeated for temperature shifts to 60 and 50°C, followed by shifting to and maintaining the temperature at 37°C. For Figures 2E and F, a somewhat different refolding protocol was used: 5 min each at 95, 90, 80, 70, 60 and 50°C, followed by transfer to 37°C (≥ 5 min).

Gel shift assay to assess 6S RNA: σ^A -RNAP complex formation

1 μ L of T7-transcribed and refolded 6S RNA (100 nM) containing trace amounts of the same 5'-³²P-labeled RNA (2,500 Cherenkov c.p.m. per gel lane), 2 μ L 5 x transcription buffer (200 mM of Tris-HCl pH 8.0, 25 mM MgCl₂, 800 mM KCl, 5 mM dithiothreitol), 2 μ L of heparin solution (400 ng/ μ L, Sigma-Aldrich), a varying concentration of native or his-tagged σ^A -RNAP (specified in the corresponding figure legend) and RNase-free ddH₂O were combined to a final volume of 10 μ L. Dilutions of σ^A -RNAP stock solutions were made in RNA polymerase storage buffer [10 mM Tris-HCl pH 8.0, 10 mM MgCl₂, 0.1 mM EDTA, 0.1 mM dithiothreitol, 0.1 M NaCl and 50% (v/v) glycerol]. The aforementioned 10 μ L reaction mixtures were incubated for 30 min at 37°C, followed by mixing with 10 μ L 2 x native loading dye [10 % (v/v) glycerol, 10 mM MgCl₂, 0.025 % (w/v) bromophenol blue and 0.025 % (w/v) xylene cyanol blue] and loading onto a native 7.5% native polyacrylamide (PAA) gel [running buffer 1 x TBE; glass plate dimensions 30 cm x 20 cm x 1 mm (L x B x H)], typically run for 3 h at 25 mA. In the experiments shown in Fig. 2C, native PAGE was conducted in an electrophoresis buffer containing 0.5 x TBE, 160 mM KOAc, 5 mM Mg(OAc)₂, 1 mM DTT, pH 8.6, with correspondingly adjusted electric field strength to prevent substantial warming of the gel during electrophoresis [17]. Gels were exposed overnight to a phosphorimaging plate (Fujifilm). Radioactive bands were visualized and quantified using a FLA-3000 Fluorescent Image Analyzer (Fujifilm) and the software BAS Reader (version 3.14) and AIDA (version 3.45.039). Data

fitting of binding curves was based on three independent experiments (if not stated otherwise), using the software Grafit, version 5.0.13 (Erithacus Software).

Native gel assay to assess NTP dependence of the pRNA-induced rearrangement of 6S-1 RNA and its release from RNAP

For the NTP concentration variation experiment in Figure 5, a set of 10.5 μL mixtures containing 3.5 μL 6S-1 RNA (100 nM stock concentration with trace amounts of 5'- ^{32}P -labeled 6S-1 RNA; a total of $\sim 9,000$ Cherenkov c.p.m. for withdrawal of 3 time point aliquots, corresponding to 2,500 c.p.m. per gel lane; see below) in 1 x TE buffer were subjected to the refolding protocol. Then, 7 μL of 5 x transcription buffer (see above), 7 μL of heparin solution (400 ng/ μL) and ~ 1 μL of ddH₂O were added per reaction. To each sample, with a time interval of 7 min, 2.5 μL of native σ^A -RNAP was added. The 7 min time delay was required for staggered incubation with NTPs and aliquot withdrawal later down the work flow. Each sample was incubated for 30 min at 37°C to reach equilibrium of 6S-1 RNA binding to σ^A -RNAP. Reactions were started by adding 7 μL of NTP mix (final reaction volume: 35 μL) to adjust the NTP concentration to either 40, 80, 120, 160 or 200 μM each NTP [A/C/G/UTP mixes of 200 μM , 400 μM , 600 μM , 800 μM and 1000 μM of each NTP were usually made from 100 mM stock solutions (Carl Roth, Karlsruhe, Germany) by dilution in ddH₂O]; the final concentration of 6S-1 RNA was 10 nM and that of σ^A -RNAP 2 μM . After 15 s, 1 min and 2 min at 37°C, 10 μL aliquots were withdrawn, mixed with 10 μL of 2 x native loading dye (see above) and put immediately on ice. The collected three aliquots were then loaded onto a 7.5% native PAA gel [running buffer 1 x TBE; glass plate dimensions 30 cm x 20 cm x 1 mm (L x B x H)] that was running at low current (~ 5 to 10 mA) to avoid diffusion of initially loaded samples from gel pockets until all pockets were loaded. Then, 7 μL of a differently concentrated NTP solution were added to the next 28- μL sample, proceeding as just described. After loading the last aliquot set, the current was increased to 25 mA for 3 h. Phosphorimaging and data evaluation were performed as described in 2.5.

Native gel assay to analyze 6S-1 RNA rearrangement kinetics at a specific NTP concentration

5.5 μL of 5'- ^{32}P -labeled 6S RNA ($\sim 2,500$ Cherenkov c.p.m per μL) were combined with 5.5 μL of 2 x TE buffer (20 mM Tris pH 8.0, 2 mM EDTA) and refolded as described in paragraph 2.4. Then, 11 μL of 5 x transcription buffer (see above), 11 μL of heparin solution (400 ng/ μL), between ~ 12 and 19 μL of His-tagged σ^{A} -RNAP (stock concentrations varied between 5.75 and 9.05 μM) and RNase-free ddH₂O were added to a total volume of 53.6 μL . The reaction mixture was incubated for 1 h at 37°C to equilibrate 6S RNA binding to σ^{A} -RNAP. Subsequently, 1.4 μL of an A/C/G/UTP mix (2 mM each NTP) was added (final volume: 55 μL) to start the reaction at 37°C. The reaction mixtures contained final concentrations of 2 μM His-tagged σ^{A} -RNAP, 50 μM each NTP and trace amounts (2,500 Cherenkov c.p.m per gel lane) of 5'- ^{32}P -labeled 6S RNA. 10 μL aliquots were withdrawn after 15 s and 2, 5, 10 and 15 min, to which 10 μL of 2 x native loading dye (see above) were added, followed by shock freezing in liquid N₂. Samples were loaded onto a native 7.5% PAA gel (running buffer 1 x TBE; gel dimensions see above) that was run for 3 h at 25 mA. Control samples lacking NTPs, or enzyme and NTPs, were prepared and handled in the same manner as the test samples before loading onto the gel (incubation time at 37°C for at least 15 min). Phosphorimaging and data evaluation were performed as described in 2.5. ATP omission experiments followed the same protocol, except that a C/G/UTP mix was added to a final concentration of 100 μM each. Data fitting of complex decay curves was based on three independent experiments using the software Gfit, version 5.0.13.

pRNA transcription assay using native σ^{A} -RNAP

For the experiment shown in Figure 3D, 2 μL of in vitro T7-transcribed 6S RNA (stock concentration: 15 μM) were combined with 2 μL of 2 x TE buffer and subjected to the refolding protocol (see above). Then 3 μL of 5 x transcription buffer (see above), 2.4 μL of native σ^{A} -RNAP (stock concentration: 15.84 μM) and 3.1 μL of RNase-free ddH₂O were added to a volume of 12.5 μL . The reaction mixture was incubated for 15 min at 37°C to equilibrate binding of

6S RNA to σ^A -RNAP. Subsequently, 2 μ L of NTP mix (ATP, GTP, CTP and UTP, each 1.5 mM) plus 0.52 μ L [α - 32 P]UTP (250,000 Cherenkov c.p.m per reaction mixture) were added. The final concentrations in the reaction mixture were 2 μ M for the 6S RNA variant, 2.5 μ M for native σ^A -RNAP and 200 μ M for each NTP. The final reaction mixture (~ 15 μ L) was incubated for up to 1 h at 37°C. After incubation, 5 μ L of the reaction mixture was withdrawn and mixed with 15 μ L of 2 x denaturing loading dye [95% (v/v) formamide, 0.025% (v/v) SDS, 0.025% (v/v) bromophenol blue, 0.025% (v/v) xylene cyanol, 0.5 mM EDTA], heated for 3 min to 98°C in a dry bath (Biometra), followed by cooling on ice for 5 min. Control samples (final volume: 15 μ L) either lacking native σ^A -RNAP or without 6S RNA were subjected to the same conditions as the test samples. Samples were loaded onto denaturing 25% PAA gel [8 M urea; running buffer 1 x TBE; gel plate dimension 42 cm x 33.5 cm x 0.3 cm (L x B x H)] that was run for 16 h at 1200 V. Phosphorimaging and data evaluation was performed as described in 2.5. A slight variation of this protocol was applied to pRNA transcription of RNAs 6S-1 wt and C44_45 (Figure 4C). Here, the differences included a final volume of 20 instead of 15 μ L, a native σ^A -RNAP final concentration of 1 μ M, and withdrawal of 5 μ L aliquots at time points 5, 20 and 60 min post-nucleotide addition.

pRNA transcription assay using His-tagged σ^A -RNAP

4 μ L of T7-transcribed 6S RNA (stock concentration ~ 15 μ M) and 4 μ L of 2 x TE buffer (20 mM Tris pH 8.0, 2 mM EDTA) were mixed and subjected to the RNA refolding procedure (see above). Then, 6 μ L of 5 x transcription buffer (see above), ~ 1 to 5 μ L of His-tagged σ^A -RNAP (stock concentration varied from 5.75 μ M to 9.05 μ M) and RNase-free ddH₂O were added to a total volume of 24.2 μ L, followed by equilibration for 15 min at 37°C. Approx. 12 μ L aliquots of this reaction mixture were transferred into two new tubes, followed by addition of 2.9 μ L of A/C/G/UTP mix or C/G/UTP mix (1.39 mM each NTP); the resulting ~ 15 μ L then contained [α - 32 P]UTP (250,000 Cherenkov c.p.m per lane), 270 μ M end concentration of each indicated NTP, 2 μ M 6S RNA and ~ 0.4 μ M His-tagged σ^A -RNAP; pRNA transcription was allowed to proceed for 1 h at 37°C. Thereafter, 5 μ L of the reaction mixture were withdrawn and mixed with 15 μ L of 2 x denaturing loading dye (see above), heated for 3 min to 98°C in a dry bath,

followed by cooling on ice for 5 min. Control samples either lacking His-tagged σ^A -RNAP or 6S RNA were treated in the same manner. For details on electrophoresis, see the preceding paragraph.

Annealing of pLNA/pRNA oligonucleotides to 6S-1 RNA

10 pmol of 6S-1 RNA were mixed with trace amounts of 5'-³²P-labeled 6S-1 RNA (10,000 Cherenkov c.p.m.) and 0.4 μ L 10 x TE buffer. The volume was adjusted to 4 μ L with RNase-free ddH₂O. Then 2 μ L of a 50 μ M stock solution of the respective pLNA or pRNA oligonucleotide was added and the mixture was successively incubated for 5 min each at 95, 90, 80, 70, 60 and 50°C, followed by transfer to 37°C for at least 5 min. Subsequently, 1 μ L of heparin (400 ng/ μ L), 2 μ L of 5 x transcription buffer (see above) and either ~ 1.1 μ L native σ^A -RNAP (stock concentration: 8 mg/mL) or 1.1 μ L double-distilled RNase-free ddH₂O (for controls without RNAP) were added. Mixtures were incubated for 30 min at 37°C, then supplemented with 10 μ L of 2 x native RNA loading dye (see above) and analyzed by 10% native PAGE.

Atomic force microscopy (AFM)

For AFM analysis, the RNA was prepared as follows: 1 μ L of a 10 μ M stock solution of *in vitro* T7-transcribed 6S-1 RNA was mixed with a tenfold molar excess of the respective pLNA oligonucleotide in a final volume of 10 μ L adjusted to 1 x TE buffer. The annealing protocol was the same as described in the preceding paragraph. To remove excess pLNA oligonucleotides, samples containing the pLNA 8- or 14-mer were centrifuged three times, with 500 μ L 1x TE buffer per round, through Amicon Ultra centrifugal filter units (molecular weight cut-off: 10 kDa). Before the actual measurements, the density of molecules was recorded in a test image; depending on the observed density, RNA mixtures were diluted with 1 x TE buffer to adjust the working concentrations to ~ 1 - 4 nM. RNA solutions were transferred to a mica surface treated with poly-L-lysine (MW 500-2000, Sigma-Aldrich) as described [24]. Pictures were taken using a Veeco Multimode Nanoscope IIIa AFM device with silicon tips (Tap300Al-G, BudgetSensors, Sophia) in tapping mode (resonance frequency: 300 kHz, scan rate: 1 Hz). Pictures were recorded with an edge length of 1 μ m. The AFM images were analyzed using 'ImageJ 1.51' [25]. Particles with a size of

0.3 to 0.64 μm^2 and a circularity ($c = 4\pi \times [\text{area}]/[\text{perimeter}]^2$) of 0.2 to 0.6 were annotated as 6S-1 RNA molecules. For each of these particles an ellipse was fitted. The ratio of the longitudinal (long) and latitudinal (short) axis length (see Figure 13C) were used to describe the molecule shape. Smaller ratios are indicative of more compact and possibly bent molecules while larger ratios indicate more stretched conformations.

RNAfold and RNAcomposer predictions

Secondary structure predictions were computed on the RNAfold web server 2.4.18 ([26]; <http://rna.tbi.univie.ac.at>) using the default parameters. For simulating complexes of 6S-1 RNA and pRNAs, the corresponding pRNA binding site was blocked using constraint folding with the 'Enforce Constrained pairing pattern' option. 3D structure predictions were performed with RNAcomposer ([27]; <https://rnacomposer.cs.put.poznan.pl>). For RNAcomposer prediction of the 6S-1:pRNA complex, the 6S-1 RNA sequence was extended at the 5'-end by a linker sequence (here 25 cytidines) and the pRNA sequence at the very 5'-end, mimicking an artificial pseudoknot structure; very similar results were obtained with U25, A25 or G25 linkers or longer homopolymeric linkers of 50, 75 or 100 nt that were analyzed in comparison.

Results

Analysis of 6S-1 RNA derivatives with large truncations

In the *E. coli* system, biochemical studies and the cryo-EM structure of the σ^{70} -RNAP complex have led to the identification of structural 6S RNA elements that correspond to the -35 and -10 regions of DNA promoters and interact with σ^{70} as well as the β and β' subunits of the core RNAP [12-14]. These 6S RNA elements coincide with the 3'-CB (-10 element) and, by inference from the *E. coli* system, roughly with the P5 helix and its two flanking internal loops (-35 element) in *B. subtilis* 6S-1 RNA (Figure 1). The P2 region interacts with β and β' while the terminal stem region (corresponding to helix P1 in Figure 1A) was shown to be dispensable for complex formation [12,13]. To gain insight into the interaction of *B. subtilis* 6S-1 RNA and σ^A -RNAP, we constructed two extensively truncated derivatives of *B. subtilis* 6S-1 RNA, a 78-nt long variant (6S₇₈) and a very similar

but circularly permuted variant ($6S_{82cp}$), 82-nt in length, both lacking the '-35' region (Figure 2A, B). The $6S_{82cp}$ variant was constructed to evaluate possible effects caused by fraying of the 5'- and 3'-termini upon helix P2 disruption during pRNA synthesis. Both truncation variants showed 50% complex formation with σ^A -RNAP at $\sim 1 \mu\text{M}$ enzyme, whereas the same enzyme bound full-length 6S-1 RNA with a K_d of $\sim 100 \text{ nM}$ (Figure 2C). Nevertheless, the truncated RNAs preserved the ability to serve as a template for the synthesis of pRNA 14/15-mers (Figure 2D, lanes 6 and 7), although with reduced efficiency relative to full-length 6S-1 RNA (lane 5), particularly in the case of RNA $6S_{82cp}$. Complexes of RNA $6S_{78}$ with pRNA formed over time, but migrated rather diffusely (Figure 2E), suggesting conformational heterogeneity possible due to end fraying of the closing helix. In the case of RNA $6S_{82cp}$, a second slower migrating band was already recognizable in the control (Figure 2F, lane 1), for unknown reasons. Time-dependent release from RNAP upon induction of pRNA synthesis was evident for RNA $6S_{78}$ (Figure 2E, cf. lanes 5-7 and 2-4). Release (Figure 2F) and pRNA transcription (Figure 2D) were particularly inefficient for RNA $6S_{82cp}$, which is likely related to the constraints imposed by the artificial capping loop of helix P2. Altogether, these findings demonstrate that the basic mechanistic features of 6S-1 RNA are maintained, though with reduced efficiency, when the RNA's size is reduced to the CB solely flanked by the immediate helical elements that confine the CB. The results also demonstrate the contribution of structural elements in the helical arms of native 6S-1 RNA, such as the putative -35 region, to ground state binding affinity of 6S-1 RNA for σ^A -RNAP.

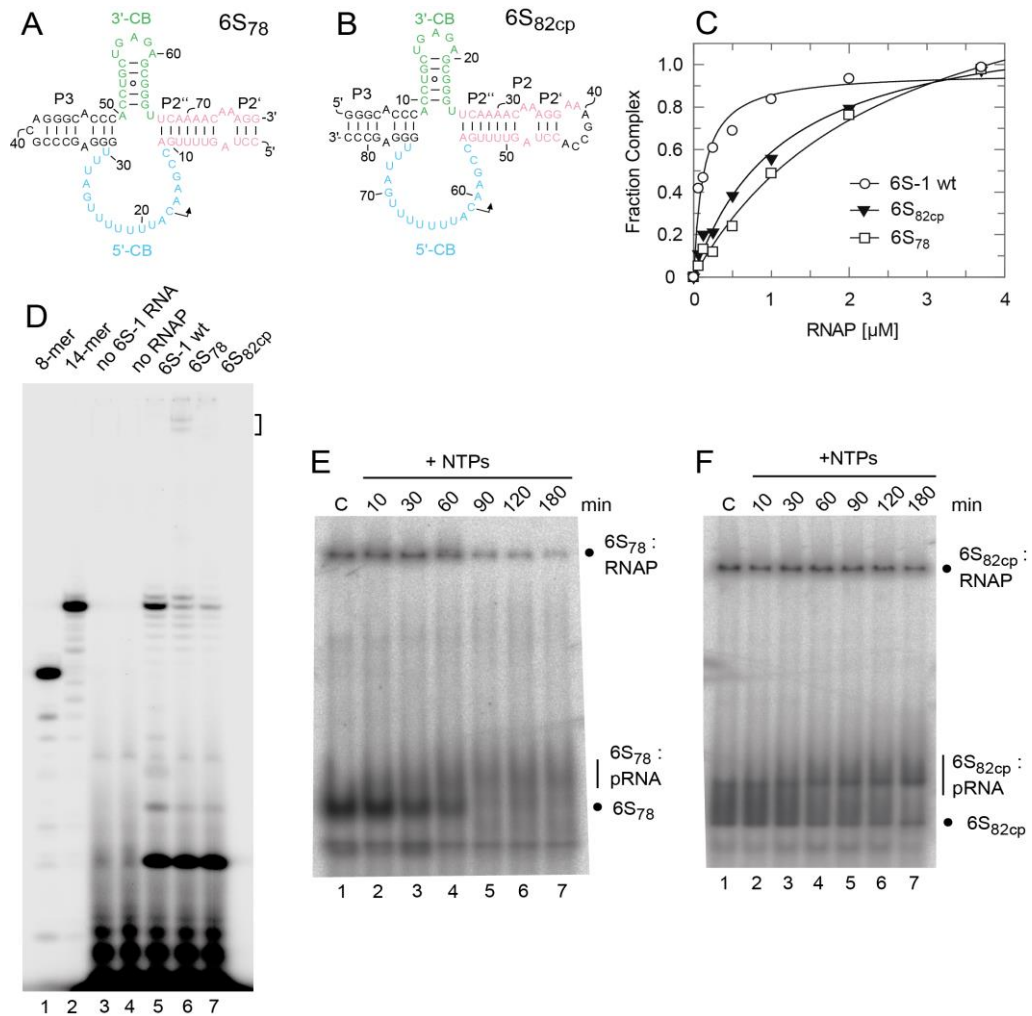


Figure 2. (A, B) Secondary structures of the truncated 6S-1 RNA derivatives (A) 6S78 (78 nt) and (B) 6S82cp (82 nt, circularly permuted) lacking larger parts of the terminal and internal stem, including the -35 region. Circular permutation was introduced to assess potential end fraying upon unwinding of the closing stem helix during pRNA transcription. The (terminal) closing stem helix P2 is depicted in pink, the 3'-central bubble (3'-CB) in green, and the 5'-central bubble (5'-CB) in light blue. (C) Binding of wt 6S-1 RNA, mutant RNA 6S82cp and mutant RNA 6S78 to σ^A -RNAP, analyzed by gel shift assay (see Materials and Methods). A representative experiment is shown. The curves are fits to a one ligand binding site model; as K_D values for the two mutant RNAs were calculated with endpoints considerably above 1, they are not given here; $K_{1/2}$ values (50% complex relative to the endpoint) were approx. 100 nM for wt 6S-1 RNA and around 1 μ M for the two mutant RNAs. (D) pRNA transcription using wt 6S-1 RNA or one of the two truncation variants as template (lanes 5-7). Lanes 1 and 2, 5'- 32 P-end-labeled (2,500 Cherenkov c.p.m.) synthetic 6S-1 pRNA 8-mer (lane 1) and 14-mer (lane 2); lanes 3 and 4, controls lacking either 6S RNA (lane 3) or enzyme (lane 4); lanes 5-7: pRNA transcription for 1 h at 37°C in the presence of 2 μ M of the respective 6S RNA variant, 2.5 μ M σ^A -RNAP, 200 μ M each NTP, and 250,000 c.p.m

of [^{32}P]-UTP per lane. The bracket at the upper right marks bands attributable to hybrids of 6S78 RNA and pRNA runoff transcripts (17-mers). (E, F) 5'- ^{32}P -end-labeled 6S78 or 6S82_{cp} RNA was preincubated with σ^{A} -RNAP for 30 min at 37°C. Then NTPs were added to the mixture to induce transcription of pRNAs and the samples were incubated at 37°C for the time period indicated above each lane. The final concentrations were 1 μM for 6S78 RNA, 2 μM for σ^{A} -RNAP and 200 μM each NTP. Lanes C, no NTPs added and incubation at 37°C for 180 min. For details, see Materials and Methods. These experiments were conducted with the native σ^{A} -RNAP.

Role of the central bubble collapse helix (CBCH) in the rearrangement and 6S-1 RNA release from RNAP

The rearrangement and release mechanism of *B. subtilis* 6S-1 RNA differs from that of 6S RNAs of *E. coli* and related γ -proteobacteria. In the latter, the 3'-CB is essentially unstructured in the free state, but an extended hairpin (9 bp) forms between nucleotides of the 3'-CB and the 3'-strand of helix P2 (also called downstream duplex; [12]), when P2 is disrupted during pRNA synthesis. This hairpin was shown to play a key role in the release mechanism in the *E. coli* system [14]. As a shorter hairpin (with 5 and potentially up to 7 bp according to RNAfold prediction; Figure 1A) already forms in the 3'-CB of free *B. subtilis* 6S-1 RNA [17] and no extended hairpin forms during pRNA synthesis, this raised the question whether the CBCH may play a supporting role in the 6S-1 RNA release process in addition to formation of the pRNA:6S-1 RNA hybrid helix. We initially approached this question by introducing the A50U mutation into 6S-1 RNA, which was expected to slightly stabilize the CBCH (Figure 1B). When we tested this mutant 6S-1 RNA for binding to σ^{A} -RNAP, we observed a two-fold increase in K_{d} (Figure 3A). Similar two- to threefold K_{d} increases were also observed for A50C and A50G mutations (Figure 3B, C), indicating that the base identity of residue A50 in the 5'-CB plays a role in the interaction with σ^{A} -RNAP. We then tested if the CBCH stabilization by the A50U mutation may energetically favor the pRNA-induced rearrangement of 6S-1 RNA and thereby somewhat shift the pRNA length pattern to shorter pRNAs. However, the pRNA length pattern did not differ substantially from that of wt 6S-1 RNA (Figure 3D). For a more substantial stabilization of the CBCH, we mutated residues U44/45 to cytosines (termed mutant C44/45 in the following), thus converting the tandem G:U to G:C pairs (Figure 1B). This double mutation decreased σ^{A} -RNAP binding affinity also

two-fold (Figure 4A) and up to three-fold with other RNAP preparations (not shown). Here, pRNA transcription assays clearly revealed a higher proportion of pRNAs shorter than 14 nt (mainly 11- and 12-mers) when using the SG7 RNAP as enzyme and the C44/45 mutant RNA as template (Figure 4B, lane 7 vs. 5, marked by the vertical line at the right margin). This effect was even enhanced (for unknown reasons) with the native RNAP (Figure 4C). These findings provided evidence that the C44/45 double mutation may energetically favor the pRNA-induced rearrangement of 6S-1 RNA to such an extent that pRNAs shorter than 14 nt (10 to 12-mers) can now more effectively trigger the rearrangement of 6S-1 RNA and its release from σ^A -RNAP.

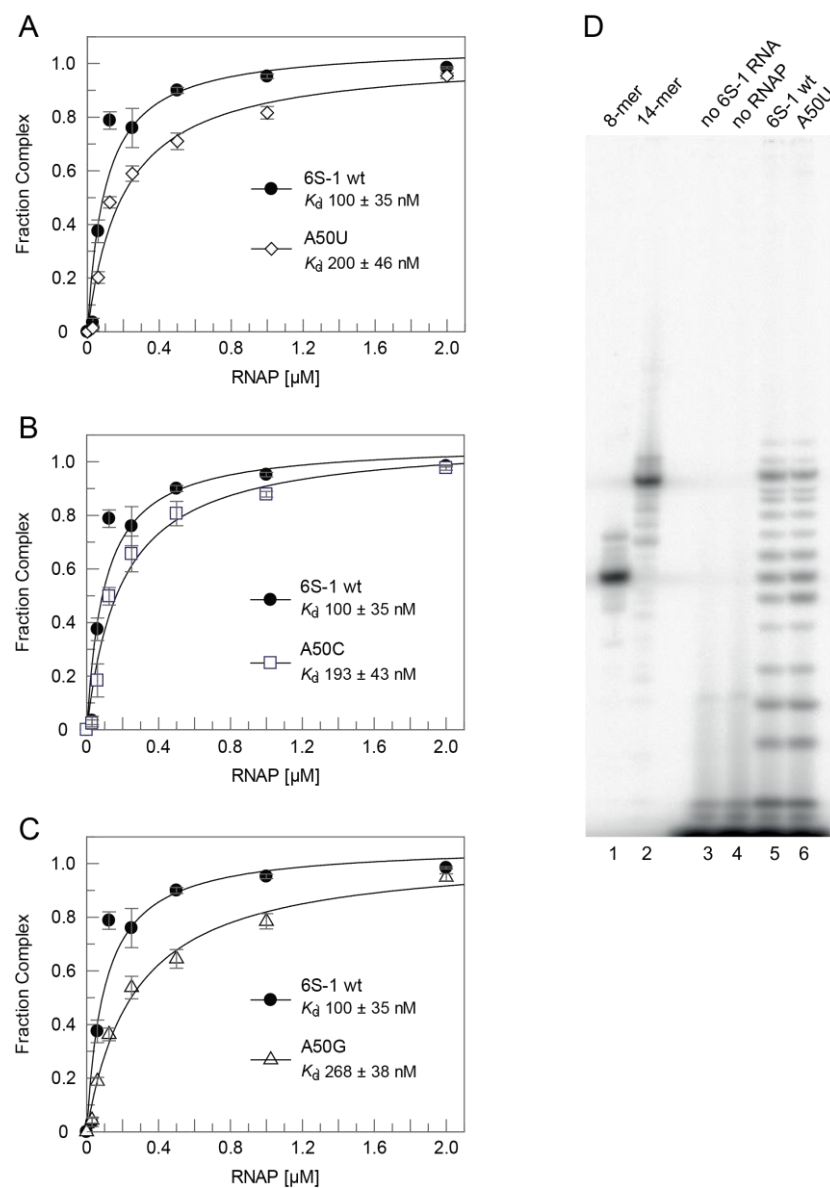


Figure 3. σ^A -RNAP affinity of 6S-1 RNA A50 mutants and pRNA transcription pattern of the A50U mutant RNA. (A-C) σ^A -RNAP affinity of mutant RNAs (A) A50U, (B) A50C and (C) A50G relative

to wt 6S-1 RNA, measured by gel shift assay using the native σ^A -RNAP. The calculated K_D values (fit to a one ligand binding site model) are indicated within each graph (error bars, SEM). (D) pRNA transcription using the wt (lane 5) and A50U mutant (lane 6) 6S-1 RNA as template, performed as in Figure 2D. Lanes 1 and 2, 5'- 32 P-end-labeled synthetic 6S-1 pRNA 8-mer (lane 1) and 14-mer (lane 2); lanes 3 and 4, controls lacking either 6S RNA (lane 3) or enzyme (lane 4). For details, see Materials and Methods. These experiments were conducted with the native σ^A -RNAP.

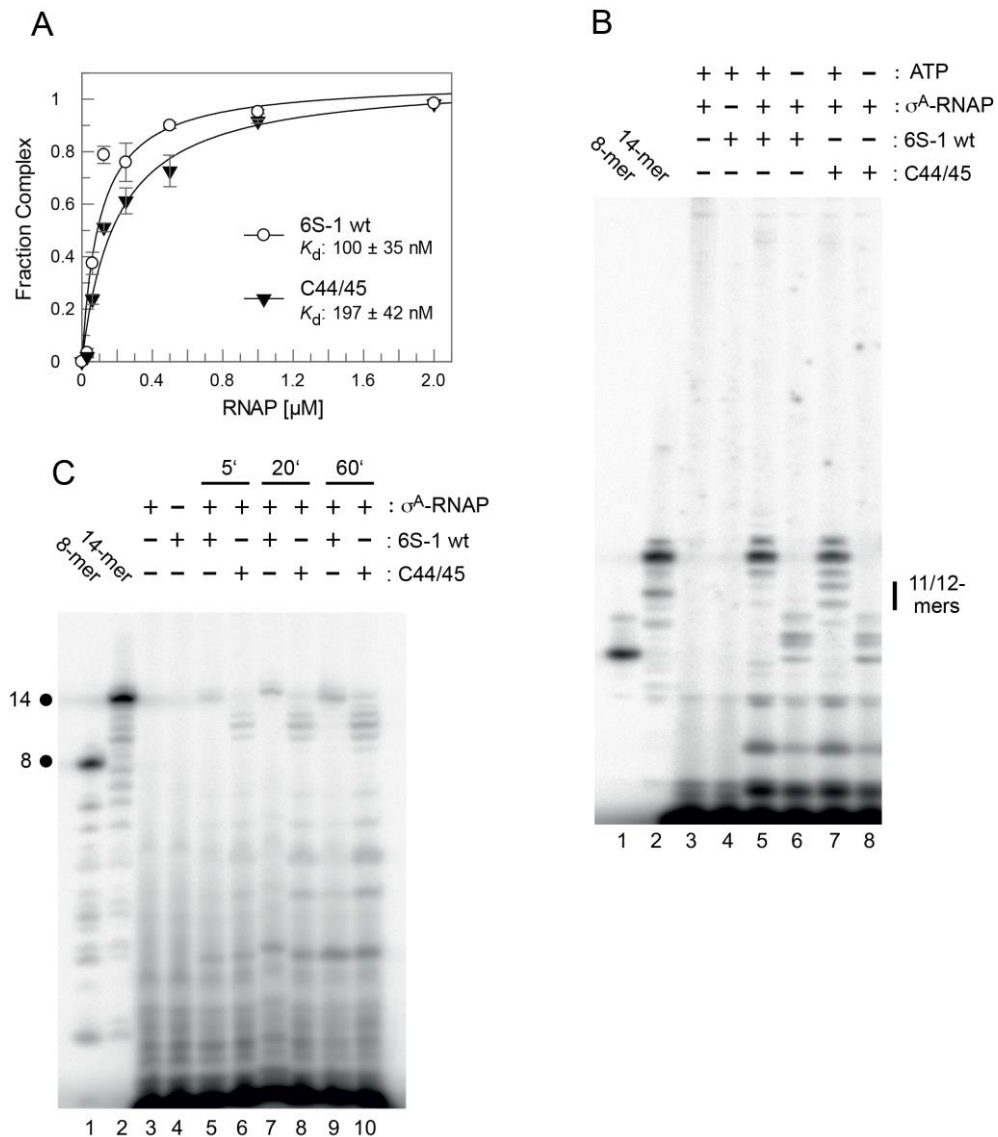


Figure 4. σ^A -RNAP binding affinity and pRNA transcription pattern for the wt and C44/45 mutant 6S-1 RNAs. (A) Binding affinity of mutant C44/45 relative to wt 6S-1 RNA (see Figure 1) to native σ^A -RNAP; K_D values, determined as in Fig. 3A-C, are indicated within the graph. (B) pRNA transcription for 1 h at 37°C using the wt (lanes 4-6) or C44/45 mutant (lanes 7 and 8) 6S-1 RNA as template (2 μ M), σ^A -RNAP (0.41 μ M) prepared from strain SG7, 270 μ M each NTP (lanes 3-5, 7), or 270 μ M CTP, UTP and GTP (lanes 6 and 8), and 250,000 c.p.m of [α - 32 P]-UTP per lane.

Lanes 1 and 2, 5'-³²P-endlabeled synthetic 6S-1 pRNA 8-mer (lane 1) and 14-mer (lane 2) used as size markers; lanes 3 and 4, controls lacking 6S RNA (lane 3) or enzyme (lane 4); the vertical line at the right margin indicates the increased abundance of mainly pRNA 11- and 12-mers in lane 7 vs. 5. The observation of pRNAs longer than 8-mers in the absence of ATP indicates non-templated product extension or misincorporation of NTPs other than ATP. For details, see Materials and Methods. (C) pRNA transcription for 1 h 37°C on wt or C44/45 mutant 6S-1 RNA (2 μM) using the native σ^A -RNAP (1 μM), 200 μM each NTP, and 250,000 c.p.m of [α -³²P]-UTP per lane. For more details, see Materials and Methods.

As a next step, we evaluated the 6S-1 RNA rearrangement/release kinetics as a function of NTP concentration (Figure 5). In this setup, complexes of 6S-1 RNA and σ^A -RNAP were preformed and pRNA transcription was induced by the addition of NTP substrates, followed by withdrawal of aliquots at different time points. The experiment illustrated in Figure 5 showed that the pRNA-mediated rearrangement of 6S-1 RNA (resulting in retarded gel mobility) and its release from σ^A -RNAP gains substantial momentum at NTP concentrations > 40 μM. Evidently, there are two subpopulations of 6S-1 RNA: σ^A -RNAP complexes, one reacting in the fast phase of the reaction (≤ 15 s) and the other reacting with slower kinetics (see also Figure 7). The subpopulation reacting in the fast phase increases with increasing NTP concentration (Figure 5). We then analyzed the rearrangement kinetics for wt 6S-1 RNA and the C44/45 mutant RNA at 100 μM each NTP to determine if the C44/45 RNA may be released faster than the wt RNA. Yet, no significant differences between the wt and C44/45 mutant RNA were observed and major fractions of both RNAs were released during the initial fast phase (≤ 15 s) (Figure 6A; quantification not shown). We also investigated the rearrangement/release kinetics under ATP omission conditions (only CTP/GTP/UTP added, which should restrict pRNA synthesis to 8-mers) to examine if the C44/45 mutant RNA might be more efficient in RNA release from RNAP, as suggested by the pRNA transcription pattern (Figure 4B, C). As expected from previous results [17], stable 6S-1 RNA:pRNA complexes could not be resolved in gel shift assays upon ATP omission (Figure 6B). The decay of 6S-1 RNA:RNAP complexes was very slow and essentially lacked an initial fast phase of release with both RNA variants (Figure 6C), suggesting that fast release requires the synthesis of pRNAs > 8-mers. The C44/45 mutant RNA showed a

trend toward somewhat faster release and lower endpoint relative to wt 6S-1 RNA (Fig. 6C).

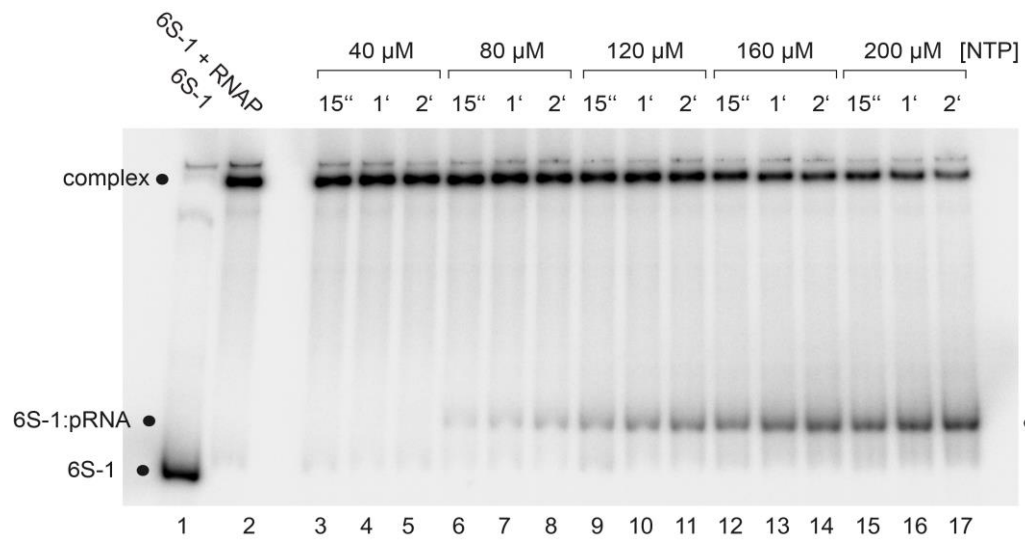


Figure 5. NTP concentration dependence of pRNA synthesis as well as 6S-1 RNA rearrangement and release, analyzed by gel shift assay. Lane 1, 6S-1 RNA (10 nM unlabeled RNA plus 2,500 Cherenkov c.p.m. of 5'-³²P-endlabeled 6S-1 RNA); lane 2, as lane 1 plus 2 μM native σ^A -RNAP; lanes 3-17, as lane 2, but followed by adjustment to the indicated NTP concentration and withdrawal of aliquots at 15 s, 1 min and 2 min post-NTP addition. Samples were loaded onto a native 7.5% PAA gel. For further details, see Materials and Methods.

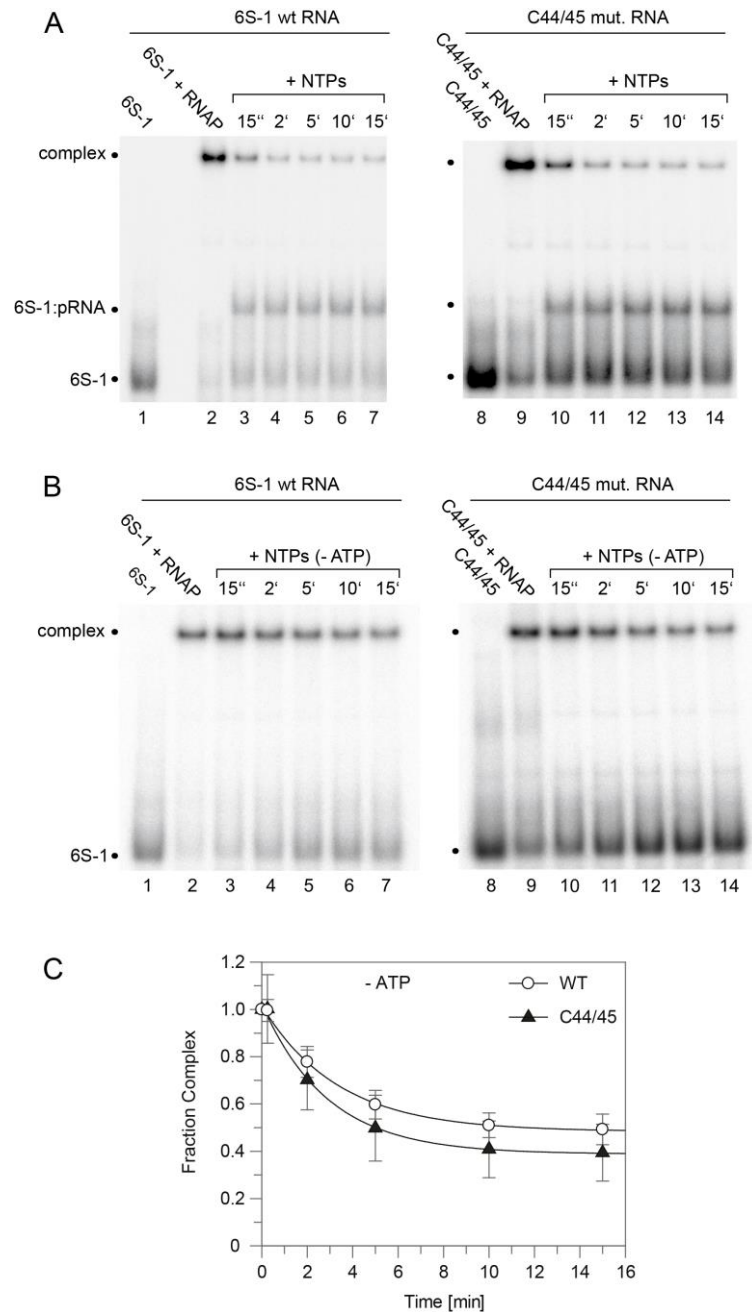


Figure 6. pRNA-induced rearrangement and release of wt and C44/45 mutant 6S-1 RNA upon addition of (A) all four NTPs or (B) CTP/GTP/UTP only. Each NTP had a final concentration of 100 μ M. (A) Lanes 1 and 8, 5'- 32 P-end-labeled 6S-1 RNA only (2,500 Cherenkov c.p.m.); lanes 2 and 9, 10 nM 6S-1 RNA incubated with 2 μ M SG7 σ^A -RNAP; lanes 3-7 and 10-14, as lanes 2 and 9, but followed by addition of NTPs and withdrawal of aliquots at the indicated time points. (B) As in panel A, but addition of CTP/GTP/UTP only (-ATP) in lanes 3-7 and 10-14. Samples were loaded onto a running native 7.5% PAA gel. (C) Kinetics of wt and C44/45 6S-1 RNA release from σ^A -RNAP upon pRNA-induced 6S-1 RNA refolding in the presence of CTP/GTP/UTP only; based on two independent experiments including the one shown in panel B (error bars, SEM). The data was fit to an equation for a single exponential with offset, yielding rate constants k of $0.3 \pm 0.03 \text{ min}^{-1}$ (wt) and $0.35 \pm 0.04 \text{ min}^{-1}$ (C44/45) and offsets (= endpoints representing release-

resistant complexes) of 0.48 ± 0.01 (wt) and $0.39 \pm 0.02 \text{ min}^{-1}$ C44/45). For further details, see Materials and Methods.

For better handling of manual kinetics, we reduced the concentration for each of the four NTPs from 100 to 50 μM each. Comparison of the release (complex decay) kinetics of wt and C44/45 mutant 6S-1 RNA yet revealed no major differences between the two (Figure 7). To accentuate the differences between wt and C44/45 mutant 6S-1 RNAs, we designed RNA variant 8M (8 mutations in P2) in the wt and C44/45 context (Figure 8A). Beforehand, we observed that major sequence changes in P2 adjacent to the CB (6S-1 RNA mutants UUUUswap and P2swap) had no or very minor effects ($< \text{two-fold}$) on ground state binding (Figure S1). The rationale for constructing the 8M mutant RNA was to change the pRNA-coding sequence such that pRNA 11-mers are transcribed in the absence of ATP (versus 8-mers in the case of wt RNA); the generated 11-mer:6S-1 8M RNA duplexes were predicted to have a ΔG of -20.7 kcal/mol (Figure 8A), thus close to the stability of the duplex formed between wt 6S-1 RNA and complementary pRNA 14-mers ($\Delta G = -22.4 \text{ kcal/mol}$; Figure 1B). With the 8M design, we speculated on seeing a more pronounced advantage of the C44/45 8M vs. wt 8M variant to undergo the structural rearrangement in the presence of such shorter pRNA:6S-1 RNA hybrids. As a side effect, the 8M mutations slightly stabilized helix P2 (predicted $\Delta G = -13$ vs. -9.2 kcal/mol for the wt RNA; Figure 8A). Again, σ^A -RNAP affinity was ~ 1.5 -fold lower for the C44/45 8M relative to the wt 8M RNA (Figure 8B), but pRNA transcription patterns were essentially identical (Figure 8C). The 8M variants now formed gel-resolvable 6S:pRNA 11-mer complexes under ATP omission conditions (Figure 9A). However, when we analyzed the 6S RNA release kinetics, we observed a much lower fraction of released 6S RNA at the endpoint for variant wt 8M (52%) relative to variant C44/45 8M (82%; Figure 8D). RNAfold analysis provided an explanation for this finding: in variant C44/45 8M, formation of the CBCH is favored upon disruption of helix P2 during pRNA synthesis, whereas a hairpin structure forming in the 3'-CB, made possible by the 8M mutations, is favored in the case of the wt 8M RNA (Figure 8A, bottom structures). This unintended effect

indicates that an extra hairpin, whenever it forms in the 3'-CB, acts as an impediment to the release from σ^A -RNAP upon pRNA synthesis.

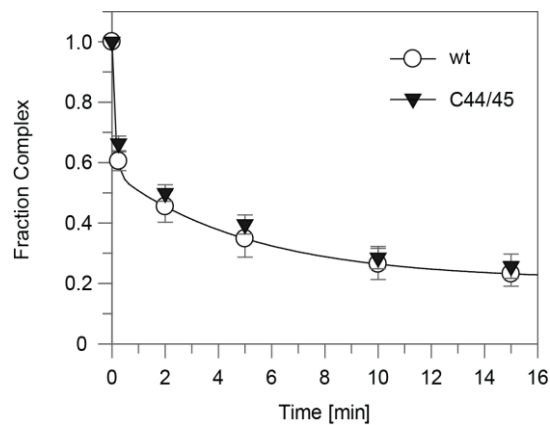


Figure 7. Kinetics of wt and C44/45 6S-1 RNA release from σ^A -RNAP (= complex decay) upon pRNA-induced 6S-1 RNA refolding. The setup was the same as in Figure 6A but conducted with only 50 μ M of each NTP. After electrophoresis, the band corresponding to the 6S-1 RNA:RNAP complex and the lane segment including free 6S-1 RNA and rearranged 6S-1 RNA:pRNA hybrids were quantified (see section 2.5) for each lane; the sum of both yielded the total radioactivity in each lane; the radioactivity of the complex band was then divided by the total radioactivity in the lane, and the resulting complex fraction was normalized to the fraction of complex at time point zero. The data was fit to an equation for a double exponential curve with offset. The rate constant k_1 for the fast phase was calculated as $8.4 \pm 0.02 \text{ min}^{-1}$ (wt) and $7.2 \pm 1.6 \text{ min}^{-1}$ (C44/45), that for the slow phase (k_2) as 0.19 min^{-1} (wt) and $0.17 \pm 0.04 \text{ min}^{-1}$ (C44/45); the release-resistant complex fraction (at the endpoint) was 0.21 (wt) and 0.22 (C44/45). For details, see Materials and Methods.

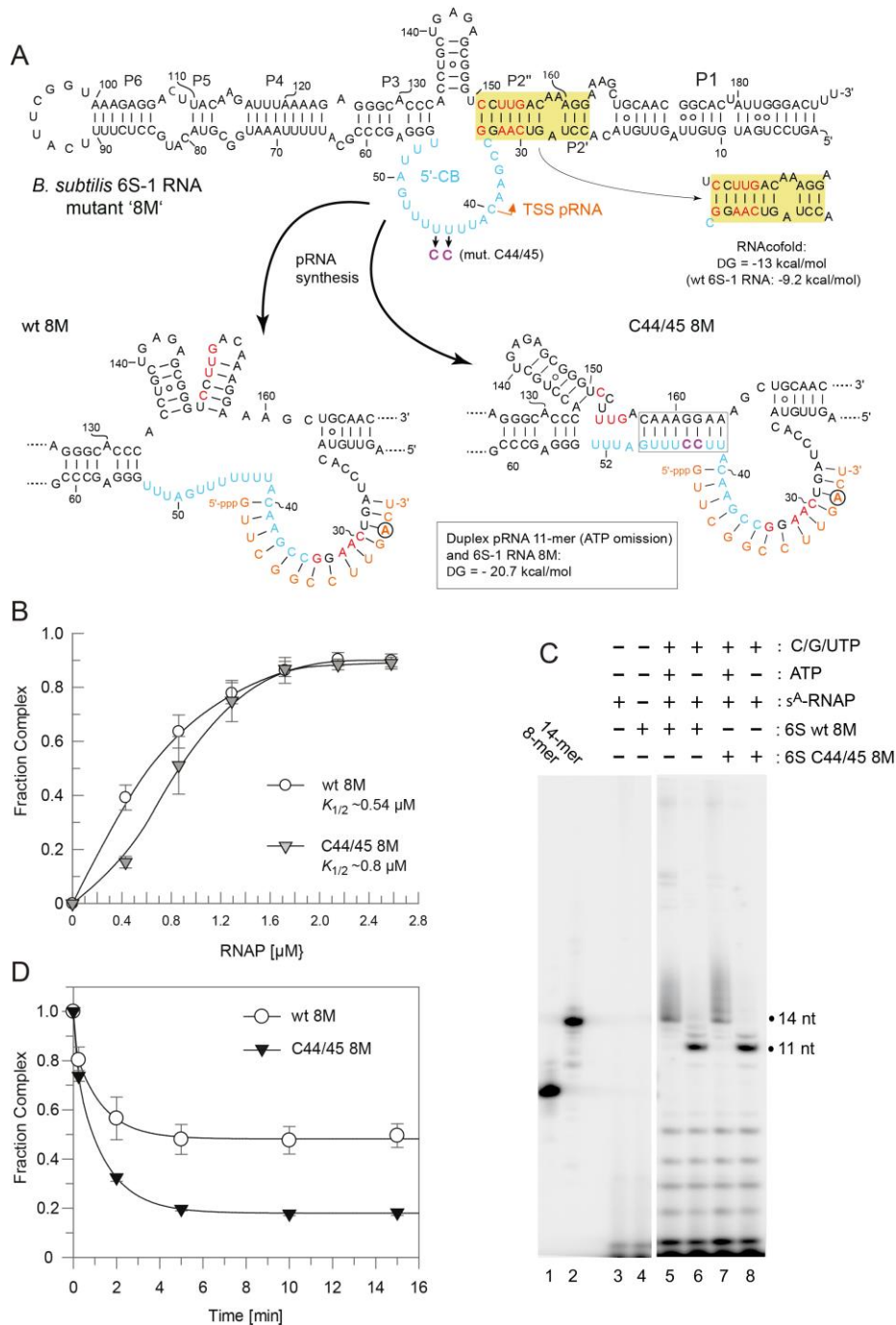


Figure 8. Characterization of wt 8M and C44/45 8M 6S-1 RNAs. (A) Secondary structure of the two 6S-1 RNA variants in the free state (top) and after the structural rearrangement (bottom) induced by pRNA transcription. The eight mutations (8M) are highlighted in red, the C44/45 mutations in magenta. In the sketches of the rearranged structures (bottom), the favored structures based on RNAfold dot plot analysis are shown. The first A residue in the pRNA sequence is marked by a circle. The ΔG of the 6S-1 8M RNA:pRNA 11-mer hybrid helix is predicted as -20.7 kcal/mol (RNAfold), compared with -22.4 for a pRNA 14-mer annealed to wt 6S-1 RNA (Figure 1B). (B) σ^A -RNAP binding affinity of the two 6S-1 RNA variants. $K_{1/2}$ gives the σ^A -RNAP concentration at half-maximal saturation. The curves are approximating curves

(B-spline of order 3; data point errors, SEM). (C) pRNA transcription by SG7 σ^A -RNAP (0.45 μM) using either wt 8M or C44/45 8M RNA (1.06 μM) as template, and in the presence of all four NTPs (each 200 μM) or with CTP, GTP and UTP (each 200 μM), but lacking ATP, as indicated above lanes 5-8. Lanes 1 and 2, 5'- ^{32}P -end-labeled synthetic 6S-1 pRNA 8-mer (lane 1) and 14-mer (lane 2) used as size markers; lanes 3 and 4, controls lacking either 6S RNA (lane 3) or enzyme (lane 4). The observation of pRNAs longer than 8-mers (lanes 6 and 8) in the absence of ATP indicates product extension by non-templated addition or misincorporation of NTPs other than ATP. For more details, see Materials and Methods. These experiments were conducted with SG7 σ^A -RNAP. (D) Kinetics of pRNA-induced complex decay for wt 8M or C44/45 8M RNAs using SG7 σ^A -RNAP (2 μM) and 100 μM each CTP, GTP and UTP; under these conditions, mainly pRNA 11-mers were synthesized based on the results shown in panel C. Complexes of 6S-1 RNA and σ^A -RNAP were preformed and pRNA transcription was induced by the addition of NTP substrates, followed by withdrawal of aliquots at different time points and their loading onto a running native 7.5% PAA gel. Data evaluation was performed as described in the legend to Figure 7 and in Materials and Methods. The rate constants k_1 for the fast phase could not be stably predicted, those for the slow phase (k_2) were $0.78 \pm 0.12 \text{ min}^{-1}$ (wt 8M) and $0.72 \pm 0.08 \text{ min}^{-1}$ (C44/45 8M), the release-resistant complex fractions were 0.48 (wt 8M) and 0.18 (C44/45 8M).

To avoid formation of this extra hairpin, we constructed variant 6M by reverting C151 and U153 in variant 8M back to U and A residues respectively (Figure 10A). This slightly reduced the predicted stability of helix P2 from $\Delta G = -9.2$ (wt 6S-1 RNA) to -7.3 kcal/mol . As a consequence, RNAfold dot plot analysis now predicted formation of the CBCH instead of P2 already in the free C44/45 6M mutant RNA, but not in the wt 6M RNA. As before, we compared σ^A -RNAP affinity of the variants wt 6M and C44/45 6M, again showing an almost three-fold reduction in RNAP affinity owing to the C44/45 mutations (Figure 10B). In the pRNA transcription pattern, 11-mers were prominent under ATP omission conditions, although non-templated 12 to 14-mers appeared as well (Figure 10C, lanes 6 and 8), somewhat more pronounced than in the case of the 8M variants (Figure 8C). Remarkably, the release extent and kinetics were now clearly increased for the 6M mutant in the C44/45 vs. wt background (Figure 10D). Furthermore, the rearranged 6S-1 RNA:pRNA hybrids formed by the 6M variants appeared as more distinct bands on native gels than the 8M mutants (cf. Figure 9A and B), suggesting that a weaker P2 helix formation potential has a stabilizing effect on the 6S-1 RNA:pRNA hybrid structures.

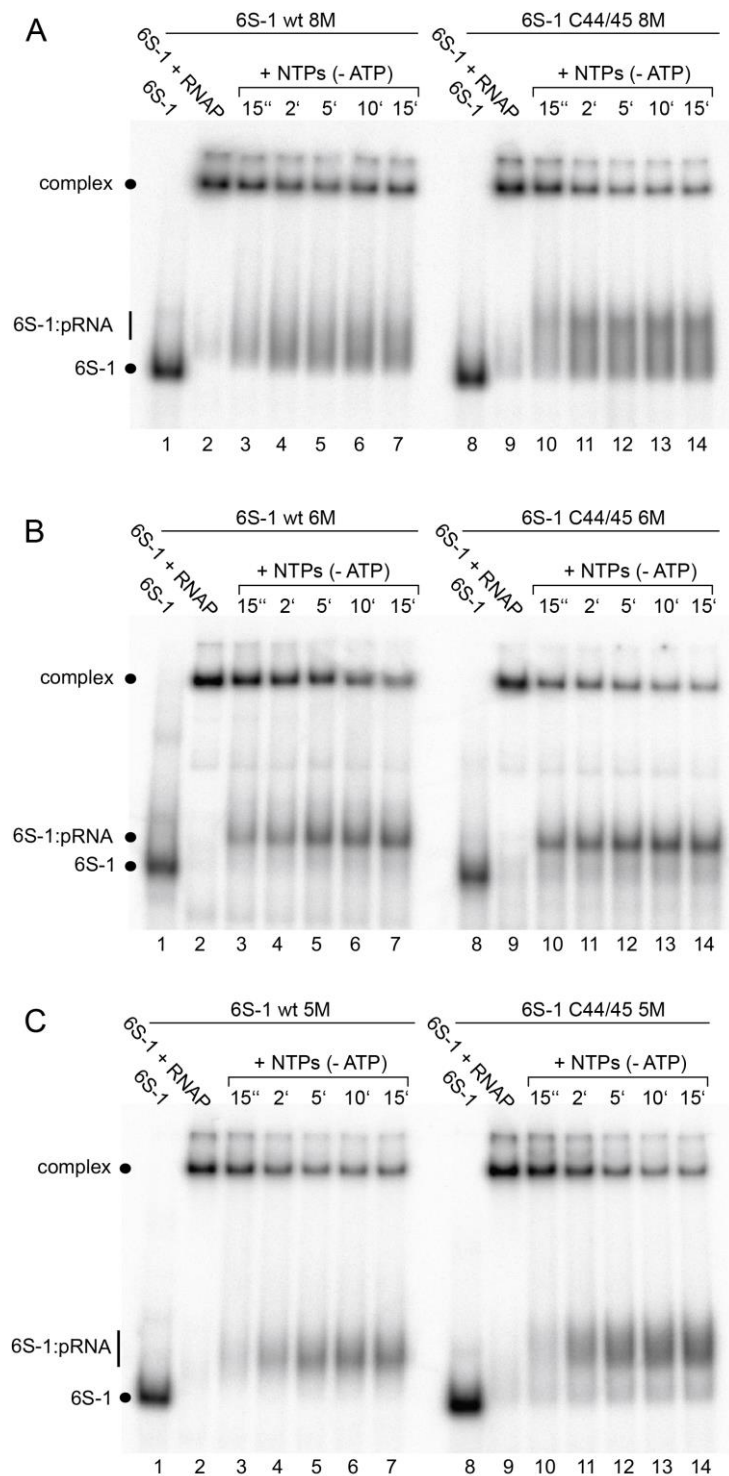


Figure 9. pRNA-induced rearrangement of 6S-1 RNA variants (A) wt and C44/45 8M, (B) wt and C44/45 6M, and (C) wt and C44/45 5M in the presence of trace amounts of 5'-³²P-endlabeled 6S-1 RNA (2,500 Cherenkov c.p.m. per lane), 2 μ M SG7 σ^A -RNAP and 100 μ M each CTP, GTP, UTP. Samples were loaded onto a running native 7.5% PAA gel. For further details, see Materials and Methods.

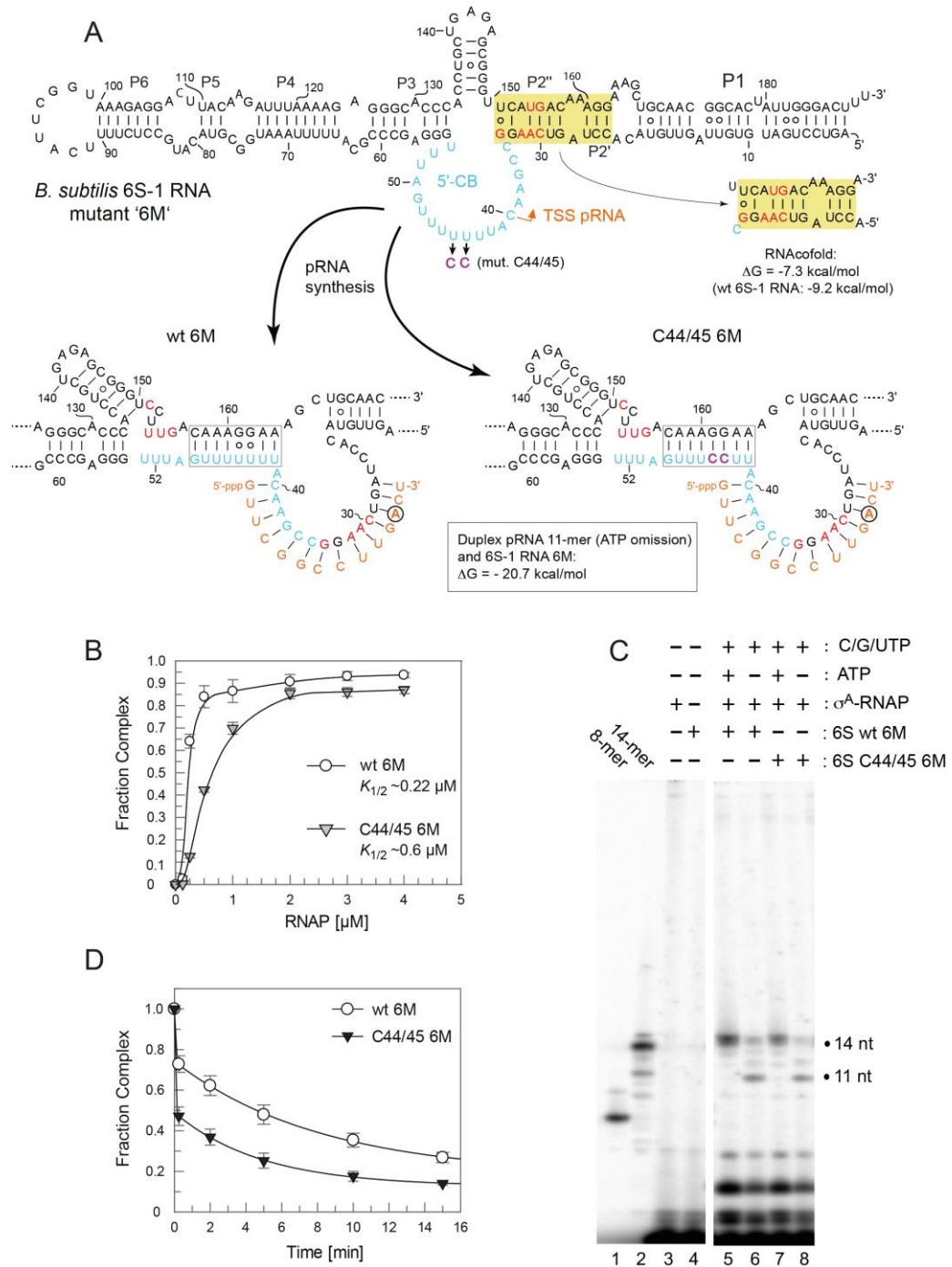


Figure 10. Characterization of 6S-1 RNA variants wt 6M and C44/45 6M (A) Secondary structure of the two 6S-1 RNA variants in the free state (top) and after the structural rearrangement (bottom) induced by pRNA transcription. The six mutations (6M) relative to the wt RNA are highlighted in red, the C44/45 mutations in magenta. In the sketches of the rearranged structures (bottom), the favored structures based on RNAfold dot plot analysis are shown. The first A residue in the pRNA sequence is marked by a circle. (B) σ^A -RNAP binding affinity for 6S-1 RNA variants wt 6M and C44/45 6M (B-spline order 3 curves). For more details, see legend to Figure 8B. (C) pRNA transcription by SG7 σ^A -RNAP using the two 6S-1 mutant RNAs as templates, as detailed in the

legend to Figure 8C. (D) Kinetics of pRNA-induced complex decay of wt 6M or C44/45 6M RNAs using SG7 σ^A -RNAP (2.6 μM) and 100 μM each CTP, GTP and UTP; under these conditions, mainly pRNA 11-mers were synthesized based on the results shown in panel C. Data evaluation was performed as described in the legend to Figure 7 and in Materials and Methods. The rate constants k_1 for the fast phase could not be stably predicted, those for slow phase (k_2) were $0.12 \pm 0.02 \text{ min}^{-1}$ (wt 6M) and $0.21 \pm 0.01 \text{ min}^{-1}$ (C44/45 6M), the release-resistant complex fractions were 0.18 (wt 6M) and 0.13 (C44/45 6M).

Finally, we again slightly reinforced helix P2 by reverting A32 to U to restore one internal base pair (variants 5M; Figure 11A; predicted P2 stability: -11.4 vs. -9.2 kcal/mol for the wt RNA). As a consequence, 8-mers were the major pRNA species expected under ATP omission conditions (Figure 11A), although 9 to 11-mers appeared as well (Figure 11C, lanes 7-10; Figure S2). These pRNAs formed gel-resolvable complexes with the 5M variants (Figure 9C). For unknown reasons, the 5M design caused a particularly pronounced deterioration of RNAP binding in the C44/45 relative to wt background (Figure 11B). Regarding extent and kinetics of release (complex decay), the wt 5M variant became slightly faster in the slow phase than the C44/45 5M variant ($k_2 = 0.45$ vs. 0.36 min^{-1}), but still formed more release-resistant complexes than the C44/45 5M RNA (0.31 vs. 0.19; Figure 11D).

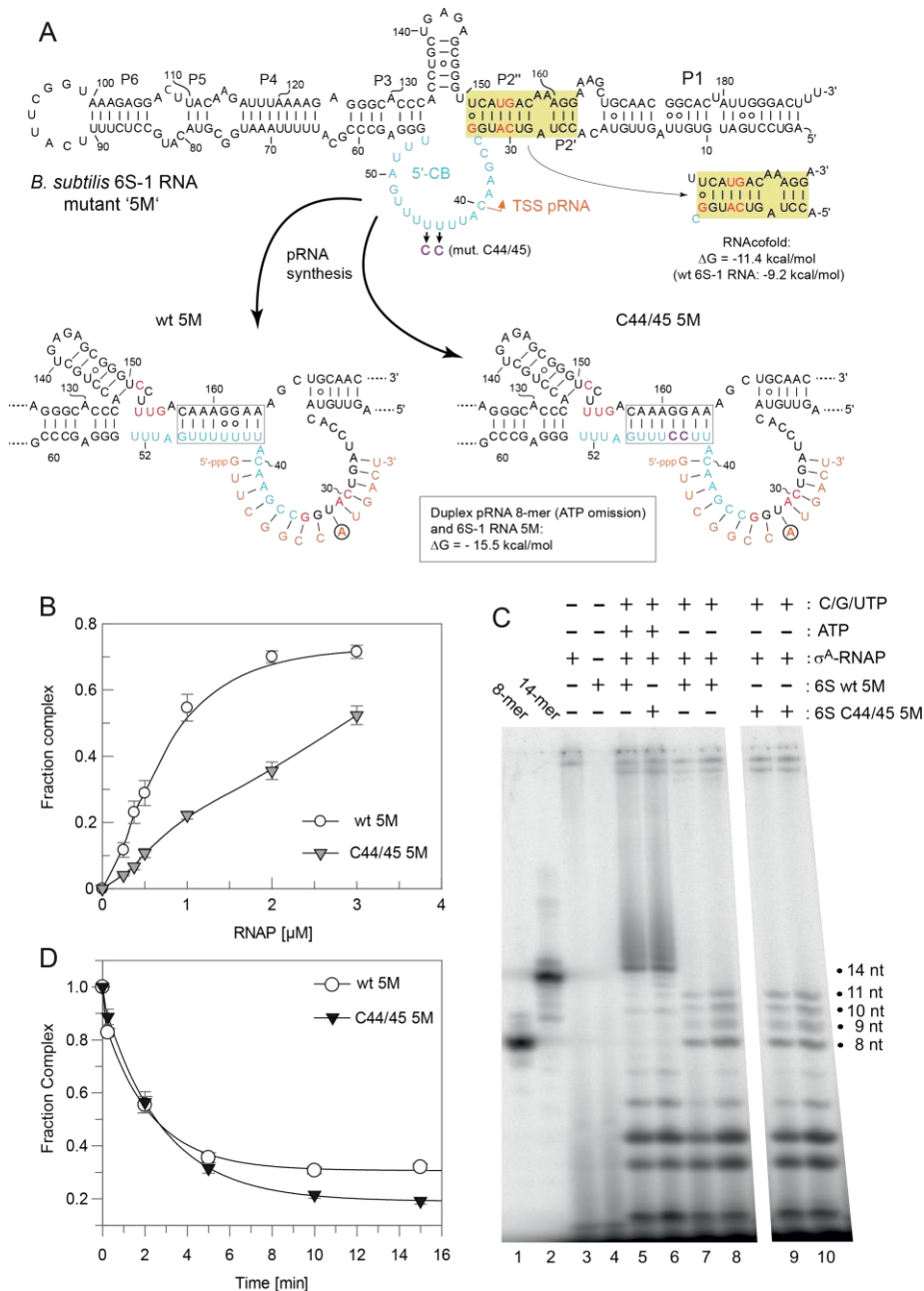


Figure 11. Characterization of 6S-1 RNA variants wt 5M and C44/45 5M (A) Secondary structure of the two 6S-1 RNA variants in the free state (top) and after the structural rearrangement (bottom) induced by pRNA transcription. The five mutations (5M) relative to the wt RNA are highlighted in red, the C44/45 mutations in magenta. In the sketches of the rearranged structures (bottom), the favored structures based on RNAfold dot plot analysis are shown. The first A residue in the pRNA sequence is marked by a circle. (B) σ^A -RNAP binding affinity for 6S-1 RNA variants wt 5M and C44/45 5M. The lines are spline curves; $K_{1/2}$ values were not calculated, as σ^A -RNAP titrations for variant C44/45 5M did not reach saturation. For more details, see legend to Figure 8B. (C) pRNA transcription by SG7 σ^A -RNAP using the two 6S-1 mutant RNAs as templates, as detailed in the legend to Figure 8C. The difference between lanes 7/8 and 9/10 is the use of 1 μ M (lanes 7 and 9) or 2 μ M (lanes 8 and 10) enzyme. In lane 7, the total amount of radioactivity was lower

than in lanes 8-10, affecting the intensity of all transcription products. (D) Kinetics of pRNA-induced decay of 6S-1 RNA:RNAP complexes for wt 5M or C44/45 5M RNAs using SG7 σ^A -RNAP (2 μ M) and 100 μ M each CTP, GTP and UTP; under these conditions, mainly pRNA 8-mers, but also 9 to 11-mers were synthesized based on the results shown in panel C. Data evaluation was performed as described in the legend to Figure 7 and in Materials and Methods. The rate constants k_1 for the fast phase could not be stably predicted, those for slow phase (k_2) were $0.45 \pm 0.06 \text{ min}^{-1}$ (wt 5M) and $0.36 \pm 0.01 \text{ min}^{-1}$ (C44/45 5M), the release-resistant complex fractions were 0.31 (wt 5M) and 0.19 (C44/45 5M).

6S-1 RNA refolding and disruption of the complex with RNAP can be induced by a stably bound oligonucleotide hexamer

We previously showed that an iso-sequential analog of a pRNA 8-mer that consists of locked nucleic acid (LNA) residues stably bound to 6S-1 RNA and retarded the RNA's mobility in native PAA gels to a very similar extent as a pRNA 14-mer [17]. Here we addressed the question whether even iso-sequential pLNA oligonucleotides shorter than 8 nt might be able to induce 6S-1 RNA refolding, such that complex formation with σ^A -RNAP is disrupted/prevented. For this purpose, we annealed chemically synthesized pLNA 6-, 7- and 8-mers to radiolabeled 6S-1 RNA and analyzed their mobilities by native PAGE. The complex of 6S-1 RNA with the pLNA 8-mer migrated almost as fast as the complex with the pRNA 14-mer used as reference (Figure 12, lines 7 and 8). Gel mobility incrementally decreased for complexes with the pLNA 7-mer and 6-mer (lanes 5 and 6), but the 6S-1:pLNA 6-mer complex still migrated substantially slower than free 6S-1 RNA (Figure 12, cf. lanes 1 and 5 with lanes 9 and 10). As the complex with the pRNA 14-mer, all three 6S-1:pLNA complexes prevented 6S-1 RNA binding to σ^A -RNAP (cf. lanes 1-4 and lane 9). Our findings demonstrate that already stable binding of a 6-meric pRNA mimic constrains or compacts the 6S-1 RNA conformation to an extent that impedes σ^A -RNAP binding.

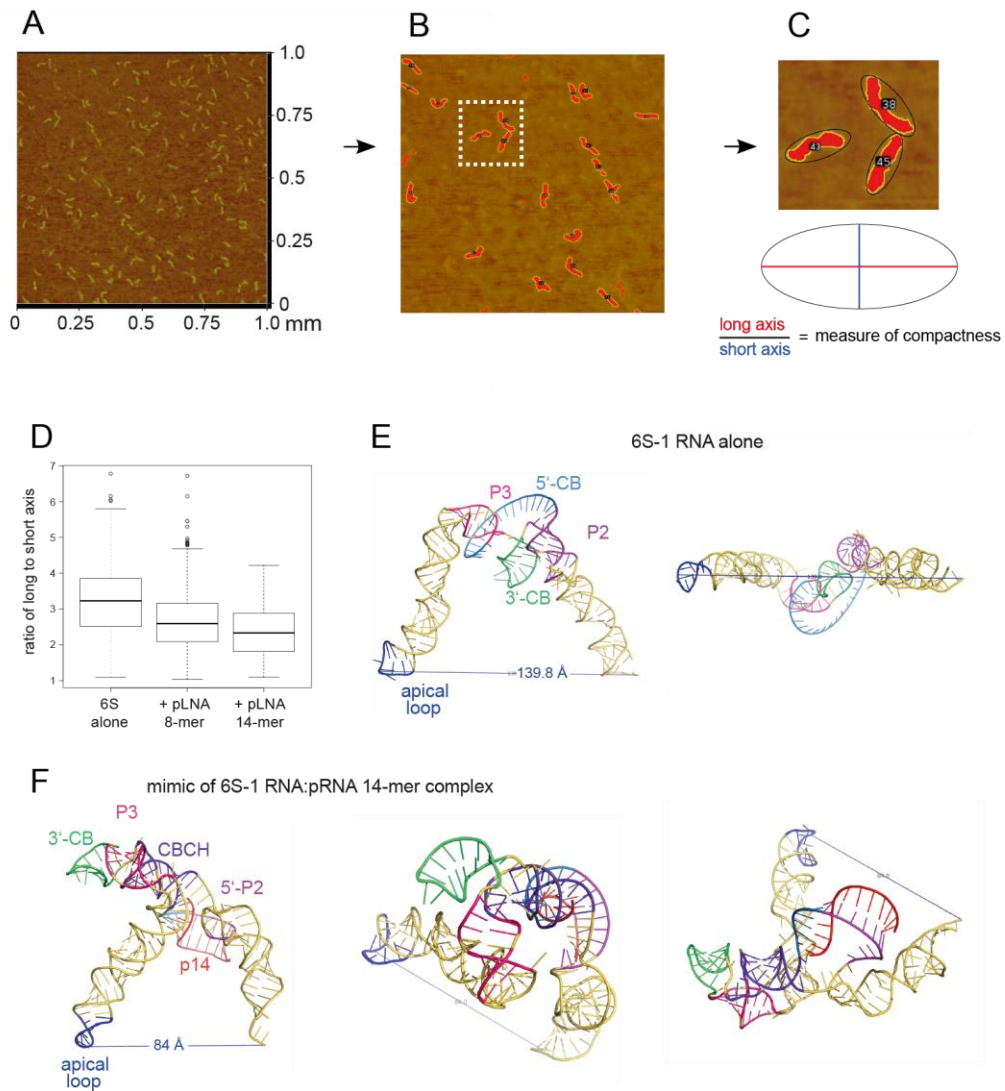


Figure 13. Atomic Force Microscopy (AFM) of *B. subtilis* 6S-1 RNA. (A) Raw image (1 x 1 μm area) of 6S-1 RNA molecules spread on a mica surface (for details, see Materials and Methods). (B) Enlarged image section after image processing with contours of individual molecules encircled by an ellipse. (C) Magnified visualization of three encircled example molecules (magnification of the area marked by the white frame in panel B) next to a cartoon of ellipse evaluation. For more individual images considered to be representative based on visual inspection, see Figure S3. (D) Boxplots displaying the ratio of long to short axis of ellipses (a value of 1 corresponds to a perfect circle) for 6S-1 RNA alone or annealed to a pLNA 8- or 14-mer; all residues were locked nucleic acid (LNA) analogs. (E, F) RNAComposer 3D approximations of 6S-1 RNA in (E) its native conformation (as in Figure 1A with unstructured 5'-CB) and (F) in its rearranged structure (Figure 1B with extended CBCH) in complex with a pRNA 14-mer. The secondary structural elements in panels E and F are indicated according to Figure 1; p14, pRNA 14-mer. The distance between the P atom of 6S-1 RNA residue U94 in the apical loop and the 3'-oxygen of the last nucleotide (U190) is depicted as well. For the 2D structure annotations used as templates for RNAcomposer, see Figure S4.

Discussion

The *B. subtilis* 6S-1 RNA truncation variant 6S₇₈ with length reductions of almost 60% still showed hallmarks of 6S RNAs, that is, served as template for transcription of pRNAs including 14-mers to form 6S RNA:pRNA hybrid structures that trigger 6S RNA release from σ^A -RNAP (Figure 2D, E). The truncations caused a ~ 10-fold decrease in affinity that may be due to the loss of contacts in the apical stem region where a -35-like contact region to the highly conserved domain 4 of σ^{70}/σ^A -like sigma factors was identified in the *E. coli* system [12]. However, in the *E. coli* system, already truncation of the distal part of the apical stem (deletion of the apical loop plus approx. P6/P5; Figure 1A) completely abolished gel-resolvable binding to σ^A -RNAP [13]. We conclude that the -35 region is more crucial for *E. coli* 6S RNA interaction with σ^{70} -RNAP than for binding of *B. subtilis* 6S-1 RNA to σ^A -RNAP. Despite the affinity reduction of variant 6S₇₈, our results demonstrate that the CB region and its adjacent short helices include all elements required for basic 6S-1 RNA function. Thus, the native length of the helical arms is not essential for the pRNA-induced disruption of 6S RNA: σ^A -RNAP complexes.

Previous investigations in the *E. coli* system focused on the '-10'-like region of the 3'-CB [12-14]. Six tested single mutations at positions 131 to 136 in the 3'-CB of *E. coli* 6S RNA (see Figure S5) had no or minor effects (~ 35% affinity reduction) on ground state binding to the σ^{70} -RNAP enzyme, of which one (C132A) caused a release defect and another one (U134A) accelerated the release rate [13]. The lack of a binding defect upon mutation of A131, U135 and G136 was confirmed in another study [12]. As nucleotides 132 to 136 form base pairs in the 3'-CB hairpin in *E. coli* 6S RNA:pRNA hybrid structures (see Figure S5), the just mentioned findings suggest a primary role of these nucleotides in the 6S RNA release mechanism during pRNA synthesis. For *B. subtilis* 6S-1 RNA [17], we observed a two- to three-fold lower affinity for a triple mutant of 6S-1 RNA (C136A/G145U/C146A) that is unable to form the 3'-CB hairpin. We also provided evidence that the triple mutant is conformationally more flexible than the native 6S-1 RNA [17]. So, it seems that the 3'-CB hairpin of *B. subtilis* 6S-1 RNA, predicted by RNAfold to stably form already in the free RNA, is either involved in ground state binding to σ^A -RNAP or indirectly supports the interaction of other

RNA elements with the holoenzyme. We conclude that the 3'-CB interaction with RNAP differs in Enterobacteriaceae such as *E. coli* compared with *B. subtilis* and related Firmicutes. This leads to the question to which extent the 5'-CB contributes to interaction with RNAP. Unfortunately, residues of the 5'-CB were not resolved in the *E. coli* cryo-EM structure [12] and ground state binding data are not available for *E. coli* 6S RNA variants with mutations in the 5'-CB. Two mutations upstream of the TSS (U44) in the 5'-CB of *E. coli* 6S RNA, namely A52U and A50U, were tested for pRNA-induced release from σ^{70} -RNAP [29]. While the A52U variant had no effect on the release rate, the A50U mutant released 2.5-fold slower than the parental 6S RNA. Surprisingly, A50U and A52U in combination were able to rescue the release defect caused by a U44A mutation at the TSS, a finding as yet not understood [29]. For *B. subtilis* 6S-1 RNA, we saw clear binding defects upon mutation of A50 to U, C or G and U44/45 to C44/45 upstream of the pRNA TSS (C40), consistent with base-specific direct contacts to the enzyme in this part of the 5'-CB. At present, it can also not be excluded that the C44/45 double mutation more indirectly reduced binding affinity through shifting the conformational equilibrium of unbound 6S-1 RNA toward conformers forming the CBCH instead of helix P2. Noteworthy, two other 6S-1 RNA mutations in the 5'-CB, U47A and U53A, had no effects on ground state binding (Figure S1), indicating that not all base identities in the 5'-CB are crucial for interaction with σ^A -RNAP.

We dedicated major efforts to evaluating the role of the CBCH in abortive pRNA transcription and pRNA-induced 6S-1 RNA release from σ^A -RNAP. We hypothesized that, if the CBCH supported pRNA-induced refolding of 6S-1 RNA, then its stabilization should lower the activation energy barrier for 6S-1 RNA release from RNAP. This could manifest either as a shift in the pRNA pattern toward slightly shorter length species or as accelerated 6S-1 RNA release kinetics. We initially introduced the A50U mutation (Figure 1) to stabilize the CBCH, but neither observed any substantial differences to the wt 6S-1 RNA in the pRNA pattern (Figure 3D) nor in release kinetics. We then reinforced stabilization of the CBCH by introducing the C44/45 double mutation that replaced two G:U with G:C pairs (Figure 1). This double mutation indeed increased the fraction of shorter pRNA in vitro transcripts (11/12-mers; Figure

4B,C), consistent with the notion that the CBCH lowers the activation barrier for pRNA-induced 6S-1 RNA refolding, to an extent depending on its relative stability and probability of formation. In our experimental setup, the kinetics of pRNA-induced 6S-1 RNA release from σ^A -RNAP (complex decay) remained indistinguishable between the wt and C44/45 mutant RNA upon pRNA synthesis in the presence of all four NTPs (Figure 7). To further carve out differences between the two, we introduced the 8M, 6M and 5M mutations into helix P2 of the wt and C44/45 6S-1 RNAs. This was conceived to adjust pRNA synthesis under ATP omission conditions to length species of 11 (8M, 6M) or 8 (5M) nucleotides and to compensate this length reduction by increasing the proportion of G:C pairs in 6S-1 RNA:pRNA hybrids. The 8M variants indeed gave rise to the synthesis of pRNA 11-mers under ATP omission conditions (Figure 8C) and to formation of gel-resolvable 6S-1 RNA:pRNA complexes (Figure 9A). The 6S-1 RNA:pRNA hybrid RNA appeared as more distinct bands in the C44/45 relative to the wt background, in line with the stabilizing effect of the CBCH (Figure 9A, cf. right and left gel image). Surprisingly, an enlarged fraction of release-resistant 6S-1 RNA: σ^A -RNAP complexes was observed in the wt background (Figure 8D). This can be explained by formation a second small hairpin in the 3'-CB that is energetically favored in the wt background, but not in the C44/45 context that favors formation of the CBCH (Figure 8A). These findings indirectly confirm the support function of the CBCH in pRNA induced 6S-1 RNA refolding and additionally reveal that formation of a second hairpin in the 3'-CB interferes with the release process. With the 6M variant we prevented formation of the artificial 3'-CB hairpin and also destabilized helix P2. With the wt and C44/45 6M variants, 6S-1 RNA:pRNA hybrids now appeared as sharp bands with identical mobility in native gels (Figure 9B). The 6M variants gave rise to primarily pRNA 11-mers, but appeared somewhat more permissive than the 8M variant to the synthesis of longer pRNAs despite the omission of ATP (Figure 10C). Here, the release process was faster and more complete in the C44/45 versus wt background (Figure 10D), again in line with the support function of the CBCH in the release process. It cannot be completely ruled out that the 2- to 3-fold decreased ground state binding affinity of the C44/45 6M mutant relative to the wt 6M variant might have contributed to its more efficient release from RNAP. We have attempted to

marginalize this possibility by analyzing 6S-1 RNA release in the presence of σ^A -RNAP concentrations considerably above the K_d for the C44/45 mutant RNA. Finally, the 5M variants harboring a re-stabilized P2 helix, gave rise to synthesis of mainly 8-mers in the absence of ATP, but was also permissive to the synthesis of 9 to 11-mers under these conditions (Figures 11C and S2). Relative to the 6M variants, the 5M derivatives showed a decreased fraction of complexes that decayed with fast kinetics (see below); the fraction of release-resistant complexes was lower for the C44/45 5M than the wt 5M RNA (Figure 11D).

Abortive pRNA transcription results from RNAP scrunching, where the enzyme remains stationary on the template but reels in RNA downstream of the TSS, thereby threading the template RNA strand through the active site for pRNA synthesis. Panchapakesan and Unrau [14] devised a model according to which formation of the extended 3'-CB hairpin upon pRNA synthesis on *E. coli* 6S RNA accumulates additional strain during scrunching, explaining why σ^{70} ejection occurs at a pRNA length of 9 nt on the wt RNA, but increases to 14 nt when the hairpin is disrupted. Our observation of a shift to shorter pRNAs with the C44/45 mutant RNA (Figure 4B,C) would be in line with the stabilized CBCH increasing strain during scrunching as well. The 3'-CB hairpin of 6S-1 RNA may also add strain during scrunching, as our 6S-1 triple mutation (C136A/G145U/C146A) that disrupts hairpin formation caused a shift to longer pRNAs including runoff-like transcripts [17]. Increased proportions of runoff-like pRNAs were also observed *in vivo* for *B. subtilis* 6S-2 RNA [30], which is less structured than 6S-1 RNA in the CB [28]. Thus, scrunching of RNAP holoenzymes and refolding of 6S RNA during pRNA synthesis are likely intertwined components of the release mechanism. A related issue is the pRNA length at which $\sigma^{A/70}$ -RNAP switches to the elongation mode. For DNA promoters, promoter escape has been reported to occur at transcript lengths of 9-15 nt [31,32]. For *E. coli* 6S RNA: σ^{70} -RNAP complexes, σ^{70} ejection, and by inference entry into the elongation mode, was observed upon synthesis of pRNA 9-mers followed by dissociation of core RNAP:6S RNA complexes at a pRNA length of 13 nt [14]. Assuming a similar length requirement for σ^A -RNAP:6S-1 RNA complexes to enter the elongation mode associated with σ^A ejection, then our 5M variants may be revealing, since pRNA 8-mers were the main products under ATP omission conditions (Figures

11D and S2). Among the 6S-1 variants tested here, the 5M variants almost lacked the fast phase of complex decay, particularly in the C44/45 background (Figure 11D). Likewise, the fast phase of complex decay was absent in the release kinetics for wt and C44/45 6S-1 RNAs under ATP omission conditions, limiting pRNA transcription to mainly 8-mers as well (Fig. 6C). Although still speculative at present, this could mean that the transition to the elongation mode of RNAP has become rate-limiting for fast release in the case of wt, C44/45, wt 5M and C44/45 5M 6S-1 RNAs under ATP omission conditions that prevent or largely decelerate the synthesis of pRNAs longer than 8-mers.

Another observation of this study is the extension of pRNAs under ATP omission conditions, despite the restriction of templated pRNAs to a length of 11 (variants 8M and 6M) or 8 (5M) nucleotides. These extensions may be due to NTP misincorporation, non-templated addition of NTPs or utilization of alternative TSSs.

We demonstrated here that already stable binding of a hexameric pLNA mimic alters the 6S-1 RNA structure to an extent that is incompatible with σ^A -RNAP binding. The bound 6-mer substantially retarded gel mobility of 6S-1 RNA, and this retardation continuously increased for the 7- and 8-mer; gel retardation of the 6S-1 RNA:pLNA 8-mer complex almost reached the extent obtained with 6S-1 RNA:pRNA 14-mer complexes. In native gels, elongated/extended/rod-shaped RNAs migrate faster than branched molecules [33]. A 6-bp helix apparently constricts conformational flexibility in the 5'-CB to an extent that disfavors formation of an elongated structure as adopted by free 6S-1 RNA. We previously showed for *A. aeolicus* 6S RNA that essentially the same gel mobility shift is obtained by annealing a pRNA 15-mer to nucleotides in the 5'-CB/5'-P2 strand compared with an artificial 'pRNA' 15-mer annealing to the opposite part of the CB, namely the 3'-strand of P2 and nucleotides in the 3'-CB [21]. This observation indicates that constricting conformational flexibility by duplex formation involving nucleotides of the 3'- or 5'-CB prevents formation of a more elongated 6S RNA structure. Thus, the latter feature seems to be the reason for the observed gel shifts, rather than formation of a specific 6S RNA:pRNA hybrid structure. More pronounced deviation from an elongated, rod-shaped structure when a pRNA is stably bound was quantitatively ascertained in our AFM particle shape analyses (Figures 13) and also qualitatively evident upon visual inspection of individual

molecule shapes (Figure S3). Upon annealing of the pLNA 8- and 14-mers, increasingly bent, thicker and shorter molecules appeared (often with three protuberances of about equal length) while slim elongated molecules seemed to be more abundant in images of free 6S-1 RNA (Figure S3). This would be in line with the RNAcomposer 3D predictions shown for free 6S-1 RNA and 6S-1 RNA:pRNA 14-mer complexes in Figure 13E and F, the latter predicted to adopt a more compact shape. We are aware that some subjective interpretations of individual AFM images (Figure S3) are at risk of overstraining the resolution power of AFM images. It might also be possible that pRNA:6S-1 RNA hybrid helices formed in the 5'-CB induce a stabilization [17] and reorientation of the 3'-CB hairpin, resulting in a more branched shape of the RNA. This could rationalize the pRNA-induced gel shift for the truncated 6S₇₈ variant that carries only short helical arms. Yet, an argument against this is the observation that the 6S-1 RNA triple mutant (C136A/G145U/C146A) with a disrupted 3'-CB hairpin still showed pronounced gel retardation in complex with pRNA [17].

Remarkably, *A. aeolicus* 6S RNA with the artificial 'pRNA' 15-mer bound to 3'-P2/3'-CB was inefficient in preventing complex formation with σ^A -RNAP and rather formed aberrantly migrating complexes with the enzyme in native PAA gels [21]. Thus, constriction of conformational flexibility in the CB may be one component of the 6S-1 RNA release mechanism, but other mechanistic components may be required as well. Conceivably, duplex formation with pRNA in the 5'-CB/5'-P2 region may specifically disrupt nearby enzyme contacts to 5'-CB nucleotides upstream of the TSS, possibly including A50 and U44/45 whose mutation was shown here to weaken ground state binding to the enzyme. If so, formation of the CBCH may support disruption of such contacts involving A50 and U44/45, as those residues are part of the CBCH.

Finally, the sensitivity of 6S-1 RNA function to certain mutations (A50B, C44/45, C136A/G145U/C146A [17]) in the CB region as well as the pleiotropic and complex phenotypes of the C44/45, 8M, 6M and 5M mutant RNAs supports the view that the 6S-1 RNA wt sequence and structure, particularly in the CB region, provides an optimal balance of all molecular features that are relevant to the different steps of the RNA's mechanistic cycle, which includes 6S-1 RNA: σ^A -RNAP ground state binding affinity as well as coordination of RNAP scrunching,

enzyme switch to the elongation mode, pRNA transcript length, conformational constriction/refolding of 6S-1 RNA and release of 6S-1 RNA:pRNA hybrids from RNAP.

Table 1. Strains and plasmids used in this study.

Strain or plasmid	Genotype	Reference or source
Strains		
<i>B. subtilis</i> His-rpoC, Δ bsrAB (SG7)	PY79 Δ bsrA:spc (Sp ^r), Δ bsrB:kan (Km ^r) <i>rpoC</i> Ω pYQ52 (Cm ^r)	[23]
<i>B. subtilis</i> 110 NA	<i>trpC2 spo0A3 su</i> ⁻	[34]
Plasmids		
pUC18_m6S1	pUC18::T7- <i>bsrA</i> -190-WT, (Amp ^r)	[16]
pGH2	pUC18::T7- <i>bsrA</i> -190-U50, (Amp ^r)	This work
pGH3	pUC18::T7- <i>bsrA</i> -190-C50, (Amp ^r)	This work
pGH5	pUC18::T7- <i>bsrA</i> -78-6S78, (Amp ^r)	This work
pGH6	pUC18::T7- <i>bsrA</i> -82-6S82cp, (Amp ^r)	This work
pGH12	pUC18::T7- <i>bsrA</i> -190-UUUUswap (Amp ^r)	This work
pGH15	pUC18::T7- <i>bsrA</i> -190-A47, (Amp ^r)	This work
pGH16	pUC18::T7- <i>bsrA</i> -190-C44/45, (Amp ^r)	This work
pGH17	pUC18::T7- <i>bsrA</i> -190-A53, (Amp ^r)	This work
pAH_P2swap	pUC18::T7- <i>bsrA</i> -190-P2swap (Amp ^r)	This work
pSG1	pUC18::T7- <i>bsrA</i> -190-G50, (Amp ^r)	This work
pSG2	pUC18::T7- <i>bsrA</i> -190-WT 8M, (Amp ^r)	This work
pSG3	pUC18::T7- <i>bsrA</i> -190-C44/45 8M, (Amp ^r)	This work
pSG4	pUC18::T7- <i>bsrA</i> -190-WT 6M, (Amp ^r)	This work
pSG5	pUC18::T7- <i>bsrA</i> -190-C44/45 6M (Amp ^r)	This work
pSG6	pUC18::T7- <i>bsrA</i> -190-WT 5M (Amp ^r)	This work
pSG7	pUC18::T7- <i>bsrA</i> -190-C44/45 5M (Amp ^r)	This work

Supplementary Materials: The following supporting information can be downloaded at: www.mdpi.com/xxx/s1, Figure S1: Binding affinity of σ^A -RNAP to 6S-1 RNA wt and other mutant RNAs; Figure S2: pRNA transcription by SG7 σ^A -RNAP using 6S RNAs wt 5M and C44/45 5M as templates; Figure S3: Example AFM images of free 6S-1 RNA and 6S-1 RNA complexes with pLNA 8- and 14-mers; Figure S4: Secondary structure dot-bracket notation of free 6S-1 RNA and the 6S-1 RNA:pRNA 14-mer complex used as input for 3D predictions by RNAcomposer; Figure S5:

Author Contributions: Conceptualization, R.K.H.; investigation, S.G., P.G.H., M.B.; software, M.L.; validation, S.G., R.K.H.; resources, M.B., M.L., R.K.H.; data curation, M.L.; writing—original draft preparation, S.G., P.G.H., R.K.H.; writing—review and editing, S.G., P.G.H., M.L., M.B., R.K.H.; visualization, S.G., P.G.H., M.L., R.K.H.; supervision, R.K.H.; project administration, R.K.H.; funding acquisition, R.K.H. All authors have read and agreed to the published version of the manuscript.”

Funding: Please add: This research was funded by Deutsche Forschungsgemeinschaft (Germany), RTG 2355, to R.K.H.

Institutional Review Board Statement: Not Applicable.

Informed Consent Statement: Not applicable.

Acknowledgments: We thank Alina Hanlon and Julia Renz for experimental support with respect to the data shown in Figure S1.

Conflicts of Interest: The authors declare no conflict of interest.

Availability:

RNAfold <http://rna.tbi.univie.ac.at/cgi-bin/RNAWebSuite/RNAfold.cgi> (accessed in Dec. 2021). RNAcomposer <https://rnacomposer.cs.put.poznan.pl/> (accessed in Dec. 2021).

References

1. Wassarman, K.M.; Storz, G. 6S RNA regulates *E. coli* RNA polymerase activity. *Cell* **2000**, *101*, 613-623.
2. Neusser, T.; Polen, T.; Geissen, R.; Wagner, R. Depletion of the non-coding regulatory 6S RNA in *E. coli* causes a surprising reduction in the expression of the translation machinery. *BMC Genomics* **2010**, *11*, 165.
3. Cavanagh, A.T.; Klocko, A.D.; Liu, X.; Wassarman, K.M. Promoter specificity for 6S RNA regulation of transcription is determined by core promoter sequences and competition for region 4.2 of sigma70. *Mol Microbiol.* **2008**, *67*, 1242-1256.
4. Cavanagh, A.T.; Wassarman, K.M. 6S RNA, a global regulator of transcription in *Escherichia coli*, *Bacillus subtilis*, and beyond. *Annu Rev Microbiol.* **2014**, *68*, 45-60.
5. Steuten, B.; Hoch, P.G.; Damm, K.; Schneider, S.; Köhler, K.; Wagner, R.; Hartmann, R.K. Regulation of transcription by 6S RNAs: insights from the *Escherichia coli* and *Bacillus subtilis* model systems. *RNA Biol.* **2014**, *11*, 508-521.
6. Wassarman, K.M. 6S RNA, a Global Regulator of Transcription. *Microbiol Spectr.* **2018**, *6*, 10.1128.
7. Wehner, S.; Damm, K.; Hartmann, R.K.; Marz, M. Dissemination of 6S RNA among bacteria. *RNA Biol.* **2014**, *11*, 1467-1478.
8. Willkomm, D.K.; Minnerup, J.; Hüttenhofer, A.; Hartmann, R.K. Experimental RNomics in *Aquifex aeolicus*: identification of small non-coding RNAs and the putative 6S RNA homolog. *Nucleic Acids Res.* **2005**, *33*, 1949-1960.
9. Nickel, A.I.; Wäber, N.B.; Gößringer, M.; Lechner, M.; Linne, U.; Toth, U.; Rossmannith, W.; Hartmann, R.K. Minimal and RNA-free RNase P in *Aquifex aeolicus*. *Proc. Natl. Acad. Sci. USA* **2017**, *114*, 11121-11126.
10. Burenina, O.Y.; Elkina, D.A.; Migur, A.Y.; Oretskaya, T.S.; Evguenieva-Hackenberg, E.; Hartmann, R.K.; Kubareva, E.A. Similarities and differences between 6S RNAs from *Bradyrhizobium japonicum* and *Sinorhizobium meliloti*. *J Microbiol.* **2020**, *58*, 945-956.

11. Barrick, J.E.; Sudarsan, N.; Weinberg, Z.; Ruzzo, W.L.; Breaker, R.R. 6S RNA is a widespread regulator of eubacterial RNA polymerase that resembles an open promoter. *RNA* **2005**, *11*, 774-784.
12. Chen, J.; Wassarman, K.M.; Feng, S.; Leon, K.; Feklistov, A.; Winkelman, J.T.; Li, Z.; Walz, T.; Campbell, E.A.; Darst, S.A. 6S RNA Mimics B-Form DNA to Regulate *Escherichia coli* RNA Polymerase. *Mol. Cell* **2017**, *68*, 388-397.e6.
13. Shephard, L.; Dobson, N.; Unrau, P.J. Binding and release of the 6S transcriptional control RNA. *RNA* **2010**, *16*, 885-892.
14. Panchapakesan, S.S.; Unrau, P.J. E. coli 6S RNA release from RNA polymerase requires sigma70 ejection by scrunching and is orchestrated by a conserved RNA hairpin. *RNA* **2012**, *18*, 2251-2259.
15. Wassarman, K.M.; Saecker, R.M. Synthesis-mediated release of a small RNA inhibitor of RNA polymerase. *Science*. **2006**, *314*, 1601-1603.
16. Beckmann, B.M.; Burenina, O.Y.; Hoch, P.G.; Kubareva, E.A.; Sharma, C.M.; Hartmann, R.K. *In vivo* and *in vitro* analysis of 6S RNA-templated short transcripts in *Bacillus subtilis*. *RNA Biol.* **2011**, *8*, 839-849.
17. Beckmann, B.M.; Hoch, P.G.; Marz, M.; Willkomm, D.K.; Salas, M.; Hartmann, R.K. A pRNA-induced structural rearrangement triggers 6S-1 RNA release from RNA polymerase in *Bacillus subtilis*. *EMBO J.* **2012**, *31*, 1727-1738.
18. Murray, H.D.; Schneider, D.A.; Gourse, R.L. Control of rRNA expression by small molecules is dynamic and nonredundant. *Mol Cell.* **2003**, *12*, 125-34.
19. Cabrera-Ostertag, I.J.; Cavanagh, A.T.; Wassarman, K.M. Initiating nucleotide identity determines efficiency of RNA synthesis from 6S RNA templates in *Bacillus subtilis* but not *Escherichia coli*. *Nucleic Acids Res.* **2013**, *41*, 7501-7511.
20. Wurm, R.; Neußer, T.; Wagner, R. 6S RNA-dependent inhibition of RNA polymerase is released by RNA-dependent synthesis of small *de novo* products. *Biol. Chem.* **2010**, *391*, 187-196.
21. Köhler, K.; Duchardt-Ferner, E.; Lechner, M.; Damm, K.; Hoch, P.G.; Salas, M.; Hartmann, R.K. Structural and mechanistic characterization of

- 6S RNA from the hyperthermophilic bacterium *Aquifex aeolicus*. *Biochimie* **2015**, *117*, 72-86.
22. Sogo, J.M.; Inciarte, M.R.; Corral, J.; Viñuela, E.; Salas, M. RNA polymerase binding sites and transcription map of the DNA of *Bacillus subtilis* phage phi29. *J Mol Biol.* **1979**, *127*, 411-436.
23. Ganapathy, S.; Wiegard, J.C.; Hartmann, R.K. Rapid preparation of 6S RNA-free *B. subtilis* σ^A -RNA polymerase and σ^A . *J Microbiol Methods.* **2021**, *190*, 106324.
24. Bussiek, M.; Schöne, A.; Nellen, W. (2014) Atomic Force Microscopy Imaging and Force Spectroscopy of RNA. In : Handbook of RNA Biochemistry (Hartmann RK, Bindereif A, Schön A, Westhof E (eds.) WILEY-VCH, Weinheim, Germany, pp. 527-546.
25. Schneider, C.A.; Rasband, W.S.; Eliceiri, K.W. NIH Image to ImageJ: 25 years of image analysis. *Nat Methods.* **2012**, *9*, 671-675.
26. Lorenz, R., Bernhart, S.H., Hoener zu Siederdissen, C., Tafer, H., Flamm, C., Stadler, P.F., Hofacker, I.L. ViennaRNA Package 2.0. *Algorithms Mol Biol.* **2011**, *6*, 26.
27. Popena, M.; Szachniuk, M.; Antczak, M.; Purzycka, K.J.; Lukasiak, P.; Bartol, N.; Blazewicz, J.; Adamiak, R.W. Automated 3D structure composition for large RNAs. *Nucleic Acids Res.* **2012**, *40*, e112
28. Burenina, O.Y.; Hoch, P.G.; Damm, K.; Salas, M.; Zatsepin, T.S.; Lechner, M.; Oretskaya, T.S.; Kubareva, E.A.; Hartmann, R.K. Mechanistic comparison of *Bacillus subtilis* 6S-1 and 6S-2 RNAs--commonalities and differences. *RNA* **2014**, *20*, 348-359.
29. Oviedo Ovando, M.; Shephard, L.; Unrau, P.J. *In vitro* characterization of 6S RNA release-defective mutants uncovers features of pRNA-dependent release from RNA polymerase in *E. coli*. *RNA* **2014**, *20*, 670-680.
30. Hoch, P.G.; Schlereth, J.; Lechner, M.; Hartmann RK. *Bacillus subtilis* 6S-2 RNA serves as a template for short transcripts *in vivo*. *RNA* **2016**, *22*, 614-622.
31. Revyakin, A.; Liu, C.; Ebright, R.H.; Strick, T.R. Abortive initiation and productive initiation by RNA polymerase involve DNA scrunching. *Science* **2006**, *314*, 1139-1143.

32. Lee, J.; Borukhov, S. Bacterial RNA Polymerase-DNA Interaction-The Driving Force of Gene Expression and the Target for Drug Action. *Front Mol Biosci.* **2016**, *3*, 73.
33. Riesner, D.; Steger, G. (2014) Temperature-gradient gel electrophoresis of RNA. In: Handbook of RNA Biochemistry, 2nd ed. (eds. Hartmann RK, Bindereif A, Schön A, Westhof E), WILEY-VCH, Weinheim, Germany, p. 427–444.
34. Muñoz-Espín, D.; Daniel, R.; Kawai, Y.; Carballido-López, R.; Castilla-Llorente, V.; Errington, J.; Meijer, W.J.; Salas, M. The actin-like MreB cytoskeleton organizes viral DNA replication in bacteria. *Proc. Natl. Acad. Sci. USA* **2009**, *106*, 13347-13352.

Supplementary

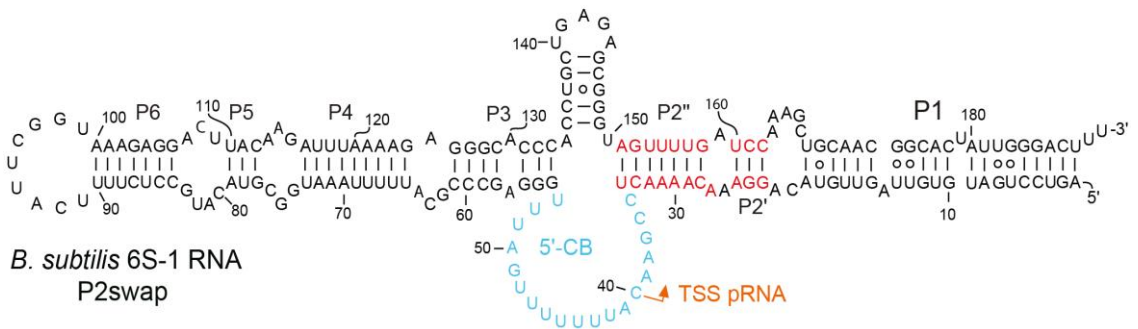
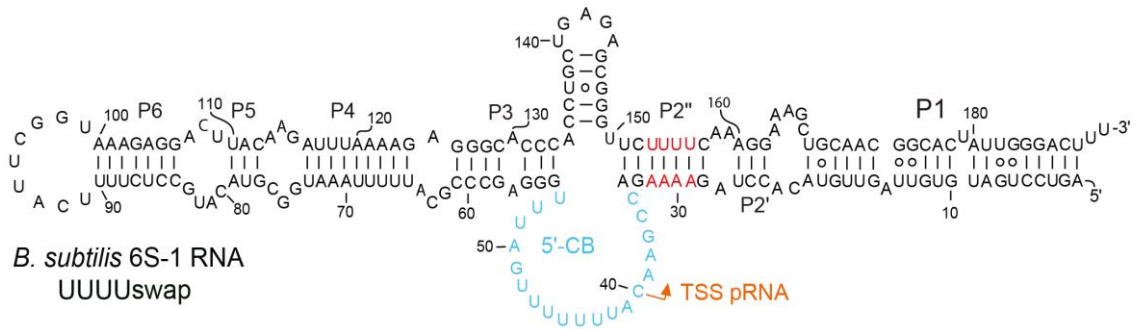
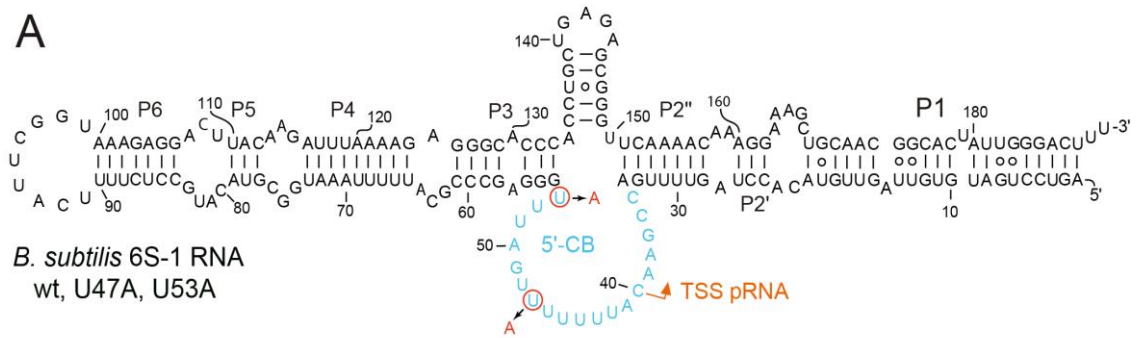
Structural and functional insight into the mechanism of *Bacillus subtilis* 6S-1 RNA release from RNA polymerase

Sweetha Ganapathy¹, Philipp G. Hoch¹, Marcus Lechner², Malte Bussiek³,
Roland K. Hartmann*

*Corresponding author:

E-mail: roland.hartmann@staff.uni-marburg.de

A



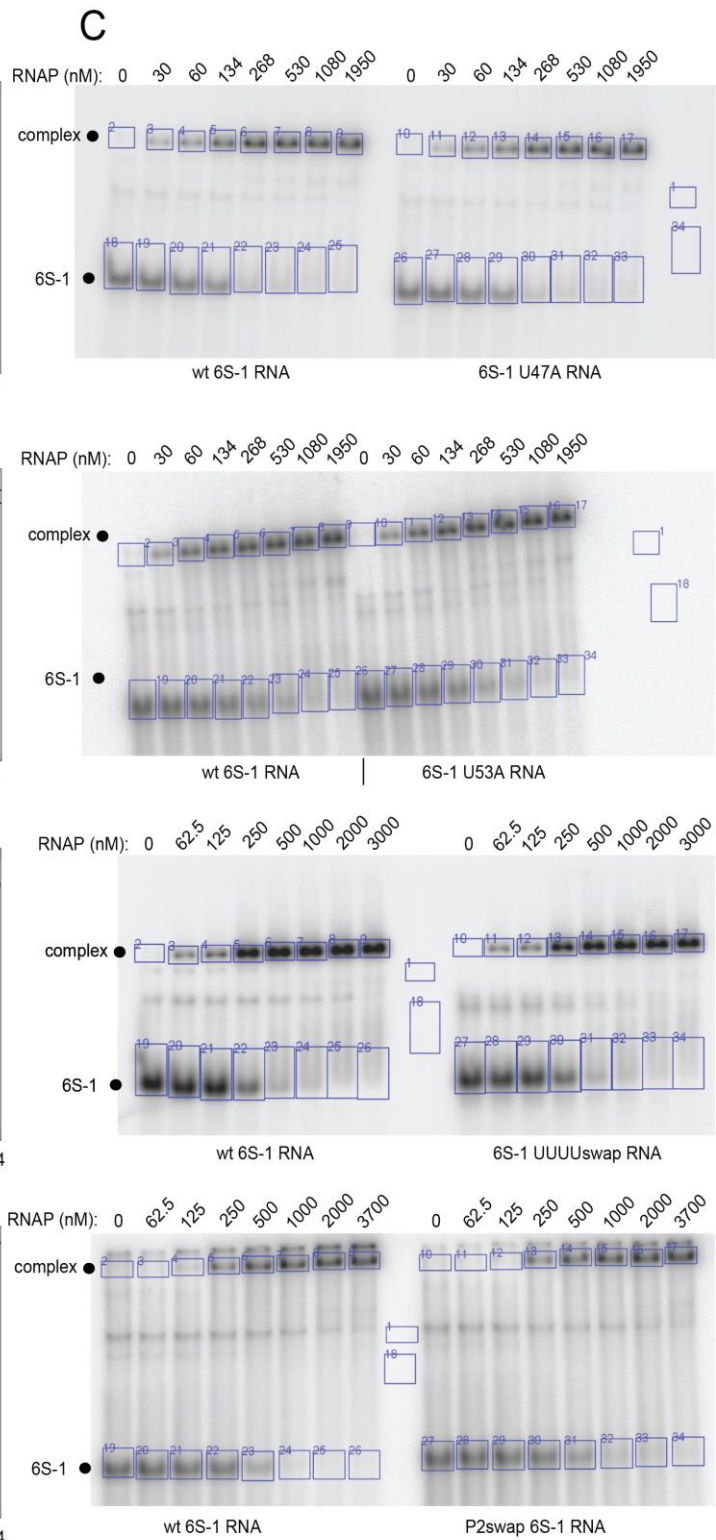
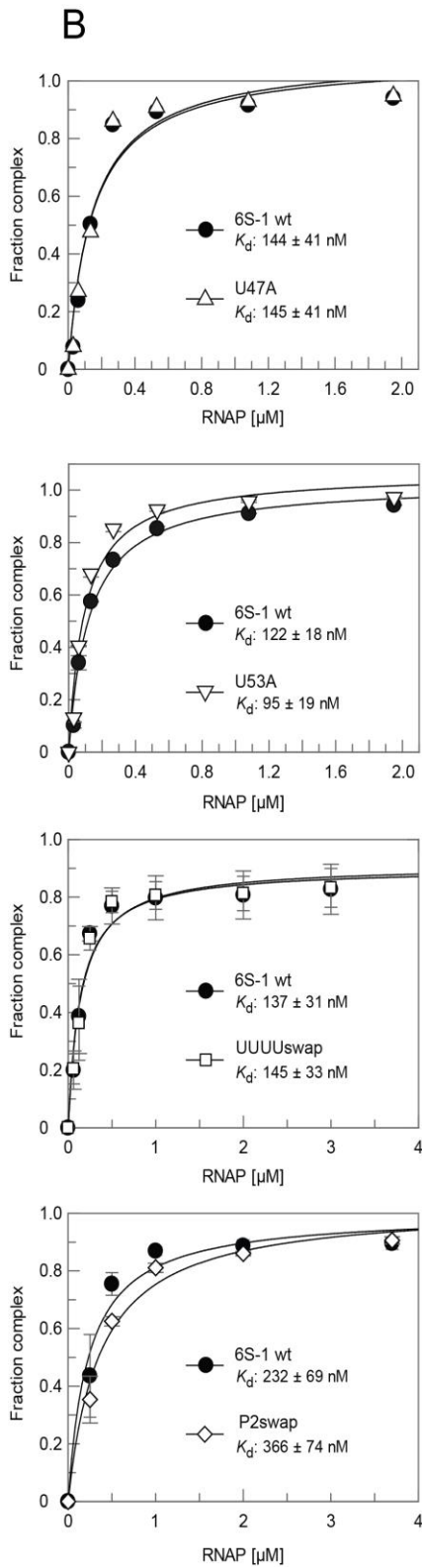


Figure S1: Binding affinity of σ^A -RNAP to 6S-1 RNA wt and other mutant RNAs. (A) Secondary structure presentation of wt 6S-1 RNA and mutants U47A and U53A thereof (top), mutant RNA UUUUswap (middle) and RNA P2swap (bottom), with mutations highlighted in red letters. (B) 6S-1 RNA: σ^A -RNAP binding affinity plotted as the fraction of complex as a function of σ^A -RNAP concentration. The data was fit to an equation for a single ligand binding site using Grafit version 5.0.13; data point errors are standard errors of the mean (SEM) and calculated K_D values are depicted within the graphs. Data for the U47A and U53A mutants are based on two and those for mutants UUUUswap and P2 swap on three individual experiments. (C) Phosphorimages of exemplary gels with quantification boxes used for K_D determination; for the example at the top, box 1 pixels were subtracted as background from boxes 2 to 17, and box 34 was subtracted from boxes 18 to 33; for the wt 6S-1 RNA panel, the calculated value for (box 2 - box 1)/[(box 2 - box 1) + (box 18 - box 34)] was defined as 0 complex formation and subtracted from the "Fraction complex" values for the corresponding lanes with boxes 3/19, 4/20, 5/21, 6/22, 7/23, 8/24 and 9/25. For more details, see Materials and Methods of the main text.

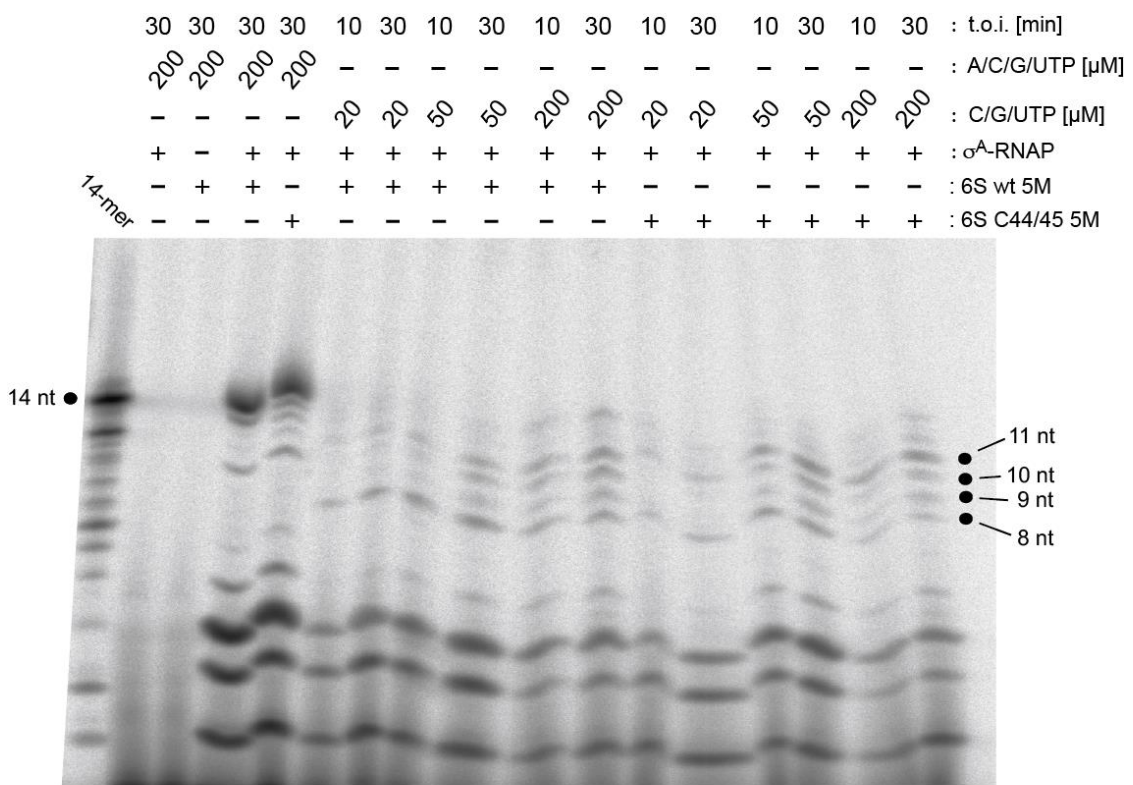


Figure S2: pRNA transcription by SG7 σ^A -RNAP using 6S RNAs wt 5M and C44/45 5M as templates. The figure illustrates that the pRNA 8-mer appears first after short incubation (10 min) and at low C/G/UTP concentrations (20 μ M each), but longer pRNA products appear under ATP omission conditions upon longer incubation periods and at higher nucleotide concentrations. The longer products can be explained by misincorporation C, G or U instead of the encoded A at position 9. For more details see Fig. 11 and Materials and Methods of the main text.

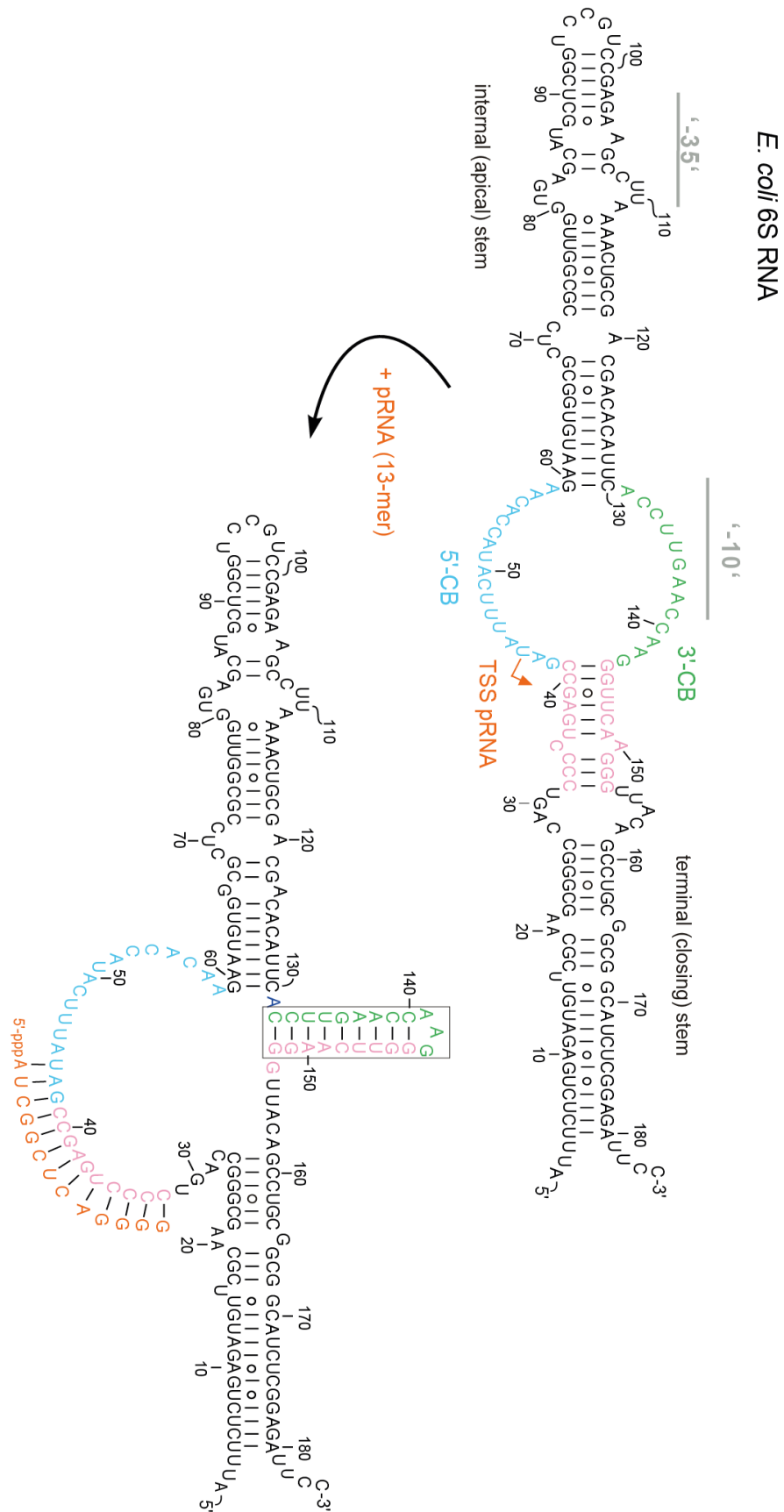


Figure S5: The pRNA-induced structural transition of *E. coli* 6S RNA. Adapted from [12,14].

For more details on abbreviations and color code, see Figure 1 of the main text.

3.2 Rapid preparation of 6S RNA-free *Bacillus subtilis*

σ^A -RNA polymerase and σ^A

Sweetha Ganapathy, Jana Christin Wiegard and Roland K. Hartmann *

¹Institut für Pharmazeutische Chemie, Philipps-Universität Marburg, Marbacher Weg 6, 35037 Marburg, Germany

*Corresponding author:

E-mail: roland.hartmann@staff.uni-marburg.de

Author Contributions: Conceptualization, R.K.H.; investigation, S.G., J. C. W.; SG7 strain construction and validation S.G.; σ^A subunit overexpression strain construction and purification J. C. W.; supervision, R.K.H.; project administration, R.K.H.; funding acquisition, R.K.H.

ABSTRACT

The regulatory 6S-1 and 6S-2 RNAs of *Bacillus subtilis* bind to the housekeeping RNA polymerase holoenzyme (σ^A -RNAP) with submicromolar affinity. We observed copurification of endogenous 6S RNAs from a published *B. subtilis* strain expressing a His-tagged RNAP. Such 6S RNA contaminations in σ^A -RNAP preparations reduce the fraction of enzymes that are accessible for binding to DNA promoters. In addition, this leads to background RNA synthesis by σ^A -RNAP utilizing copurified 6S RNA as template for the synthesis of short abortive transcripts termed product RNAs (pRNAs). To avoid this problem, we constructed a *B. subtilis* strain expressing His-tagged RNAP but carrying deletions of the two 6S RNA genes. The His-tagged, 6S RNA-free σ^A -RNAP holoenzyme can be prepared with sufficient purity and activity by a single affinity step. We also report expression and separate purification of *B. subtilis* σ^A that can be added to the His-tagged RNAP to maximize the amount of holoenzyme and, by inference, *in vitro* transcription activity.

INTRODUCTION

The Gram-positive, spore-forming bacterium *Bacillus subtilis*, representing the phylum Firmicutes, is a major bacterial model organism in general and for studies on regulation of gene expression in particular. The *B. subtilis* core RNA polymerase with the subunit composition $\beta\beta'(\alpha)_2\epsilon\omega$ (~ 350 kDa) predominantly associates with the housekeeping sigma factor σ^A for recognition of housekeeping DNA promoters during exponential growth phase. However, ~ 20 alternative or phage sigma factors, numerous transcription regulators and cofactors such as HelD, RpoE, NusA, GreA, Btr, CshA, MgsR, CcpA, CodY, PcrA and Spx (for overview, see SubtiWiki; Zhu and Stülke, 2018), as well as the two non-coding RNAs 6S RNAs (6S-1 and 6S-2 RNA; Trotochaud and Wassarman, 2005) have been identified as interaction partners of *B. subtilis* RNAP. They change promoter specificity and gene expression profiles, affect the kinetics of transcription and modulate the transcription process primarily in response to altered environmental and multiple stress conditions. Moreover, >200 DNA-binding transcription factors were identified in *B. subtilis* (Moreno-Campuzano *et al.*, 2006). Altogether, this justifies a central interest in RNAP purification protocols for the *in vitro* study of many aspects of gene expression control in *B. subtilis* (Delumeau *et al.*, 2011, Sierro *et al.*, 2008; Zhu and Stülke, 2018).

Initial protocols described the preparation of the native *B. subtilis* RNAP holoenzyme ($\sigma^A\beta\beta'\alpha_2$) via phase partitioning, ammonium sulfate precipitation, weak anion-exchange (DEAE cellulose) and DNA cellulose chromatography (Avila *et al.*, 1971; Jiménez *et al.*, 1974), or by heparin agarose chromatography, glycerol gradient centrifugation and chromatography on a single-stranded DNA agarose column (Davison *et al.*, 1979). However, these procedures are complex, laborious and in our hands hard to reproduce. Later, derivatives of *B. subtilis* strain JH642 carrying a chromosomal *rpoC* copy encoding a β' subunit with a C-terminal His tag were constructed, enabling the isolation of the *B. subtilis* RNAP holoenzyme by a single Ni-NTA affinity chromatography step (Qi and Hulett, 1998; Fujita and Sadaie, 1998). For preparation of His-tagged core RNAP without σ^A from strain MH5636 (Qi and Hulett, 1998), eluates from the Ni-NTA column were further passed through a phosphocellulose column (Qi and Hulett, 1998), or through a Superdex 200 gel filtration column followed by Mono Q

anion-exchange chromatography (Anthony *et al.*, 2000). The first strategy has the disadvantage that phosphocellulose matrices have become commercially unavailable. Size exclusion steps, applied in the second strategy, are usually critical in purification schemes and require expensive gel filtration media with tailored resolution in the size range of bacterial core RNAP (~ 350 kDa); here, column size is critical, as small columns restrict the input sample volume and large columns largely dilute the protein preparations. In another approach, plasmid-encoded *B. subtilis* core RNAP including a His-tagged *rpoC* subunit was overexpressed in *E. coli* and purified by Ni-NTA affinity and MonoQ anion-exchange chromatography (Yang *et al.*, 2008). In our hands, this approach has the drawback that the large, 13-kb plasmid encoding the α , β and β' subunits of *B. subtilis* RNAP under control of a T7 promoter gives rise to only moderate expression levels. Overall, the robust and efficient methodology of isolating a homologous, His-tagged RNAP has become prevalent and has also given rise to *B. subtilis* derivative strains with inactivated RNAP cofactor genes (*heiD*, *rpoE*); such strains were expedient in studies investigating the functional interplay between such cofactors and *B. subtilis* RNAP (Wiedermannova *et al.*, 2014, Rabatinová *et al.*, 2013).

Although more robust and efficient than multi-step protocols for the isolation of native RNAP, approaches based on a single-step isolation of His-tagged RNAP directly from cell lysates bear the risk of co-purifying cellular interaction partners. The copurification of transcription factor HeiD with His-tagged *B. subtilis* RNAP from lysates of strain MH5636 strain was already described (Wiedermannova *et al.*, 2014). We isolated *B. subtilis* RNAP from strain MH5636 for interaction studies with *B. subtilis* 6S-1 mutant RNAs. 6S RNAs mimic an open DNA promoter structure and thereby inactivate housekeeping RNAP holoenzymes (Barrick *et al.*, 2005; Steuten *et al.*, 2014; Chen *et al.*, 2017). One assay to study the function of 6S RNAs is pRNA transcription, where σ^A -RNAP utilizes the bound 6S RNA as template in an RNA-dependent RNA polymerase reaction to synthesize short abortive transcripts, named product RNAs (pRNAs). When these pRNAs reach a certain length (~ 14 nt), they remain stably bound to 6S RNA and persistently rearrange its structure. This leads to dissociation of the σ^A -RNAP:6S RNA complex and releases σ^A -RNAP from the 6S RNA block (Beckmann *et al.*, 2011, 2012; Burenina *et al.*, 2014; Hoch *et al.*,

of σ^A -RNAP (no σ^A -RNAP). Samples were analyzed by 25 % denaturing PAGE and phosphor-imaging. For more details, see Materials and Methods.

RESULTS and DISCUSSION

Endogenous 6S RNA copurifies with His-tagged σ^A -RNAP isolated from *B. subtilis* strain LK782

In pRNA transcription assays using the His-tagged σ^A -RNAP isolated from *B. subtilis* strain LK782 and *B. subtilis* 6S-1 RNA as template we noticed some contamination with endogenous 6S RNA. This was evident in controls without addition of *in vitro* transcribed 6S-1 RNA template (Fig. 1, lane 3). As the pRNA pattern was remarkably similar in lane 3 versus 5 (with addition of exogenous 6S-1 RNA), we concluded that primarily endogenous 6S-1 RNA was copurified with the His-tagged σ^A -RNAP.

Construction of strain SG7

To be able to prepare His-tagged σ^A -RNAP without traces of endogenous 6S RNAs, we transferred the *rpoC* gene encoding the C-terminally His-tagged β' subunit of strain MH5636 into the genome of *B. subtilis* PY79 $\Delta bsrAB$ lacking both 6S RNA genes (Hoch *et al.*, 2015). Using a modified competence medium protocol (Spizizen *et al.*, 1958), homologous recombination was triggered between the genomic DNAs of strain MH5636 (Qi and Hulett, 1998) and the competent cells of strain PY79 $\Delta bsrAB$. In the latter strain, the genes encoding 6S-1 RNA (*bsrA*) and 6S-2 RNA (*bsrB*) were replaced by spectinomycin and kanamycin resistance genes, respectively (Hoch *et al.*, 2015), while strain MH5636 encodes a chloramphenicol resistance gene next to the *rpoC* gene (Fig. S1). This allowed selection of recombinants on agar plates containing all three antibiotics. Genomic DNA was isolated from triple-resistant overnight colonies and analyzed with the primer pair *rpoC_for* and *rpoC_rev* specific for the *rpoC* gene.

Promising candidate clones were identified by colony PCR using the primer pair *rpoC_for* and *rpoC_rev*. Fig. 2A (lanes 2-4) shows the PCR products obtained with this primer pair and using either genomic DNA from *B. subtilis* strain MH5636, strain W168 used as control, or from the SG7 clone representing the

newly constructed strain. Our selected clone SG7 gave rise to the same PCR product as strain MH5636, demonstrating successful recombination at the *rpoC* locus of the PY79 $\Delta bsrAB$ strain (see schematic representation in Fig. 2B). To rule out the possibility of cellular re-uptake of 6S RNA genes into their native genome locations during recombination, PCR reactions with primer pairs targeting the genomic context of the *bsrA* (6S-1) and *bsrB* (6S-2) loci, respectively, were set up (Fig. 3). Genomic DNA of strain SG7 gave rise to fragments with sizes exactly expected for its PY79 $\Delta bsrAB$ strain background, while the MH5636 genomic DNA gave shorter PCR products representing the lengths of the wild type *bsrA/B* loci (Fig. 3A, lanes 4 and 6 versus 3 and 5). This and partial sequencing (see Fig. 3) of the two genomic regions in strain SG7 confirmed the absence of *bsrA/B* genes in strain SG7.

To verify the identity of the His-tagged *rpoC* gene insertion into our PY79 $\Delta bsrAB$ strain background and the absence of mutations, we sequenced the entire genomic region (~ 8 kb) by primer walking (Fig. S2). The recombinant *rpoC* gene region of strain SG7 was directly compared to the original *rpoC* gene region of PY79 and deduced to be free of mutations from the sequenced end of the *rpoB* gene to the region encoding the C-terminal His₁₀ tag of the recombinant *rpoC* gene. This unequivocally confirmed the Campbell style insertion of the His₁₀ tagged *rpoC* gene 3' end into the genome of the PY79 $\Delta bsrAB$ recipient strain according to Fig. S1.

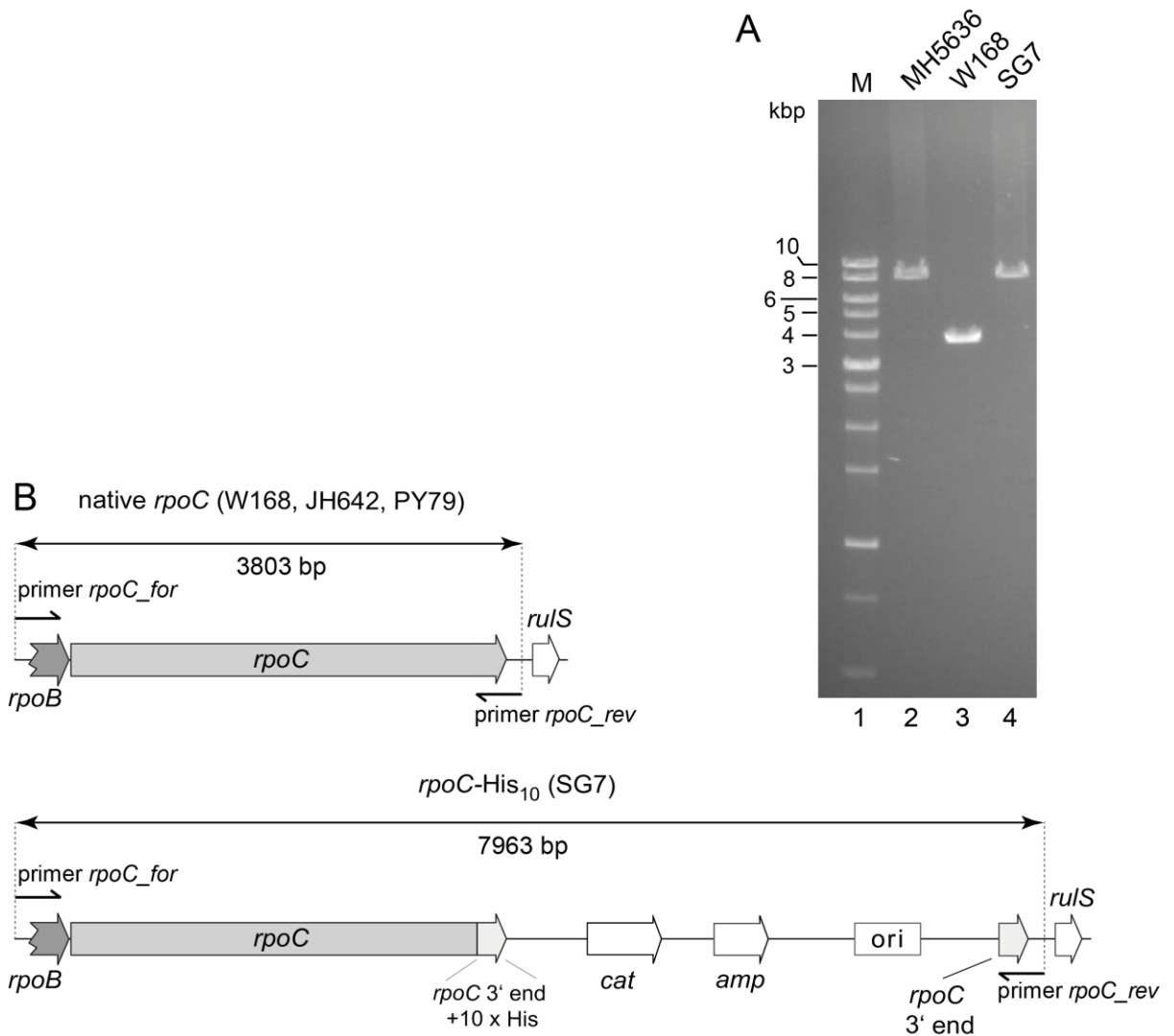


Fig. 2. PCR amplification products of the native and engineered *rpoC* locus. (A) Primer pair *rpoC_for* and *rpoC_rev* (see Table 1) was used to check the size of the *rpoC* gene region in strains MH5636 (JH642 derivative strain), W168 and the constructed strain SG7 (lanes 2-4). The engineered *rpoC* locus of *B. subtilis* strains MH5636 (lane 2) and SG7 (lane 4) includes the entire integration vector pYQ52, resulting in a longer PCR product than obtained for the native *rpoC* locus as present in strain W168 (lane 3). Lane 1, dsDNA size marker (1 kb ladder, CytoGen GmbH, Sinn, Germany), with relevant fragment sizes (in bp) indicated at the left margin. **(B)** Graphical representation predicting the size of the PCR amplification products of the native and engineered *rpoC* locus. The native *rpoC* gene (sequence-identical in *B. subtilis* strains W168, JH642 and PY79) is 3.8 kbp long, the engineered one ~ 8 kbp.

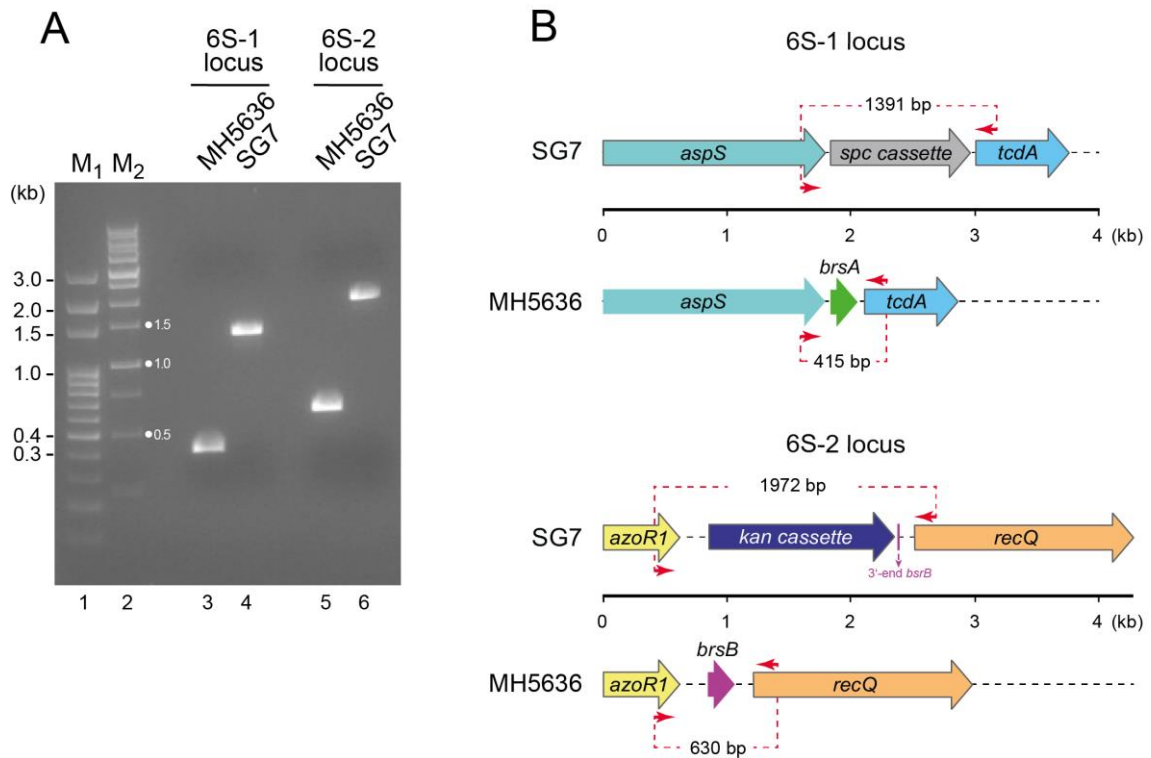


Fig. 3. Strain SG7 lacks 6S RNA genes. The presence of 6S-1 and 6S-2 RNA gene loci was analyzed by PCR to exclude that these genes were reinserted into their native genome locations in strain SG7 during recombination of the MH5636 and PY79 Δ *bsrAB* chromosomes. **(A)** PCR fragments (lanes 3-6) amplified from genomic DNA of strains SG7 and MH5636 using the primer pairs 6S-1_for_SG/6S-1_rev_SG or 6S-2_for_SG/6S-2_rev_SG (see Table 1). Lanes 1 and 2 (M₁ and M₂) are 100 bp and 1 kb DNA ladders (CytoGen GmbH, Sinn, Germany), respectively, with relevant fragment sizes indicated. **(B)** Schematic representation of the anticipated 6S-1 RNA (*bsrA*) and 6S-2 RNA (*bsrB*) loci in strains SG7 versus MH5636. The PCR primer pairs are depicted as red arrowheads. The extant 3'-terminal 32 bp of the *bsrB* gene at the *bsrB* locus of strain SG are indicated in magenta. The anticipated PCR fragment sizes (1391, 415, 1972 and 630 bp) are consistent with the sizes inferred from the gel in panel A. We further validated the *bsrA/bsrB* loci of strain SG7 by sequencing into the antibiotic cassettes from both sides using sequencing primers (see Table 1) annealing in the *aspS* and downstream of the *tcdA* (= *yrvM*) genes (6S-1 locus, primers 6S-1_seq_for and 6S-1_seq_rev), or in the *azoR1* (= *azoJ*, *yocJ*) and the *recQ* (= *yocI*) genes (6S-2 locus, primers 6S-2_seq_for and 6S-2_seq_rev).

Purification of SG7 RNAP

For purification of SG7 RNAP, cells were lysed by sonication. After centrifugation, the cleared cell lysate was loaded onto a Ni-NTA column (Fig. 4; for details, see Material and Methods). The bulk of RNAP often elutes in a single fraction (5 mL). One may collect this single fraction to maximize the final protein concentration.

We also pooled either 2 fractions (when there is a second fraction with second most protein; corresponding to fraction e and f in Fig. 4) or 4 fractions when aiming at collecting as much RNAP as possible (this would correspond to collecting fractions d to g in Fig. 4). The single or pooled fraction(s) were dialyzed into storage buffer and stored at -20 °C (for details, see Materials and Methods). After dialysis against the glycerol-containing storage buffer, the sample volume is shrunk to ~ 50 % of the initial volume. The yield of σ^A -RNAP was in our hands 6 to 8 mL with a protein concentration of 1 to 2 mg/mL when 4 fractions were pooled. This option is advised if one wants to conduct a series of experiments with the same enzyme preparation, provided that the enzyme concentration of 1 to 2 mg/mL is sufficient for this purpose. In the case of collecting only the main elution fraction, the yield was ~ 2.5 mL with a concentration of up to ~ 4 mg/mL. The His-*rpoC* protein expression of SG7 strain is stable and multiple purification batches of SG7 RNAP were compared, demonstrating reproducible enzyme activities (Fig. S3).

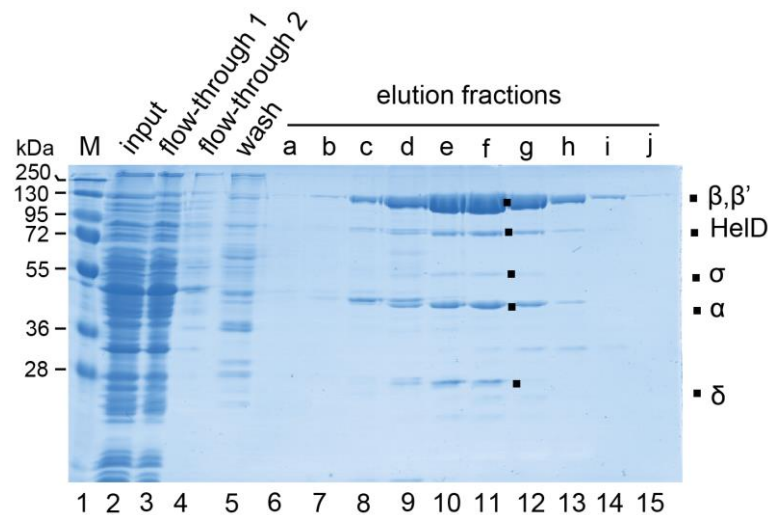


Fig. 4. Ni-NTA affinity chromatography effectively purifies His-tagged σ^A -RNAP from strain SG7. The gel depicted is a 12 % SDS gel and protein bands visualised are Coomassie stained. Lane 1, PageRuler™ Plus prestained Protein ladder (Thermo Scientific™) used as size marker (in kDa); lane 2, crude cell lysate from strain SG7 (input) loaded onto the column; lane 3 and 4, flow-through; lane 5, wash fraction; lanes 6-15, elution fractions; fractions d to g were selected and dialyzed into storage buffer and stored at -20 °C (for details, see Material and Methods).

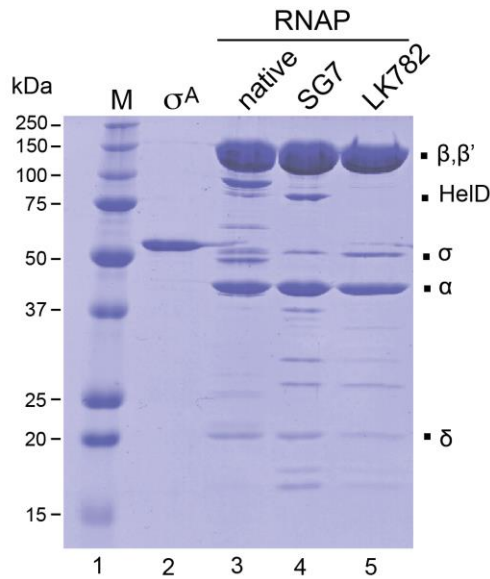


Fig. 5. 12 % SDS-PAGE analysis of *B. subtilis* σ^A and σ^A -RNAP preparations. Lane 1, 5 μ L Precision Plus Protein™ All Blue Prestained Protein Standards (Bio-Rad, #1610373) used as size marker; lane 2, 5 μ g N-terminally His₆-tagged *B. subtilis* σ^A protein (~43 kDa) prepared in this study; note that the recombinant protein migrates somewhat slower than native σ^A owing to the His tag; lane 3, native σ^A -RNAP isolated from *B. subtilis* strain 110NA (native *rpoC*); lanes 4 and 5, His-tagged σ^A -RNAP isolated from *B. subtilis* strains LK782 and SG7, respectively. RNAP subunits are depicted on the right. 15 μ g protein were loaded in lanes 3-5.

SG7 RNAP isolated via a single Ni-NTA affinity purification step was analyzed by SDS-PAGE along with purified native σ^A -RNAP (prepared according to Sogo *et al.* 1979), His-tagged σ^A -RNAP from strain LK782 isolated in the same manner, and recombinant His-tagged σ^A (Fig. 5, lanes 2-5). Subunits β , β' , σ^A , α and δ were identifiable in all three RNAP preparation (lanes 3-5). A band assignable to the helicase HelD based on size and its known association with RNAP (Wiedermannová *et al.*, 2014) was prominent in the SG7 preparation. Overall, The SG7 RNAP preparation was satisfactorily pure with fair enrichment of the major RNAP subunits after Ni-NTA chromatography (Fig. 5). It was shown that HelD stimulates transcription in an ATP-dependent manner by enhancing transcriptional cycling and elongation, and this effect was enhanced in the presence of δ (Wiedermannová *et al.*, 2014). As HelD removes nucleic acids from the active site of RNAP (Newing *et al.*, 2020; Pei *et al.*, 2020), we considered the possibility that copurification of 6S-1 RNA with σ^A -RNAP from LK782 cells might be due to the *helD* knockout in this strain. Yet, we also observed copurification of

6S-1 RNA in σ^A -RNAP preparations from *B. subtilis* strain 110 NA and the MH5636 derivative strain LK637 (Rabatinová et al., 2013), both expressing HelD.

Transcriptional activity of SG7 RNAP

In vitro transcription reactions were set up to assess the enzymatic activity of native σ^A -RNAP (from strain 110 NA) as well as His-tagged σ^A -RNAP from strains SG7 and LK782. For this purpose, we used a linear DNA fragment encoding the σ^A -dependent *veg* promoter that is constitutively expressed during vegetative growth (Fukushima et al., 2003). The *veg* template gave rise to two runoff transcripts, 148 and 190 nt in length, when using the His-tagged σ^A -RNAP enzymes (Fig 6A, lanes 6 and 8). The minor transcript can be assigned to transcription initiated from an alternative start site upstream of the conventional start site (6B) as described in Guiziou et al. (2016). For unknown reasons, the native σ^A -RNAP preparation was essentially inactive on such linear PCR fragments (Fig. 6A, lane 4), although the same enzyme was active in pRNA transcription. We had observed this before (Burenina et al., 2014) and there switched to σ^A -RNAP preparations from strain MH5636 for transcription of linear DNA templates. We then compared the two His-tagged σ^A -RNAP enzymes for pRNA transcription as a function of adding *B. subtilis* 6S-1 RNA as template. This demonstrated the absence of endogenous 6S-1 RNA in the preparation from strain SG7 relative to that from strain LK782 (Fig. 7, lanes 3 and 5 versus 6 and 8). We also obtained similar results with three independent σ^A -RNAP preparations (batches) from strain SG7 analyzed in the same assay (Fig. S3). Thus, the quality of independent SG7 σ^A -RNAP preparations was reproducible.

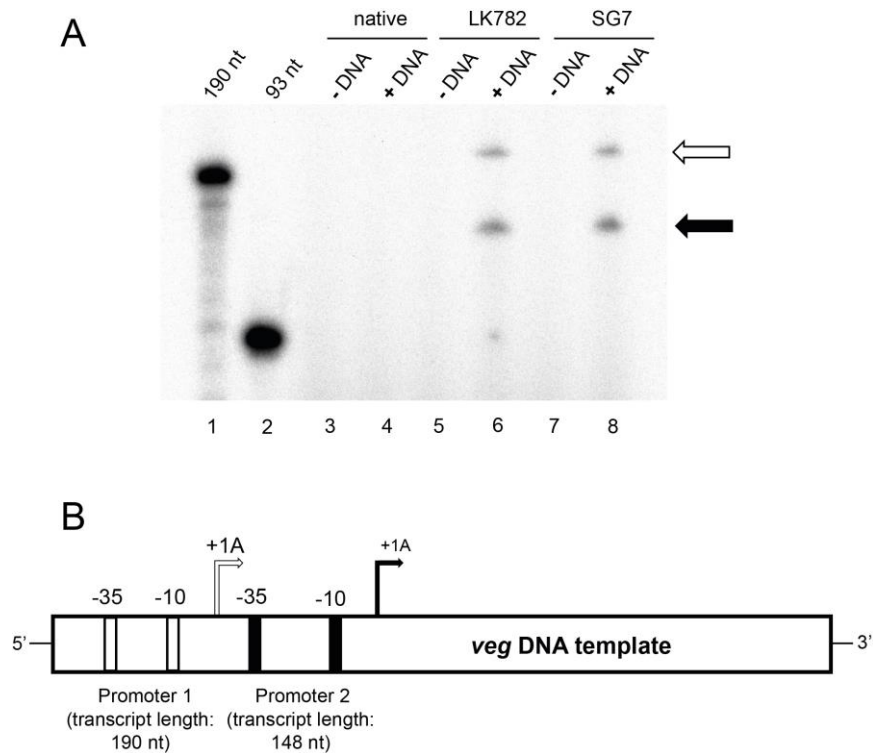


Fig. 6. Transcriptional activity of σ^A -RNAP enzymes using the *veg* template (A) *In vitro* transcription reactions in the presence α - 32 P-UTP using a 288 bp long PCR template of the *veg* gene locus and the σ^A -RNAP preparations illustrated in Fig. 5 (native, LK782 and SG7). Lanes 1 and 2, 5'- 32 P-labeled RNA size markers with sizes indicated above the lanes; lanes 3-8, reactions with the three σ^A -RNAP preparations as indicated, each with *veg* template (+DNA) or without (-DNA). **(B)** Graphical representation illustrating the two promoters (-35 and -10 boxes) and transcription start sites (TSS) on the *veg* DNA template. The first TSS results in a ~190 nt long runoff transcript, marked by the open arrow in panel A; transcription initiation at the main promoter yields a 148 nt runoff transcript, depicted by the black arrow in panel A. Both transcripts were reported to start with an A residue (Guiziou *et al.*, 2016).

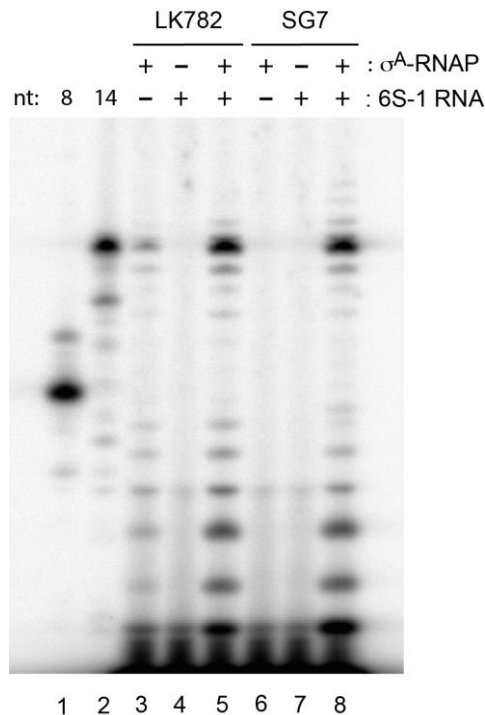


Fig. 7. pRNA transcription confirms the absence of endogenous 6S RNA in σ^A -RNAP preparations from strain SG7. Lanes 1 and 2, chemically synthesized and 5'-³²P-labeled 6S-1 pRNA 8-mer (5'-GUUCGGUC) or 14-mer (5'-GUUCGGUCAAAACU) used as size markers; lanes 3 and 5, pRNA *in vitro* transcription by LK782 σ^A -RNAP with (lane 5) or without (lane 3) added 6S-1 RNA; lane 4, as lane 5 but omission of enzyme; lanes 6-8, as lanes 3-5, but using SG7 σ^A -RNAP. Samples were analyzed by 25 % denaturing PAGE and phosphor-imaging. For more details, see Materials and Methods.

Preparation of recombinant *B. subtilis* σ^A

The housekeeping sigma factor (σ^A) of *B. subtilis* mediates promoter recognition and transcription initiation. We recombinantly expressed His-tagged *B. subtilis* σ^A for mechanistic studies. A previously published protocol described the purification of a tag-free recombinant σ^A (Chang *et al.*, 1990). This necessitated guanidine hydrochloride treatment because σ^A was expressed in inclusion bodies, followed by several purification steps including weak anion-exchange chromatography (DEAE-cellulose), ammonium sulfate precipitation and gel filtration. To minimize the methodological effort, we utilized a robust and efficient protocol for recombinant σ^A preparation that builds on published procedures (Rollenhagen *et al.*, 2003; Johnston *et al.*, 2009) but makes use of overexpression at lower temperature (IPTG induction for 16 h at 15 °C) to improve protein folding. For example, expression at lower temperature (16 °C) was shown

to yield a substantially higher proportion of soluble and functional GFP than expression at 30 or 37 °C in *E. coli* BL21 (DE3) cells (Vera *et al.*, 2006). Using the T7 expression system, high amounts of soluble N-terminally His-tagged σ^A were recombinantly expressed in *E. coli*, followed by a quick and efficient single-step purification via Ni-NTA affinity chromatography directly from cell lysates (for details, see Materials and Methods). In three independent preparations, application of the protocol resulted in reproducible yields of soluble and active protein of high purity (20-24 mg σ^A per liter of cell culture). We further compared σ^A expression at 15 °C, 25 °C and 37 °C. Our results (illustrated in Fig. S4) revealed expression of ~50 % soluble σ^A protein upon IPTG induction for 16 h at 15 °C (terminal OD₆₀₀ = 1.5). At 37 °C, when cells were grown to a comparable OD₆₀₀, the insoluble σ^A fraction increased. Surprisingly, expression at 25° C yielded less protein when cells were grown to an OD₆₀₀ of 1.5 as applied to induction at 15 °C, but the fraction of soluble σ^A increased to > 50 %. Overnight induction (16 h) at 25 °C, relative to 15 °C, again increased the fraction of insoluble σ^A . Thus, induction at 25°C for 2 h (or somewhat longer, but definitely much shorter than 16 h) might be considered as an alternative to induction at 15 °C for 16 h. All in all, the 15 °C expression protocol stands out in terms of its robustness and by combining acceptable protein yields with a relatively high proportion of soluble σ^A protein.

As inferred from the *E. coli* system, heparin-resistant binding of 6S RNA depends on the housekeeping sigma factor (σ^{70} in *E. coli*, σ^A in *B. subtilis*) (Gildehaus *et al.*, 2007; Klocko and Wassarman, 2009). Here we tested the σ^A protein (induction at 15 °C) in our standard gel shift assay used to analyze 6S-1 RNA binding to RNAP. Adding a 10-molar excess of σ^A to our SG7 σ^A -RNAP increased the affinity for 6S-1 RNA ~ two-fold (Fig. 8). Recombinant σ^A was reported to be saturating at a 5-fold excess over core RNAP (Sudzinová *et al.*, 2021), but 10 to 15-fold excesses were reported in other studies (Holátko *et al.*, 2012). In addition, our binding assay was performed at 100 nM 6S-1 RNA and excess concentrations (the lowest being 370 nM) of preassembled SG7 σ^A -RNAP. σ^A saturation effects may manifest differently in σ^A titration assays using core RNAP and excess amounts of 6S-1 RNA. Finally, we cannot exclude that a subfraction of our recombinant σ^A may not be fully functional. Nonetheless,

the experiment in Fig. 8 shows that our recombinant, His-tagged σ^A preparation contains substantial amounts of functional σ^A factor. Likewise, the result also demonstrates that the SG7 σ^A -RNAP already includes sufficient σ^A amounts for functional studies on its own.

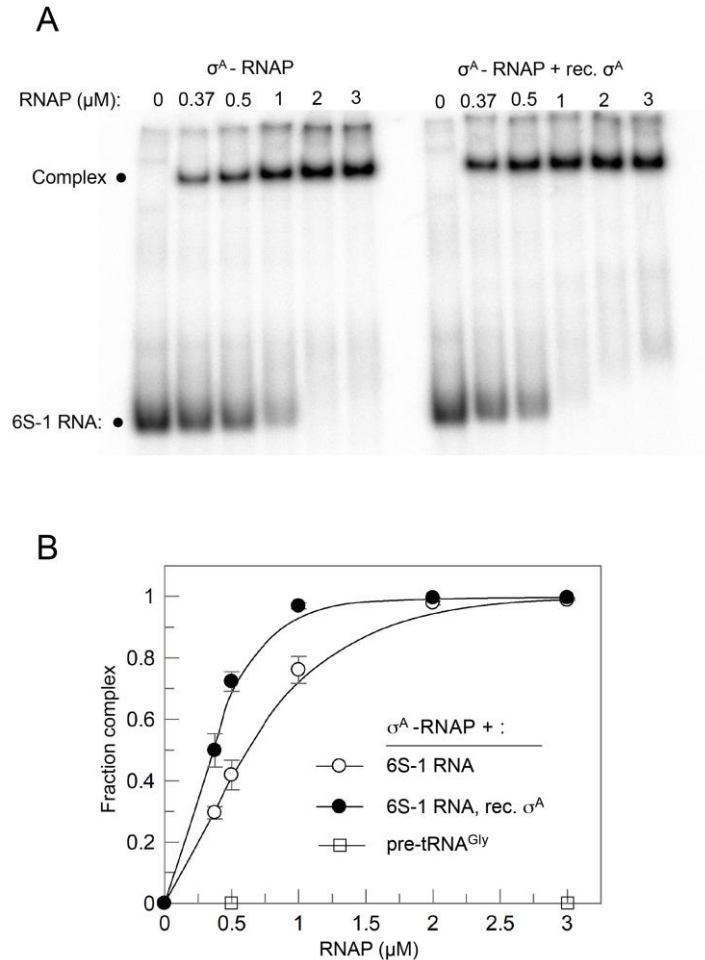


Fig. 8. Binding affinity of SG7 RNAP to 6S-1 RNA improves upon σ^A factor supplementation. (A) Complex formation of 6S-1 RNA and SG7 σ^A -RNAP as a function of σ^A -RNAP concentration, analyzed by gel shift assay. The position of the specific complex and free 6S-1 RNA ($5'$ - ^{32}P -end-labeled) is depicted at the left margin. In the gel on the right, the concentration of SG7 σ^A -RNAP was varied as in the gel on the left, but enzyme was supplemented with a 10-fold molar excess of recombinantly expressed σ^A at each RNAP concentration. (B) The binding affinity was evaluated by plotting the fraction of complex against the RNAP concentration. The data points were connected by a spline curve. The RNAP concentration required to reach 50 % of RNA binding at saturation was 0.6 μM for σ^A -RNAP alone (●) and 0.38 μM for σ^A -RNAP supplemented with recombinant σ^A (●). Pre-tRNA^{Gly} from the bacterium *Thermus thermophilus* (Brillante *et al.*, 2016), carrying a 14-nt single-stranded 5'-flank, was analyzed at 0.5 and 3 μM to control for non-specific RNA binding to σ^A -RNAP (□) (see also Fig S4). Data points are mean

values of three independent experiments, with errors indicating the standard error of the mean (SEM) calculated using Grafit version 3.04 (Erithacus Software).

Materials and Methods

Bacterial strains

B. subtilis MW Δ *bsrAB* is a prototrophic derivative of strain PY79 described as PY79 Δ *bsrA:spc* (Sp^r) Δ *bsrB:kan* (Km^r) (Hoch *et al.*, 2015). *B. subtilis* MH5636 is a derivative of strain JH642 and harbors an *rpoC*-His10 allele (Qi and Hulett, 1998); *B. subtilis* LK782 was derived from strain MH5636 and additionally carries an inactivated *helD* gene (Wiedermannová *et al.*, 2014). 1.5 % LB agar plates and liquid LB medium were used for bacterial growth unless otherwise indicated. Concentrations of antibiotics used for strain selection were 10 μ g/mL for kanamycin (Km), 100 μ g/mL for spectinomycin (Sp), 100 μ g/mL for ampicillin (Amp) and 2.5 μ g/mL for chloramphenicol (Cm). The here constructed strains SG7 and DE3 σ^A nHis are available from the authors upon request.

Strain construction

6 mL of LB broth overnight culture (supplemented with Cm) was inoculated with a single colony of strain MH5636. OD₆₀₀ was measured at 1:10 dilution to calculate cell count (standard conversion factor OD₆₀₀ of 1 corresponds to 8×10^8 cells/mL). 2×10^9 (1.34 mL of overnight culture) was centrifuged at $\sim 7300 \times g$ for 10 min. The supernatant was discarded and the cell pellet was resuspended in lysis buffer and processed further as instructed by the protocol of the DNeasy Blood and Tissue extraction kit (Qiagen, Cat. No. / ID: 69504). The eluted genomic DNA of strain MH5636 was quantified using UV spectroscopy. *B. subtilis* strain PY79 Δ *bsrAB* was streaked onto LB plates containing Km and Sp. Isolated colonies were picked and inoculated into 7 mL LB medium (supplemented with Km and Sp) in a 100 mL baffled Erlenmeyer flask that was incubated at 30°C overnight in a water bath (Aquatron, Infors AG, Switzerland) under shaking at 200 rpm. The OD was measured at 600 nm (1:10 dilution); approx. 150 μ l of the overnight culture were added to 10 mL modified competence medium in a 250 mL baffled flask, thereby adjusting the OD₆₀₀ to 0.08; this culture was shaken at 200 rpm and 37 °C. The modified competence medium is

composed of 10 % (v/v) 10 x MC, 3.33 % (v/v) 1 M MgSO₄, in H₂O. The 10x MC medium consists of 0.62 M potassium phosphate dibasic trihydrate, 0.39 M potassium phosphate monobasic, 1.11 M glucose anhydrous (added as powder), 33 mM trisodium citrate, 0.84 mM ferric ammonium citrate, 0.01 g/ml casein hydrolysate, 0.11 M potassium glutamate and ddH₂O. The 10x MC medium was not autoclaved instead sterile filtered and stored at -20 °C in small aliquots that are easily discarded after one time use. At an OD₆₀₀ of ~ 1.4, 1 mL of cell culture was transferred to a 13 mL polypropylene reaction tube (Sarstedt, order number 62.515.006) and 500 ng of genomic DNA (MH5636) was added. The reaction mixture was shaken at 200 rpm, 37 °C and for 2 h in a warm air shaking incubator (GFL). 200 µL of the suspension was then plated on antibiotic screening plates (containing 10 µg/mL Km, 100 µg/mL Sp and 2.5 µg/mL Cm) and incubated overnight at 37 °C. Screening and selection of positive clones was achieved by genomic DNA extraction from overnight colonies, followed by a PCR reaction with the locus-specific primer pair *rpoC_for* and *rpoC_rev* (Table 1) to confirm the presence of the recombined locus encoding a His-tagged RpoC (β') subunit. Specific primer pairs flanking the *bsrA* (6S-1) and *bsrB* (6S-2) locus (6S-1_for_SG/6S-1_rev_SG and 6S-2_for_SG/6S-2_rev_SG; Table 1) were used to test and rule out the possibility of a reinsertion of the *bsrA* and *bsrB* genes at their respective native genome locations.

Cell culture and harvest of strain SG7

A single colony of strain SG7 was picked to inoculate 40 mL LB broth (containing 10 µg/mL Km, 100 µg/mL Sp and 2.5 µg/mL Cm), followed by overnight growth at 37 °C in the warm air shaking incubator (GFL) at 200 rpm. The overnight culture was used to inoculate 1.8 L LB medium (prewarmed to 37° C, containing Km, Sp and Cm) in a 5 L baffled Erlenmeyer flask, and the culture was grown at 37 °C under shaking (220 rpm) to late exponential phase (OD₄₂₀ of 1.5 to 2.0; OD₄₂₀ is ~ 1.7-fold than OD₆₀₀) and then harvested by centrifugation at 17,700 x g (JA - 10 rotor, Beckmann ultracentrifuge). Growth curves measured using OD₆₀₀ was consistent to OD₄₂₀ in terms of phases of growth curve although the OD value itself changes. Cell pellets were snap-frozen in liquid nitrogen and stored at - 80 °C until further use. Strain LK782 was grown according to the same

protocol with the exception that chloramphenicol was the only antibiotic to be added.

Purification of His-tagged σ^A -RNAP

15 g of harvested cells were resuspended in optimally 35 mL sonication buffer (50 mM Tris-HCl pH 7.8, 300 mM NaCl, 5 mM MgCl₂, 20 % Glycerol) containing lysozyme (f. c. 4 mg/mL) by stirring thoroughly for 30 min on ice or at 4 °C. Then phenyl methyl sulfonyl fluoride (f. c. 1 mM) was added and the cells were sonicated on ice (output 20 %, duty cycle 50 %, S-250 Branson sonifier) in 8 cycles each lasting 30 s with intervals of 2 min. The sonicated cell lysate was centrifuged at ~ 10,200 x g for 1 h at 4 °C. The supernatant was processed further by filtering through 0.2 µm filters (Sarstedt) and stored on ice. For subsequent Ni-NTA chromatography, buffers differing in imidazole concentration were used, namely binding buffer (50 mM Tris-HCl pH 7.8, 300 mM NaCl, 5 mM MgCl₂, 20 % Glycerol and 30 mM imidazole) and elution buffer (50 mM Tris-HCl pH 7.8, 300 mM NaCl, 5 mM MgCl₂, 20 % Glycerol and 400 mM imidazole). The Ni-NTA column (HisTrap HP 5 mL, GE Healthcare) was equilibrated by passing 5 column volumes (CV) of ddH₂O, 5 CV elution buffer and 10 CV sonication buffer (flow rate 5 mL/min). Then the filtered supernatant (≤ 50 mL) was loaded onto the column at a flow rate of 5 mL/min. After loading the supernatant, the column was washed with binding buffer until the baseline of the detector at 280 nm was reached (~ 10-15 CV). Then elution was performed by applying a linear gradient from 30 mM (binding buffer) to 400 mM (elution buffer) imidazole over 15 CV, collecting fractions of 5 mL. Aliquots of the eluted fractions (9 µL per fraction) were analyzed by 12 % SDS-PAGE and fractions containing σ^A -RNAP were pooled and dialyzed into storage buffer (10 mM Tris pH 8.0, 10 mM MgCl₂, 0.1 mM EDTA, 0.1 mM DTT, 0.1 M NaCl and 50 % (v/v) Glycerol) and stored at - 20 °C.

Purification of native RNA polymerase

Native *B. subtilis* σ^A -RNA polymerase holoenzyme was prepared as described in Sogo *et al.* (1979).

***In vitro* transcription of *B. subtilis* 6S-1 RNA**

Mature 6S-1 RNA (190 nt; gene *bsrA*) was transcribed from a pUC18 derivative plasmid encoding 6S-1 RNA (pUC18_m6S1) under control of the class III T7 promoter. 14 µg of plasmid template (linearized with HindIII) was transcribed in a volume of 200 µL containing 33 mM MgCl₂, 80 mM Hepes pH 7.5, 1 mM Spermidine, 5 mM DTT, 0.05 U Phosphatase, 4 mM NTPs (each), 5 % DMSO and 4 µL of T7 RNA polymerase (40 U/µL) (purified as described in Zawadzki *et al.*, 1991). After an incubation period of 2 h at 37 °C, a second 4 µL aliquot of T7 RNA polymerase was added followed by incubation at 37° C for another 2 h. The sample was then mixed with 2 x denaturing loading dye [95 % (v/v) formamide, 0.025 % (v/v) SDS, 0.025 % (v/v) bromophenol blue, 0.025 % (v/v) xylene cyanol, 0.5 mM EDTA], heated for 3 min to 98 °C followed by cooling on ice for 5 min. Samples were subjected to 7.5 % denaturing (8 M urea) polyacrylamide gel electrophoresis (PAGE; running buffer 1 x TBE) for 3 h at 25 mA. The 6S-1 RNA band was identified by UV shadowing, excised from the gel and eluted in 1 M NaOAc at 4 °C overnight. The eluted RNA was recovered using ethanol precipitation, redissolved in ddH₂O and quantified using UV spectroscopy.

pRNA transcription assay

0.7 µL of a ~ 15.2 µM 6S-1 RNA solution were mixed with 0.7 µL of 2 x TE buffer (20 mM Tris-HCl pH 8.0, 2 mM EDTA) and heated to 80 °C in a PCR machine; after 2 min at 80 °C, the temperature was lowered to 70 °C, kept for 2 min at 70 °C; this was repeated for temperature shifts to 60 and 50 °C, followed by shifting the temperature to 37 °C for further use. To this mixture, 2 µL of transcription buffer (final concentration 20 mM Tris HCl pH 8.0, 2.5 mM MgCl₂, 80 mM KCl, 0.5 mM DTT), varying volumes of σ^A-RNAP and ddH₂O were added to a volume of ~ 8 µL, followed by incubation for 15 min at 37 °C to allow binding of 6S-1 RNA to σ^A-RNAP. The transcription reaction was initiated by the addition of 1 µL 2 mM NTP mix (f.c. of 200 µM ATP, GTP, CTP and UTP each) and 250,000 c.p.m (~ 1 µL) of radioactive α-³²P-UTP, resulting in final volume 10 µL. After 60 min of incubation at 37 °C, 5 µL of the reaction mixture was mixed with 15 µL of 2 x denaturing loading dye [95 % (v/v) formamide, 0.025 % (v/v) SDS, 0.025 % (v/v) bromophenol blue, 0.025 % (v/v) xylene cyanol, 0.5 mM EDTA],

heated for 3 min to 98 °C, followed by cooling on ice for 5 min. Samples were subjected to denaturing 25 % PAGE (8 M Urea, 1 x TBE) for 16 h at 1200 V.

Sequencing the *rpoC* gene insert

The *rpoC* gene region in the genome sequence of *B. subtilis* strain JH642 (NCBI accession number NZ_CP007800) was used to design primers mapping to *rpoC* and its flanking regions. Primers against the *cat* (chloramphenicol acetyltransferase) gene were designed using plasmid vector pC194 (NCBI: NC_002013.1). A 25 µL PCR reaction containing the long PCR master mix (Thermo Fisher Scientific), unique set of primer pairs in each reaction vial and 100 ng of genomic DNA template from strain SG7 His-tag positive clone was set up to amplify shorter PCR fragments. The sizes of PCR products ranged from 1.5 to 7 kbp and were visualized on 0.5 % agarose gels. The PCR products were eluted using the gel elution kit (Promega), recovered in 15 µL elution volume and directly sequenced using the sequencing primers specified in Fig. S2.

Amplification of the *veg* template DNA

A PCR reaction (final volume 50 µL) containing 1x Phusion master mix (Thermo Fisher Scientific), *veg_primer_for*, *veg_primer_rev* and 300 ng of genomic DNA isolated from *B. subtilis* strain 168 was performed according to the manufacturer's recommendations. The resulting PCR product, 288 bp in size, was eluted using the Monarch PCR & DNA Cleanup Kit (New England Biolabs).

***veg* template transcription assay**

Transcription reactions contained 50 nM *veg* DNA template (288 bp), 100 nM *B. subtilis* σ^A -RNAP and 40 ng/µL heparin in transcription buffer (20 mM Tris HCl pH 8.0, 2.5 mM MgCl₂, 80 mM KCl, 0.5 mM DTT). After incubation for 10 min at 37 °C to facilitate DNA:RNAP complex formation, transcription was initiated by the addition of cold NTPs (f.c 50 µM ATP, 50 µM GTP, 50 µM CTP, 12.5 µM UTP) and 50,000 Cherenkov c.p.m. of α -³²P-UTP per lane. Reactions were incubated for 30 min at 37 °C and subsequently terminated by addition of 2 x denaturing loading dye (see above) and heating for 3 min at 98 °C followed by cooling on ice

for 5 min. Samples were analyzed by 7.5 % denaturing PAGE (8 M Urea, 1 x TBE) for 3 h at 30 mA.

Strain construction of His-tagged sigma protein (σ^A nHis)

The σ^A gene of *B. subtilis* was amplified from chromosomal DNA of *B. subtilis* strain 168 using primers sigA_forward and sigA_reverse (Table 1). Plasmid pET28a(+) (Novagen) was amplified using the primer pair vector_forward and vector_reverse (Table 1). This generated PCR products of insert and vector with overlapping ends. After gel elution of amplified insert and vector DNAs using a gel purification kit (Wizard® SV Gel and PCR Clean-Up System, Promega), the overlapping DNA fragments were ligated using Gibson Assembly Master Mix (New England Biolabs; Gibson D G, 2011) according to the manufacturer's instructions. The resulting plasmid pET28a(+): σ^A nHis, encoding σ^A with an N-terminal His₆ tag, was transformed into expression strain *E. coli* BL21 (DE3) and verified by sequencing.

Overexpression and purification of His-tagged sigma protein (σ^A nHis)

1 L cell culture of the expression strain *E. coli* BL21 (DE3) harboring plasmid pET28a(+): σ^A nHis was grown at 37 °C to an OD₆₀₀ of 0.6 to 0.8; then, IPTG (Isopropyl β -D-1-thiogalactopyranoside, Roth) was added to a final concentration of 1 mM. Cells were allowed to grow for 16 h at 15 °C, harvested by centrifugation at 2.000 x g (A-4-81 rotor, Eppendorf 5810R), washed once and resuspended in 30 mL buffer NPI-20 (50 mM NaH₂PO₄, 300 mM NaCl, 20 mM imidazole, pH 7.0). After mechanical disruption via FastPrep (3 cycles of 20 s, 5 min break on ice in between, MP biomedical), the cell lysate was clarified by centrifugation at 6,000 x g (F-34-6-38 rotor, Eppendorf 5810R). For subsequent purification, the supernatant was filtered through 0.2 μ M filters (Sarstedt) and loaded onto a Ni-NTA affinity column (HisTrap HP 1ml, GE Healthcare) that was pre-equilibrated with 5 mL buffer NPI-20, using a flow rate of 1 mL/min. Unspecifically bound proteins were removed by washing with 10 mL buffer NPI-20, and the protein was eluted by applying a linear gradient from 20 to 500 mM imidazole over 15 column volumes (= 15 mL), collecting fractions of 1 mL. Aliquots of the eluted fractions (6 μ L per fraction) were analyzed by 12 %

SDS-PAGE. Fractions containing σ^A nHis were pooled, dialyzed into storage buffer (10 mM Tris-HCl, pH 8.0, 10 mM MgCl₂, 0.1 mM EDTA, and 0.1 mM DTT, 0.1 M NaCl, 50 % glycerol) and stored at -20 °C.

Gel shift assay

A 10 μ L reaction mixture consisting of heparin (f. c 80 ng/ μ L), transcription buffer master mix (f. c 20 mM Tris HCl pH 8.0, 2.5 mM MgCl₂ 80 mM KCl, 0.5 mM DTT), cold 6S-1 RNA or pre-tRNAGly (f. c 100 nM; pre-tRNAGly used to rule out non-specific RNA binding), trace amounts of radioactive 6S-1 RNA or pre-tRNAGly (2,500 c.p.m. per lane) and SG7 σ^A -RNAP (\pm recombinant σ^A) was added in the described order and mixed. The reaction mixture was incubated at 37°C for 30 min. For experiments that included recombinant purified His-tagged σ^A factor (see above), purified SG7 σ^A -RNAP was mixed with a 10-fold molar excess of σ^A factor, followed by preincubation at 30°C for 15 min before addition of the other components. After the main incubation, 10 μ L of native loading dye [10 % (v/v) glycerol, 10 mM MgCl₂, 0.025 % (w/v) BPB and 0.025 % (w/v) XCB] were added to the reaction mixture and loaded onto a native 7.5 % PAA gel (1x TBE). Electrophoresis was carried out for 3 h at 25 mA.

Table 1. Primers used in this study

Primer name	Sequence
<i>rpoC_for</i>	5' GAGCCGGAAGAAACAGCATCTGC 3'
<i>rpoC_rev</i>	5' GATTTCGTTCTTCTCATAGAGTGACTTTTT 3'
<i>rpoC_start_rev</i>	5' GACGGTGTTACAACCGGTTTACCATC 3'
<i>rpoC_mid_rev</i>	5' CTTAGCAAGAATGCCTCGGTCAG 3'
<i>rpoC_mid_for</i>	5' CCGTGAAGGTCTGACAGTATTGGAGTAC 3'
<i>rpoC_380_bp_for</i>	5' GGTGACACTGATGTGCTTCCA 3'
<i>rpoC_his_tag_rev</i>	5' TTAATGATGATGATGATGATGATGATGATGAT GTTCAACCGGGACCATATCGT 3'
6S-1_for_SG	5' CAGCTTGACGAGCTTCATCTTTCTATC 3'
6S-1_rev_SG	5' GCTAATTCATTGCGTGAAAAGTGGTG 3'
6S-2_for_SG	5' GGTTTACAAGAAGCAAAGATCTTGCTG 3'

6S-2_rev_SG	5' CCAGAAGGGATTGGGCTCTATGTAAC 3'
cat_rev	5' GTTTTGGGAAACAATTTCCCCGAACC 3'
cat_for	5' TGAACCAACAAACGACTTTTAGTATAACCACA 3'
GEX3_rev_25	5' GAGCTGCATGTGTCAGAGG 3'
ori_primer	5' GGGAAGCGTGGCGCTTTCTCATAGC 3'
veg_primer_for	5' CATAATTTACCGAAACTTGCGG 3'
veg_primer_rev	5' CAGAAGGGTACGTCTCAGC 3'
sigA_forward	5'CAACTCAGCTTCCTTTTCGGGTTATTCAAGGAAAT CTTTCAAACGTTTACTTCTGCTAGG 3'
sigA_reverse	5' TGGTGCCGCGCGGCAGCCATATGGCTGATAA ACAAACCCACGAG 3'
vector_forward	5' TGGGTTTGTTCATCAGCCATATGGCTGCCG CG 3'
vector_reverse	5' TGAAAGATTTCTTGAATAACCCGAAAGGAAG CTGAGTTGG 3'
6S-1_seq_for	5' CATCAATGTAAAAGGCGGTGC 3'
6S-1_seq_rev	5' GCCATTCTGGCAATCGATGA 3'
6S-2_seq_for	5' CCAAGCAAGTACACCGATATTAG 3'
6S-2_seq_rev	5' GATTCGTTTCAATCTCTCATATATCCG 3'

Strain	Characteristics	Source
<i>B. subtilis</i> MH5636 His- <i>rpoC</i>	<i>pheA1</i> , <i>trpC2</i> , and <i>rpoC</i> Ω pYQ52(Cm ^r)	Qi and Hulett, 1998
<i>B. subtilis</i> MW Δ bsrAB	PY79 Δ <i>bsrA</i> :spc (Sp ^r) <i>\Delta</i> <i>bsrB</i> :kan (Km ^r)	Hoch <i>et al.</i> , 2015
<i>B. subtilis</i> 110 NA	<i>trpC2 spo0A3 su</i> ⁻	Muñoz-Espín <i>et al.</i> , 2009

<i>B. subtilis</i> LK782	<i>pheA1</i> , <i>trpC2</i> , and <i>rpoCΩ pYQ52(Cm^r), <i>helD</i>:MLS</i>	Wiedermannová <i>et al.</i> , 2014
<i>E. coli</i> pBB T7 6S-1 190	pUC18: <i>bsrA</i> , (Amp ^r)	Beckmann <i>et al.</i> , 2011
<i>B. subtilis</i> PY79 His- <i>rpoC</i> , Δ <i>bsrAB</i> (SG7)	PY79 Δ <i>bsrA</i> : <i>spc</i> (Sp ^r), Δ <i>bsrB</i> : <i>kan</i> (Km ^r) <i>rpoCΩ pYQ52 (Cm^r)</i>	This work
BL21 (DE3) σ^A nHis	F- <i>ompT hsdSB</i> (rB-, mB-) <i>gal dcm</i> (DE3) pET28a(+): σ^A nHis	This work

Acknowledgments

We like to thank Marietta Thüring for introduction into genetic recombination of *B. subtilis*. The *B. subtilis* LK782 strain was kindly provided by the laboratory of Libor Krasny (Prague, Czech Republic). This work was supported by the Deutsche Forschungsgemeinschaft (GRK 2355).

References

- Anthony LC, Artsimovitch I, Svetlov V, Landick R, Burgess RR. Rapid purification of His(6)-tagged *Bacillus subtilis* core RNA polymerase. *Protein Expr Purif.* 2000 Aug;19(3):350-4. PMID: 10910724.
- Avila J, Hermoso JM, Vinuela E, Salas M. Purification and properties of DNA-dependent RNA polymerase from *Bacillus subtilis* vegetative cells. *Eur J Biochem.* 1971 Aug 25;21(4):526-35. PMID: 4999759.
- Barrick JE, Sudarsan N, Weinberg Z, Ruzzo WL, Breaker RR. 6S RNA is a widespread regulator of eubacterial RNA polymerase that resembles an open promoter. *RNA.* 2005 May;11(5):774-84. Epub 2005 Apr 5. PMID: 15811922; PMCID: PMC1370762.

- Beckmann BM, Hoch PG, Marz M, Willkomm DK, Salas M, Hartmann RK. A pRNA-induced structural rearrangement triggers 6S-1 RNA release from RNA polymerase in *Bacillus subtilis*. *EMBO J*. 2012 Apr 4;31(7):1727-38. Epub 2012 Feb 14. PMID: 22333917; PMCID: PMC3321203.
- Beckmann BM, Burenina OY, Hoch PG, Kubareva EA, Sharma CM, Hartmann RK. In vivo and in vitro analysis of 6S RNA-templated short transcripts in *Bacillus subtilis*. *RNA Biol*. 2011 Sep-Oct;8(5):839-49. Epub 2011 Sep 1. PMID: 21881410.
- Brillante N, Gößringer M, Lindenhofer D, Toth U, Rossmann W, Hartmann RK. Substrate recognition and cleavage-site selection by a single-subunit protein-only RNase P. *Nucleic Acids Res*. 2016 Mar 18;44(5):2323-36. PMID: 26896801.
- Burenina OY, Hoch PG, Damm K, Salas M, Zatsepin TS, Lechner M, Oretskaya TS, Kubareva EA, Hartmann RK. Mechanistic comparison of *Bacillus subtilis* 6S-1 and 6S-2 RNAs--commonalities and differences. *RNA*. 2014 Mar;20(3):348-59. Epub 2014 Jan 24. PMID: 24464747; PMCID: PMC3923129.
- Chang BY, Doi RH. Overproduction, purification, and characterization of *Bacillus subtilis* RNA polymerase sigma A factor. *J Bacteriol*. 1990 Jun;172(6):3257-63. PMID: 2111806; PMCID: PMC209133.
- Chen J, Wassarman KM, Feng S, Leon K, Feklistov A, Winkelman JT, Li Z, Walz T, Campbell EA, Darst SA. 6S RNA Mimics B-Form DNA to Regulate *Escherichia coli* RNA Polymerase. *Mol Cell*. 2017 Oct 19;68(2):388-397.e6..Epub 2017 Oct 5. PMID: 28988932; PMCID: PMC5683422.
- Davison BL, Leighton T, Rabinowitz JC. Purification of *Bacillus subtilis* RNA polymerase with heparin-agarose. In vitro transcription of phi 29 DNA. *J Biol Chem*. 1979 Sep 25;254(18):9220-6. PMID: 113409.
- Delumeau O, Lecointe F, Muntel J, Guillot A, Guédon E, Monnet V, Hecker M, Becher D, Polard P, Noirot P. The dynamic protein partnership of RNA polymerase in *Bacillus subtilis*. *Proteomics*. 2011 Aug;11(15):2992-3001. Epub 2011 Jun 28. PMID: 21710567.
- Fujita M, Sadaie Y. Rapid isolation of RNA polymerase from sporulating cells of *Bacillus subtilis*. *Gene*. 1998 Oct 23;221(2):185-90. PMID: 9795209.

- Fukushima T, Ishikawa S, Yamamoto H, Ogasawara N, Sekiguchi J. Transcriptional, functional and cytochemical analyses of the *veg* gene in *Bacillus subtilis*. *J Biochem*. 2003 Apr;133(4):475-83. PMID: 12761295.
- Gibson DG. Enzymatic assembly of overlapping DNA fragments. *Methods Enzymol*. 2011; 498:349-61. PMID: 21601685; PMCID: PMC7149801.
- Gildehaus N, Neusser T, Wurm R, Wagner R. Studies on the function of the riboregulator 6S RNA from *E. coli*: RNA polymerase binding, inhibition of in vitro transcription and synthesis of RNA-directed de novo transcripts. *Nucleic Acids Res*. 2007;35(6):1885-96. PMID: 17332013.
- Guiziou S, Sauveplane V, Chang HJ, Clerté C, Declerck N, Jules M, Bonnet J. A part toolbox to tune genetic expression in *Bacillus subtilis*. *Nucleic Acids Res*. 2016 Sep 6;44(15):7495-508. Epub 2016 Jul 8. PMID: 27402159; PMCID: PMC5009755.
- Hoch PG, Burenina OY, Weber MH, Elkina DA, Nesterchuk MV, Sergiev PV, Hartmann RK, Kubareva EA. Phenotypic characterization and complementation analysis of *Bacillus subtilis* 6S RNA single and double deletion mutants. *Biochimie*. 2015 Oct;117:87-99. Epub 2015 Jan 8. PMID: 25576829.
- Holátko J, Silar R, Rabatinová A, Sanderová H, Halada P, Nešvera J, Krásný L, Pátek M. Construction of in vitro transcription system for *Corynebacterium glutamicum* and its use in the recognition of promoters of different classes. *Appl Microbiol Biotechnol*. 2012 Oct;96(2):521-9. PMID: 22885668.
- Jiménez F, Avila J, Viñuela E, Salas M. Initiation of the transcription of ϕ 29 DNA by *Bacillus subtilis* RNA polymerase. *Biochim Biophys Acta*. 1974 May 31;349(3):320-7. PMID: 4210355.
- Johnston EB, Lewis PJ, Griffith R. The interaction of *Bacillus subtilis* sigmaA with RNA polymerase. *Protein Sci*. 2009 Nov;18(11):2287-97. PMID: 19735077; PMCID: PMC2788283.
- Klocko AD, Wassarman KM. 6S RNA binding to Esigma(70) requires a positively charged surface of sigma(70) region 4.2. *Mol Microbiol*. 2009 Jul;73(2):152-64. PMID: 19538447.
- Moreno-Campuzano S, Janga SC, Pérez-Rueda E. Identification and analysis of DNA-binding transcription factors in *Bacillus subtilis* and other Firmicutes--a

- genomic approach. *BMC Genomics*. 2006 Jun 13; 7:147. PMID: 16772031; PMCID: PMC1524751.
- Muñoz-Espín D, Daniel R, Kawai Y, Carballido-López R, Castilla-Llorente V, Errington J, Meijer WJ, Salas M. The actin-like MreB cytoskeleton organizes viral DNA replication in bacteria. *Proc Natl Acad Sci U S A*. 2009 Aug 11;106(32):13347-52. PMID: 19654094; PMCID: PMC2726393.
- Newing TP, Oakley AJ, Miller M, Dawson CJ, Brown SHJ, Bouwer JC, Tolun G, Lewis PJ. Molecular basis for RNA polymerase-dependent transcription complex recycling by the helicase-like motor protein HelD. *Nat Commun*. 2020 Dec 18;11(1):6420. PMID: 33339820.
- Pei HH, Hilal T, Chen ZA, Huang YH, Gao Y, Said N, Loll B, Rappsilber J, Belogurov GA, Artsimovitch I, Wahl MC. The δ subunit and NTPase HelD institute a two-pronged mechanism for RNA polymerase recycling. *Nat Commun*. 2020 Dec 18;11(1):6418. PMID: 33339827.
- Qi Y, Hulett FM. PhoP-P and RNA polymerase sigmaA holoenzyme are sufficient for transcription of Pho regulon promoters in *Bacillus subtilis*: PhoP-P activator sites within the coding region stimulate transcription in vitro. *Mol Microbiol*. 1998 Jun;28(6):1187-97. PMID: 9680208.
- Rabatinová A, Šanderová H, Jirát Matějčková J, Korelusová J, Sojka L, Barvík I, Papoušková V, Sklenár V, Žídek L, Krásný L. The δ subunit of RNA polymerase is required for rapid changes in gene expression and competitive fitness of the cell. *J Bacteriol*. 2013 Jun;195(11):2603-11. Epub 2013 Mar 29. PMID: 23543716; PMCID: PMC3676059.
- Rollenhagen C, Antelmann H, Kirstein J, Delumeau O, Hecker M, Yudkin MD. Binding of sigma(A) and sigma(B) to core RNA polymerase after environmental stress in *Bacillus subtilis*. *J Bacteriol*. 2003 Jan;185(1):35-40. PMID: 12486038; PMCID: PMC141833.
- Sierro N, Makita Y, de Hoon M, Nakai K. DBTBS: a database of transcriptional regulation in *Bacillus subtilis* containing upstream intergenic conservation information. *Nucleic Acids Res*. 2008 Jan;36(Database issue):D93-6. Epub 2007 Oct 25. PMID: 17962296; PMCID: PMC2247474.
- Sogo JM, Inciarte MR, Corral J, Viñuela E, Salas M. RNA polymerase binding sites and transcription map of the DNA of *Bacillus subtilis* phage phi29. *J Mol Biol*. 1979 Feb 5;127(4):411-36. PMID: 107317.

- Spizizen J. Transformation of biochemically deficient strains of *Bacillus subtilis* by deoxyribonucleate. Proc Natl Acad Sci U S A. 1958 Oct 15;44(10):1072-8. PMID: 16590310; PMCID: PMC528696.
- Steuten B, Hoch PG, Damm K, Schneider S, Köhler K, Wagner R, Hartmann RK. Regulation of transcription by 6S RNAs: insights from the *Escherichia coli* and *Bacillus subtilis* model systems. RNA Biol. 2014;11(5):508-21. doi: 10.4161/rna.28827.
- Sudzinová P, Kambová M, Ramaniuk O, Benda M, Šanderová H, Krásný L. Effects of DNA Topology on Transcription from rRNA Promoters in *Bacillus subtilis*. Microorganisms. 2021 Jan 1;9(1):87. PMID: 33401387.
- Thüring M, Ganapathy S, Schlüter MAC, Lechner M, Hartmann RK. 6S-2 RNA deletion in the undomesticated *B. subtilis* strain NCIB 3610 causes a biofilm derepression phenotype. RNA Biol. 2021 Jan;18(1):79-92. Epub 2020 Aug 30. PMID: 32862759; PMCID: PMC7834083.
- Trotochaud AE, Wassarman KM. A highly conserved 6S RNA structure is required for regulation of transcription. Nat Struct Mol Biol. 2005 Apr;12(4):313-9. PMID: 15793584.
- Vera A, González-Montalbán N, Arís A, Villaverde A. The conformational quality of insoluble recombinant proteins is enhanced at low growth temperatures. Biotechnol Bioeng. 2007 Apr 15;96(6):1101-6. PMID: 17013944.
- Wiedermannová J, Sudzinová P, Kovač T, Rabatinová A, Šanderová H, Ramaniuk O, Rittich Š, Dohnálek J, Fu Z, Halada P, Lewis P, Krásný L. Characterization of HelD, an interacting partner of RNA polymerase from *Bacillus subtilis*. Nucleic Acids Res. 2014 Apr;42(8):5151-63. PMID: 24520113; PMCID: PMC4005671.
- Yang X, Lewis PJ. Overproduction and purification of recombinant *Bacillus subtilis* RNA polymerase. Protein Expr Purif. 2008 May;59(1):86-93. Epub 2008 Jan 24. PMID: 18289874.
- Zawadzki V, Gross HJ. Rapid and simple purification of T7 RNA polymerase. Nucleic Acids Res. 1991 Apr 25;19(8):1948. PMID: 2030975; PMCID: PMC328134.
- Zhu B, Stülke J. SubtiWiki in 2018: from genes and proteins to functional network annotation of the model organism *Bacillus subtilis*. Nucleic Acids Res. 2018 Jan 4;46(D1):D743-D748. PMID: 29788229; PMCID: PMC5753275.

Supplementary Information

Rapid preparation of 6S RNA-free *Bacillus subtilis* σ^A -RNA polymerase and σ^A

Sweetha Ganapathy, Jana Christin Wiegard and Roland K. Hartmann *

¹Institut für Pharmazeutische Chemie, Philipps-Universität Marburg, Marbacher Weg 6, 35037 Marburg, Germany

*Corresponding author:

E-mail: roland.hartmann@staff.uni-marburg.de

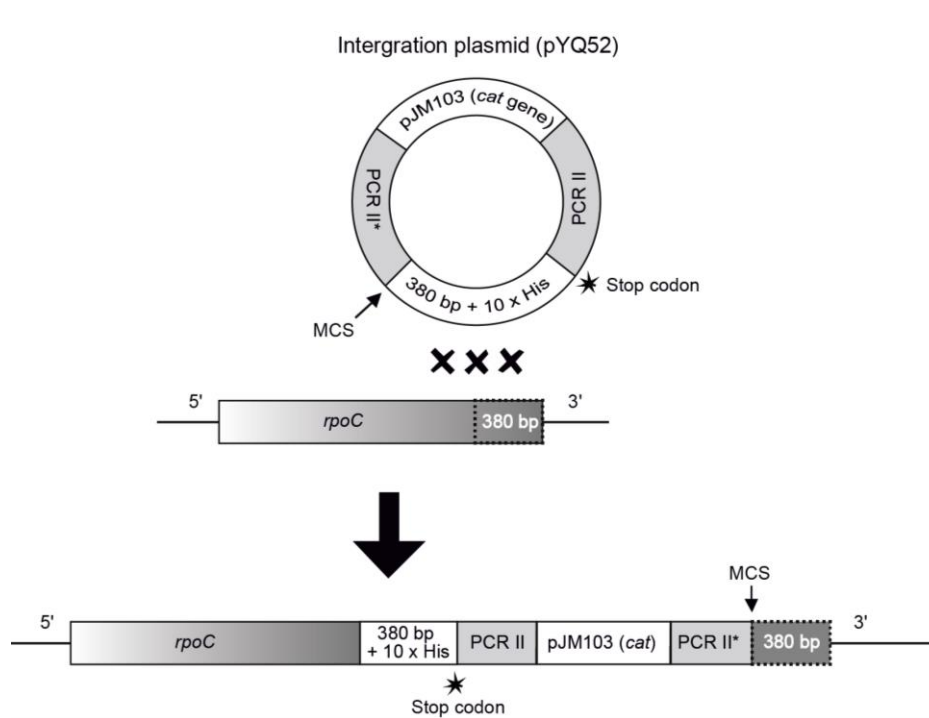


Fig. S1. History of the previously constructed *B. subtilis* strain MH5636 expressing a His-tagged *rpoC* gene product (Qi and Hulett, 1998). An integrational hybrid plasmid (pYQ52), carrying components of shuttle vector PCR II (Invitrogen), integrational vector pJM103 and a 380 bp fragment resembling the 3' end of the *rpoC* gene extended by 10 consecutive His codons, was constructed as described in Qi and Hulett (1998). When linearized, the 380 bp 3' end fragment of the plasmid is homologous to the native *rpoC* 3' portion to trigger a Campbell style integration of the complete pYQ52 plasmid into the genome. The native 3' end of the *rpoC* gene (untagged) was relocated as a result of the integration and remained in the genome as a non-functional entity. The strain acquired a chloramphenicol resistance (*cat*) encoded on the pJM103 vector. MCS, multiple cloning site.

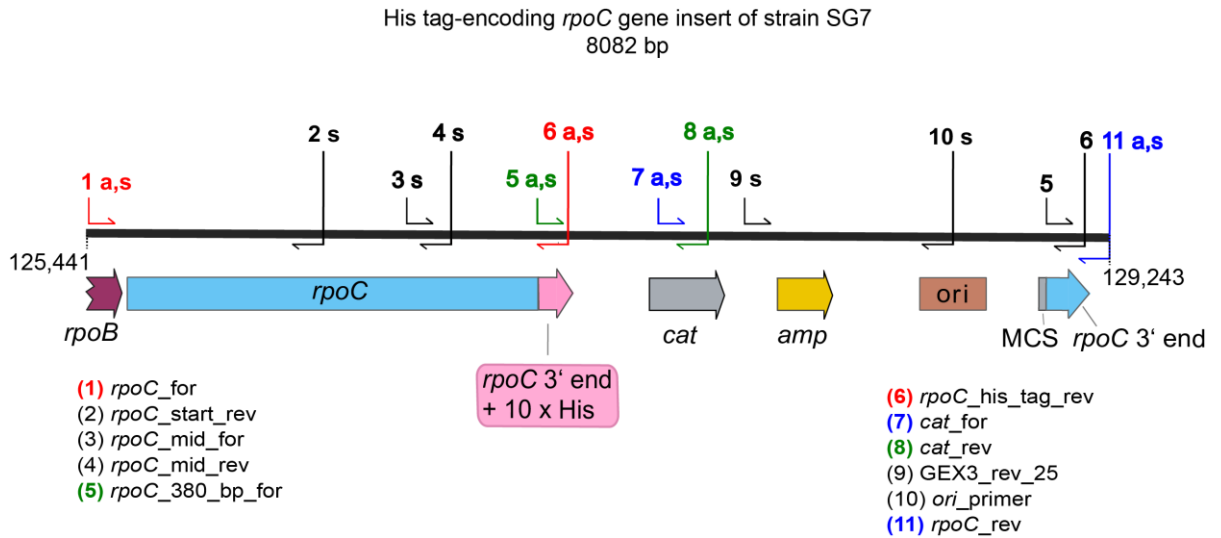


Fig. S2. Sequenced chromosomal region harboring the His-*rpoC* gene with C-terminal His₁₀ tag in strain SG7. The entire chromosomal region of ~ 8 kbp was sequenced by primer walking using PCR subfragments of the entire 8 kbp region as templates. The end positions of the region are numbered according to the genome positions of *B. subtilis* strain PY79 (GenBank: CP006881.1). Primers, illustrated by half arrows, were numbered, with the suffix 'a' indicating the use of the primer for amplification and/or 's' indicating its use for sequencing; primers of identical color were used as pairs to amplify subfragments of the region. For primer sequences, see Table 1 of the main text; *rpoB*, β -subunit of RNAP; *rpoC*, β '-subunit of RNAP; *cat*, chloramphenicol acetyltransferase gene; *amp*, ampicillin resistance gene (β -lactamase); ori, origin of replication derived from plasmid pYQ52; MCS, multiple cloning site derived from the same plasmid.

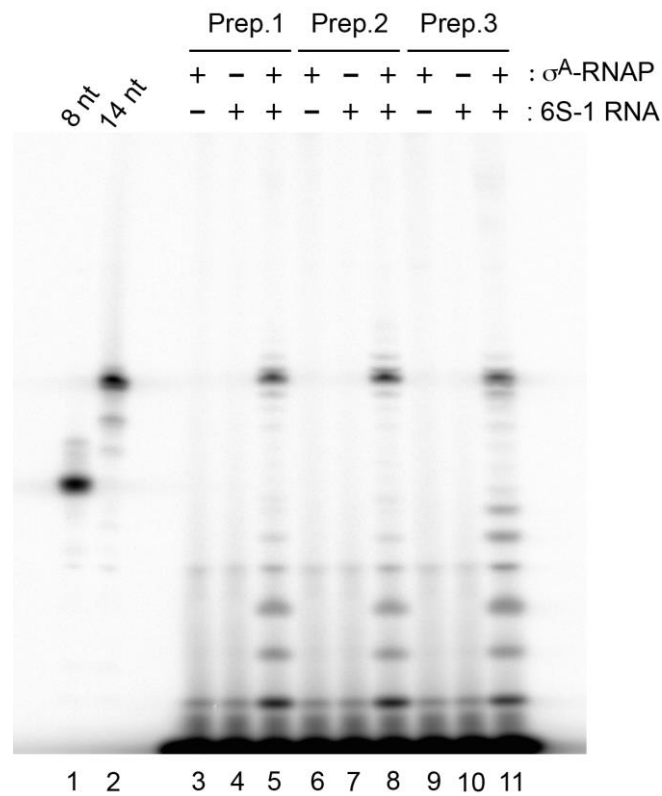


Fig. S3. pRNA transcription catalyzed by three independent σ^A -RNAP preparations from strain SG7. *In vitro* transcription of ^{32}P -labeled pRNAs was performed with three independent σ^A -RNAP preparations purified from strain SG7 RNAP using 6S-1 RNA as template. Lanes 1, 2: chemically synthesized, 5'- ^{32}P -endabeled 6S-1 pRNAs 8- and 14-mers used as size markers; lanes 3, 6, 9: reactions with σ^A -RNAP but without addition of 6S-1 RNA; lanes 4, 7, 10: omission of enzyme; lanes 5, 8, 11: pRNA transcription in the presence of σ^A -RNAP and 6S-1 RNA. For details, see Materials and Methods of the main text.

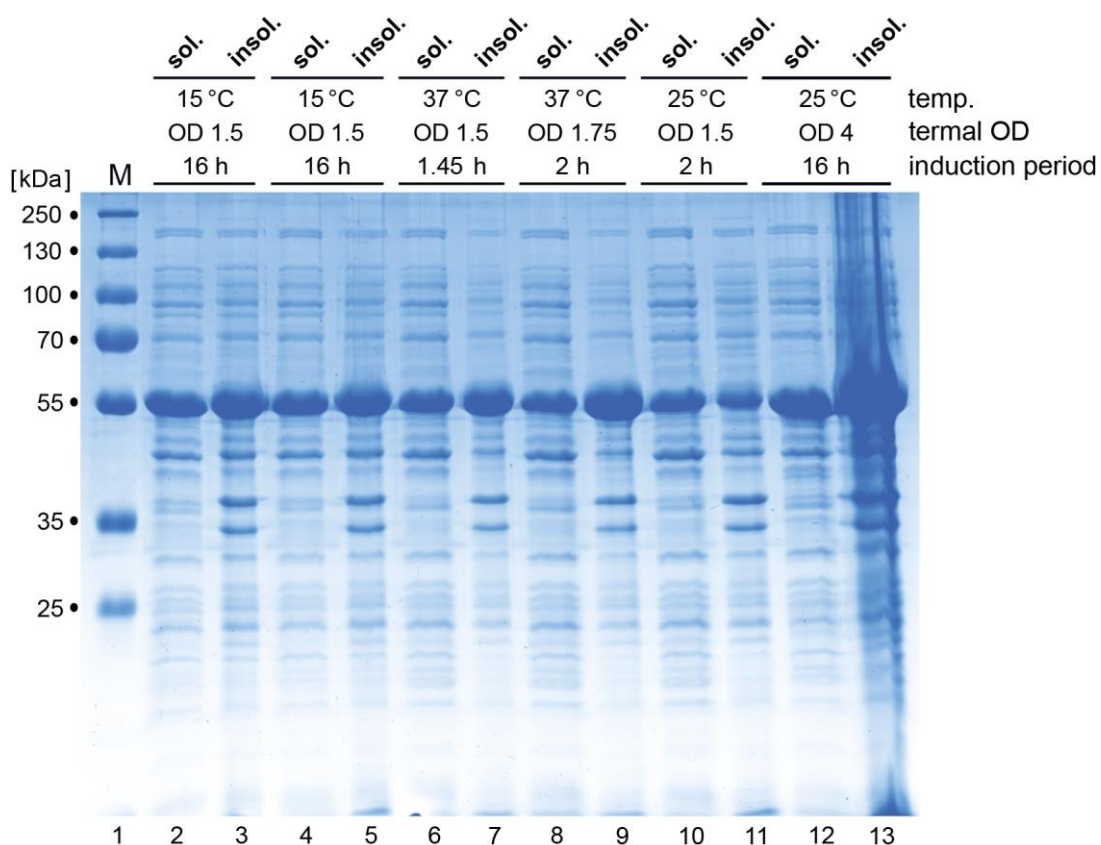


Fig. S4. Representative 12 % SDS-PAGE analysis of σ^A factor solubility at different temperatures during protein expression induction. The DE3 σ^A strain was grown at 37°C until an OD₆₀₀ of 0.6 to 0.8 was reached. Protein expression was induced by addition of 1 mM IPTG and cells were grown at 15°C (lanes 2-5), 37°C (lanes 6-9) or 25°C (lanes 10-13) until the indicated terminal OD₆₀₀ was reached; the length of the induction period is indicated as well above each lane. Then 20 mL of each cell culture were harvested and cells were resuspended in 1 mL NPI-20 buffer, followed by cell lysis as described (see Material and Methods of the main text). To separate soluble and insoluble proteins, cell lysates were centrifuged for 1 h at 16,060 x g (Biofuge fresco, Heraeus) with the resulting supernatant (~1 mL) containing soluble proteins and the pellet containing insoluble proteins. To analyze insoluble protein fractions, pellets were resuspended in 1 mL TUS buffer (50 mM Tris-HCl, pH 7.6, 100 mM NaCl, 8 M urea) (same volume as the supernatant). Lane 1, 5 μ L PageRuler™ Plus Prestained Protein Ladder (Thermo Scientific™, #26620) used as size marker. 3 μ L sample volume were loaded in all other lanes. Lane 13 shows blurred signals due to high viscosity of the sample owing to high cell density and large protein amounts; sol., soluble; insol., insoluble; temp., temperature; OD = OD₆₀₀.

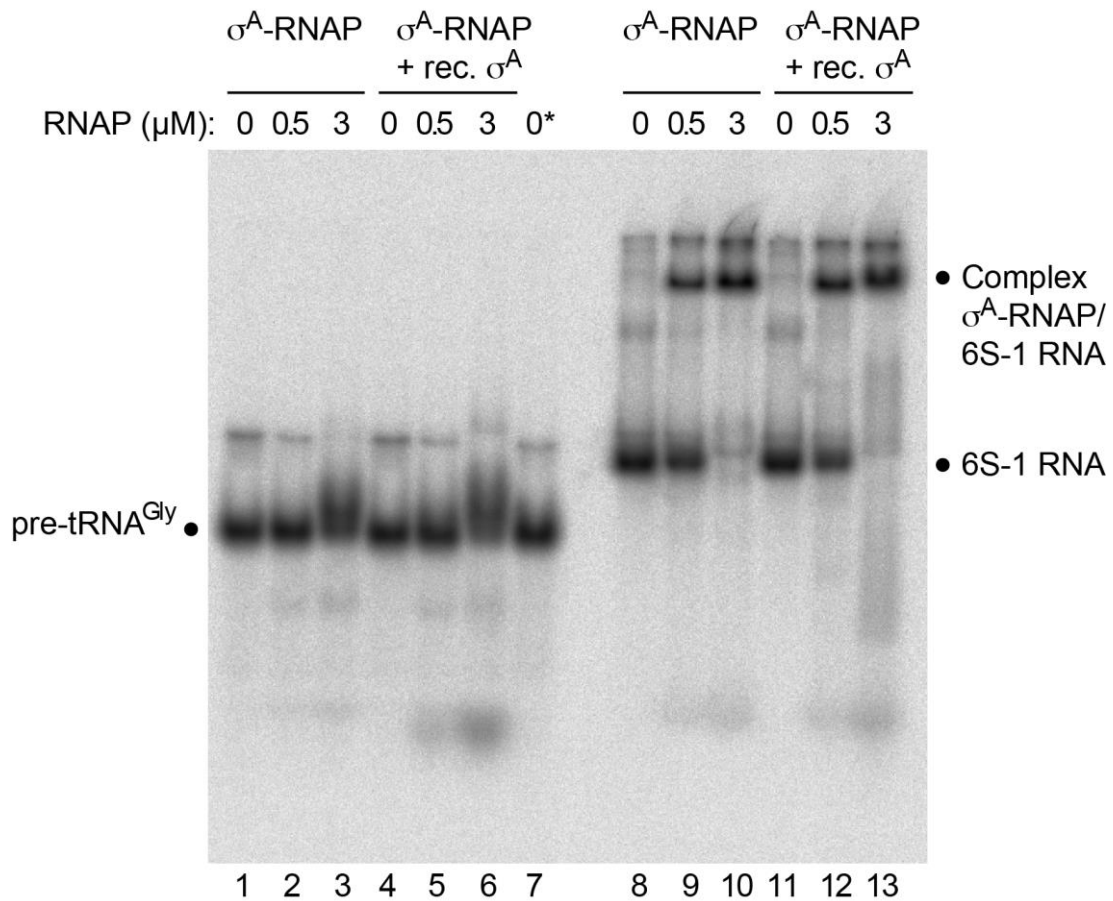


Fig. S5. Binding affinity of SG7 RNAP to 6S-1 RNA versus pre-tRNA^{Gly} to control for non-specific RNA binding. Analysis of complex formation of 5'-³²P-endlabeled pre-tRNA^{Gly} (lanes 1-7) versus 6S-1 RNA (lanes 8-13) with SG7 σ^A -RNAP at σ^A -RNAP concentrations of 0.5 and 3 μ M, analyzed by gel shift assay. A 10-fold molar excess of recombinant σ^A was added to the respective σ^A -RNAP concentration in lanes 4-6 and 11-13. In lane 7, RNAP storage buffer but neither σ^A -RNAP nor recombinant σ^A were added to control whether the glycerol in the storage buffer was responsible for the slight retardation of pre-tRNA at 3 μ M enzyme, which, however, was not the case. The positions of free pre-tRNA^{Gly} and 6S-1 RNA as well as the σ^A -RNAP:6S-1 RNA complex are depicted at the margins. For further experimental details, see Materials and Methods of the main text.

3.3 6S-2 RNA deletion in the undomesticated *B. subtilis* strain NCIB 3610 causes a biofilm derepression phenotype

Marietta Thüring¹, Sweetha Ganapathy¹, M. Amri C. Schlüter¹, Marcus Lechner² and Roland K. Hartmann^{1, *}

¹Institut für Pharmazeutische Chemie, Philipps-Universität Marburg, Marbacher Weg 6, 35037 Marburg, Germany

²Center for Synthetic Microbiology, Bioinformatics core facility, Hans-Meerwein-Str. 6, 35032 Marburg

*Corresponding author:

E-mail: roland.hartmann@staff.uni-marburg.de

Author Contributions: Conceptualization, R.K.H.; investigation, S.G., M.T., M.A.C.; overnight growth curve experiment, S.G., M.A.C.; sporulation and motility assay, S.G, M.T; supervision, R.K.H.; project administration, R.K.H.; funding acquisition, R.K.H.

ABSTRACT

Bacterial 6S RNA regulates transcription via binding to the active site of RNA polymerase holoenzymes. 6S RNA has been identified in the majority of bacteria, in most cases encoded by a single gene. Firmicutes including *Bacillus subtilis* encode two 6S RNA paralogs, 6S-1 and 6S-2 RNA. Hypothesizing that the regulatory role of 6S RNAs may be particularly important under natural, constantly changing environmental conditions, we constructed 6S RNA deletion mutants of the undomesticated *B. subtilis* wild-type strain NCIB 3610. We observed a strong phenotype for the Δ 6S-2 RNA strain that showed increased biofilm formation on solid media and the ability to form surface-attached biofilms in liquid culture. This phenotype remained undetected in derived laboratory strains (168, PY79) that are defective in biofilm formation. Quantitative RT-PCR data revealed transcriptional upregulation of biofilm marker genes such as *tasA*, *epsA* and *bslA* in the Δ 6S-2 RNA strain, particularly during transition from exponential to stationary growth phase. Salt stress, which blocks sporulation at a very early stage, was found to override the derepressed biofilm phenotype of the Δ 6S-2 RNA strain. Furthermore, the Δ 6S-2 RNA strain showed retarded swarming activity and earlier spore formation. Finally, the Δ 6S-1&2 RNA double deletion strain showed a prolonged lag phase of growth under oxidative, high salt and alkaline stress conditions, suggesting that the interplay of both 6S RNAs in *B. subtilis* optimizes and fine-tunes transcriptomic adaptations, thereby contributing to the fitness of *B. subtilis* under the unsteady and temporarily harsh conditions encountered in natural habitats.

Results

The $\Delta 6S-2$ RNA knockout strain has retarded swarming ability

As biofilm formation was found to be enhanced in the $\Delta 6S-2$ strain, we asked if swarming motility may also be affected in this mutant. For this purpose, liquid cultures of strains WT *amyE:cat*, $\Delta 6S-2$ *amyE:cat* and $\Delta 6S-2$ *amyE:6S-2:cat* were grown in LB medium with shaking at 220 rpm using baffled Erlenmeyer flasks. Under these conditions, biofilm formation of the $\Delta 6S-2$ strain was less evident (Fig. S1), likely due to vigorous aeration and associated mechanical forces. At a defined OD₆₀₀ of 2.0, 2 μ L of liquid culture were spotted onto 0.7 % TG swarm agar plates (for details, see Material and Methods), followed by incubation of the plates at 28 °C. Every hour the distance from the colony center to the swarm front (= radius) was measured (Fig. 1A). The resulting graph (radius over time) revealed slower swarming kinetics of the $\Delta 6S-2$ strain and restoration of wild-type-like swarming kinetics for the 6S-2 RNA complementation strain (Fig. 1B). Thus, we identified another physiologically relevant function affected by the 6S-2 RNA knockout in the NCIB 3610 background.

The $\Delta 6S-2$ RNA knockout strain shows accelerated spore formation

As biofilm formation and sporulation are interdigitated cellular processes (Vlamakis et al., 2013), it seemed possible that the $\Delta 6S-2$ strain also differs from the parental NCIB 3610 wild-type strain in some aspect of sporulation. We grew the four strains in sporulation medium and withdrew cell culture aliquots at different time points (6, 8, 10 and 24 h), which were split into two fractions. One fraction was plated directly in serial tenfold dilutions, and the other fraction was heated to 80°C for 20 min before plating which kills vegetative cells, yielding the ratio of colony numbers after heat treatment divided by those before heating. In these experiments we noticed that the fraction of spores was negligible at 6 h and approached its maximum at 10 h for all strains (65 to 80 % spores, not shown). However, after 8 h, we reproducibly observed a higher fraction of spores for the $\Delta 6S-2$ strain and a considerably reduced fraction for the double knockout strain (Fig. 2).

Discussion

The use of the undomesticated NCIB 3610 wild-type strain for studying the consequences of 6S RNA gene deletions revealed previously unrecognized phenotypes for the 6S-2 RNA single and the double knockout strains. No new phenotypic features were observed for the 3610 Δ 6S-1 strain under the conditions tested in the present study. The latter mutant strain showed reduced optical density during extended stationary growth), a feature shared with the laboratory derivative strain PY79 (Hoch *et al.*, 2015). One possible explanation is that cells lacking 6S-1 RNA consume nutrients more rapidly than the parental strain and initiate processes mediated by nutrient deprivation, such as cell lysis, cell size alterations and/or sporulation, more rapidly. Major support for this notion came from a study of a 6S-1 RNA knockout in the *B. subtilis* 168 strain background, showing that the absence of 6S-1 RNA leads to an earlier onset of sporulation which is attributable to faster consumption of nutrients (Cavanagh and Wassarman, 2013).

In the PY79 Δ 6S-1&2 strain, we observed two growth phenotypes that were more pronounced for the double knockout than for any of the corresponding single knockouts: (i) accelerated decrease of optical density toward extended stationary phase and (ii) faster outgrowth from stationary phase under alkaline stress conditions (pH 9.8) (Hoch *et al.*, 2015). These phenotypes of the PY79 Δ 6S-1&2 strain was not evident here in the analysis of the NCIB 3610 Δ 6S-1&2 strain, illustrating the importance of strain background.

Our study further revealed retarded swarming behavior of the 6S-2 RNA knockout mutant (Fig. 1). Biofilms and bacterial swarms feature multicellular communities, where division of labor drives the specialization of phenotypically different subpopulations to increase fitness of the entire bacterial population (Dragoš *et al.*, 2018; Lopez *et al.*, 2009). For instance, motile cells, surfactin producers, competent cells, matrix producers, spores and cannibal-like cells are able to coexist within a multicellular biofilm colony (Mielich-Süss and Lopez, 2015). With respect to our NCIB 3610 Δ 6S-2 strain we cannot decide at present whether the strain's phenotype of enhanced biofilm formation is caused by an increase in the number of matrix-producing cells or whether this subpopulation remains constant but individual cells of this subpopulation strongly overexpress

the matrix genes. In the former case, 6S-2 RNA would be involved in the regulation of *B. subtilis* cell differentiation. Finally, relative to the wild-type, we observed earlier spore formation for the NCIB 3610 Δ 6S-2 strain, retarded spore formation of the double knockout strain and little change in the case of the Δ 6S-1 strain (Fig. 2). The finding for the Δ 6S-2 strain illustrates the tight interdigitation of biofilm formation and sporulation. Previously, a 6S-1 RNA knockout and 6S-1&2 double knockouts (but not a 6S-2 knockout) in the *B. subtilis* 168 laboratory strain background were reported to result in earlier sporulation (Cavanagh and Wassarman, 2013). For the *B. subtilis* 168 Δ 6S-1 strain, this could be ascribed to an earlier onset of sporulation without affecting the time elapsing between initiation and completion of spore formation (Cavanagh and Wassarman, 2013). We do not know yet if earlier spore formation observed for our NCIB 3610 Δ 6S-2 strain is due to an earlier onset of sporulation or faster completion of spore formation. The seemingly contradictory sporulation phenotypes of 6S RNA deletion strains in the *B. subtilis* 168 versus NCIB 3610 background are not understood at present, but again emphasize the remarkable differences between *B. subtilis* laboratory and wild-type like strains.

Material and methods

General methods

All bacterial strains and plasmids used in this study are listed in appendix E and F. Cloning and transformation of *E. coli* DH5 α cells were carried out according to standard techniques (Sambrook and Russell, 2001). *E. coli* cultures were grown in LB medium, supplemented with 100 μ g/mL ampicillin for plasmid maintenance. All plasmid constructs were verified by DNA sequencing. *B. subtilis* cells were streaked from frozen glycerol stocks onto LB agar plates (supplemented with antibiotics if necessary) that were incubated overnight at 37°C. A single colony was used for inoculation of a liquid culture that was grown overnight at 37°C and under shaking. On the next day, fresh prewarmed LB medium (antibiotics added as indicated) was inoculated with 1/1000 volume of overnight culture; this preculture was grown to early exponential phase (0.3 to 0.5 OD₆₀₀) and used to inoculate the main culture to a starting OD₆₀₀ of 0.05. The growth curve at OD₆₀₀ of the main culture was periodically monitored and recorded. Depending on the

strain, antibiotics were added to final concentrations of 10 µg/mL in the case of chloramphenicol and kanamycin, and 100 µg/mL in the case of spectinomycin.

Motility/swarming assay

To study the influence of 6S-2 RNA on the motility of *B. subtilis*, bacterial growth was investigated on swarm plates. Single colonies of NCIB 3610 derivative strains WT *amyE:cat*, Δ 6S-2 *amyE:cat* and Δ 6S-2 *amyE:6S-2:cat* (see appendix E for more details) grown on LB plates (1.5 % agar, 5 µg/mL chloramphenicol [CM]) overnight at 37°C were used to inoculate 3 mL LB medium containing 5 µg/mL CM, followed by growth at 37°C overnight in a warm air shaker. Then 20 µL of overnight culture were introduced into 20 mL of LB medium (in 100-mL unbaffled Erlenmeyer flasks containing 5 µg/mL CM) prewarmed to 37°C (1:1000 dilution), followed by growth at 37 °C in a water bath shaker (Aquatron, 220 rpm) to an OD₆₀₀ of 0.3 to 0.6. This preculture was used to inoculate 50 mL LB medium (in a 250-mL baffled Erlenmeyer flask) to a starting OD₆₀₀ of 0.05; cultures were grown at 37°C under shaking (220 rpm in the water bath shaker). At an OD₆₀₀ of 2.0, 2 µl of cell suspension were spotted onto a 0.7 % TG swarming plate [peptone 1 % (w/v), meat extract 1 % (w/v), NaCl 0.5 % (w/v), 55 mM glucose, 0.3 mM 2,3,5 tri-phenyl tetrazolium chloride (Sigma-Aldrich Merck), 0.7% (w/v) agar] (Bordner *et al.*, 1978). TG plates were freshly poured, air-dried for 20 min at room temperature without lid and then stored with cover at room temperature for use on the next day. After spotting, plates were incubated at 28°C and the distance from the spot center to the outer swarm front (= radius) was documented every hour with a documentation equipment (Dark Hood HD-50 + Gerix 1000, Biosteps, adjusting the lens manual focus to f/4 iris, 12x zoom, 7/20 focus, 0.04x illumination). For improved recognizability of the swarm front, a radius line was drawn manually on the plate bottom which was measured digitally using the ImageJ 1.51p software; the graph shown in Fig. 1B was generated with GraphPad Prism 8.

Sporulation assay

To quantify spores in a liquid culture, we exploited the heat resistance of *B. subtilis* spores for distinguishing them from heat-sensitive vegetative cells (Nicholson and Setlow, 1990; Cavanagh and Wassarman, 2013). Preculture preparation was done as described above under "Bacterial strains, plasmids, media and growth conditions, General methods". Cells of the preculture grown to early exponential phase (0.3 to 0.5 OD₆₀₀) were centrifuged and, after removal of the LB medium, the cell pellet was resuspended in DSM medium. Main cultures were then inoculated to an OD₆₀₀ of 0.05 in 100 mL prewarmed DSM medium in 1-L baffled Erlenmeyer flasks (DSM medium, per 1 L: 8 g Difco nutrient broth, 1 g KCl, 1 mL of 1 M MgSO₄, 1 mL of 10 mM MnCl₂; after autoclaving, 0.5 mL 1 M CaCl₂ [1M] and 100 µL FeSO₄ [100 µM] were added). Cultures were agitated in a water bath shaker at 37°C, 220 rpm. After 8 h of incubation, 1-mL culture samples of each strain were withdrawn to make serial tenfold dilutions in PBS buffer (pH 7.4). 100 µL of each dilution sample were directly plated onto LB agar plates (quantification of all types of viable cells). The remaining 900 µL were heated to 80 °C for 20 min and again 100 µL of each dilution sample were plated onto LB agar (quantification of heat-resistant spores only). After incubation of plates for 24 h at 37 °C, colonies were counted on plates with streaked dilutions that yielded 10 to 700 distinguishable colonies per plate. To determine the fraction of spores within the cultures, the ratio of heated to non-heated colony numbers in the same volume of cell suspension was calculated. The presented data are based three independent biological replicates.

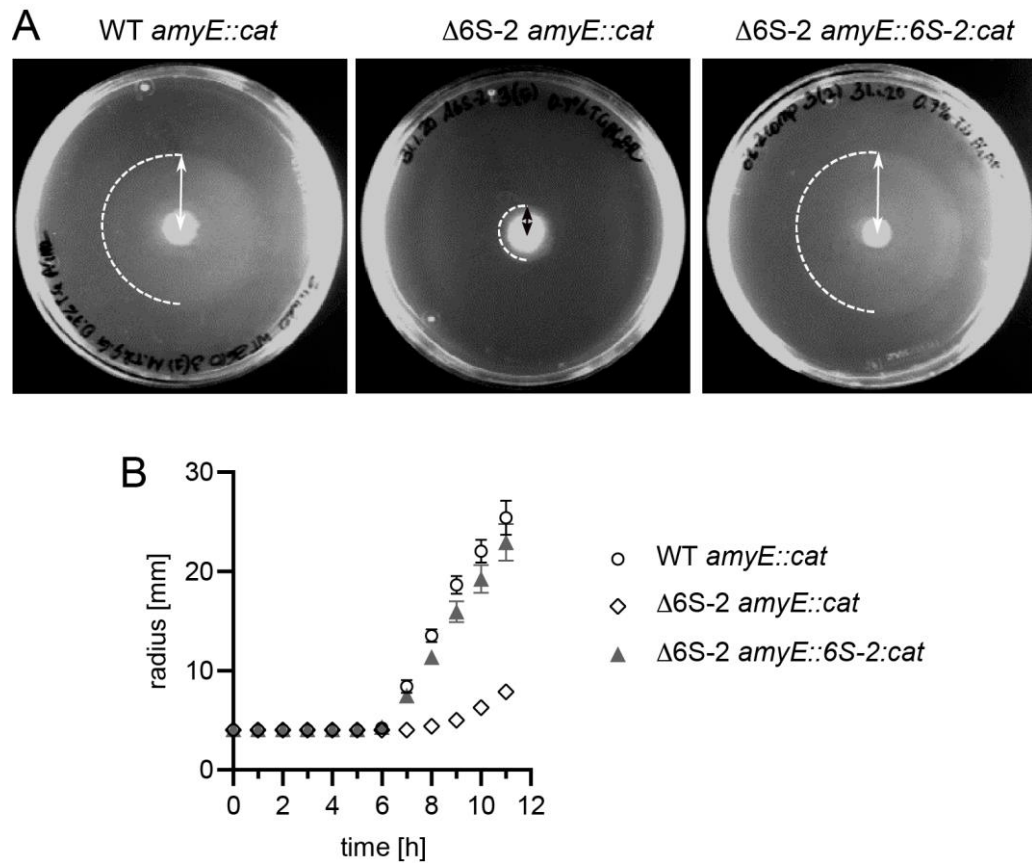


Fig. 1: Bacteria lacking 6S-2 RNA show retarded swarming behavior. Strain NCIB 3610 *amyE::cat* (WT *amyE::cat*), the derived 6S-2 RNA knockout mutant strain (Δ 6S-2 *amyE::cat*) and the latter complemented with the 6S-2 RNA gene (Δ 6S-2 *amyE::cat:6S-2*) were analyzed for the time dependence of swarming. When liquid cell cultures grown at 37 °C reached an OD₆₀₀ of 2.0, 2 μ L of culture were spotted in the center of a swarm plate (0.7 % TG agar) that was incubated at 28 °C. **(A)** Example swarm plates after 10 h of incubation at 28 °C. Dashed semi-circles mark the boundary of the swarm area; the distance/radius from the initial spot center to the outer swarm front (double arrows) was measured at various time points, providing the basis for the graph in panel B. **(B)** Swarming kinetics of the three analyzed strains. Values are based on three independent experiments with five technical replicates each. Error bars indicate standard errors of the mean (SEM). For more details, see Materials and Methods.

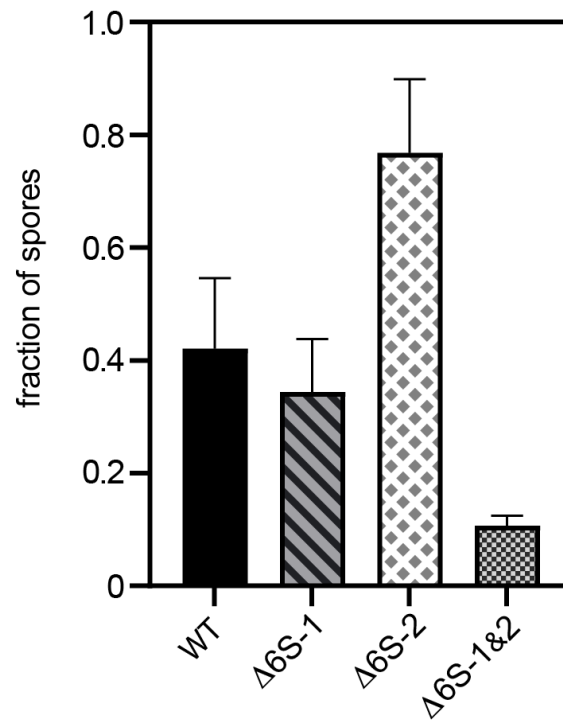


Fig. 2: Fraction of spores after 8 h of growth in sporulation medium. The fraction of spores was determined by counting the number of colonies before and after heating cell culture dilutions to 80 °C for 20 min and calculating the ratio of "colonies heated / colonies not heated". At 10 h, the relative number of spores became more similar for all strains (65 to 80 %, not shown), suggesting earlier spore formation in the Δ6S-2 strain. For details, see Materials and methods.

Supplementary Figures

6S-2 RNA deletion in the undomesticated *B. subtilis* strain NCIB 3610 causes a biofilm derepression phenotype

Marietta Thüring¹, Sweetha Ganapathy¹, M. Amri C. Schlüter¹, Marcus Lechner² and Roland K. Hartmann^{1, *}

¹Institut für Pharmazeutische Chemie, Philipps-Universität Marburg, Marbacher Weg 6, 35037 Marburg, Germany

²Center for Synthetic Microbiology, Hans-Meerwein-Str. 6, 35032 Marburg

*Corresponding author:

E-mail: roland.hartmann@staff.uni-marburg.de

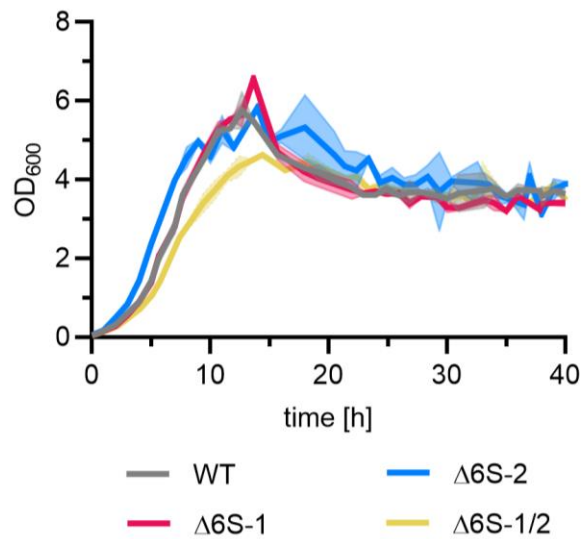


Fig. S1: Growth of the four *B. subtilis* NCIB 3610 strains. Precultures (for details, see Materials and Methods of main text, paragraph "Bacterial strains, plasmids, media and growth conditions") were used to inoculate the main culture to a starting OD₆₀₀ of 0.05 (100 mL LB medium in 1-L baffled Erlenmeyer flasks). Cultures were incubated at 28°C in a waterbath under shaking (220 rpm). Curves are based on two biological replicates.

3.4 RemA and RNA polymerase transcription assay

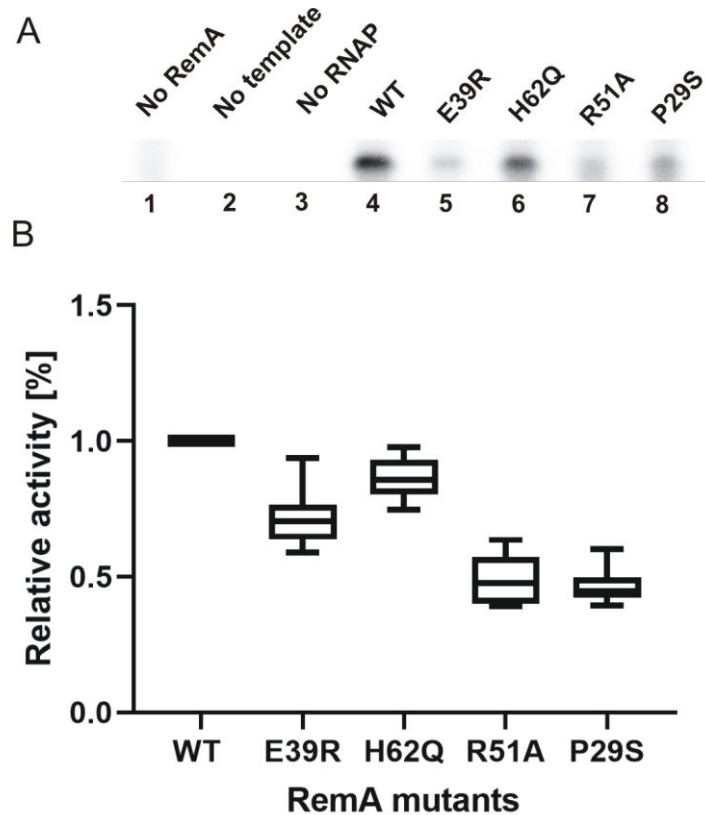


Fig 1: *In vitro* radiolabeled transcription assay on *epsA* gene by RemA mutants: (A) 7.5 % denaturing gel assay indicates the presence of 140 nucleotide transcript product of *epsA* gene upon activation by RemA wild type and RemA mutants in lanes 4 - 8 with varying efficacy. Lanes 1 - 3 are control lanes that indicate the absence of transcript product upon omission of (lane 1) RemA protein, (lane 2) supercoiled plasmid template and (lane 3) His-tagged σ^A -RNAP. (B) Box plot indicating the transcription efficacy of RemA mutants on *epsA* gene normalised against the RemA wild type. The intensity of the radioactive bands was evaluated using AIDA (version 3.45.039) and visualised using GraphPad prism 9 (for more details regarding procedure see section 2.4.6 RemA and RNA polymerase transcription assay).

RemA wild type and RemA mutants with single amino acid mutations namely E39R, H62Q, R51A and P29S were checked for transcription activation efficacy of the *epsA* gene. The *epsA* gene promoter sequence from position -165 bp to +35 bp was amplified from the genomic DNA of NCIB 3610 strain. The amplicon was digested and ligated into a standard plasmid upstream to *rrnB1* terminator (see Plasmid card AL0170 for more details) (Winkelman JT et al., 2013). The RNA product resulting from successful transcription using this plasmid carrying

the *epsA* gene as template was 140 nucleotides in length. The RemA protein is a DNA binding protein involved in the biofilm formation of *B. subtilis* through expression of *epsA* gene and *apA-sipW-tasA* operon. *epsA* gene codes for exopolysaccharide, necessary for the formation of the exoskeleton of biofilm. Therefore, the project aimed to check for correlation between activation of the *epsA* gene and biofilm formation. Previously, *in vivo* biofilm assays could show that bacterial strain expressing wild type RemA protein exhibited normal biofilm formation whereas with mutation in RemA position E39R, the bacteria exhibited an unregulated always “on” biofilm formation phenotype. With mutation in RemA position H62Q, the bacterial strain exhibited an abnormal biofilm formation phenotype and mutation in RemA position R51A resulted in a strain which was completely devoid of any biofilm formation. Finally, mutant with mutation in RemA position P29S could build biofilm but it also looked abnormal. The data obtained from *in vitro* transcription activation efficacy of *epsA* gene by RemA mutants correlated poorly with the *in vivo* biofilm formation data. RemA mutant E39R, producing more biofilm *in vivo* than the wild-type protein, showed less transcription activation of the *epsA* gene than wild-type RemA and even less than the RemA mutant H62Q that caused an abnormal biofilm formation phenotype. Moreover, transcription activation efficacy of *epsA* gene by RemA mutant R51A and P29S are quite comparable in spite of producing completely different biofilm phenotypes such as no biofilm formation and abnormal biofilm formation during plate assays respectively. This inconsistency only illustrates the complexity of the molecular networks responsible for biofilm formation. Especially when more than one operon (*eps* operon, *apA-sipW-tasA* operon), different sigma factors (RpoA σ^A , RpoB σ^B), matrix proteins (TasA, SipW, EpsE) and many protein activators/inhibitors (RemA, SinI, SinR) are involved in regulation of the biofilm network.

4. Summary and Outlook

Through my primary project, we could understand in depth about the impact of secondary structure of *Bacillus subtilis* 6S-1 RNA on σ^A -RNAP binding, pRNA transcription and structural rearrangement. We could show that the integrity of 5' Central Bulge (CB) is important in recognition and binding of 6S RNA to σ^A -RNAP. The formation of Central Bulge Collapse helix (CBC) is important for the optimal functioning of *B. subtilis* 6S-1 RNA; 6S-1 RNA variant rearranged more effectively and released itself from σ^A -RNAP faster in the presence of the stabilized CBC compared to a wild type without a stabilised CBC. We found that introducing a second short hairpin in 3'-CB is detrimental to 6S-1 RNA release and therefore, propose that the CBC formation subtly supports pRNA-induced 6S-1 RNA rearrangement and release. Truncation of the -35 promoter equivalent region of the 6S-1 RNA did not lead to a complete loss in σ^A -RNAP binding activity; a phenomenon contrary to data reported in *E. coli*. This feature could be due to the fact that contacts formed between *B. subtilis* 6S-1 RNA and RNAP are different from those present in the *E. coli* system. We found that even short pLNA mimics as short as 6 nt can sufficiently increase duplex stability to rearrange 6S RNA. Using such pLNAs, we studied the 6S-1:pLNA hybrid structures using atomic force microscopy and found that these structures adopt a more bent/constrained structure than 6S-1 RNA alone. The aforementioned pLNA experiments help us draw a conclusion that 6S-1 RNA rearrangement is not a binary process with a flip mechanism resulting in either "free" or "rearranged" state; but instead is a step-wise process of many intermediate states ultimately yielding into one constrained and putatively bent structure. Finally, increasing the nucleotide concentration increases the rate of 6S-1 rearrangement and by inference, RNAP release, this piece of data supports the role of 6S-1 RNA during nutrient re-supply.

For this project, the technique primarily used are gel assays. Native gel assays are neither representative of the cellular environment nor conditions where equilibrium binding and multiple turnovers can occur. Furthermore, the gel assays run unidirectionally under the influence of electrical current, resulting in an irreversible dissociation of complex as soon as thermodynamic threshold for

binding is not fulfilled. Nevertheless, gel assays first indicated the formation of pRNA:6S-1 RNA complex in *B. subtilis* published by Beckmann B et al. (2011); these complexes could now be confirmed *in vivo* using a technique called Grad-seq (Gerovac M et al., 2021). The Grad-seq technique did not exist in 2011. Therefore, gel assays can provide valuable insights on point-to-point interaction and predict *in vivo* interactions with great accuracy.

In my secondary project, a useful strain namely SG7 was constructed for the purpose of quick and robust preparation of 6S RNA-free σ^A -RNAP. Using the strain *B. subtilis* MW Δ bsrAB as background, a C-terminal His₁₀ tag was transferred onto the 3' end of β' subunit resulting in SG7. Additionally, we describe the construction and purification of σ^A subunit that can be externally supplemented to the RNAP preparation to improve performance. The genomic integrity of the SG7 strain and the purity of the σ^A -RNAP was also thoroughly validated.

In my tertiary project, the phenotypic aspects of 6S RNA knockouts in the wild-type strain 3610 were studied. Overnight growth curve studies were conducted on 6S RNA knockout mutants in 1-L flasks and did not reveal any strong phenotype, correlating to the lack of any strong phenotype under nutrient rich conditions from previous studies. When stress situations were applied to induce special adaptations such as motility or sporulation, 6S-2 RNA knockout mutant in the wild-type background exhibited retarded swarming ability and accelerated sporulation. It would be intriguing to study the possibility of sub-populations or transcriptomic/proteomic changes contributing to the rise of such phenotypes.

Generally, there are many aspects of the 6S RNA that remain unsolved until date. A single and definite, phylogenetically conserved function of 6S RNA is not yet known. As our phenotype analysis of 3610 strain pointed to a stress response function of 6S-2 RNA, studying the role of 6S-2 RNA in alternative sigma factor mediated transcription of special genes in regard to stress adaptation and bacterial survival would be interesting. In order to study the alternative sigma factors, a stable and reproducible purification protocol of core *B. subtilis* RNAP

would come in handy. It might be worthwhile to work further in order to establish a core RNAP purification protocol from the SG7 strain background. There are multiple copies of 6S RNAs in some organisms and it will be interesting to explore how their functions have diverged since the assumed gene duplication events. Lastly, through the secondary structure analysis of 6S-1 RNA in *B. subtilis*, we could show that the 6S-1 RNA functions differently to *E. coli* 6S RNA and identify critical factors such as central bulge collapse helix, P2 helix and pRNA length that contribute to rearrangement kinetics. Hoch et al. 2015 found that 6S-1 RNA knockout mutant exhibited decreased growth (optical density) phenotype towards extended stationary phase, Now, it would be interesting to clone our modified 6S RNA with altered rearrangement properties/secondary structure into this construct and to check for an *in vivo* consequence of our mutations.

5. Literature review

Anagha Joshi, Julia Romanowska, Chapter Twenty-Eight - Recent advances in computational-based approaches in epigenetics studies, Editor(s): Trygve Tollefsbol, In *Translational Epigenetics, Epigenetics Methods*, Academic Press, Volume 18, 2020, Pages 569-590, ISSN 25425358, ISBN 9780128194140.

Barrick JE, Sudarsan N, Weinberg Z, Ruzzo WL, Breaker RR. 6S RNA is a widespread regulator of eubacterial RNA polymerase that resembles an open promoter. *RNA*. 2005 May;11(5):774-84. Epub 2005 Apr 5. PMID: 15811922; PMCID: PMC1370762.

Beckmann BM, Burenina OY, Hoch PG, Kubareva EA, Sharma CM, Hartmann RK. In vivo and in vitro analysis of 6S RNA-templated short transcripts in *Bacillus subtilis*. *RNA Biol*. 2011 Sep-Oct;8(5):839-49. Epub 2011 Sep 1. PMID: 21881410.

Beckmann BM, Hoch PG, Marz M, Willkomm DK, Salas M, Hartmann RK. A pRNA-induced structural rearrangement triggers 6S-1 RNA release from RNA polymerase in *Bacillus subtilis*. *EMBO J*. 2012 Apr 4;31(7):1727-38. Epub 2012 Feb 14. PMID: 22333917; PMCID: PMC3321203.

Bordner R, Winter JA, Scarpino P, editors. *Microbiological methods for monitoring the environment: water and wastes*. Environmental Protection Agency, Office of Research and Development, Environmental Monitoring and Support Laboratory; 1978.

Brownlee GG. Sequence of 6S RNA of *E. coli*. *Nat New Biol*. 1971 Feb 3;229(5):147-9. PMID: 4929322.

Burenina OY, Elkina DA, Migur AY, Oretskaya TS, Evguenieva-Hackenberg E, Hartmann RK, Kubareva EA. Similarities and differences between 6S RNAs from *Bradyrhizobium japonicum* and *Sinorhizobium meliloti*. *J*

Microbiol. 2020 Nov;58(11):945-956. Epub 2020 Oct 30. PMID: 33125669.

Burenina OY, Hoch PG, Damm K, Salas M, Zatsepin TS, Lechner M, Oretskaya TS, Kubareva EA, Hartmann RK. Mechanistic comparison of *Bacillus subtilis* 6S-1 and 6S-2 RNAs--commonalities and differences. *RNA*. 2014 Mar;20(3):348-59. Epub 2014 Jan 24. PMID: 24464747; PMCID: PMC3923129.

Cabrera-Ostertag IJ, Cavanagh AT, Wassarman KM. Initiating nucleotide identity determines efficiency of RNA synthesis from 6S RNA templates in *Bacillus subtilis* but not *Escherichia coli*. *Nucleic Acids Res*. 2013 Aug; 41(15):7501-11. Epub 2013 Jun 12. PMID: 23761441; PMCID: PMC3753640.

Cavanagh AT, Chandrangu P, Wassarman KM. 6S RNA regulation of *relA* alters ppGpp levels in early stationary phase. *Microbiology (Reading)*. 2010 Dec;156(Pt 12):3791-3800. Epub 2010 Sep 9. PMID: 20829285; PMCID: PMC3068707.

Cavanagh AT, Klocko AD, Liu X, Wassarman KM. Promoter specificity for 6S RNA regulation of transcription is determined by core promoter sequences and competition for region 4.2 of sigma70. *Mol Microbiol*. 2008 Mar;67(6):1242-56. Epub 2008 Jan 15. PMID: 18208528.

Cavanagh AT, Sperger JM, Wassarman KM. Regulation of 6S RNA by pRNA synthesis is required for efficient recovery from stationary phase in *E. coli* and *B. subtilis*. *Nucleic Acids Res*. 2012 Mar;40(5):2234-46. Epub 2011 Nov 18. PMID: 22102588; PMCID: PMC3299989.

Cavanagh AT, Wassarman KM. 6S-1 RNA function leads to a delay in sporulation in *Bacillus subtilis*. *J Bacteriol*. 2013 May;195(9):2079-86. Epub 2013 Mar 1. PMID: 23457253; PMCID: PMC3624594.

- Chen H, Dutta T, Deutscher MP. Growth Phase-dependent Variation of RNase BN/Z Affects Small RNAs: REGULATION OF 6S RNA. *J Biol Chem*. 2016 Dec 16;291(51):26435-26442. Epub 2016 Nov 8. PMID: 27875308; PMCID: PMC5159504.
- Chen J, Wassarman KM, Feng S, Leon K, Feklistov A, Winkelman JT, Li Z, Walz T, Campbell EA, Darst SA. 6S RNA Mimics B-Form DNA to Regulate *Escherichia coli* RNA Polymerase. *Mol Cell*. 2017 Oct 19;68(2):388-397.e6. Epub 2017 Oct 5. PMID: 28988932; PMCID: PMC5683422.
- Delumeau O, Lecointe F, Muntel J, Guillot A, Guédon E, Monnet V, Hecker M, Becher D, Polard P, Noirot P. The dynamic protein partnership of RNA polymerase in *Bacillus subtilis*. *Proteomics*. 2011 Aug;11(15):2992-3001. Epub 2011 Jun 28. PMID: 21710567.
- Dennis PP, Omer A. Small non-coding RNAs in Archaea. *Curr Opin Microbiol*. 2005 Dec; 8(6):685-94. Epub 2005 Oct 26. PMID: 16256421.
- Drecktrah D, Hall LS, Brinkworth AJ, Comstock JR, Wassarman KM, Samuels DS. Characterization of 6S RNA in the Lyme disease spirochete. *Mol Microbiol*. 2020 Feb;113(2):399-417. Epub 2019 Dec 11. PMID: 31742773; PMCID: PMC7047579.
- Elkina D, Weber L, Lechner M, Burenina O, Weisert A, Kubareva E, Hartmann RK, Klug G. 6S RNA in *Rhodobacter sphaeroides*: 6S RNA and Prna transcript levels peak in late exponential phase and gene deletion causes a high salt stress phenotype.
- Erickson RP, Izant JG, editors. *Gene regulation: biology of antisense RNA and DNA*. Lippincott Williams & Wilkins; 1992.
- Fadouloglou VE, Lin HT, Tria G, Hernández H, Robinson CV, Svergun DI, Luisi BF. Maturation of 6S regulatory RNA to a highly elongated structure. *FEBS J*. 2015 Dec;282(23):4548-64. doi: 10.1111/febs.13516. Epub 2015

Oct 13. PMID: 26367381; PMCID: PMC7610929.

Faucher SP, Friedlander G, Livny J, Margalit H, Shuman HA. Legionella pneumophila 6S RNA optimizes intracellular multiplication. Proc Natl Acad Sci U S A. 2010 Apr 20;107(16):7533-8. Epub 2010 Apr 5. PMID: 20368425; PMCID: PMC2867745.

Fujita M, Sadaie Y. Rapid isolation of RNA polymerase from sporulating cells of *Bacillus subtilis*. Gene. 1998 Oct 23;221(2):185-90. PMID: 9795209.

Gerovac M, Wicke L, Chihara K, Schneider C, Lavigne R, Vogel J. A Grad-seq View of RNA and Protein Complexes in *Pseudomonas aeruginosa* under Standard and Bacteriophage Predation Conditions. mBio. 2021 Feb 9;12(1):e03454-20. PMID: 33563827.

Gildehaus N, Neusser T, Wurm R, Wagner R. Studies on the function of the riboregulator 6S RNA from *E. coli*: RNA polymerase binding, inhibition of in vitro transcription and synthesis of RNA-directed de novo transcripts. Nucleic Acids Res. 2007;35(6):1885-96. Epub 2007 Mar 1. PMID: 17332013; PMCID: PMC1874619.

Glyde R, Ye F, Darbari VC, Zhang N, Buck M, Zhang X. Structures of RNA Polymerase Closed and Intermediate Complexes Reveal Mechanisms of DNA Opening and Transcription Initiation. Mol Cell. 2017 Jul 6;67(1):106-116.e4. Epub 2017 Jun 1. PMID: 28579332; PMCID: PMC5505868.

Gottesman S. Micros for microbes: non-coding regulatory RNAs in bacteria. Trends Genet. 2005 Jul; 21(7):399-404. PMID: 15913835.

Graumann LP, *Bacillus: Cellular and Molecular Biology* (Third edition). Caister Academic Press. Mar 2017. ISBN: 978-1-910190-57-9

Heilmann B, Hakkila K, Georg J, Tyystjärvi T, Hess WR, Axmann IM, Dienst D. 6S RNA plays a role in recovery from nitrogen depletion in *Synechocystis*

sp. PCC 6803. *BMC Microbiol.* 2017 Dec 8;17(1):229. PMID: 29216826; PMCID: PMC5721685.

Hindley J. Fractionation of ³²P-labelled ribonucleic acids on polyacrylamide gels and their characterization by fingerprinting. *J Mol Biol.* 1967 Nov 28;30(1):125-36. PMID: 4865141.

Hoch PG, Burenina OY, Weber MH, Elkina DA, Nesterchuk MV, Sergiev PV, Hartmann RK, Kubareva EA. Phenotypic characterization and complementation analysis of *Bacillus subtilis* 6S RNA single and double deletion mutants. *Biochimie.* 2015 Oct;117:87-99. Epub 2015 Jan 8. PMID: 25576829.

Hoch PG, Schlereth J, Lechner M, Hartmann RK. *Bacillus subtilis* 6S-2 RNA serves as a template for short transcripts in vivo. *RNA.* 2016 Apr;22(4):614-22. Epub 2016 Feb 12. PMID: 26873600; PMCID: PMC4793215.

Jones AJ, Venkataramanan KP, Papoutsakis T. Overexpression of two stress-responsive, small, non-coding RNAs, 6S and tmRNA, imparts butanol tolerance in *Clostridium acetobutylicum*. *FEMS Microbiol Lett.* 2016 Apr;363(8):fnw063. Epub 2016 Mar 16. PMID: 26989157.

Kim KS, Lee Y. Regulation of 6S RNA biogenesis by switching utilization of both sigma factors and endoribonucleases. *Nucleic Acids Res.* 2004 Nov 18;32(20):6057-68. PMID: 15550566; PMCID: PMC534622.

Klocko AD, Wassarman KM. 6S RNA binding to Esigma (70) requires a positively charged surface of sigma (70) region 4.2. *Mol Microbiol.* 2009 Jul;73(2):152-64. Epub 2009 Jun 16. PMID: 19538447; PMCID: PMC2758106.

Köhler K, Duchardt-Ferner E, Lechner M, Damm K, Hoch PG, Salas M, Hartmann RK. Structural and mechanistic characterization of 6S RNA from the

hyperthermophilic bacterium *Aquifex aeolicus*. *Biochimie*. 2015 Oct; 117:72-86. Epub 2015 Mar 11. PMID: 25771336.

Lal A, Krishna S, Seshasayee ASN. Regulation of Global Transcription in *Escherichia coli* by Rsd and 6S RNA. *G3 (Bethesda)*. 2018 May 31;8(6):2079-2089. PMID: 29686109; PMCID: PMC5982834.

Lee SY, Bailey SC, Apirion D. Small stable RNAs from *Escherichia coli*: evidence for the existence of new molecules and for a new ribonucleoprotein particle containing 6S RNA. *J Bacteriol*. 1978 Feb;133(2):1015-23. PMID: 342486; PMCID: PMC222114.

Li Z, Zhu L, Yu Z, Liu L, Chou SH, Wang J, He J. 6S-1 RNA Contributes to Sporulation and Parasporal Crystal Formation in *Bacillus thuringiensis*. *Front Microbiol*. 2020 Nov 26; 11:604458. PMID: 33324388; PMCID: PMC7726162.

Lorenz AR, Bernhart SH, Neubock R, Hofacker IL. The vienna RNA websuite. *Nucleic Acids Res*. 2008;36(Suppl 2): W70-4.

Mikulík K, Bobek J, Zídková J, Felsberg J. 6S RNA modulates growth and antibiotic production in *Streptomyces coelicolor*. *Appl Microbiol Biotechnol*. 2014 Aug;98(16):7185-97. Epub 2014 May 24. PMID: 24859522.

Moreno-Campuzano S, Janga SC, Pérez-Rueda E. Identification and analysis of DNA-binding transcription factors in *Bacillus subtilis* and other Firmicutes—a genomic approach. *BMC Genomics*. 2006 Jun 13;7:147. PMID: 16772031; PMCID: PMC1524751.

Narra HP, Sahni A, Alsing J, Schroeder CLC, Golovko G, Nia AM, Fofanov Y, Khanipov K, Sahni SK. Comparative transcriptomic analysis of *Rickettsia conorii* during in vitro infection of human and tick host cells. *BMC Genomics*. 2020 Sep 25;21(1):665. PMID: 32977742; PMCID:

PMC7519539.

Neidle S. Nucleic acid structure and recognition. Oxford University Press, USA; 2002.

Neusser T, Gildehaus N, Wurm R, Wagner R. Studies on the expression of 6S RNA from *E. coli*: involvement of regulators important for stress and growth adaptation. *Biol Chem*. 2008 Mar; 389(3):285-97. PMID: 18177266.

Neusser T, Polen T, Geissen R, Wagner R. Depletion of the non-coding regulatory 6S RNA in *E. coli* causes a surprising reduction in the expression of the translation machinery. *BMC Genomics*. 2010 Mar 11;11:165. PMID: 20222947; PMCID: PMC2848244.

Oviedo Ovando M, Shephard L, Unrau PJ. In vitro characterization of 6S RNA release-defective mutants uncovers features of pRNA-dependent release from RNA polymerase in *E. coli*. *RNA*. 2014 May;20(5):670-80. Epub 2014 Mar 28. PMID: 24681966; PMCID: PMC3988568.

Palazzo AF, Lee ES. Non-coding RNA: what is functional and what is junk? *Front Genet*. 2015 Jan 26; 6:2. PMID: 25674102; PMCID: PMC4306305.

Panchapakesan SS, Unrau PJ. *E. coli* 6S RNA release from RNA polymerase requires σ^{70} ejection by scrunching and is orchestrated by a conserved RNA hairpin. *RNA*. 2012 Dec;18(12):2251-9. Epub 2012 Nov 1. PMID: 23118417; PMCID: PMC3504675.

Peeters E, Sass A, Mahenthiralingam E, Nelis H, Coenye T. Transcriptional response of *Burkholderia cenocepacia* J2315 sessile cells to treatments with high doses of hydrogen peroxide and sodium hypochlorite. *BMC Genomics*. 2010 Feb 5; 11:90. PMID: 20137066; PMCID: PMC2830190.

Qi Y, Hulett FM. PhoP-P and RNA polymerase sigmaA holoenzyme are sufficient for transcription of Pho regulon promoters in *Bacillus subtilis*: PhoP-P

activator sites within the coding region stimulate transcription in vitro. *Mol Microbiol.* 1998 Jun;28(6):1187-97. PMID: 9680208.

Rediger A, Geißen R, Steuten B, Heilmann B, Wagner R, Axmann IM. 6S RNA – an old issue became blue-green. *Microbiology (Reading).* 2012 Oct;158 (Pt 10):2480-2491. Epub 2012 Jul 5. PMID: 22767549.

Ren J, Sang Y, Qin R, Cui Z, Yao YF. 6S RNA is involved in acid resistance and invasion of epithelial cells in *Salmonella enterica* serovar Typhimurium. *Future Microbiol.* 2017 Sep; 12:1045-1057. Epub 2017 Aug 10. PMID: 28796533.

RNA Biol. 2017 Nov 2;14(11):1627-1637. Epub 2017 Sep 13. Erratum in: *RNA Biol.* 2018 Jan 2;15(1):156. PMID: 28692405; PMCID: PMC5785217.

Shephard L, Dobson N, Unrau PJ. Binding and release of the 6S transcriptional control RNA. *RNA.* 2010 May;16(5):885-92. Epub 2010 Mar 30. PMID: 20354151; PMCID: PMC2856883.

Šíková M, Janoušková M, Ramaniuk O, Páleníková P, Pospíšil J, Bartl P, Suder A, Pajer P, Kubičková P, Pavliš O, Hradilová M, Vítovská D, Šanderová H, Převorovský M, Hnilicová J, Krásný L. Ms1 RNA increases the amount of RNA polymerase in *Mycobacterium smegmatis*. *Mol Microbiol.* 2019 Feb;111(2):354-372. Epub 2018 Dec 11. PMID: 30427073.

Steuten B, Hoch PG, Damm K, Schneider S, Köhler K, Wagner R, Hartmann RK. Regulation of transcription by 6S RNAs: insights from the *Escherichia coli* and *Bacillus subtilis* model systems. *RNA Biol.* 2014;11(5):508-21. Epub 2014 Apr 23. PMID: 24786589; PMCID: PMC4152359.

Steuten B, Setny P, Zacharias M, Wagner R. Mapping the spatial neighborhood of the regulatory 6S RNA bound to *Escherichia coli* RNA polymerase holoenzyme. *J Mol Biol.* 2013 Oct 9;425(19):3649-61. Epub 2013 Jul 15. PMID: 23867276.

- Steuten B, Wagner R. A conformational switch is responsible for the reversal of the 6S RNA-dependent RNA polymerase inhibition in *Escherichia coli*. *Biol Chem*. 2012 Dec;393(12):1513-22. PMID: 23667906.
- Trotochaud AE, Wassarman KM. 6S RNA function enhances long-term cell survival. *J Bacteriol*. 2004 Aug;186(15):4978-85. PMID: 15262935; PMCID: PMC451630.
- Trotochaud AE, Wassarman KM. 6S RNA regulation of *pspF* transcription leads to altered cell survival at high pH. *J Bacteriol*. 2006 Jun;188(11):3936-43. PMID: 16707685; PMCID: PMC1482906.
- Trotochaud AE, Wassarman KM. A highly conserved 6S RNA structure is required for regulation of transcription. *Nat Struct Mol Biol*. 2005 Apr; 12(4):313-9. Epub 2005 Mar 27. PMID: 15793584.
- Ul-Haq I, Müller P, Brantl S. Intermolecular Communication in *Bacillus subtilis*: RNA-RNA, RNA-Protein and Small Protein-Protein Interactions. *Front Mol Biosci*. 2020 Aug 7; 7:178. PMID: 32850966; PMCID: PMC7430163.
- Vandevenne M, Delmarcelle M, Galleni M. RNA Regulatory Networks as a Control of Stochasticity in Biological Systems. *Front Genet*. 2019 May 7; 10:403. PMID: 31134128; PMCID: PMC6514243.
- Warrier I, Hicks LD, Battisti JM, Raghavan R, Minnick MF. Identification of novel small RNAs and characterization of the 6S RNA of *Coxiella burnetii*. *PLoS One*. 2014 Jun 20;9(6):e100147. PMID: 24949863; PMCID: PMC4064990.
- Wassarman KM, Saecker RM. Synthesis-mediated release of a small RNA inhibitor of RNA polymerase. *Science*. 2006 Dec 8;314(5805):1601-3. PMID: 17158328.
- Wassarman KM, Storz G. 6S RNA regulates *E. coli* RNA polymerase activity.

Cell. 2000 Jun 9;101(6):613-23. PMID: 10892648.

Wassarman KM. 6S RNA, a Global Regulator of Transcription. *Microbiol Spectr.* 2018 May; 6(3): 10.1128 / microbiolspec. RWR-0019-2018. PMID: 29916345; PMCID: PMC6013841.

Wehner S, Damm K, Hartmann RK, Marz M. Dissemination of 6S RNA among bacteria. *RNA Biol.* 2014;11(11):1467-78. PMID: 25483037; PMCID: PMC4615782.

Wiedermannová J, Sudzinová P, Koval' T, Rabatinová A, Šanderova H, Ramaniuk O, Rittich Š, Dohnálek J, Fu Z, Halada P, Lewis P, Krásny L. Characterization of HelD, an interacting partner of RNA polymerase from *Bacillus subtilis*. *Nucleic Acids Res.* 2014 Apr;42(8):5151-63. PMID: 24520113; PMCID: PMC4005671.

Willkomm DK, Minnerup J, Hüttenhofer A, Hartmann RK. Experimental RNomics in *Aquifex aeolicus*: identification of small non-coding RNAs and the putative 6S RNA homolog. *Nucleic Acids Res.* 2005 Apr 6;33(6):1949-60. PMID: 15814812; PMCID: PMC1074721.

Winkelman JT, Bree AC, Bate AR, Eichenberger P, Gourse RL, Kearns DB. RemA is a DNA-binding protein that activates biofilm matrix gene expression in *Bacillus subtilis*. *Mol Microbiol.* 2013 Jun;88(5):984-97. doi: 10.1111/mmi.12235. Epub 2013 May 7. PMID: 23646920; PMCID: PMC3732408.

Wurm R, Neusser T, Wagner R. 6S RNA-dependent inhibition of RNA polymerase is released by RNA-dependent synthesis of small de novo products. *Biol Chem.* 2010 Feb-Mar;391(2-3):187-96. PMID: 20030589.

Yan Y, Su S, Meng X, Ji X, Qu Y, Liu Z, Wang X, Cui Y, Deng Z, Zhou D, Jiang W, Yang R, Han Y. Determination of sRNA expressions by RNA-Seq in *Yersinia pestis* grown in vitro and during infection. *PLoS One.* 2013 Sep

11;8(9): e74495. PMID: 24040259; PMCID: PMC3770706.

Yang X, Lewis PJ. Overproduction and purification of recombinant *Bacillus subtilis* RNA polymerase. *Protein Expr Purif*. 2008 May;59(1):86-93. Epub 2008 Jan 24. PMID: 18289874

Zeigler DR, Prágai Z, Rodriguez S, Chevreux B, Muffler A, Albert T, Bai R, Wyss M, Perkins JB. The origins of 168, W23, and other *Bacillus subtilis* legacy strains. *J Bacteriol*. 2008 Nov;190(21):6983-95. Epub 2008 Aug 22. PMID: 18723616; PMCID: PMC2580678.

Zeigler DR. *Bacillus Genetic Stock Center Catalog of Strains, Volume 1: Bacillus subtilis 168*. Bacillus Genetic Stock Center. 2000 Nov 8.

Zhu B, Stülke J. SubtiWiki in 2018: from genes and proteins to functional network annotation of the model organism *Bacillus subtilis*. *Nucleic Acids Res*. 2018 Jan 4;46(D1):D743-D748. PMID: 29788229; PMCID: PMC5753275.

Appendix

A. Equipment and disposables

Instrument	Manufacturer
Autoclave V 95	Systemec
Power supply PowerPac 3000	Bio-rad
Cell lysis:	
Fast prep	MP Biomedicals
Ultrasonifier	Branson sonifier
Centrifuge:	
Biofuge Fresco	Heraeus
Centrifuge 5415R	Eppendorf
Centrifuge 5810R	Eppendorf
Micro centrifuge 5415D	Eppendorf
Minispin® plus	Eppendorf
Documentation devices:	
ChemiDoc™ MP Imaging system	Bio-Rad
Dark Hood DH-50 and Gerix 1000	Biostep
Gel Chambers:	
Mini-Sub® Cell GT systems	Bio-Rad
Mini-PROTEAN tetra vertical electrophoresis cell	Bio-Rad
PAA gel chamber	University of Lübeck
Dry Bath:	
Thermoblock TB1	Biometra
Incubator:	
Falcon rolling incubator	Phoenix Instrument GmbH
Laboratory incubator BE 400	Memmert
Shaking incubator 3033	GFL
Water shaking incubator	Aquatron
PCR cycler:	

TGradient	Biometra
Tone 96 G	Biometra
Spectrophotometer:	
UV-Vis Spectrophotometer 7305	Jenway
Nanodrop ND1000	Peqlab
UV5Nano	Mettler Toledo
Miscellaneous:	
Äkta	GE Healthcare
Electro-blotter	Bio-Rad
Fractionator	GE Healthcare
Gel scanner	Bio-Rad
Gilson™ electronic pipette	Thermo Fisher Scientific
Laminar flow hood Heraeus Herasafe®	Thermo Fisher Scientific
Magnetic stirrer	Heidolph instrument
Microwave 8020 E	Privileg
Peristaltic pump	Fisher Scientific
pH-meter inoLab pH level 1	WTW
Phospho-imager	Fujifilm
Pipettes	Eppendorf
Scintillator Tricarb	Perkin Elmer
Thermomixer 5436	Eppendorf
UV lamp	Camag
Vortex mixer 7-2020	neoLab
Weighing machine	Sartorius
Water bath MT	Lauda

Disposable materials	Manufacturer
Filtropur BT 50 bottle top filter, 500 mL	Sarstedt
Petri plates	Sarstedt
Pipette tips with filter	Sarstedt

Pipette tips without filter	Starlab
Eppendorf vials:	
1.5 / 2 mL	Sarstedt
Falcons 15, 50 mL	Sarstedt
Filtropur S Syringe filter 0.2 µM	B. Braun
Multiply®- µStrip Pro, 8 vials (0.2 mL)	Greiner Bio-one
Serological Pipette	Sarstedt
Surgical Scalpel Blade No. 21	B. Braun
Syringe needles	Sarstedt

B. Chemicals

Name	Manufacturer
100 bp DNA ladder	Cytogen
1 kb DNA ladder	Cytogen
Acrylamide M-bis (24:1) 50 %	Gerbu
Agar (RNA / DNA electrophoresis grade)	Roth
Agar (Bacteriology grade)	Roth
Ampicillin sodium salt	Roth
Ammonium persulfate	ACS
Bovine serum albumin (BSA)	Roth
Boric acid (99.8 % p.a)	ACS
Protein assay dye reagent concentrate	Bio-Rad
Bromophenol blue	Merck
Casein peptone	Roth
Chloroform	Merck
Chloramphenicol	Sigma
Disodium phosphate (Na₂HPO₄)	Merck
Dithiothreitol (DTT)	Gerbu
Ethanol (99.8 % p.a.)	Roth
Ethylenediaminetetraacetic acid (EDTA)	Gerbu

Formamide (99.5 % p.a.)	Roth
Gel Red	Merck
Glacial acetic acid	Roth
Glucose	Roth
Glycerol (99.5 %)	Gerbu
Glycoblue™	Thermo Fisher Scientific
Heparin	Sigma-Aldrich
Hydrochloric acid (HCl) concentrated	Roth
Kanamycin	Roth
Magnesium Chloride (MgCl₂)	Roth
Monopotassium phosphate (KH₂PO₄)	Roth
Meat Extract	Roth
N, N, N', N'- Tetramethylethylenediamine (TEMED)	Sigma-Aldrich
Phenylmethylsulfonyl fluoride (PMSF)	Roth
Polyethylene glycol	Roth
Potassium chloride (KCl)	Merck
Pyrophosphatase	Roche Diagnostics GmbH
Roti®-phenol/chloroform/Isoamylalcohol	Roth
Rotiphoresis gel acrylamide (37.5:1 acrylamide/bis acrylamide)	Roth
Sodium acetate (NaCH₃COO)	Grüssig GmbH
Sodium chloride (NaCl)	Roth
Sodium phosphate monobasic (NaH₂PO₄)	Merck
Sodium hydroxide (NaOH)	Fluka
Spectinomycin	Fluka
Spermidine	Roth
Tri-phenyl tetrazolium Chloride	Sigma-Aldrich
Tris (Hydroxymethyl) aminomethane (Tris)	Roth
Tryptone	Roth
Urea	Gerbu
Yeast extract	Gerbu
Xylene cyanol blue	Roth

C. Proteins and Enzymes

Proteins and Enzymes	Manufacturer
2 x Phusion master mix	Thermo Fisher Scientific
2 x PowerUp™ SYBR™ green master mix	Thermo Fisher Scientific
5 x Cytopol hot bench MM	Cytogen GmbH
10 x Fast digest green buffer	Thermo Fisher Scientific
FastAP™ thermosensitive alkaline phosphatase	Thermo Fisher Scientific
Fast digest DpnI	Thermo Fisher Scientific
Fast digest HindIII	Thermo Fisher Scientific
Glycoblu™	Thermo Fisher Scientific
Long PCR polymerase	Thermo Fisher
PageRuler™ Prestained Protein Ladder	Thermo Fisher Scientific
Precision Plus Protein™ All Blue Pre- stained Protein Standards	Bio-Rad
Precision Plus Protein™ Unstained Protein Standards	Bio-Rad
Rabbit 6 x his tagged antibody	Invitrogen
Superfi polymerase	Thermo Fisher Scientific
T4 DNA ligase	Thermo Fisher Scientific
T4 Polynucleotide kinase	Thermo Fisher Scientific

D. Kits

Kits	Manufacturer
Clarity™ Western ECL substrate	Bio-Rad
GeneJET Plasmid Miniprep Kit	Thermo Fisher Scientific
Monarch DNA Gel Extraction Kit	New England Biolabs
Monarch® PCR & DNA Clean up Kit (5 µg)	New England Biolabs
NucleoBond Xtra Maxi kit	Macherey-Nagel
TGX gel	Bio-Rad
Wizard® SV Gel and PCR Clean-Up system	Promega

E. Bacterial strains and antibiotics

Strain	Characteristics	Source
<i>B. subtilis</i> MH5636 his-rpoC	<i>pheA1</i> , <i>trpC2</i> , and <i>rpoC</i> Ω pYQ52(Cm ^r)	Qi et al., 2002
<i>B. subtilis</i> MWΔ<i>bsrAB</i>	PY79 Δ <i>bsrA</i> :spc (Sp ^r) Δ <i>bsrB</i> :kan (Km ^r)	Hoch et al., 2015
<i>B. subtilis</i> 110 NA	<i>trpC2 spo0A3</i> su ⁻	Muñoz-Espín et al., 2009
<i>B. subtilis</i> LK782	<i>pheA1</i> , <i>trpC2</i> , and <i>rpoC</i> Ω pYQ52(Cmr), <i>helD</i> ::MLS	Wiedermannová et al., 2014
<i>E. coli</i> σ^A overexpression strain	F ⁻ ompT <i>hsdS_B</i> (r _B ⁻ , m _B ⁻) gal dcm (DE3) pET28a(+>:: σ^A nHis	From Jana C. Wiegard
<i>E. coli</i> pBB T7 6S-1 190	ϕ 10 pUC18:: <i>bsrA</i> , (Amp ^r)	Beckmann et al., 2011
<i>B. subtilis</i> WT 3610 (<i>amyE</i>:cat)	NCIB 3610 (<i>amyE</i> ::cat)	Thüring et al., 2021
Δ6S-1 <i>amyE</i>:cat	NCIB 3610 (Δ <i>bsrA</i> <i>amyE</i> ::cat)	Thüring et al., 2021
Δ6S-2 <i>amyE</i>:cat	NCIB 3610 (Δ <i>bsrB</i> <i>amyE</i> ::cat)	Thüring et al., 2021
Δ6S-2 <i>amyE</i>:6S-2:cat	NCIB 3610 (Δ <i>bsrB</i> <i>amyE</i> ::6S-2::cat)	Thüring et al., 2021
Δ6S-1&2 <i>amyE</i>:cat	NCIB 3610 (Δ <i>bsrA</i> Δ <i>bsrB</i> <i>amyE</i> ::cat)	Thüring et al., 2021
<i>B. subtilis</i> His-rpoC, Δ<i>bsrAB</i> (SG7)	PY79 Δ <i>bsrA</i> :spc (Sp ^r), Δ <i>bsrB</i> ::kan (Km ^r) <i>rpoC</i> Ω pYQ52 (Cm ^r)	This work

Antibiotics	Stock concentration	Final concentration	Strains
Ampicillin (Amp)	100 mg/mL in ddH ₂ O	100 µg/mL	<i>E. coli</i> T7 6S-1 RNA strain & derivative
Kanamycin (Km)	50 mg/mL in ddH ₂ O	10 µg/mL	PY79 double knockout, SG7
Spectinomycin (Sp)	100 mg/mL in ddH ₂ O	100 µg/mL	PY79 double knockout, SG7
Chloramphenicol (Cm)	34 mg/mL in EtOH	2.5 µg/mL	MH5636, LK782 SG7
Chloramphenicol (Cm)	34 mg/mL in EtOH	10 µg/mL	NCIB 3610 and derivatives

F. Plasmids

All plasmids listed below are carried by vector *E. coli* T7 6S-1 strain with *bsrA* sequence carrying the described modifications:

Plasmid	Characteristics	Source
pBB1	pUC18::T7- <i>bsrA</i> -190, (Amp ^r)	Beckmann et al., 2011
pGH2	pUC18::T7- <i>bsrA</i> -190-A50U, (Amp ^r)	From Philipp G. Hoch
pGH3	pUC18::T7- <i>bsrA</i> -190-A50C, (Amp ^r)	From Philipp G. Hoch
pGH5	pUC18::T7- <i>bsrA</i> -78-78nt, (Amp ^r)	From Philipp G. Hoch
pGH6	pUC18::T7- <i>bsrA</i> -82-82cp, (Amp ^r)	From Philipp G. Hoch
pGH16	pUC18::T7- <i>bsrA</i> -190-U44_45C, (Amp ^r)	From Philipp G. Hoch
pGH17	pUC18::T7- <i>bsrA</i> -190-GGGG, (Amp ^r)	From Philipp G. Hoch
P170	pRLG770:: <i>epsA</i> (Amp ^r)	From AG Bange
pSG1	pUC18::T7- <i>bsrA</i> -190-A50G, (Amp ^r)	This work
pSG2	pUC18::T7- <i>bsrA</i> -190-WT 8m, (Amp ^r)	This work

pSG3	pUC18::T7- <i>bsrA</i> -190-U44_45C 8m, (Amp ^r)	This work
pSG4	pUC18::T7- <i>bsrA</i> -190- WT 8mb, (Amp ^r)	This work
pSG5	pUC18::T7- <i>bsrA</i> -190-U44_45C 8mb (Amp ^r)	This work
pSG6	pUC18::T7- <i>bsrA</i> -190- WT 8mb_U32 (Amp ^r)	This work
pSG7	pUC18::T7- <i>bsrA</i> -190-U44_45C 8mb_U32 (Amp ^r)	This work

For detailed overview of plasmid construction and sequence information, please refer Appendix J.

G. Terminology of 6S RNA mutants

Plasmid	RNA mutant	Alias
pBB1	6S-1 RNA	Wild type (WT)
pGH2	A50U	U50
pGH3	A50C	C50
pGH5	78nt	-
pGH6	82cp	-
pGH16	U44_45C	C44_45
pGH17	GGGG	-
pSG1	A50G	G50
pSG2	WT 8m	-
pSG3	U44_45C 8m	C44_45 8m
pSG4	WT 8mb	WT 6m
pSG5	U44_45C 8mb	C44_45 6m
pSG6	WT 8mb_U32	WT 5m
pSG7	U44_45C 8mb_U32	C44_45 5m

H. Primers

DNA primers and synthetic oligonucleotides

Primer name	Sequence
<i>rpoC_for</i>	5' GAGCCGGAAGAAACAGCATCTGC 3'
<i>rpoC_rev</i>	5' GATTCGTTCTTCTCATAGAGTGACTTTTT 3'
<i>rpoC_start_rev</i>	5' GACGGTGTTACAACCGGTTTACCATC 3'
<i>rpoC_mid_rev</i>	5' CTTAGCAAGAATGCCTCGGTCAG 3'
<i>rpoC_mid_for</i>	5' CCGTGAAGGTCTGACAGTATTGGAGTAC 3'
<i>rpoC_380_bp_for</i>	5' GGTGACACTGATGTGCTTCCA 3'
<i>rpoC_his_tag_rev</i>	5' TTAATGATGATGATGATGATGATGATGATGAT GTTCAACCGGGACCATATCGT 3'
6S-1_for_SG	5' CAGCTTGACGAGCTTCATCTTTCTATC 3'
6S-1_rev_SG	5' GCTAATTCATTGCGTGAAAAGTGGTG 3'
6S-2_for_SG	5' GGTTTACAAGAAGCAAAAGATCTTGCTG 3'
6S-2_rev_SG	5' CCAGAAGGGATTGGGCTCTATGTAAC 3'
6S-1_seq_for	5' CATCAATGTAAAAGGCGGTGC 3'
6S-1_seq_rev	5' GCCATTCTGGCAATCGATGA 3'
6S-2_seq_for	5' CCAAGCAAGTACACCGATATTAG 3'
6S-2_seq_rev	5' GATTCGTTTCAATCTCTCATATATCCG 3'
<i>cat_rev</i>	5' GTTTTGGGAAACAATTTCCCCGAACC 3'
<i>cat_for</i>	5' TGAACCAACAAACGACTTTTAGTATAACCACA 3'
GEX3_rev_25	5' GAGCTGCATGTGTCAGAGG 3'
<i>ori_primer</i>	5' GGGAAGCGTGGCGCTTTCTCATAGC 3'
<i>veg_primer_for</i>	5' CATAATTTACCGAAACTTGCGG 3'
<i>veg_primer_rev</i>	5' CAGAAGGGTACGTCTCAGC 3'
<i>sigA_forward</i>	5' CAACTCAGCTTCCTTTTCGGGTTATTCAAGGA AATCTTTCAAACGTTTACTTCTGCTAGG 3'
<i>sigA_reverse</i>	5' TGGTGCCGCGCGGCAGCCATATGGCTGATAA ACAAACCCACGAG 3'

vector_forward	5' TGGGTTTGTTCATCAGCCATATGGCTGCCCGC G 3'
vector_reverse	5' TGAAAGATTTCTTGAATAACCCGAAAGGAA GCTGAGTTGG 3'
pRNA 8 mer	5' GUUCGGUC 3'
pRNA 14 mer	5' GUUCGGUCAAAACU 3'
A50U_6S-1_for	5' CAAAACAAAAAATGTTTCGGTCAAACACTAG GTG 3'
A50U_6S-1_rev	5' GGAGCCCGCATTTTTTAAATGGC 3'
A50C_6S-1_for	5' CAAAGCAAAAAAATGTTTCGGTCAAACACTAG GTGT 3'
A50C_6S-1_rev	5' GGAGCCCGCATTTTTTAAATGGCGTA 3'
A50G_6S-1_for	5' GCGGGCTCCCAAACCAAAAAAATGTTTCGGT C 3'
A50G_6S-1_rev	5' GACCGAACATTTTTTTGGTTTGGGAGCCCG C 3'
78nt_6S-1_for	5' ATGGAATTCTAATACGACTCACTATAGGCCTAG TTTTGACCGAACATTTTTTTG 3'
78nt_6S-1_rev	5' ATGAAGCTTCCTTTGTTTTGAACCCGCTCTCAG CAGGTGGGTGCCCTGCGGGCTCCCAAATCAAA AAAATG 3'
82cp_6S-1_for	5' ATGAAGCTTGGGCTCCCAAATCAAAAAAATGTT CGGTCAAACACTAGGTGGCTTTCCTTTGTTTTGA ACCCGCTCTCAGC 3'
82cp_6S-1_rev	5' ATGGAATTCTAATACGACTCACTATAGGGCAC CCACCTGCTGAG 3'
U44_45C_for	5' GGTCAAACACTAGGTGTACAACACACATCA GGA 3'
U44_45C_rev	5' GAACATTCCTTTGATTTGGGAGCCCG 3'
8m C30_G34_wt_1	5' AAAATGTTTCGGCCTTGACTAGGTGTACAAC AACA 3'
8m C151_G155_wt_1	5' GCTTTCCTTTGTCAAGGACCCGCTCTCA 3'

8m C30_G34_btb_3	5' TTTGATTTGGGAGCCCCGC 3'
8m C151_G155_btb_3	5' TGCAACGGCACTATTGGG 3'
8m C30_G34_U44_45C_1	5' GGAATGTTTCGGCCTTGACTAGGTGTACAAC AACA 3'
8mb U151_G155_1	5' GCTTTCCTTTGTCATGAACCCGCTCTCA 3'
8mb_C30_G34_U44_45C_1	5' GGAATGTTTCGGCCTTGACTAGGTGTACAAC TAACA 3'
8mb_U32_C30_G34_WT_1	5' AAAATGTTTCGGCCATGACTAGGTGTAC AACTAACA 3'
8mb_U32_C30_G34_U44_45C_1	5' GGAATGTTTCGGCCATGACTAGGTGTACAAC TAACA 3'
GGGG_rev	5' AAAGGAAAGCTGCAACGGCACTATTG 3'
GGGG_for	5' GCCCCGAACCCGCTCTCAG 3'

I. Softwares

Softwares used	Purpose
Graphpad prism 9	Data analysis, Illustration
Grafit 5	Kinetics evaluation
RNAfold (Vienna web-package)	Secondary structure prediction
RNAcofold (Vienna web-package)	Binding prediction
CoreIDRAW 11	Illustration
Inkscape	Illustration
Snappgene 4.1.9	Cloning and sequencing
Image lab version 6.1 (Bio-Rad)	Evaluation of SDS gels
BAS Reader 3.14 (Fujiifilm)	Visualisation of radioactive gels
AIDA image analyser 3.45.039 (Fujifilm)	Evaluation of radioactive gels

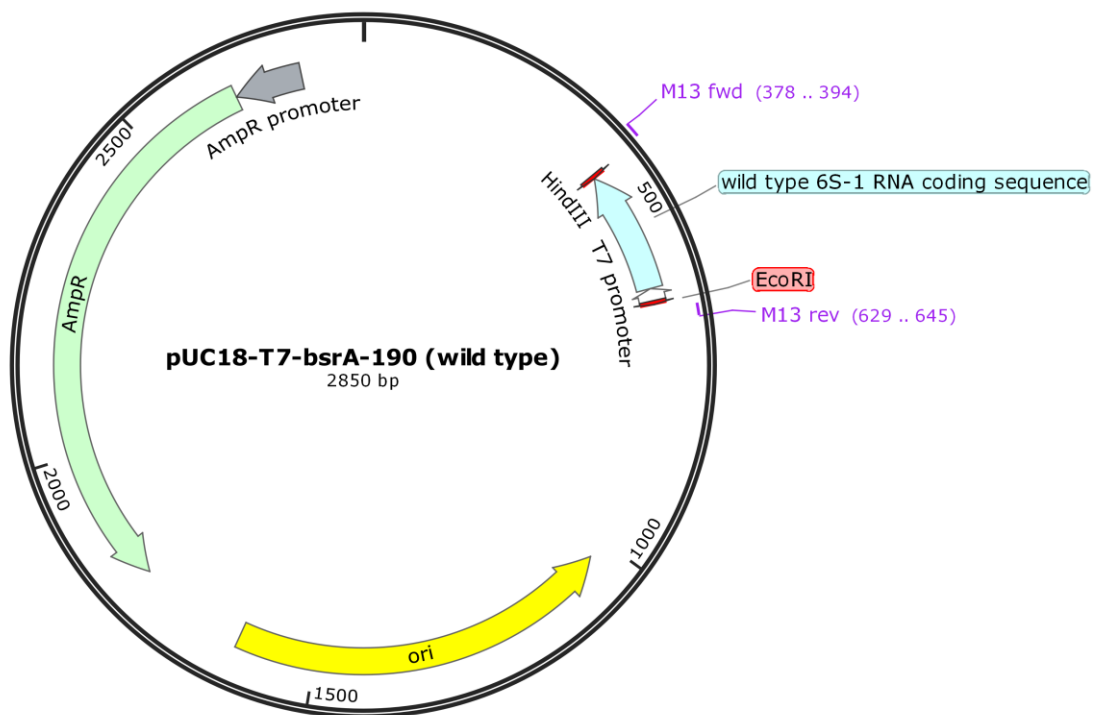
J. Plasmid cards

pUC18-T7-bsrA-190

Also known as pBB1, is a derivative of plasmid pUC18 with EcoRI and HindIII restriction sites, T7 promoter and the coding sequence of mature *B. subtilis* 6S-1 RNA. The plasmid also carries an ampicillin resistance cassette that serves as selection marker. The RNA transcribed from this plasmid construct is referred to as wild type (WT).

Alias: pBB1

Created with SnapGene®



Wild type sequence

5' GAATTCTAATACGACTCACTATAGGAGTCCTGATGTGTTAGTTGTACAC
CTAGTTTTGACCGAACATTTTTTTGATTTGGGAGCCCGCATTTTTAAATGGC
GTACATGCCTCTTTTCATTCGGTAAAGAGGACTTACAAGATTTAAAAGAGG
GCACCCACCTGCTGAGAGCGGGTTCAAACAAAGGAAAGCTGCAACGGCA
CTATTGGGACTTTAAGCTT 3'

EcoRI

T7 promoter

WT 6S-1 RNA coding sequence

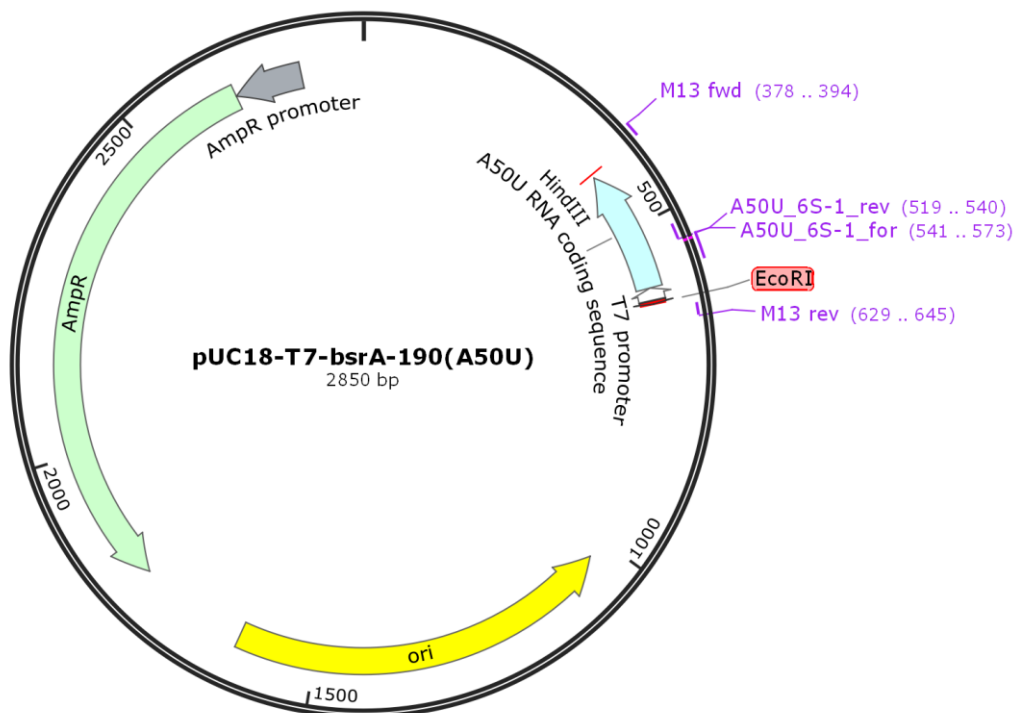
HindIII

pGH2 (pUC18-T7-bsrA-190-A50U)

as pBB1, with an A to T point mutation at position 50 of the mature 6S-1 RNA sequence. In this and the following maps for 6S-1 RNA mutant constructs, the primers used for their construction are indicated within the maps. In the sequences below the plasmid maps, mutated bases are marked by **bold underlined** letters. The RNA transcribed from this plasmid construct (pGH2) is referred to as A50U.

Alias: pGH2

Created with SnapGene®

**A50U mutant sequence**

5' GAATTCTAATACGACTCACTATAGGAGTCCTGATGTGTTAGTTGTACACC
TAGTTTTGACCGAACATTTTTTTG**T**TTTGGGAGCCCGCATTTTTAAATGGCG
TACATGCCTCTTTTCATTCGGTAAAGAGGACTTACAAGATTTAAAAGAGGG
CACCCACCTGCTGAGAGCGGGTTCAAACAAAGGAAAGCTGCAACGGCAC
TATTGGGACTTT**AAGCTT** 3'

EcoRI

T7 promoter

A50U RNA coding sequence

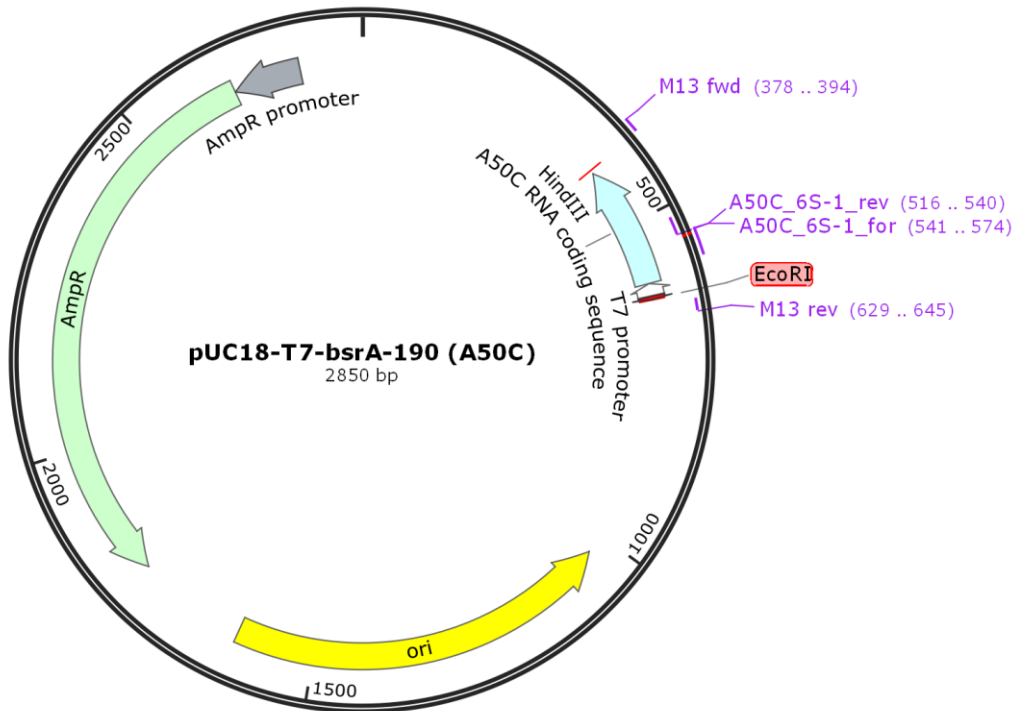
HindIII

pGH3 (pUC18-T7-bsrA-190-A50C)

as pBB1, with an A to C point mutation at position 50 of the mature 6S-1 RNA sequence. The RNA transcribed from this plasmid construct is referred to as A50C.

Alias: pGH3

Created with SnapGene®

**A50C mutant sequence**

5' **GAATTC**TAATAC**GA**CTCACTATAGGAGTCCTGATGTGTTAGTTGTACACC
 TAGTTTTGACCGAACATTTTTTTT**G**TTTGGGAGCCCGCATTTTTAAATGGC
 GTACATGCCTCTTTTCATTCGGTAAAGAGGACTTACAAGATTTAAAGAGG
 GCACCCACCTGCTGAGAGCGGGTTCAAACAAAGGAAAGCTGCAACGG
 CACTATTGGGACTTT**AAGCTT** 3'

EcoRI

T7 promoter

A50C RNA coding sequence

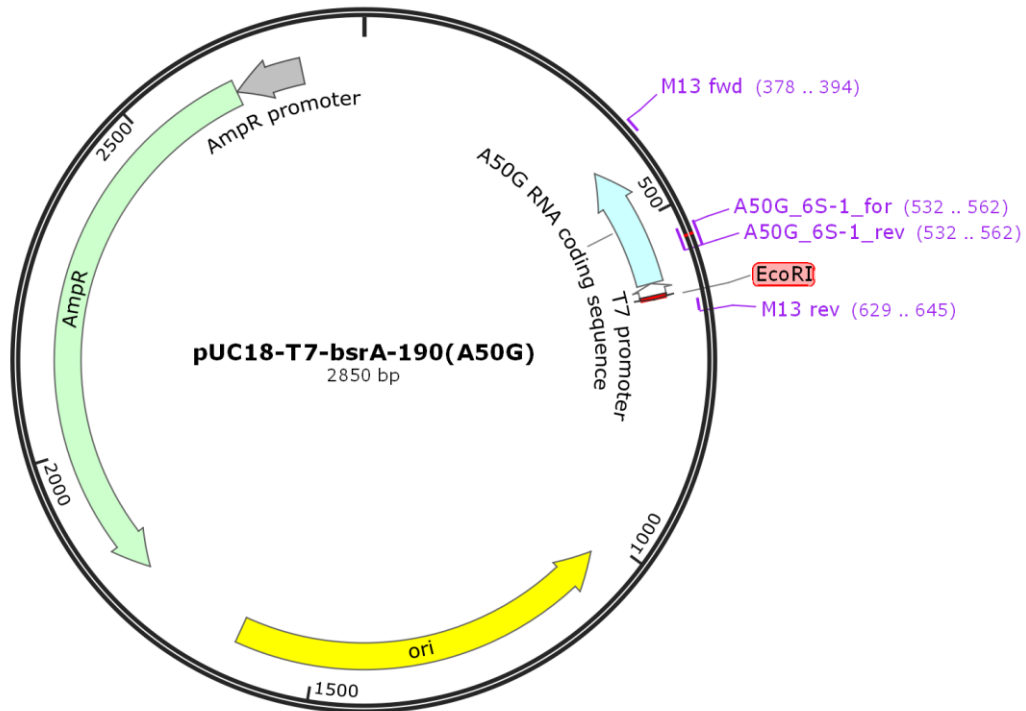
HindIII

pSG1 (pUC18-T7-bsrA-190-A50G)

as pBB1, with an A to G point mutation at position 50 of the mature 6S-1 RNA sequence. The RNA transcribed from this plasmid construct is referred to as A50G.

Alias: pSG1

Created with SnapGene®

**A50G mutant sequence**

5' GAATTCTAATACGACTCACTATAGGAGTCCTGATGTGTTAGTTGTACACC
TAGTTTTTGACCGAACATTTTTTTTGGTTTGGGAGCCCGCATTTTTAAATGGCG
TACATGCCTCTTTTCATTCGGTAAAGAGGACTTACAAGATTTAAAAGAGGG
CACCCACCTGCTGAGAGCGGGTTCAAACAAAGGAAAGCTGCAACGGCAC
TATTGGGACTTTAAGCTT 3'

EcoRI

T7 promoter

A50G RNA coding sequence

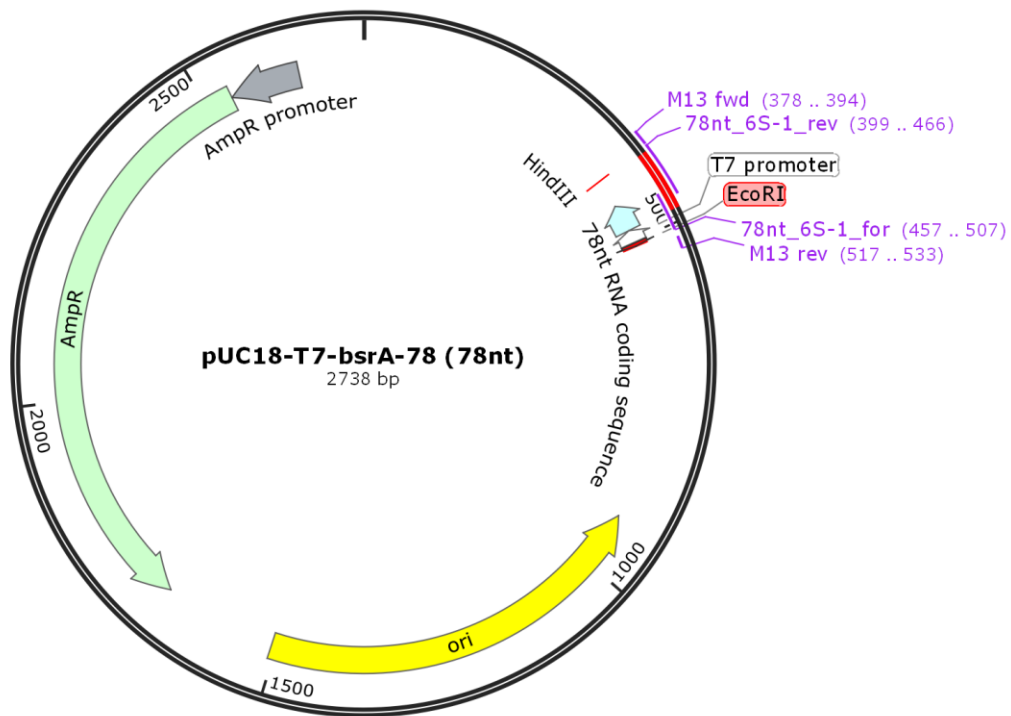
HindIII

pGH5 (pUC18-T7-bsrA-78)

pBB1 derivative with a shortened sequence of 6S-1 RNA (78 nt). The RNA transcribed from this plasmid construct is referred to as 6S₇₈.

Alias: pGH5

Created with SnapGene®

**78nt mutant sequence**

5' GAATTCTAATACGACTCACTATAGGCCTAGTTTTGACCGAACATTTTTTTT
GATTTGGGAGCCCGCAGGGCACCCACCTGCTGAGAGCGGGTTCAAACA
AAGGAAGCTT 3'

EcoRI

T7 promoter

78nt RNA coding sequence

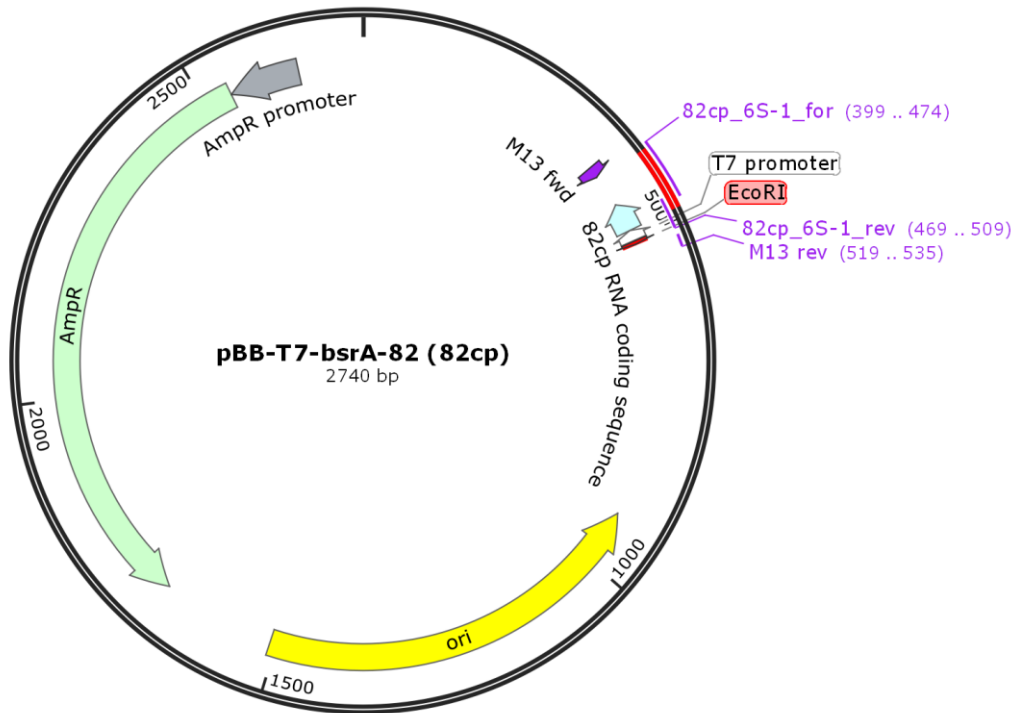
HindIII

pGH6 (pUC18-T7-bsrA-82)

pBB1 derivative, encoding a circularly permuted 6S-1 RNA derivative shortened to 82 nt. The RNA transcribed from this plasmid construct is referred to as 6S_{82cp}.

Alias: pGH6

Created with SnapGene®

**82cp mutant sequence**

5' GAATTCTAATACGACTCACTATAGGGGGCACCCACCTGCTGAGAGCGG
 GTTCAAACAAAGGAAAGCCACCTAGTTTTGACCGAACATTTTTTTGATTTG
 GGAGCCCAAGCTT 3'

EcoRI

T7 promoter

82cp RNA coding sequence

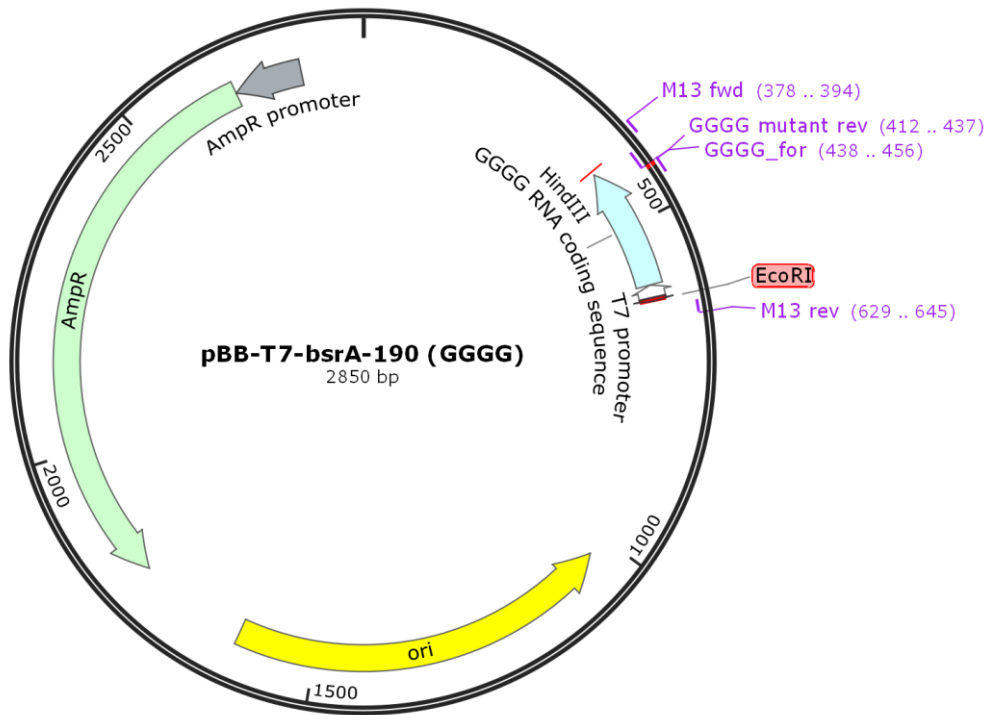
HindIII

pGH17 (pUC18-T7-bsrA-190-GGGG)

pBB1 derivative, with a quadruple substitution mutation introducing C residues at positions 29, 30, 31, 32 and G residues at positions 153, 154, 155 and 156. The RNA transcribed from this plasmid construct is referred to as 6S-1 RNA variant GGGG.

Alias: pGH17

Created with SnapGene®

**GGGG mutant sequence**

5' GAATTCTAATACGACTCACTATAGGAGTCCTGATGTGTTAGTTGTACACC
TAGCCCCGACCGAACATTTTTTTGATTTGGGAGCCCGCATTTTTAAATGGC
GTACATGCCTCTTTTCATTCGGTAAAGAGGACTTACAAGATTTAAAAGAGG
GCACCCACCTGCTGAGAGCGGGTTCGGGGCAAAGGAAAGCTGCAACGGC
ACTATTGGGACTTTAAGCTT 3'

EcoRI

T7 promoter

GGGG RNA coding sequence

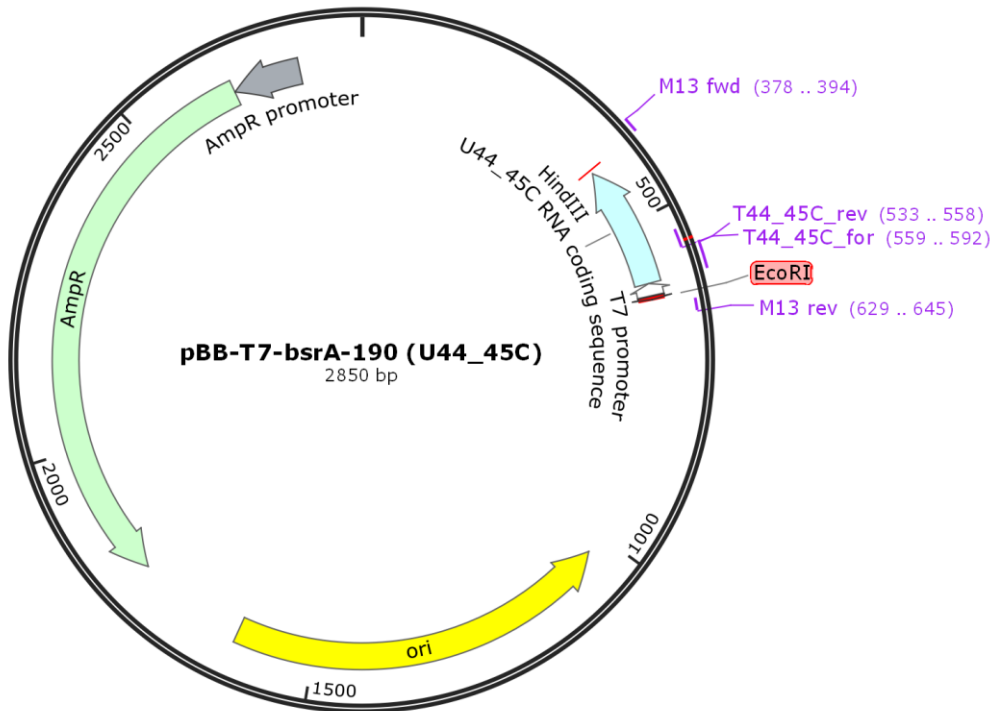
HindIII

pGH16 (pUC18-T7-bsrA-190-U44_45C)

pBB1 derivative, with double mutation at position 44 and 45. The RNA transcribed from this plasmid construct is referred to as to as 6S-1 RNA variant U44_45C or C44/45.

Alias: pGH16

Created with SnapGene®

**U44_45C mutant sequence**

5' GAATTCTAATACGACTCACTATAGGAGTCCTGATGTGTTAGTTGTACACC
 TAGTTTTGACCGAACATTCCTTTTGATTTGGGAGCCCGCATTTTTAAATGGC
 GTACATGCCTCTTTTCATTCGGTAAAGAGGACTTACAAGATTTAAAAGAGG
 GCACCCACCTGCTGAGAGCGGGTTCAAACAAAGGAAAGCTGCAACGGCA
 CTATTGGGACTTTAAGCTT 3'

EcoRI

T7 promoter

U44_45C RNA coding sequence

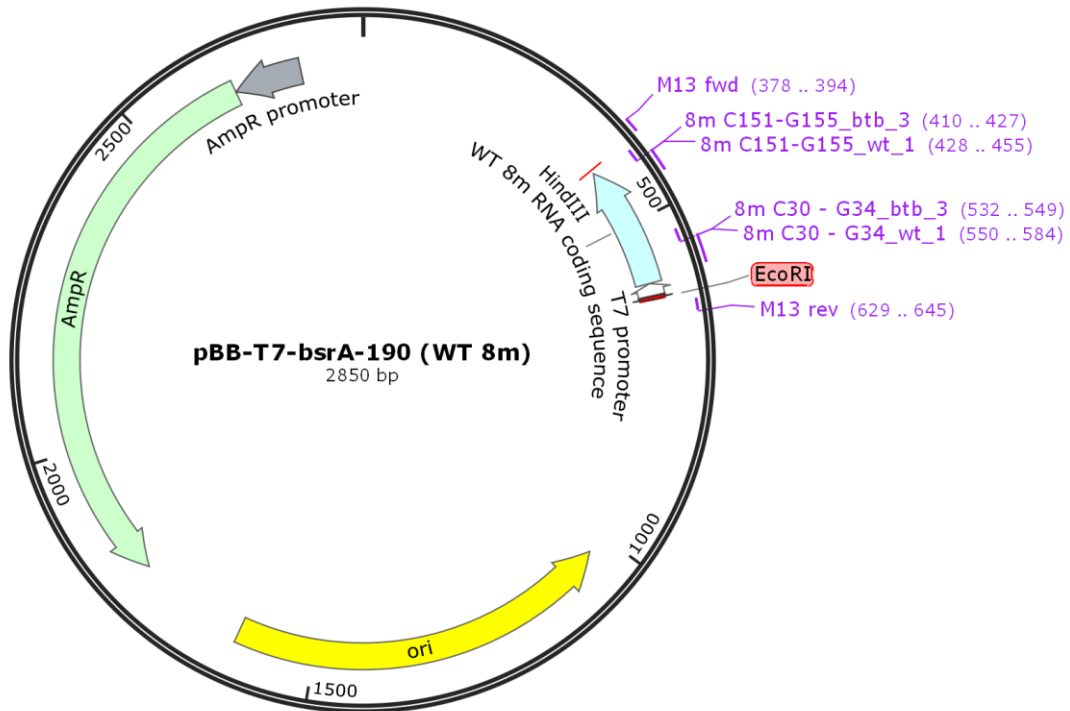
HindIII

pSG2 (pUC18-T7-bsrA-190-WT 8m)

as pBB1, with 8 point mutations at positions 30, 31, 32, 34, 151, 153, 154 and 155 as indicated in the sequence below. The RNA transcribed from this plasmid construct is referred to as WT 8M.

Alias: pSG2

Created with SnapGene®

**WT 8m mutant sequence**

5' **GAATTCTAATACGACTCACTATAGG**AGTCCTGATGTGTTAGTTGTACACC
 TAGT**CAAGG**CCGAACATTTTTTTGATTTGGGAGCCCGCATTTTTAAATGGC
 GTACATGCCTCTTTTCATTCGGTAAAGAGGACTTACAAGATTTAAAAGAGG
 GCACCCACCTGCTGAGAGCGGGT**CCTTG**ACAAAGGAAAGCTGCAACGGC
 ACTATTGGGACTTT**AAGCTT** 3'

EcoRI

T7 promoter

WT 8m RNA coding sequence

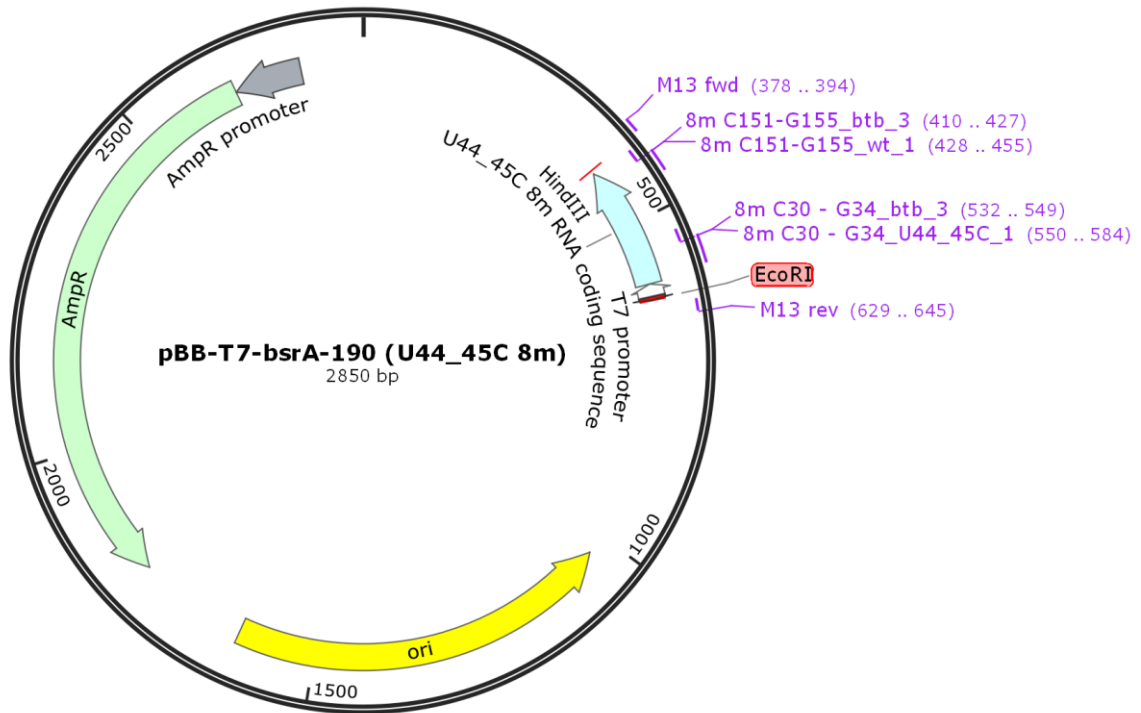
HindIII

pSG3 (pUC18-T7-bsrA-190-U44_45C 8m)

combination of pGH16 and pSG2. The RNA transcribed from this plasmid construct is referred as U44_45C or C44/45 8M.

Alias: pSG3

Created with SnapGene®

**U44_45C 8m mutant sequence**

5' **GAATTC**TAATACGACTCACTATAGGAGTCCTGATGTGTTAGTTGTACACC
 TAGT**CAAGG**CCGAACATT**CC**TTTTGATTTGGGAGCCCGCATTTTTAAATGGC
 GTACATGCCTCTTTTCATTCGGTAAAGAGGACTTACAAGATTTAAAAGAGG
 GCACCCACCTGCTGAGAGCGGGT**CTT**GACAAAGGAAAGCTGCAACGGC
 ACTATTGGGACTTT**AAGCTT** 3'

EcoRI

T7 promoter

U44_45C 8m RNA coding sequence

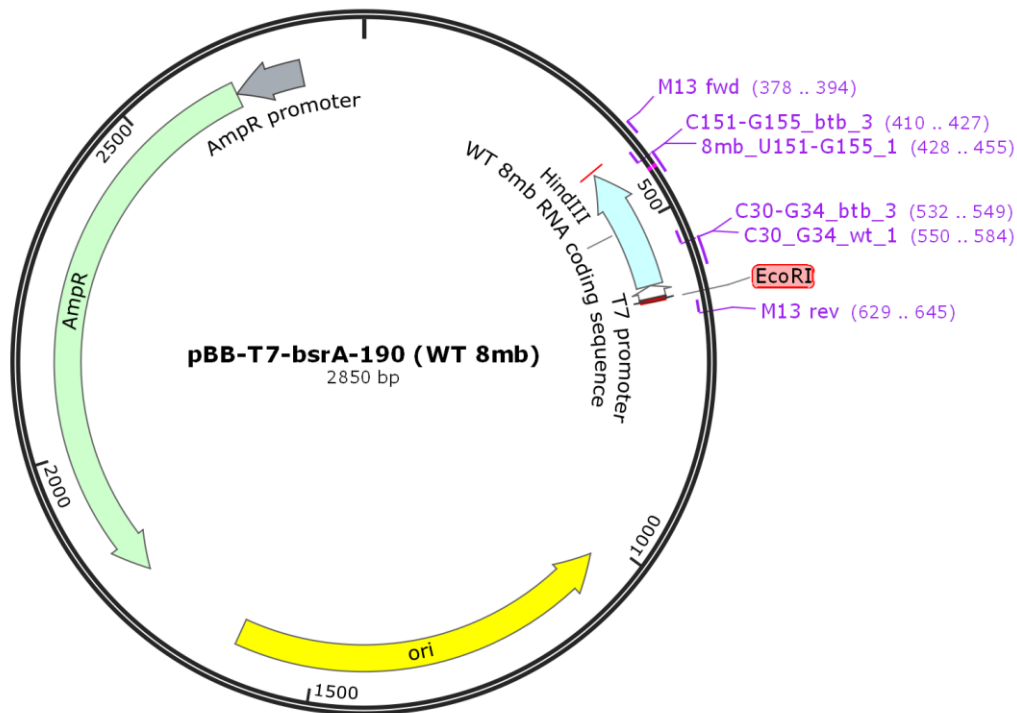
HindIII

pSG4 (pUC18-T7-bsrA-190-WT 8mb)

as pSG2, but positions 151 and 153 reverted back to the WT sequence. The RNA transcribed from this plasmid construct was originally referred to as WT 8mb and later renamed to WT 6M.

Alias: pSG4

Created with SnapGene®

**WT 8mb mutant sequence**

5' GAATTCTAATACGACTCACTATAGGAGTCCTGATGTGTTAGTTGTACACC
TAGTCAAGGCCGAACATTTTTTTGATTTGGGAGCCCGCATTTTTAAATGGC
GTACATGCCTCTTTTCATTCGGTAAAGAGGACTTACAAGATTTAAAAGAGG
GCACCCACCTGCTGAGAGCGGGTTCATGACAAAGGAAAGCTGCAACGGC
ACTATTGGGACTTTAAGCTT 3'

EcoRI

T7 promoter

WT 8mb RNA coding sequence

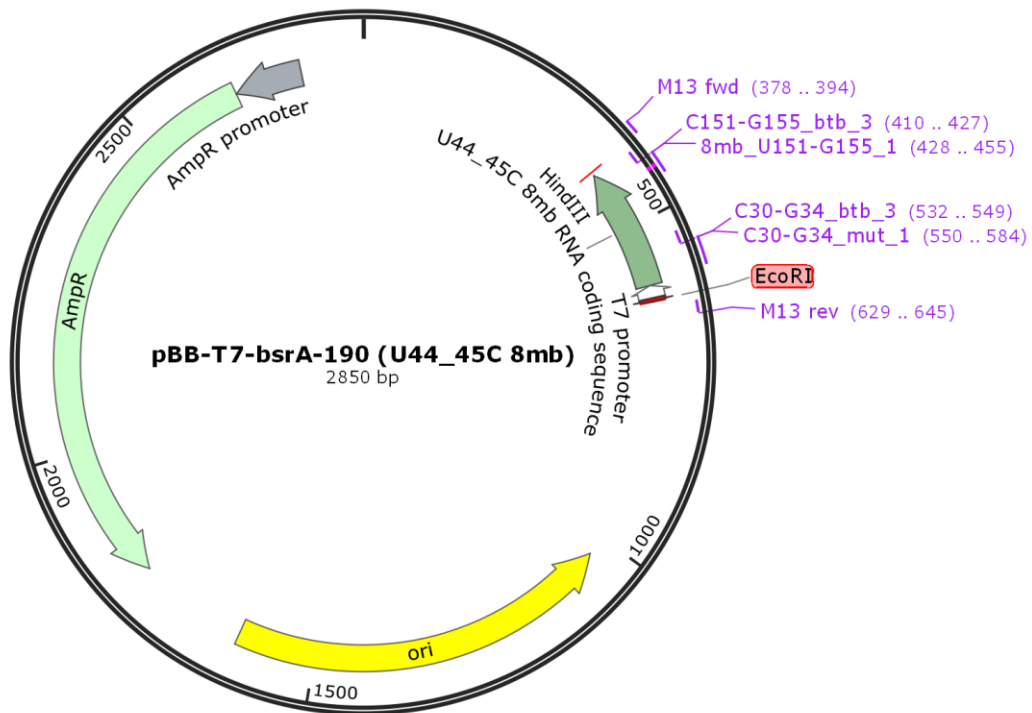
HindIII

pSG5 (pUC18-T7-bsrA-190-U44_45 8mb)

as pSG3, but positions 151 and 153 reverted back to the WT sequence. The RNA transcribed from this plasmid construct was originally referred to as U44_45 8mb and later renamed to C44/45 6M.

Alias: pSG5

Created with SnapGene®

**U44_45C 8mb mutant sequence**

5' **GAATTCTAATACGACTCACTATAGG**AGTCCTGATGTGTTAGTTGTACACC
 TAGT**CAAGGCCGAACATTCC**TTTGATTTGGGAGCCCGCATTTTTAAATGGC
 GTACATGCCTCTTTTCATTCGGTAAAGAGGACTTACAAGATTTAAAAGAGG
 GCACCCACCTGCTGAGAGCGGGT**TCATG**ACAAAGGAAAGCTGCAACGGC
 ACTATTGGGACTTT**AAGCTT** 3'

EcoRI

T7 promoter

U44_45C 8mb RNA coding sequence

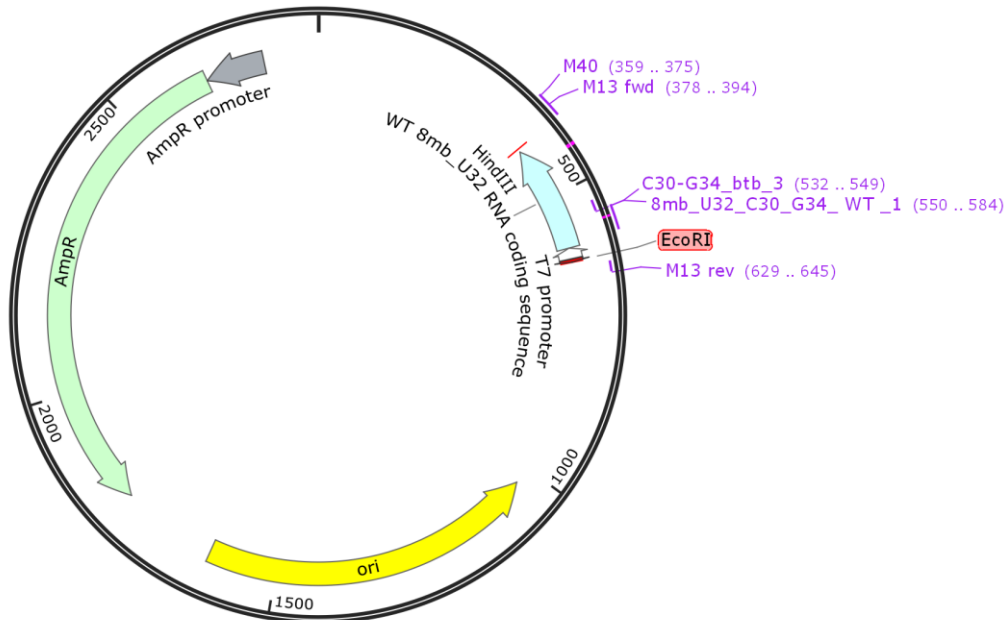
HindIII

pSG6 (pUC18-T7-bsrA-190-WT 8mb_U32)

as pSG4, but also position 32 reverted back to the WT sequence. The RNA transcribed from this plasmid construct was originally referred to as WT 8mb_U32 and later renamed to WT 5M.

Alias: pSG6

Created with SnapGene®



pUC18-T7-bsrA-190 (WT 8mb_U32)
2850 bp

WT 8mb_U32 mutant sequence

5' GAATTC TAATACGACTCACTATAGG AGTCCTGATGTGTTAGTTGTACACC
TAGT CATGG CCGAACATTTTTTTGATTTGGGAGCCCGCATTTTTAAATGGC
GTACATGCCTCTTTTCATTCGGTAAAGAGGACTTACAAGATTTAAAAGAGG
GCACCCACCTGCTGAGAGCGGGT ICATG ACAAGGAAAGCTGCAACGGC
ACTATTGGGACTTTAAGCTT 3'

EcoRI

T7 promoter

WT 8mb_U32 RNA coding sequence

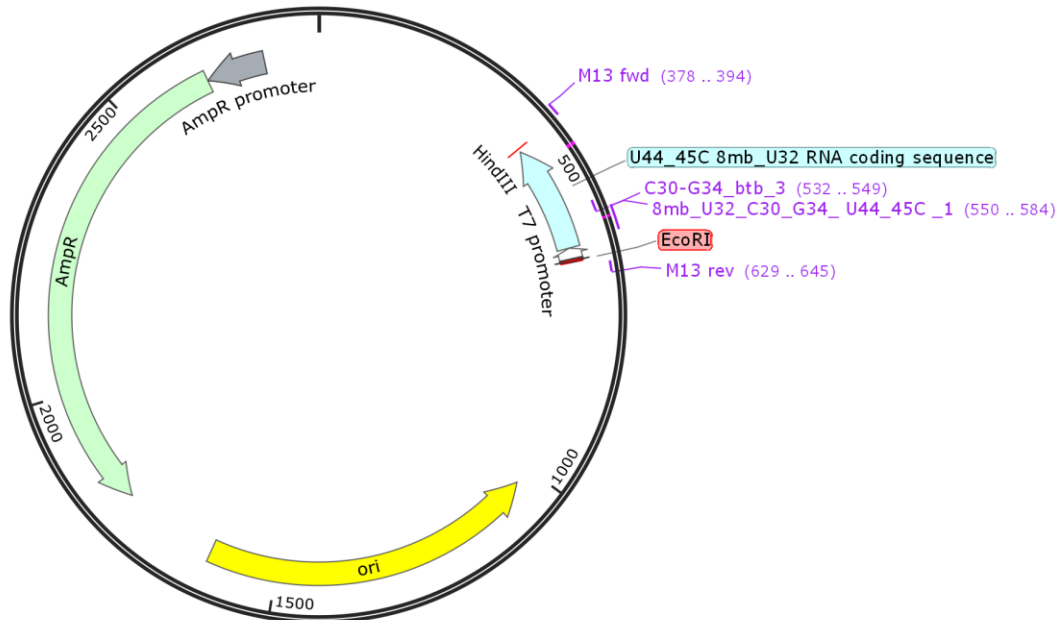
HindIII

pSG7 (pUC18-T7-bsrA-190-U44_45C 8mb_U32)

as pSG5, but also position 32 reverted back to the WT sequence. The RNA transcribed from this plasmid construct was originally referred to as U44_45C 8mb_U32 and later renamed to C44/45 5M.

Alias: pSG7

Created with SnapGene®



pUC18-T7-bsrA-190 (U44_45C 8mb_U32)
2850 bp

U44_45C 8mb_U32 mutant sequence

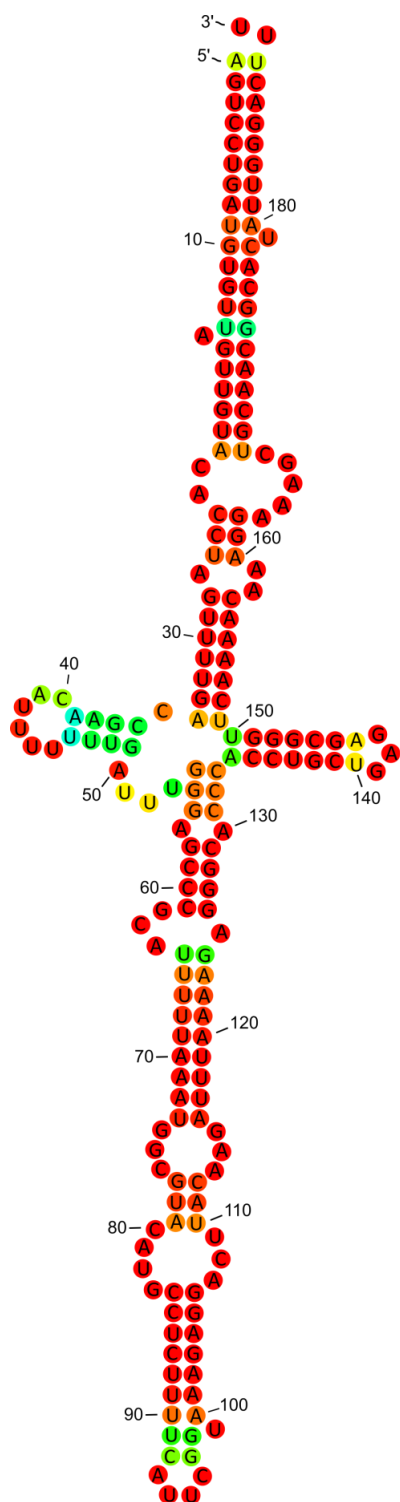
5' **GAATTC**TAATACGACTCACTATAGGAGTCCTGATGTGTTAGTTGTACACC
TAGT**CATGG**CCGAACATT**CC**TTTGATTTGGGAGCCCGCATTTTTAAATGGC
GTACATGCCTCTTTTCATTCGGTAAAGAGGACTTACAAGATTTAAAAGAGG
GCACCCACCTGCTGAGAGCGGGT**ICATG**ACAAAGGAAAGCTGCAACGGC
ACTATTGGGACTTT**AAGCTT** 3'

EcoRI

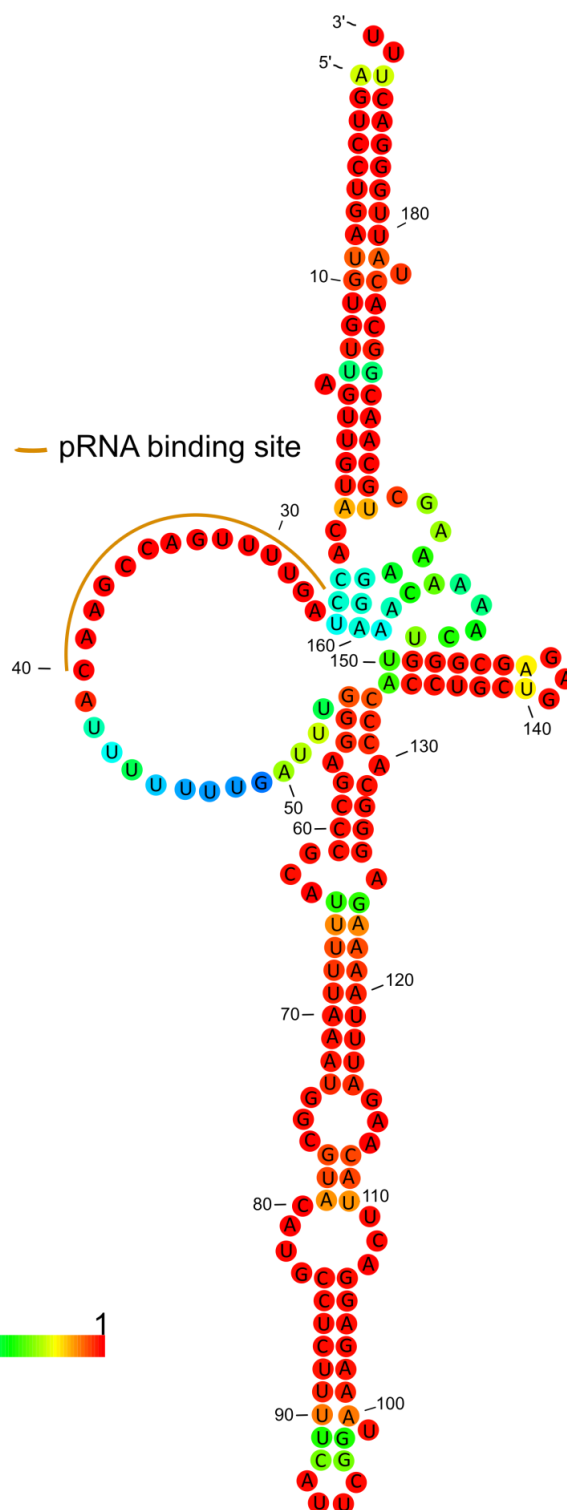
T7 promoter

U44_45C 8mb_U32 RNA coding sequence

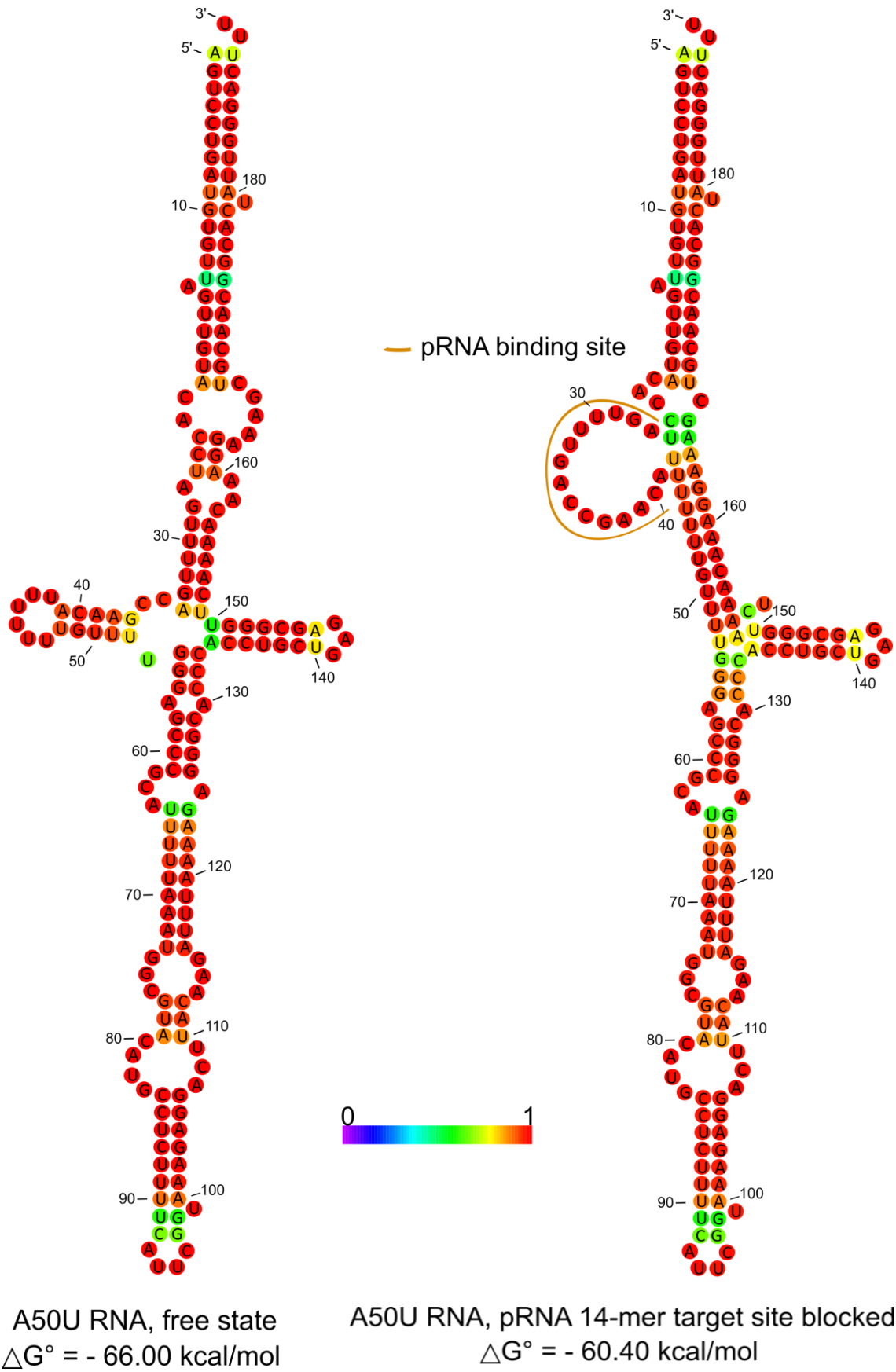
HindIII

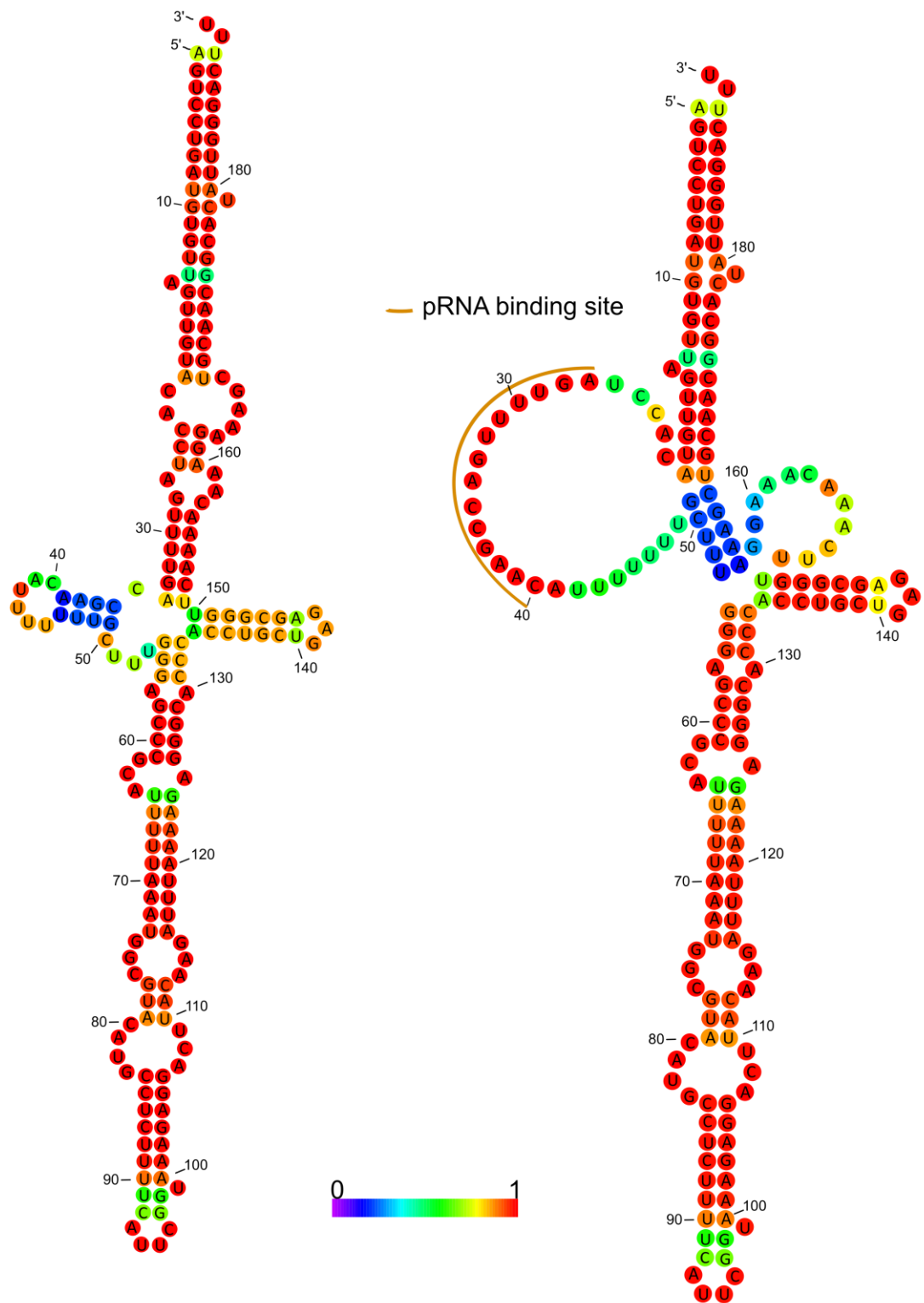


6S-1 RNA, free state
 $\Delta G^\circ = -63.50$ kcal/mol



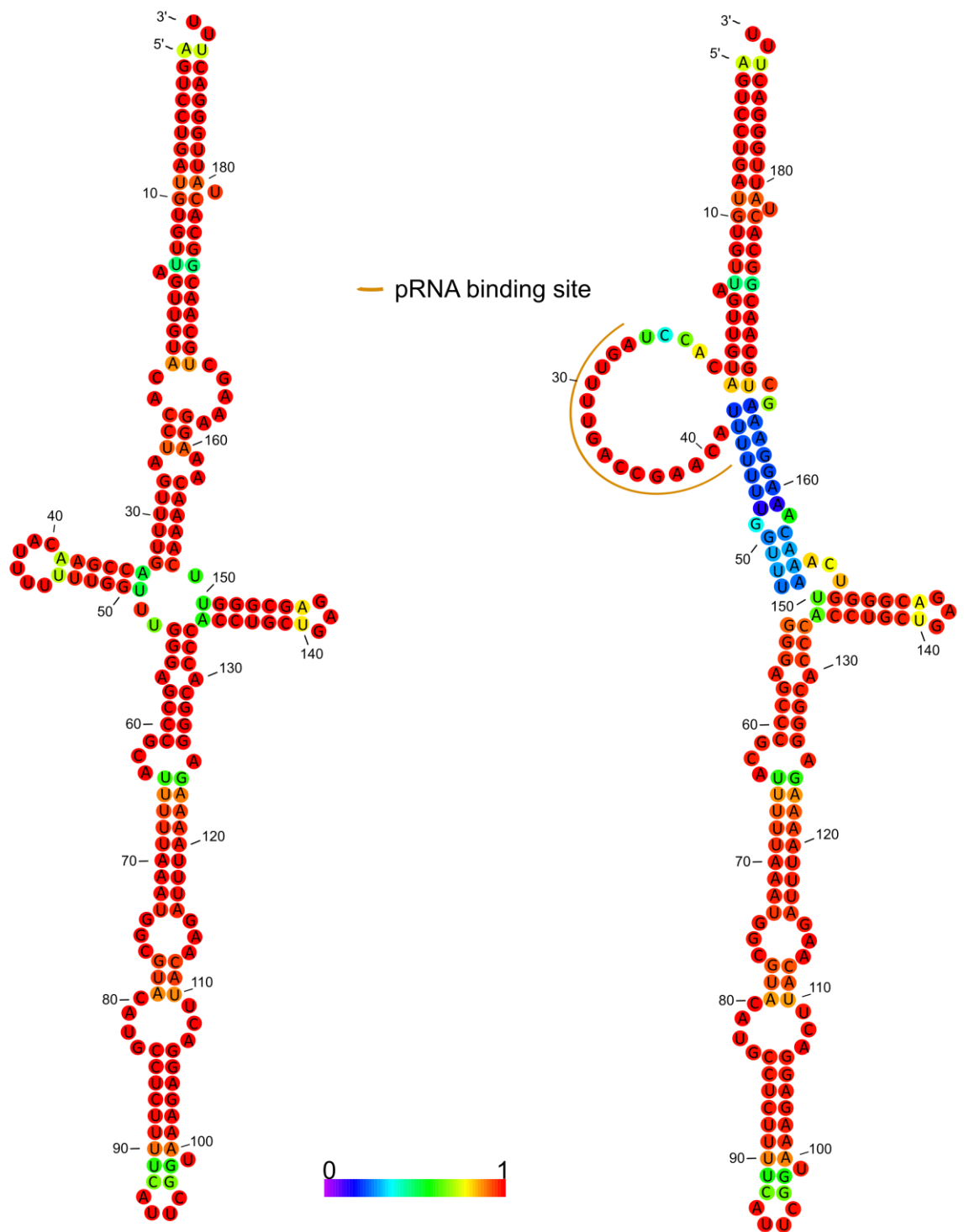
6S-1 RNA, pRNA 14-mer target site blocked
 $\Delta G^\circ = -59.79$ kcal/mol





A50C RNA, free state
 $\Delta G^\circ = -62.70$ kcal/mol

A50C RNA, pRNA 14-mer target site blocked
 $\Delta G^\circ = -56.80$ kcal/mol



A50G RNA, free state
 $\Delta G^\circ = -66.60$ kcal/mol

A50G RNA, pRNA 14-mer target site blocked
 $\Delta G^\circ = -57.00$ kcal/mol

78nt RNA sequence

5' CCUAGUUUUUGACCGAACAUUUUUUUUGAUUUUGGGAGCCCGCAGGGCA
 CCCACCUGCUGAGAGCGGGUUCAAAACAAAGG 3'

78nt RNA, free state

Predicted base pairing probability

(((((.....))))....(((.....))))(((((.....)))))).....))

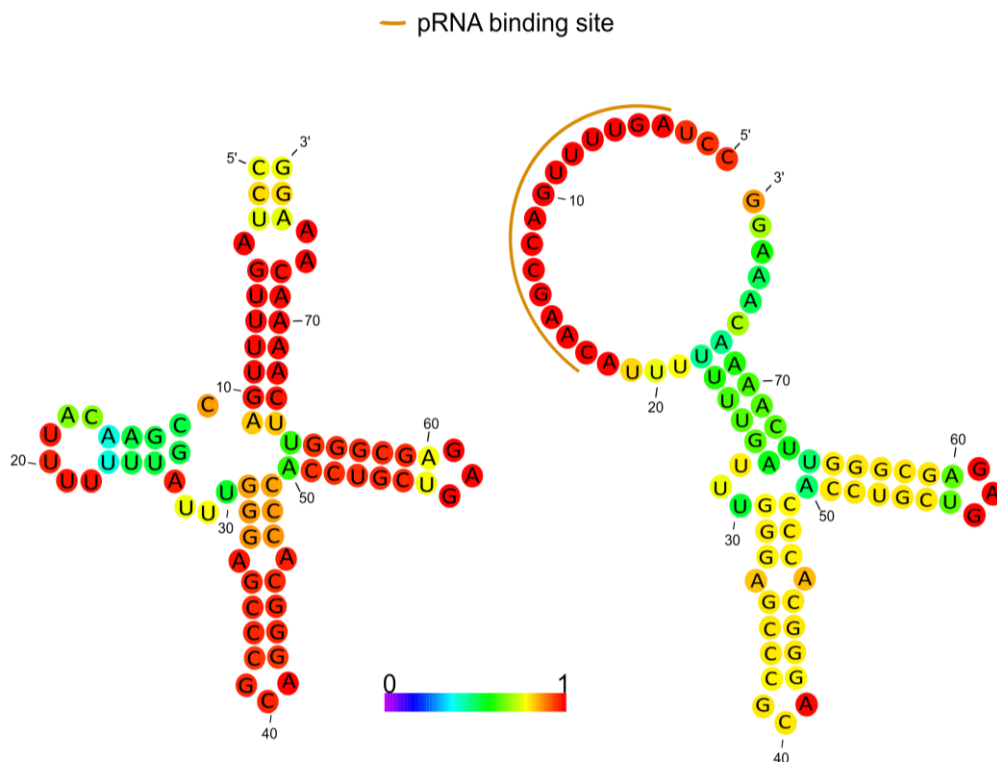
78nt RNA, pRNA 14-mer target site blocked

pRNA 14-mer constrain parameters

...xxxxxxxxxxxxx.....

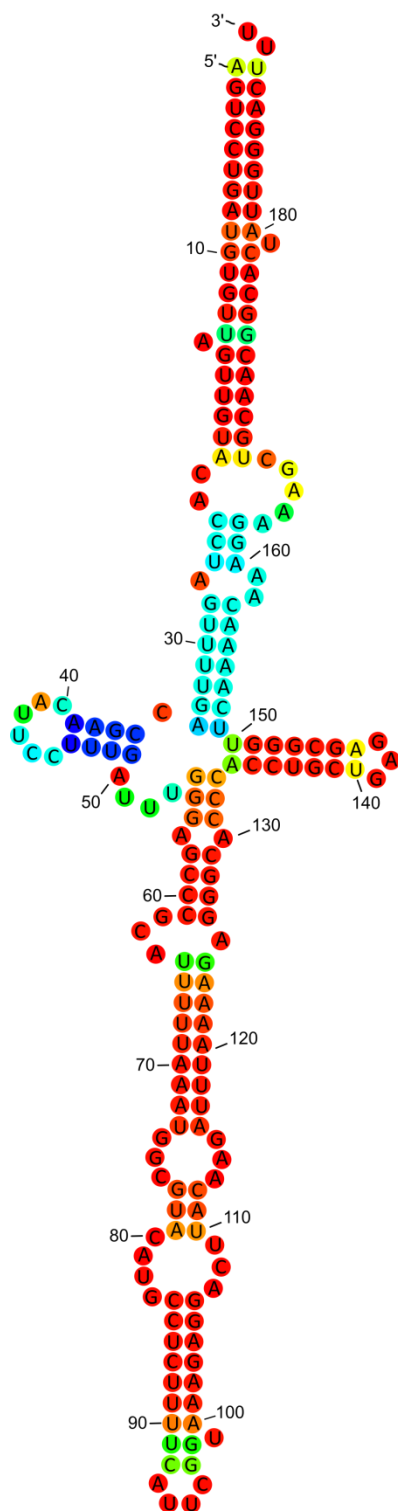
Predicted base pairing probability

.....((((.....(((.....))))))((((.....)))))).....

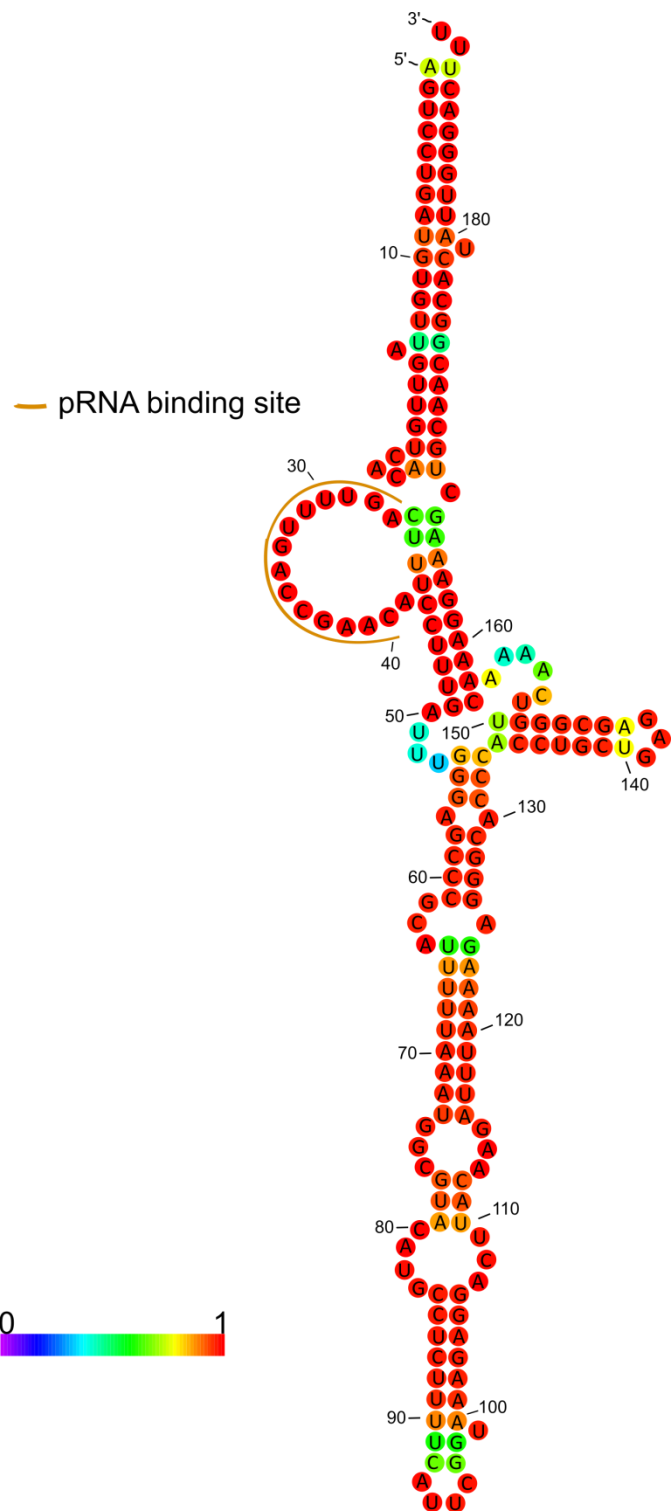


78nt RNA, free state
 $\Delta G^\circ = - 26.70$ kcal/mol

78nt RNA, pRNA 14-mer target site blocked
 $\Delta G^\circ = - 21.60$ kcal/mol



U44_45C RNA, free state
 $\Delta G^\circ = -63.50$ kcal/mol



U44_45C RNA, pRNA 14-mer target site blocked
 $\Delta G^\circ = -61.70$ kcal/mol

GGGG RNA sequence

5' AGUCCUGAUGUGUUAGUUGUACACCUAGCCCCGACCGAACAUUUUUU
UGAUUUGGGAGCCCGCAUUUUUAAAUGGCGUACAUGCCUCUUUUCAUU
CGGUAAAGAGGACUUACAAGAUUUAAAAGAGGGCACCCACCUGCUGAGA
GCGGGUUCGGGGCAAAGGAAAGCUGCAACGGCACUAUUGGGACUUU 3'

GGGG RNA, free state

Predicted base pairing probability

(((((.....)))).....(((.....)))).....(((.....)))).....(((.....)))).....
.....)))).....)))).....)))).....)))).....)))).....)))).....)))).....))..

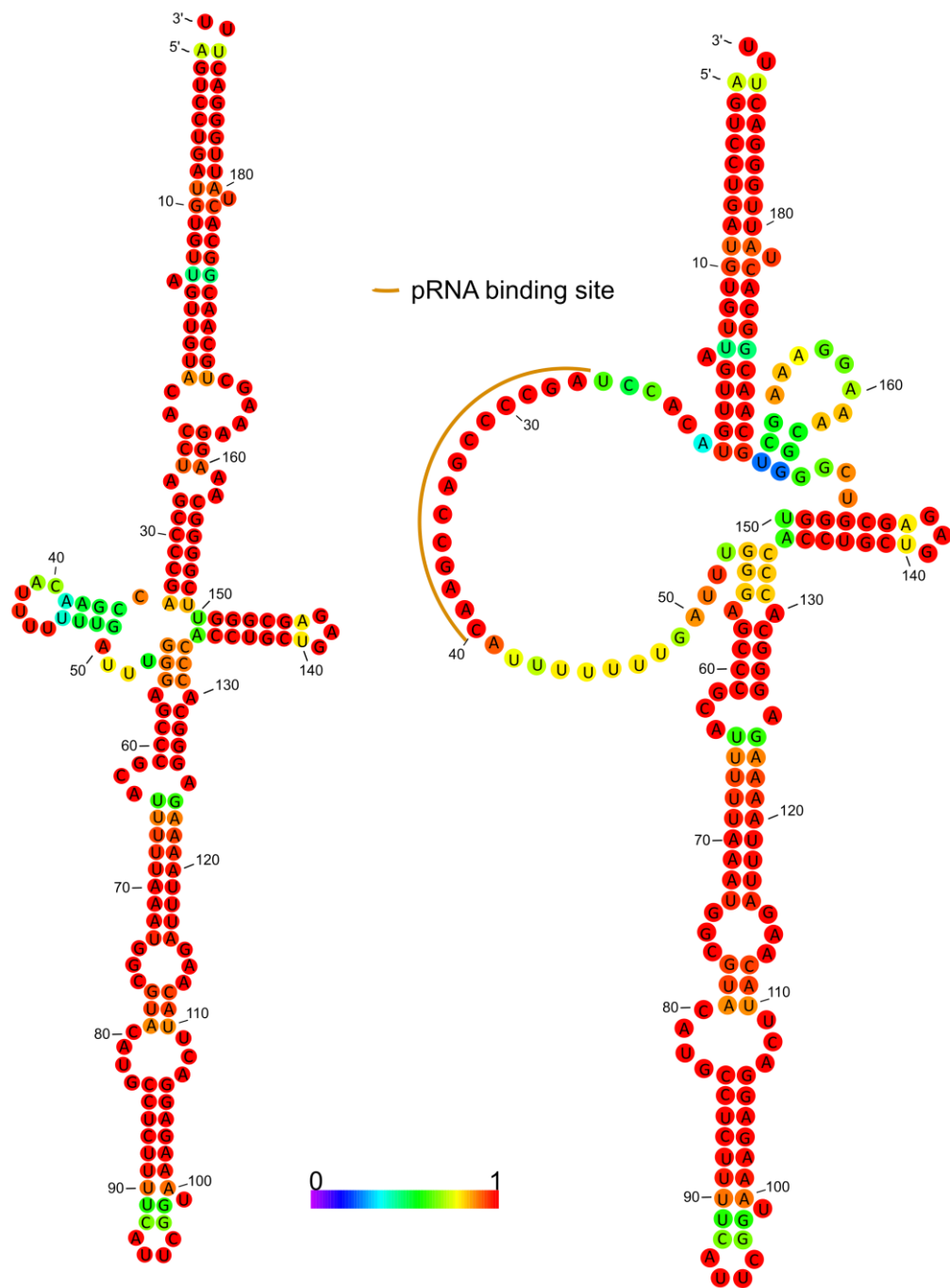
GGGG RNA, pRNA 14-mer target site blocked

pRNA 14-mer constrain parameters

.....XXXXXXXXXXXX.....
.....

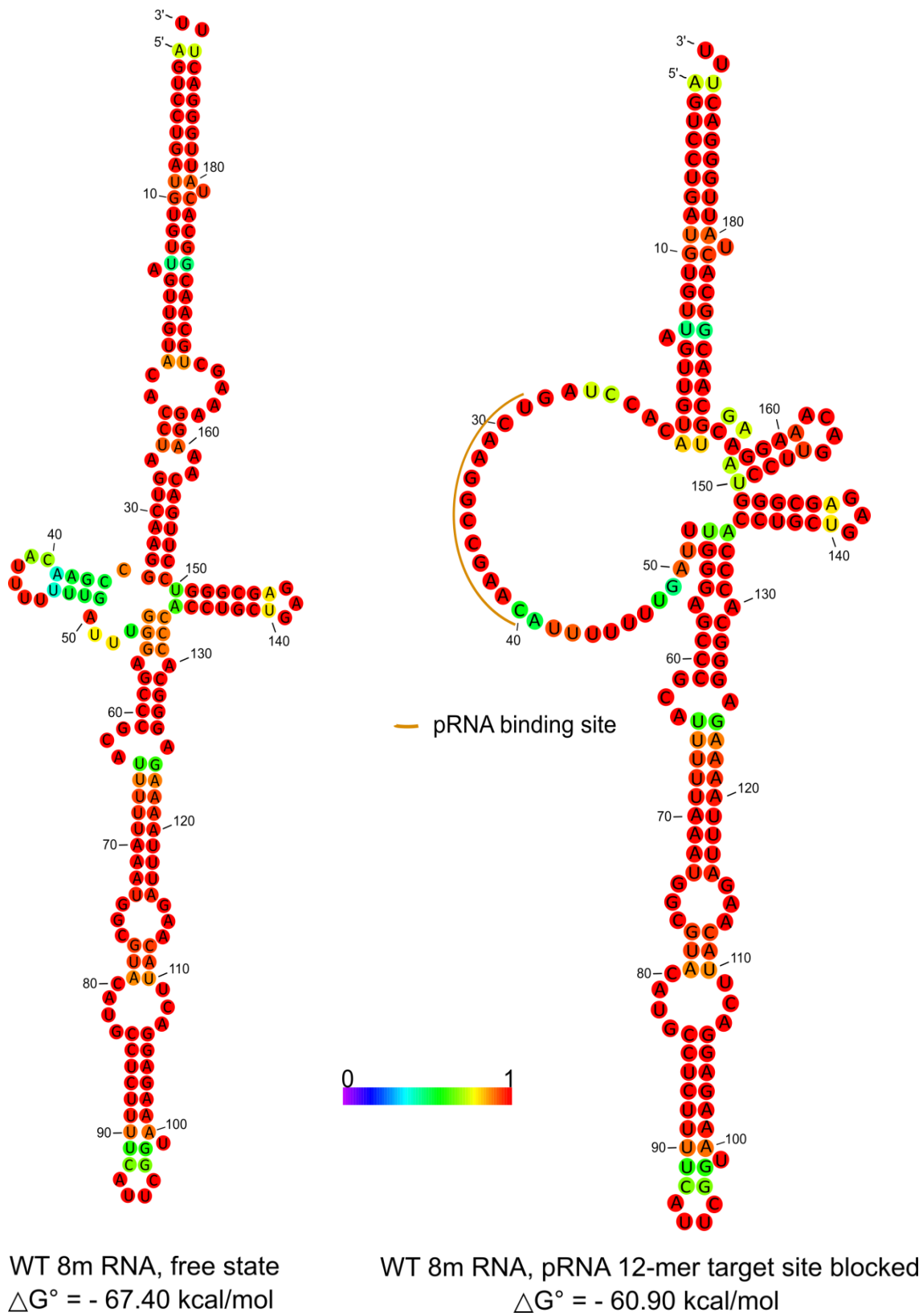
Predicted base pairing probability

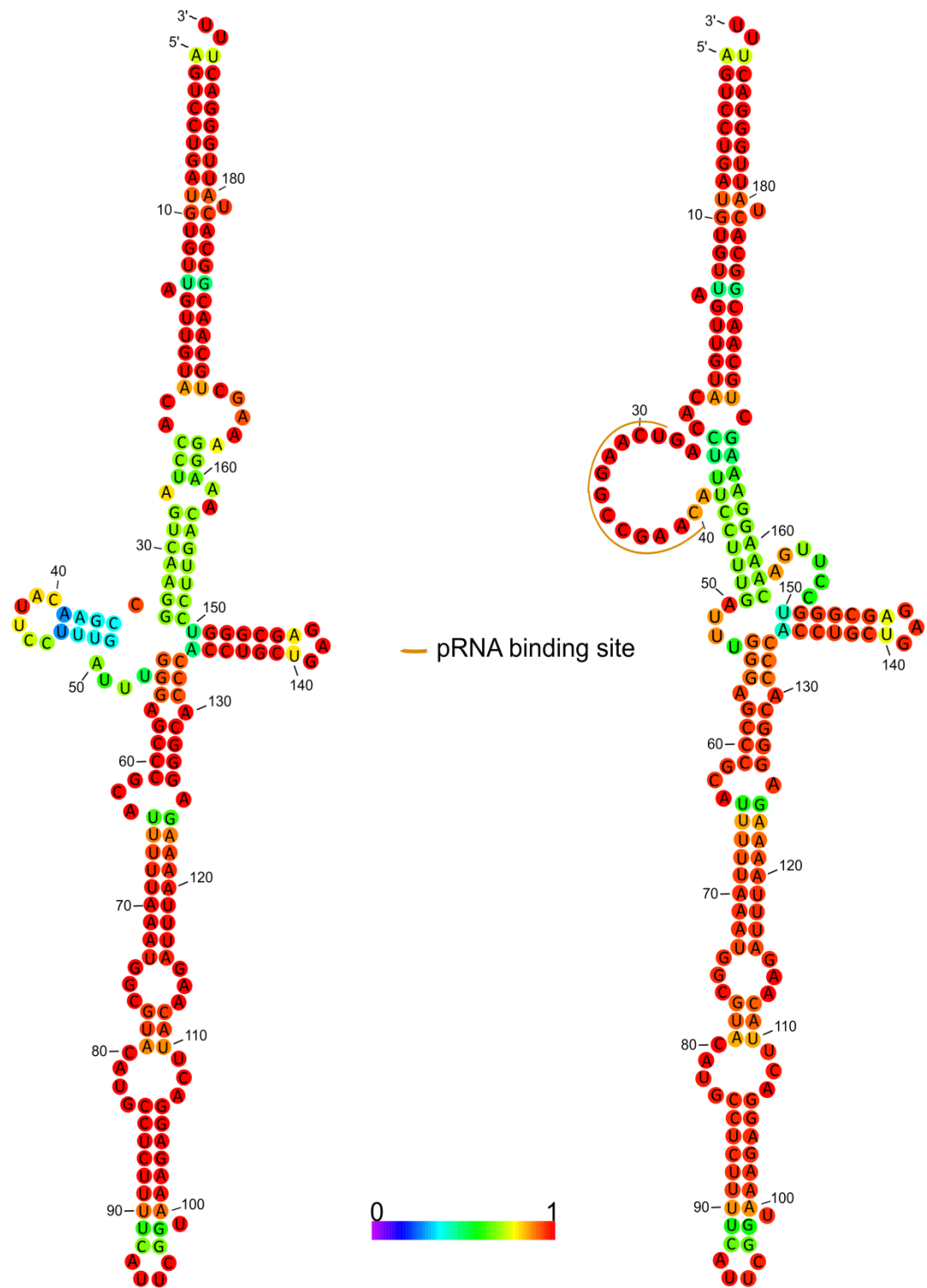
(((((.....)))).....(((.....)))).....(((.....)))).....(((.....)))).....
.....)))).....)))).....)))).....)))).....)))).....)))).....)))).....))..



GGGG RNA, free state
 $\Delta G^\circ = - 72.20$ kcal/mol

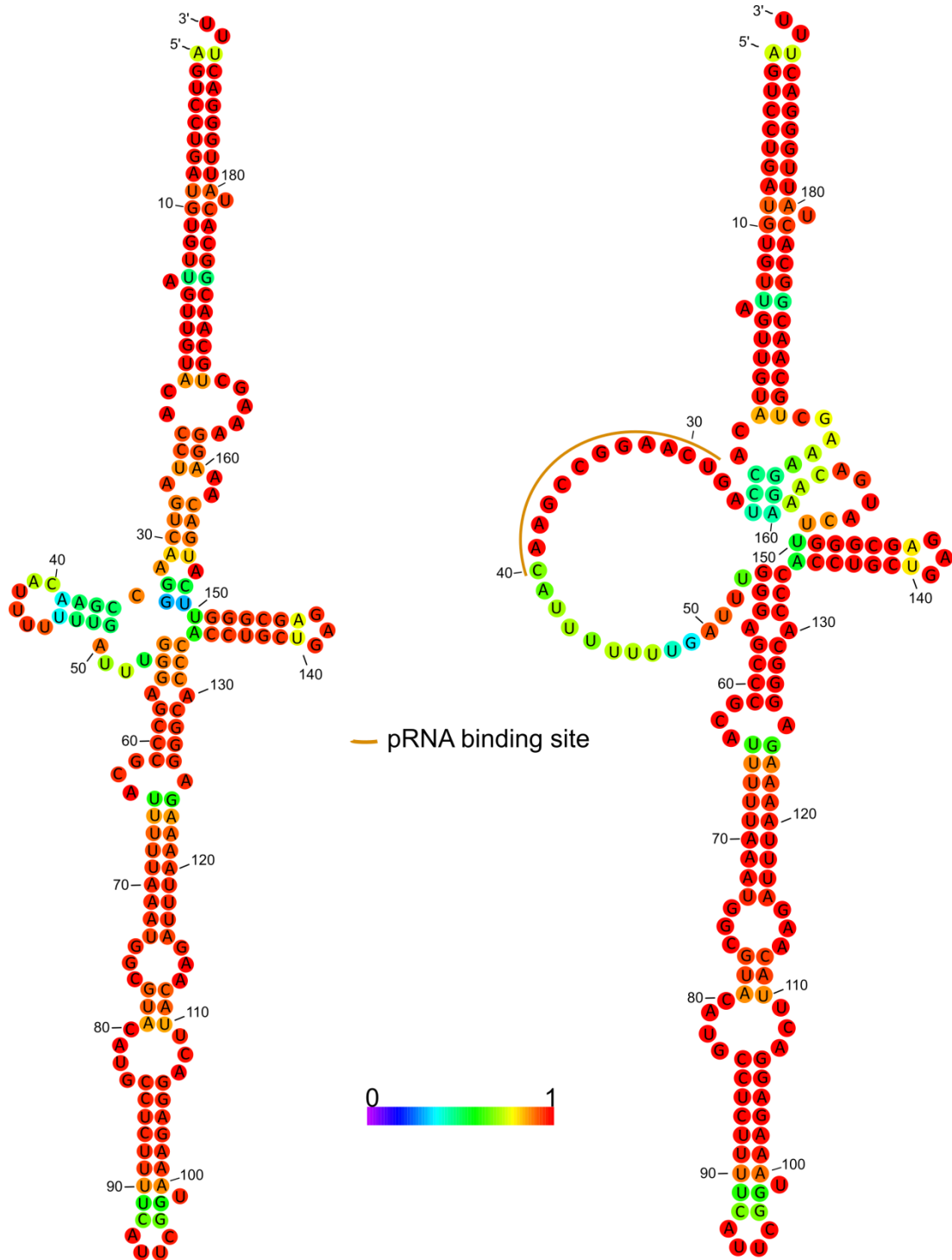
GGGG RNA, pRNA 14-mer target site blocked
 $\Delta G^\circ = - 57.30$ kcal/mol





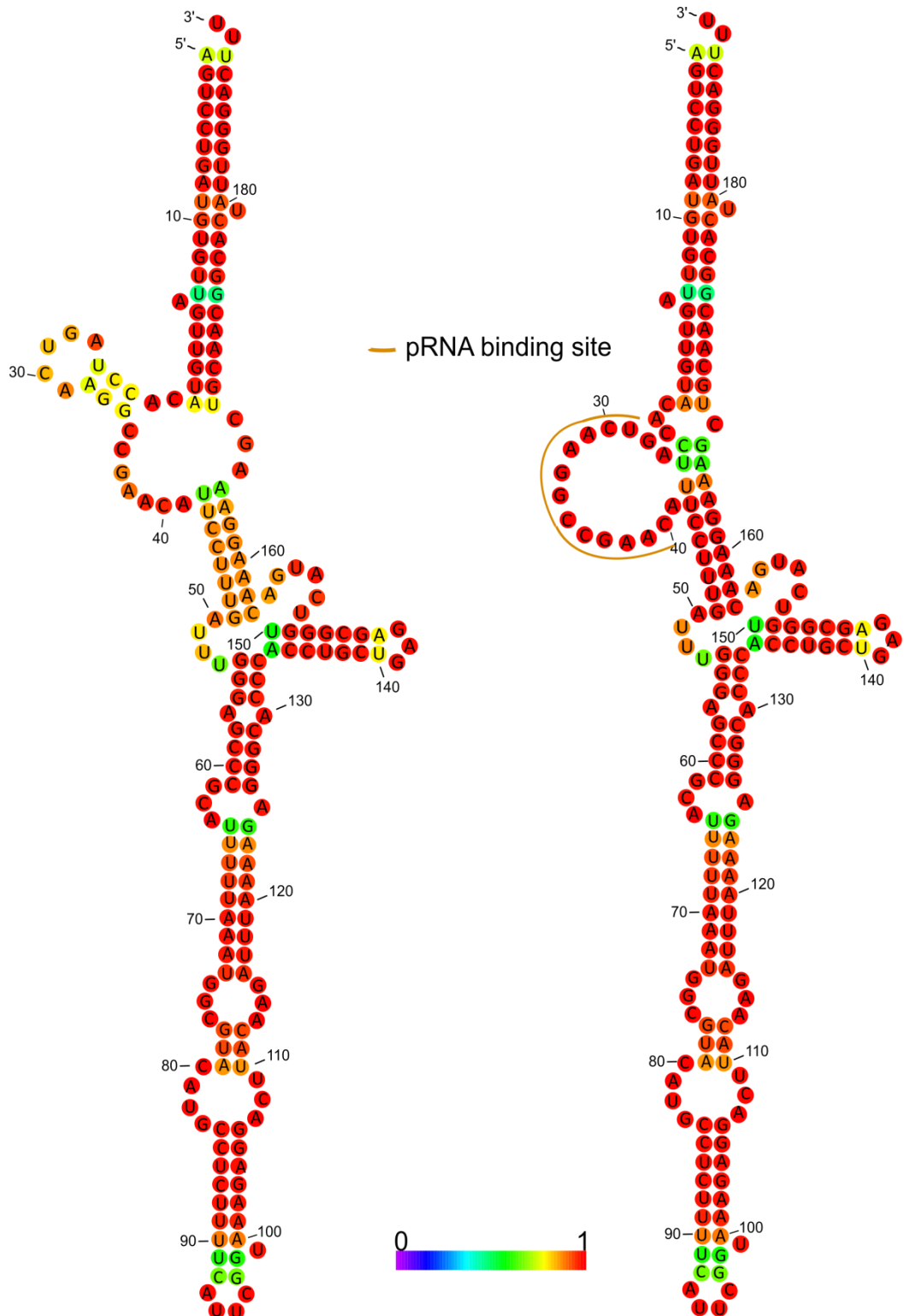
U44_45C 8m RNA, free state
 $\Delta G^\circ = -67.40$ kcal/mol

U44_45C 8m RNA, pRNA 12-mer target site blocked
 $\Delta G^\circ = -61.70$ kcal/mol



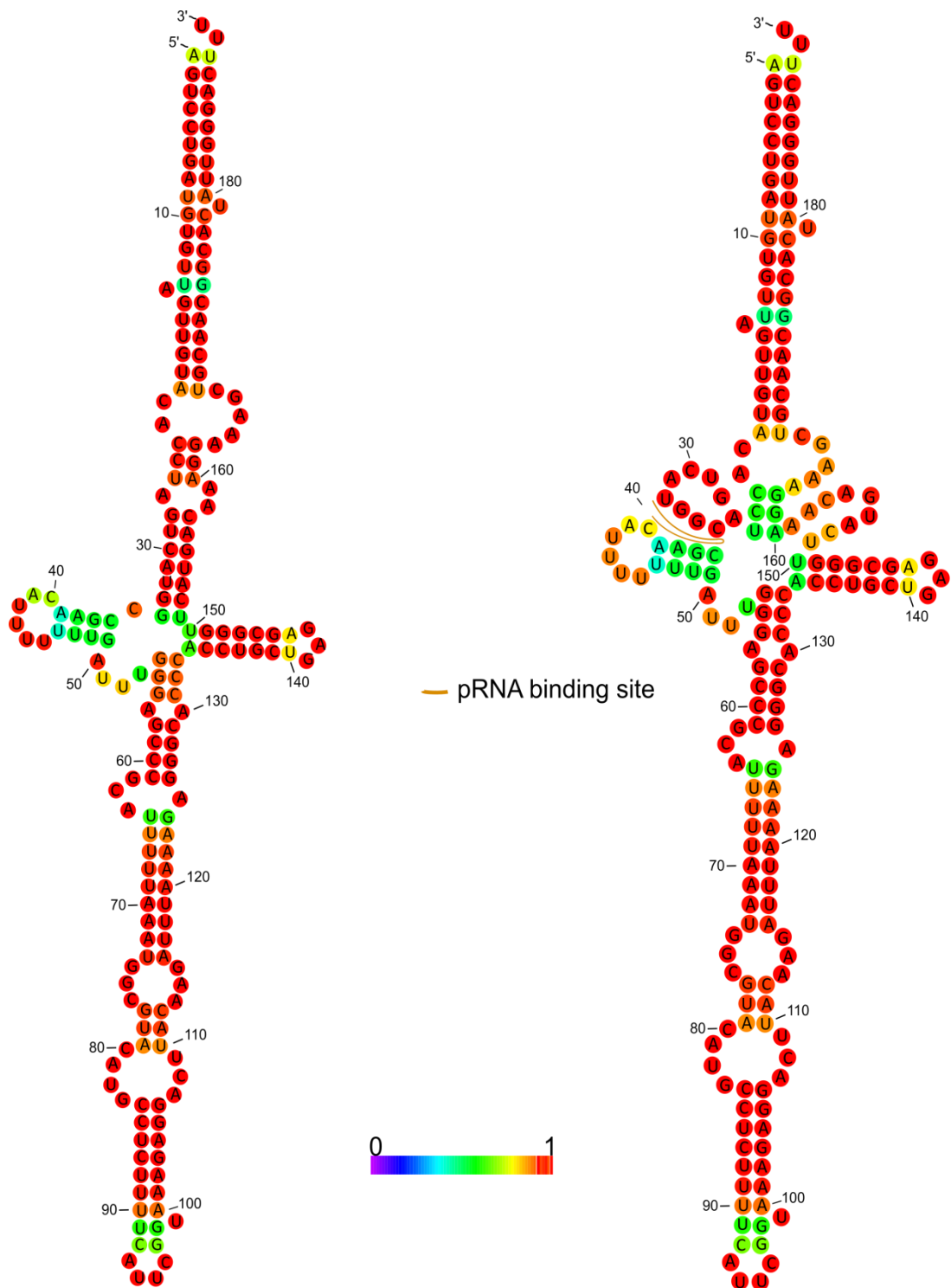
WT 8mb RNA, free state
 $\Delta G^\circ = -61.10$ kcal/mol

WT 8mb RNA, pRNA 12-mer target site blocked
 $\Delta G^\circ = -56.60$ kcal/mol



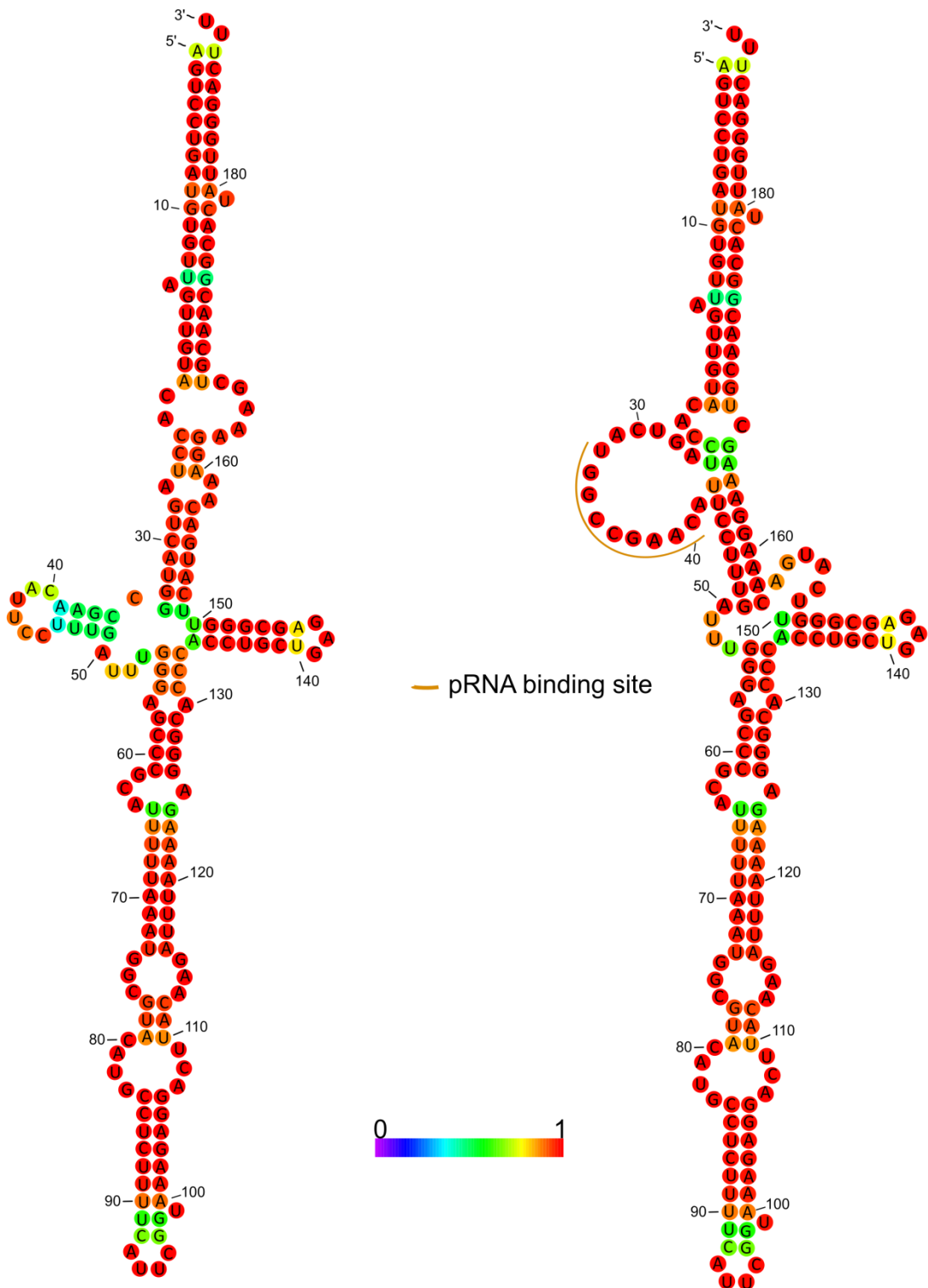
U44_45C 8mb RNA, free state
 $\Delta G^\circ = -64.20$ kcal/mol

U44_45C 8mb RNA, pRNA 12-mer target site blocked
 $\Delta G^\circ = -61.70$ kcal/mol



WT 8mb_U32 RNA, free state
 $\Delta G^\circ = -65.50$ kcal/mol

WT 8mb_U32 RNA, pRNA 9-mer target site blocked
 $\Delta G^\circ = -57.40$ kcal/mol



U44_45C 8mb_U32 RNA, free state
 $\Delta G^\circ = -65.50$ kcal/mol

U44_45C 8mb_U32 RNA, pRNA 9-mer target site blocked
 $\Delta G^\circ = -61.70$ kcal/mol

L. Scientific CV

sweethabiotechnologist@gmail.com phone +49 17663287197

Personal details

Name Ganapathy, Sweetha
Date of birth 17th September 1992
Place of birth Chennai, India
Nationality Indian

Education

Since 2016 Ph.D. in RNA Biochemistry
Institute of Pharmaceutical Chemistry, Philipps-University Marburg

2014 – 2016 Master of Technology (M. Tech.), Industrial Biotechnology
Shanmugha Arts, Science, Technology and Research Academy

2010 – 2014 Bachelor of Technology (B.Tech.), Biotechnology
Sri Venkateswara College of Engineering

Ph. D. thesis

Title 6S RNAs in *Bacillus subtilis* - Investigation of biological function
and molecular mechanism

Supervisor Prof. Dr. Roland K. Hartmann

Experience

Expertise Molecular biology, RNA biochemistry, Microbiology

Teaching Supervision of undergraduate students as Scientific assistant

Working Research Intern, December 2015 - May 2016 (6 months)
Novozymes, Bengaluru, Karnataka India

Scientific skills and methods

Molecular Biology Handling genetically modified organisms, strain construction, DNA based techniques (PCR, cloning, preparation and modification)

RNA Methods RNA isolation, *in vitro* transcription, secondary structure prediction, analysis of RNA-protein binding

Protein Methods Protein purification (Ni-NTA column, Size exclusion column)
Standard protein techniques (SDS-PAGE/Western blotting)

Assays *In vitro* radiolabeled transcription assays, Motility and Sporulation assay

Certificates

Training GMP, GLP and GCP course by MARA Academy, Marburg

IELTS International English Language Testing System 7.5 / 9, 2019

M. Scientific contributions

Scientific achievements

- Talks “Phenotypic characteristics of 6S RNA knockout mutants” during annual meeting of non-coding RNA research groups, Hirscheegg, 2019
- “Role of 6S RNAs in *Bacillus subtilis* mechanistic and physiological aspects (An update)” during annual meeting of non-coding RNA research groups, Hirscheegg, 2018
- “Role of 6S RNAs in *Bacillus subtilis*: mechanistic and physiological aspects” during annual meeting of non-coding RNA research groups, Hirscheegg, 2017
- “Function and regulation of two 6S RNAs in *Bacillus subtilis*”, Bacell 2018, Bath, UK, presented by Hartmann, R. K.
- Poster **Ganapathy, S.**, Hartmann, R. K. “Role of 6S-1 RNA in *Bacillus subtilis*: a study on mechanistic aspects” during conference on Sensory and Regulatory RNA in Prokaryotes, Giessen 2018
- Ganapathy, S.**, Hartmann, R. K. “Role of 6S-1 RNA in *Bacillus subtilis*: a study on mechanistic aspects” during GBM RNA Biochemistry workshop 2018, Bonn
- Manuscript **Ganapathy, S.**, Hoch, P. G., Hartmann, R. K. Structural and functional insight into the mechanism of *Bacillus subtilis* 6S-1 RNA release from RNA polymerase (In preparation)
- Publication Thüring, M., **Ganapathy, S.**, Schlüter, M. A. C., Lechner, M., Hartmann R. K., 6S-2 RNA deletion in the undomesticated *B. subtilis* strain NCIB 3610 causes a biofilm derepression phenotype. RNA Biol. 2021 Jan;18(1):79-92. Epub 2020 Aug 30.

PMID: 32862759; PMCID: PMC7834083.

Ganapathy S, Wiegard JC, Hartmann RK. Rapid preparation of 6S RNA-free *B. subtilis* σ^A -RNA polymerase and σ^A . J Microbiol Methods. 2021 Sep 8;190:106324. doi: 10.1016 /j. mimet. 2021. 106324 . Epub ahead of print. PMID: 34506811.

Erklärung zum selbstständigen Verfassen einer Arbeit**ERKLÄRUNG****gemäß § 10 der Promotionsordnung des Fachbereichs Pharmazie (FB 16)
der Philipps-Universität Marburg**

Ich versichere, dass ich meine Dissertation

**“6S RNAs in *Bacillus subtilis*
Investigation of biological function and molecular mechanism”**

selbständig ohne unerlaubte Hilfe angefertigt und mich dabei keiner anderen als der von mir ausdrücklich bezeichneten Quellen bedient habe. Alle vollständig oder sinngemäß übernommenen Zitate sind als solche gekennzeichnet.

Die Dissertation wurde in der jetzigen oder einer ähnlichen Form noch bei keiner anderen Hochschule eingereicht und hat noch keinen sonstigen Prüfungszwecken gedient.

Marburg, den 06.12.2021

.....

(Sweetha Ganapathy)